AD NUMBER: AD0466293
LIMITATION CHANGES
TO: Approved for public release; distribution is unlimited.
FROM: Distribution authorized to DoD Components only; Administrative/Operational Use; 8 Jul 1965. Other requests shall be referred to US Army Electronics Laboratories, Fort Monmouth, NJ 07703.
AUTHORITY
USAEC ltr dtd 1 Aug 1967

FOR OFFICIAL USE ONLY

FEASIBILITY STUDY OF SHIELDING TECHNIQUES

D6-8597-5

Contract No. DA36-039 AMC-02308(E)

Department of the Army

Project No. 1E6-20501-D-449-01-18

FINAL REPORT

1 JUNE 63 to 30 NOVEMBER 64

U. S. Army Electronics Laboratories, Fort Monmouth, New Jersey

THE BOEING COMPANY
AIRPLANE GROUP . PRODUCT DEVELOPMENT
RENTON, WASHINGTON

DATA REGARDING CANCELLATION OF PROTECTIVE MARKINGS CANNOT BE PREDETERMINED

FOR OFFICIAL USE ONLY

NOTICE: When government or other drawings, specifications or other data are used for any purpose other than in connection with a definitely related government procurement operation, the U. S. Government thereby incurs no responsibility, nor any obligation whatsoever; and the fact that the Government may have formulated, furnished, or in any way supplied the said drawings, specifications, or other data is not to be regarded by implication or otherwise as in any manner licensing the holder or any other person or corporation, or conveying any rights or permission to manufacture, use or sell any patented invention that may in any way be related thereto.

DDC AVAILABILITY NOTICE

For Official Use Only. DDC release to CFSTI not authorized. U. S. Government agencies may obtain copies of this report directly from DDC.

RELEASE OR ANNOUNCEMENT TO THE PUBLIC IS NOT AUTHORIZED.

DISCLAIMER

The citation of trade names and names of manufacturers in this report is not to be construed as official Government indorsement or approval of commercial products or services referenced herein.

The findings in this report are not to be construed as an official Department of the Army position, unless so designated by other authorized documents.

FOR OFFICIAL USE ONLY

FEASIBILITY STUDY OF SHIELDING TECHNIQUES

D6-8597-5

Contract No. DA36-039 AMC-02308(E)

Signal Corps Technical Requirement
SCL-7681, dated 27 August 1962

Department of the Army Project No. 1E6-20501-D-449-01-18

FINAL REPORT

1 June 63 to 30 November 64

OBJECT OF THE STUDY: To obtain reliable data for use by design personnel in assessing the effectiveness of a given electromagnetic shielding configuration with a great degree of accuracy and confidence.

Prepared by Vellar C. Plantz
Vellar C. Plantz

David R. Brush
David R. Brush

THE BOEING COMPANY
PRODUCT DEVELOPMENT
AIRPLANE GROUP
RENTON, WASHINGTON

Approved by RBSchulz
Richard B. Schulz
8 July 1965

FOR OFFICIAL USE ONLY

CONTENTS

Page

ILLUSTRATIONS

Figure		Page
24	UHF Setup (at Resonance Below 1 Gc)	71
25	Coordinate System Relative to Enclosures	72
26	Klystron Transmitting Test Setup (Shown in Screen Room)	75
27	10 Gigacycle Test Setup — Exterior View	75
28	Antenna Tower — Rotational Scheme (Side View)	76
29	E Plane of Pyramidal Horn; Geometric Representation	78
30	Transmitting Horn	79
31	Transmitting Horn Beam Width Representation; E Plane	79
32	Transmitting Horn; Beam Clearance	80
33	Helmholtz Indicator Current Source, Generator Amplifier Equipment	81
34	Phase Angle Determination Equipment, Amplitude Comparison Techniques	82
35	Correction Nomograph — Low Signal-to-Noise Ratio	83
36	Phase Angle Determination Equipment, Direct Reading Method	86
37	Phase Comparator Block Hook-Up Diagram	87
38	Enclosure No. -15 Phase Differential Versus Frequency	89
39	Enclosure No. -53 Phase Differential Versus Frequency	90
40	Transmitting Horn, Test Enclosure Relationship at the Zero-Angle Rotational Reference	91
41	10 Gigacycle Test Setup — Interior View	91
42	X-Band Field Pattern Data Interpolation Chart	92
43	Standardized Magnetic-Sensing Antenna Locations	93

TABLES

1.0 PURPOSE

The purpose of this Study is to provide reliable and readily applicable information to design personnel so that electromagnetic shielding configurations may be designed to provide, or verified as providing, a required degree of attenuation of intercepted electromagnetic waves. Although much shielding data has been available prior to this study, it has been relatively uncoordinated and difficult to apply to a given shielding design objective with a high degree of confidence because practical shields do not conform in detail to the ideally uniform materials and transmission media hypothesized in theoretical calculations.

1.1 Study Phases

The required research was accomplished in two overlapping phases: Phase I is a study of electromagnetic shielding for frequencies between 50 cps and 1.0 Gc. Phase II extends the study through 10 Gc. In addition, The Boeing Company has supported a companion study for the purpose of determining shielding effectiveness per unit of weight per unit of area for a given shielding material, and the effects of adverse environments upon shielding effectiveness.

1.2 Shielding Effectiveness Factors

The major objectives of the study are to isolate and measure the several discrete factors contributing to the total shielding effectiveness of enclosures. Since total shielding effectiveness, S, may be expressed as a function of all factors constitutive of a shielding situation, each individual factor is isolated and its dependence upon varying shielding configurations is determined. Then, for any given combination of the various factors in a specific enclosure, the shielding effectiveness can be determined from the contributions of the factors involved. Table A lists the variables considered. Practical considerations such as procurement lead time for materials, fabrication facilities response time and analytic or empiric ease of factor isolation determined the sequence in which the factors were separated.

2.0 ABSTRACT

This is the final report of an 18-month study program. Two significant results of basic utility in understanding and designing electromagnetic shielding are presented along with two resulting patent disclosures. It also details the basic theory and analytic and experimental approaches employed in obtaining these results.

2.1 Shielding Design

A technique based upon sound engineering principles was developed for the design of shielding enclosures. Substantiating though limited design data has been obtained. The basic approach was to consider transmission of wave energy through a shielding barrier in a manner analogous to conventional transmission-line theory. Transmission through each leakage path such as a seam, air inlet, electrical filter, etc., was considered to be in parallel with that through the shielding material itself. This fundamental theoretical development is presented in Sections 5.0 and 6.0. Design data resulting from this approach is given in Section 9.0 and substantiating experimental data is given in Appendices A, B, and C. The significance of the basic approach taken is that it is the first technique yielding good agreement between theory, design, and predicted performance of practical shielding enclosures.

2.2 Low-Frequency Resonance

During the performance of the study, resonance effects in a number of shielding enclosures were observed in the frequency range of 5 to 150 kc (Appendix A). These are explained as resulting from large differences in phase shift between parallel transmission paths; one through the shielding material and the other through seams under certain conditions of transmission. Since these effects are believed to be newly discovered, they serve as the basis for two patent disclosures made under the program which describe (1) a resonant filter for electromagnetic waves and (2) a metal seam and flaw evaluator. The patent disclosures are more fully described in Section 4.0.

Previous page was blank, therefore not filmed.

3.0 PUBLICATIONS, LECTURES, REPORTS AND CONFERENCES

3.1 Publications

(1) A technical paper, "Shielding Theory and Practice," by R. B. Schulz, V. C. Plantz and D. R. Brush, was published in the Proceedings of the Ninth Tri-Service Conference on Electromagnetic Compatibility, Illinois Institute of Technology Research Institute.

(2) A technical publication, by R. B. Schulz, for an Army Electronics Laboratories Seminar, "Feasibility Study of Shielding Techniques," dated 21 May 1964.

(3) A technical paper, by R. B. Schulz, V. C. Plantz, and D. R. Brush, "Low-Frequency Shielding Resonance," has been published in the Proceedings of the 1965 IEEE International Convention, March 1965.

3.2 Lectures

(1) R. B. Schulz, V. C. Plantz and D. R. Brush, "Shielding Theory and Practice," presented at the Ninth Tri-Service Conference on Electromagnetic Compatibility, Illinois Institute of Technology Research Institute, 15-17 October 1963, Chicago, Illinois.

(2) R. B. Schulz, "Feasibility Study of Shielding Techniques," to the Interference Reduction Branch of the U. S. Army Electronics Laboratories, Fort Monmouth, New Jersey, 21 May 1964. (Based on publication of same title).

(3) R. B. Schulz, V. C. Plantz, and D. R. Brush, "Low-Frequency Shielding, Resonance," presented at the 1965 IEEE International Convention, March 1965.

3.3 Reports

Five Quarterly Progress Reports entitled "Feasibility Study of Shielding Techniques," Department of the Army Project Number, 1E6-20501-D-499-01-18, released in September and December 1963, and March, June, and September 1964.

3.4 Conferences

3.4.1 On 11 July 1963 at Boeing, Seattle, Washington; concerned with directions and progress of subject Study. Attended by Mr. Guy Johnson of the U. S. Army Electronics Research and Development Laboratory, and Messrs. Schulz, Plantz, and Brush of the Boeing Company. Objectives and considerations agreed upon were as follows:

(1) The Study was to result in a compilation of shielding data and formulas in a form readily usable by design engineers. This would permit an accurate evaluation of shielding effectiveness of any given enclosure.

(2) The attenuation and phase shift effects upon an E or H field passing through a shielding medium were to be discussed in the First Quarterly Report.

(3) The reasons for measuring only the H field at low frequencies were to be explained.

(4) An explanation of why a single shield is less effective than two shields not in contact with each other, but having the same total thickness of metal, was requested.

(5) Frequencies at which a given metal shielding sample would appear to be "electrically thick" were to be considered more significant in tests than the specific test frequency of 1.0 Gc.

3.4.2 On 20 January 1964 at the U. S. Army Electronics Research and Development Laboratories, Fort Monmouth, New Jersey. Concerned with the validity of the technical approach taken on subject Study. Attended by R. B. Schulz, Boeing, and Messrs. Melvin Morris and William Stirrat of U. S. Army Electronics Laboratories. No common agreement was reached except that the technical aspects of the study would be reviewed.

3.4.3 On 22-23 April 1964 at Boeing: a visit and review of activities on the Study, to that date, by Mr. William Stirrat of USAEL, Fort Monmouth.

3.4.4 On 21-22 May 1964 at Fort Monmouth: a technical presentation of interim progress on the study of shielding techniques. Presented by R. B. Schulz.

3.4.5 On 18-20 August 1964 at Boeing: a visit by Mr. William Stirrat of the U. S. Electronics Laboratory to review past progress and future effort on subject Study. Because low-frequency shielding resonance had been obtained unexpectedly, the decision was made to concentrate the remainder of the study on understanding this and other major effects and to put little effort on minor shielding factors.

3.4.6 On 22 October 1964 at U. S. Army Electronics Laboratories, Fort Monmouth, a meeting was held between Mr. R. B. Schulz and Mr. William Stirrat. The shielding study progress was reviewed. Mr. Stirrat made several suggestions on the closing aspects of the study with special emphasis on separation of a seam factor.

3.4.7 On 12 February 1965 at U. S. Army Electronics Laboratories, Fort Monmouth, a meeting was held between Mr. R. B. Schulz and Mr. William Stirrat. The first draft of the Final Report had been intensively reviewed by Mr. Stirrat and his comments and suggestions were discussed at this meeting. Chief among Mr. Stirrat's contributions was the discussion of non-normal wave incidence (Par. 5.1.6).

4.0 PATENT DISCLOSURES

Two patent disclosures have been made as a result of this program. Both are based upon the phenomenon of low-frequency shielding resonance as described in this report.

4.1 Resonant Filter for Electromagnetic Waves

A resonant filter for electromagnetic waves which depends upon control of the parameters that cause resonance is disclosed. Frequency of resonance is determined primarily by electrical properties and thickness of the shielding material. A device, such as a shutter over a hole in the shield, controls the degree of peaking by varying the amount of leakage.

4.2 Metal Seam and Flaw Evaluator

Two versions of a metal seam and flaw evaluator have been disclosed. Both require a signal source driving a transmitting loop at one side of the metal and a pickup coil and voltmeter at the other side.

(1) In one version the source signal sweeps through the resonance range. The maximum voltmeter indication is calibrated in terms of flaw or seam leakage.

(2) The other version requires a double source coil and a double receiver coil. One receiver coil over good material and the other over a seam or flaw are arranged in series opposition for a signal cancellation in the absence of a defect. With a defect present the resultant voltmeter reading can be calibrated in terms of leakage.

5.0 FACTUAL DATA - UNIFORM SHIELDING THEORY

The development of plane wave theory in this section is largely in accordance with Schelkunoff (Ref. 1) and based on the preliminary development in "Shielding Theory and Practice" (Ref. 2). Typical calculations have been extracted from the invaluable work of Vasaka (Ref. 3). This section begins with a compilation of shielding theory intended to assist in understanding the mechanism of shielding behavior; the following section continues with a development of theory specifically applicable to the requirements of this study. Parallel experimental research and results are presented in the following sections and in the appendices.

The following list contains those symbols that have been used consistently throughout this report. Symbols used are in accord with those used in current texts and with IEEE recommendations. Because of the large number of parameters to be represented, it has been necessary on occasion to use some symbols with subscripts or superscripts to represent related quantities. In every instance the symbol has been defined wherever introduced to avoid misinterpretation.

Symbol	Quantity Represented	Units
A	Penetration loss term	db
B	Re-reflection correction term	db
c	Velocity of light (free space)	meters/sec.
e	Naperian base (2.71828...)	- -
E	Electric field strength	volts/meter
f	Frequency	cps
H	Magnetic field strength	amp/meter
i, I	Current	amp
Im	Imaginary part of ...	- -
j	Unit imaginary number $\sqrt{-1}$	- -
k	Impedance ratio; $k = \frac{Zw}{\eta}$	- -
ℓ	Length or thickness	meters, inches
p	Transmission coefficient	- -
q	Reflection coefficient	- -

Symbols	Quantity Represented	Units
r	Distance	meters, inches
R	Reflection loss term	db
Re	Real part of ...	- -
S	Shielding effectiveness	db
v	Phase velocity	meters/sec.
Y	Admittance per unit length of transmission line	mhos/meter
Z	Impedance per unit length of transmission line	ohms/meter
$Z(\ell)$	Impedance at point ℓ	ohms
Z_o	Characteristic impedance	ohms
Z_W	Wave impedance outside shield	ohms
α	Attenuation constant	nepers/meter
β	Phase-shift constant $\beta = 2\pi/\lambda$	radians/meter
β_o	Phase-shift constant in air (Par. 5.1.2)	radians/meter
γ	Propagation constant	$(\text{meter})^{-1}$
ϵ	Dielectric constant	farads/meter
ϵ_o	Dielectric constant of air	farads/meter
ϵ_r	Dielectric constant relative to air	- -
η	Intrinsic impedance	ohms
η_o	Intrinsic impedance of air	ohms
η_W	Wave impedance inside shield	ohms
θ	Net angular phase displacement	radians, degrees
θ_p	Phase displacement of path p	radians, degrees
λ	Wavelength	meters
λ_o	Wavelength in air	meters
μ	Initial magnetic permeability	henries/meter

Symbol	Quantity Represented	Unit
μ_o	Initial magnetic permeability of air	henries/meter
μ_r	Initial magnetic permeability relative to air	- -
2π	2 x 3.14159 . . .	radians/cycle
σ	Electrical conductivity	mhos/meter
σ_r	Electrical conductivity relative to copper	- -
ω	Angular frequency	radians
Ω	Resistance	ohms

5.1 Basic Plane-Wave Shielding; Basic Theory

The manner in which an electromagnetic shield transmits plane electromagnetic waves has been shown to be analogous to the manner in which a conventional two-wire transmission line transmits electrical current and voltage. Except where otherwise noted, MKS units are used in the theoretical derivations and English fps units are used in design formulas.

NOTE: The theoretical development and derivations which follow in this and the succeeding sections through 5.1.6 are closely based on original development and concepts of Mr. William A. Stirrat, Project Engineer on this contract for USAEL, Fort Monmouth. His approach is a generalization of that taken by the contractor to include the effects of oblique incidence.

5.1.1 Penetration Loss: A For the conducting metal of a shield, $\sigma \gg \omega\epsilon$ so that

$$\eta = \sqrt{\frac{j\omega\mu}{\sigma}} = (1+j)\sqrt{\frac{\omega\mu}{2\sigma}} = (1+j)\frac{|\eta|}{\sqrt{2}} \tag{1}$$

For dielectrics, $\sigma \ll \omega\epsilon$ so that

$$\eta = \sqrt{\frac{\mu}{\epsilon}} \tag{2}$$

In general,

$$\gamma = \alpha + j\beta \tag{3}$$

so that for a metallic sheet

$$\gamma = \sqrt{j\omega\mu\sigma} = (1+j)\sqrt{\omega\mu\sigma/2} \tag{4}$$

$$\alpha = \beta = \sqrt{\omega\mu\sigma/2} \tag{5}$$

and for a dielectric

$$\gamma = \sqrt{-\omega^2\mu\varepsilon} = j\omega\sqrt{\mu\varepsilon} = j\beta \tag{6}$$

$$\alpha = 0 \tag{7}$$

The transmission loss in passing through a shield of thickness ℓ is

$$A = 20\log_{10}|e^{\gamma\ell}| = 20\log_{10} e^{\alpha\ell}$$

$$A = 8.686\ \frac{\text{decibels}}{\text{neper}}\ \alpha\ell \tag{8}$$

5.1.2 Constants for Traveling Waves (See 5.1.3) The phase velocity v of the traveling wave is ω/β.

For a dielectric

$$v = 1/\sqrt{\mu\varepsilon} \tag{9}$$

and for metals

$$v = \sqrt{2\omega/\mu\sigma} \tag{10}$$

which is radically slower.

For air:

$$\varepsilon = \varepsilon_o = (1/36\pi)10^{-9}\ \text{farad/m}$$

$$\mu = \mu_o = 4\pi \times 10^{-7}\ \text{henries/m}$$

$$\eta = \eta_o = \sqrt{\mu_o/\varepsilon_o} = 120\pi\ \text{ohms} \tag{11}$$

$$v = c = 1/\sqrt{\mu_o\varepsilon_o} = 3\times10^8\ \text{m/sec}$$

$$\beta = \beta_o = \omega\sqrt{\mu_o\varepsilon_o} = (2\pi/3)\ 10^{-8}\ \frac{\text{radians}}{\text{meter}}\ \frac{\text{f}}{\text{cps}} \tag{12}$$

For copper,

$$\epsilon \simeq \epsilon_o, \quad \mu \simeq \mu_o{}^*$$

$$\sigma = 5.80 \times 10^7 \text{ mhos/m} \tag{13}$$

$$\eta = (1+j)\sqrt{\frac{\pi f \times 4\pi \times 10^{-7}}{5.8 \times 10^7 \text{ cps}} \text{ohm}^2}$$

$$= (1+j)\, 2.61 \times 10^{-7} \text{ ohms} \sqrt{\frac{f}{\text{cps}}}$$

$$v = \sqrt{\frac{4\pi f\, m^2}{4\pi \times 10^{-7} \times 5.8 \times 10^7 \text{cps sec}^2}}$$

$$= .415 \frac{m}{\text{sec}} \sqrt{\frac{f}{\text{cps}}}$$

$$\alpha = (15.1 \text{ nepers/m}) \sqrt{\frac{f}{\text{cps}}} \tag{14}$$

For dielectrics in general,

$$\eta = 120\pi \text{ ohms} \sqrt{\frac{\mu_r}{\epsilon_r}}$$

$$v = (3 \times 10^8 \text{ m/sec}) / \sqrt{\mu_r \epsilon_r} \tag{15}$$

$$\beta = \left(\frac{2\pi}{3}\right) 10^{-8} \ \frac{\text{radians}}{\text{m}} \ \frac{f}{\text{cps}} \sqrt{\mu_r \epsilon_r}$$

and for conductors in general,

* *Although this is a common assumption, a recent measurement shows* $\mu = 0.868\,\mu_o$ *for copper.*

$$\eta = (1+j)\ 2.61 \times 10^{-7}\,\text{ohms}\ \sqrt{\frac{f}{\text{cps}}}\ \sqrt{\frac{\mu_r}{\sigma_r}} \tag{16}$$

$$v = \left(.415\ \frac{\text{m}}{\text{sec}}\ \sqrt{\frac{f}{\text{cps}}}\right) \Big/ \sqrt{\mu_r \sigma_r} \tag{17}$$

$$\alpha = (15.1\ \text{nepers/m})\ \sqrt{\mu_r \sigma_r f/\text{cps}} \tag{18}$$

Associated with the phase velocity in a shield is a wavelength drastically shorter than the wavelength λ_o in air:

$$\lambda = \frac{v}{f} = \lambda_o \frac{v}{c} \tag{19}$$

$$= 1.38 \times 10^{-9}\,\lambda_o \sqrt{\frac{f/\text{cps}}{\mu_r \sigma_r}}$$

5.1.3 The Traveling Wave. A traveling wave is defined as one where propagation is in one direction only and there is no standing wave. For this wave the solution of Maxwell's equations produces

$$\frac{E}{H} = \eta = \sqrt{\frac{\mu}{\varepsilon}\ \frac{1}{(1+\sigma/j\omega\varepsilon)}} \tag{20}$$

and the complex velocity of propagation is

$$\sqrt{j\omega/\mu(\sigma+j\omega\varepsilon)} = j\omega/\gamma \tag{21}$$

for the special case where

$$j\omega E = \dot{E} = \partial E/\partial t. \tag{22}$$

Note that for all mediums

$$\gamma\eta = j\omega\mu \tag{23}$$

The intrinsic impedance η is the wave impedance (see 5.1.4) of this propagation. For this application in air, $\gamma = j\beta_o$.

5.1.4 Wave Impedance.

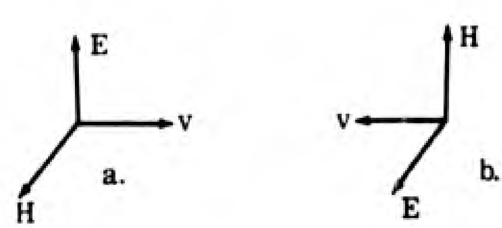

Fig. 1 Power Flow Conventions, Positive and Negative Flow Directions

In general, the following rules apply:

(1) There is no propagation in any direction in which there is no power flow.
(2) Components of E and H fields in the direction of propagation do not contribute to that propagation.
(3) The power flow per unit area through a plane perpendicular to the direction of propagation is determined by the product of E and H in that plane.
   (a) Only that component of H perpendicular to E contributes to the power flow.
   (b) Using the right hand rule, the power flow is in a positive direction for the orientations shown in Fig. 1a, and in the negative direction for the orientations shown in Fig. 1b.
(4) In complex analysis, the power flow may be complex.
(5) The wave impedance for propagation in a particular direction is the ratio E/H where the E and H fields are the same as in the product EH that produces the power flow in that direction. In a traveling wave these are the only fields present.
(6) If two traveling waves of the same frequency are combined as shown in Fig. 2, the power flow per unit area in the direction of v_2 is

$$(H_1+H_2)(E_2+E_1\cos\phi)$$

and the corresponding wave impedance is

$$\eta_{resultant} = \frac{E_2+E_1\cos\phi}{H_1+H_2}$$

Both the power flow and the wave impedance are complex if E_1 and E_2 are not in phase. Since the wavefront of the v_1 wave propagates in the v_2 direction at the rate $v_1/\cos\phi$ with a wavelength $\lambda/\cos\phi$, the wave impedance changes from point to point. In the high impedance field of Par. 5.1.8 the H fields of the traveling waves are all in the same direction but the E fields are not all in the same direction, as in Fig. 2. In the low impedance field case of Par. 5.1.10 the condition is reversed, so that the E fields are all in the same direction. (While fields may be in the same direction they may differ by π radians in phase.)

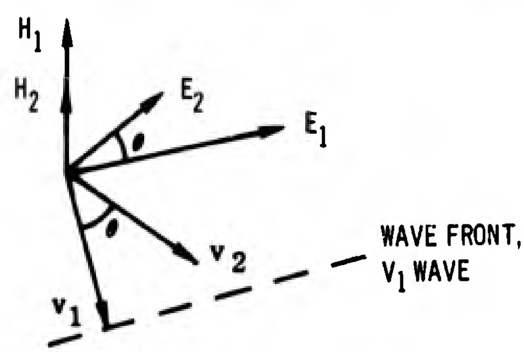

Fig. 2 High-Impedance Wave

5.1.5 **Transmission Through the Shield.**

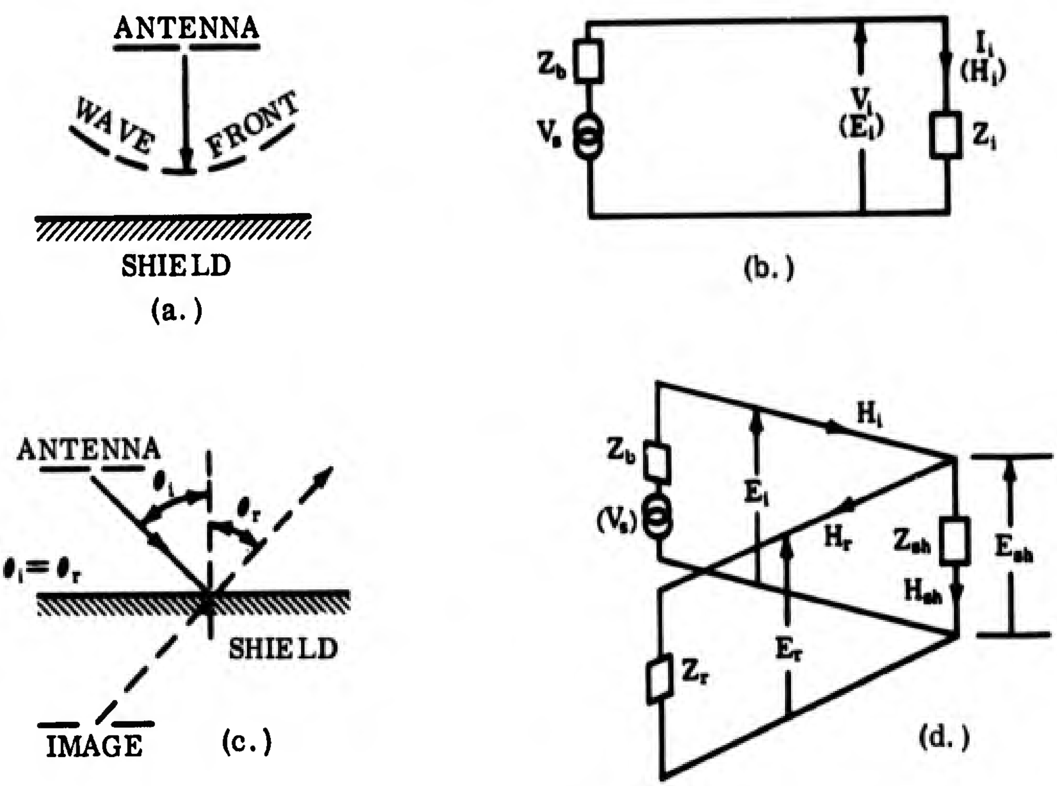

Fig. 3 Surface Reflection and Transmission Line Analogues

Consider a wave front set up by an antenna and propagated as shown in Fig. 3a. Until the wavefront reaches the shield the ratio of E to H (incident wave impedance, Z_i) is analogous to the ratio of V_i to I_i with Z_i the impedance looking forward, on the transmission line of Fig. 3b.

Note that Z_i is not affected by the shield since the incident wave has not yet reached the shield.

At the surface of the shield in Fig. 3c the wave is reflected with an angle of reflection equal to the angle of incidence. Since the wave impedance in free space is geometry determined, the reflected wave has the same forward impedance, Z_r, as the incident. Note that in reflection one of the fields in the plane of the shield must reverse direction, since the wave reverses direction with respect to the normal to the shield.

With E analogous to voltage and H analogous to current; with the subscript $_i$ denoting incident, $_r$ denoting reflected, and $_{sh}$ applying to fields entering the shield; and with Z_{sh} representing the wave impedance looking into the shield, the following equations can be written for the transmission line analogy in Fig. 3d:

$$E_i = H_i Z_i$$
$$E_r = H_r Z_r$$
$$E_{sh} = H_{sh} Z_{sh} \tag{24}$$

(Note that in the confinement of a transmission line Z_r would have been Z_b)

$$E_i + E_r = E_{sh} \tag{25a}$$

$$H_i - H_r = H_{sh} \tag{25b}$$

By addition of variations of equations (25)

$$Z_r \frac{E_i}{Z_i} - E_r = \frac{E_{sh}}{Z_{sh}} Z_r \tag{26}$$

yields

$$E_i \left[\frac{Z_r}{Z_i} + 1\right] = E_{sh}\left[\frac{Z_r}{Z_{sh}} + 1\right] \tag{27}$$

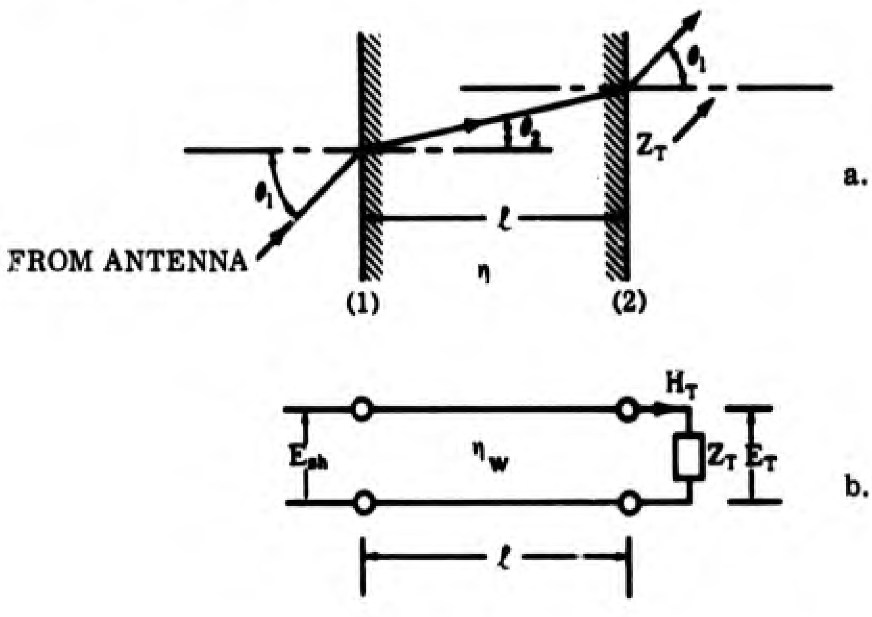

Fig. 4 Wave Refraction and Transmission Line Analogue

As shown in Fig. 4a, the field follows the laws of refraction. The transmission line analogy is shown in Fig. 4b. Here Z_T , the transmission line termination is analogous to the wave impedance seen by the fields E_T , H_T looking into space when leaving the shield at side (2). From transmission line equations,

$$E_{sh} = E_T \cosh \gamma \ell + \eta_w H_T \sinh \gamma \ell \tag{28}$$

$$H_{sh} = H_T \cosh \gamma \ell + \left(\frac{E_T}{\eta_W}\right) \sinh \gamma \ell \tag{29}$$

Then

$$\frac{E_i}{E_T}\left[1+\frac{Z_r}{Z_i}\right] = \frac{E_{sh}}{E_T}\left[1+\frac{Z_r}{Z_{sh}}\right] = \frac{E_{sh}}{E_T} + \frac{H_{sh}Z_r}{H_T Z_T}$$

$$= \left(1+\frac{Z_r}{Z_T}\right)\cosh \gamma \ell + \left(\frac{\eta_W}{Z_T} + \frac{Z_r}{\eta_W}\right)\sinh \gamma \ell, \tag{30}$$

where η_W is a wave impedance equal to η only if the direction of propagation considered is in the same direction as the traveling wave.

Let $$k_T = \frac{Z_T}{\eta_W}, \; k_r = \frac{Z_r}{\eta_W}. \tag{31}$$

Then with the use of

$$\cosh \gamma \ell = \frac{e^{\gamma \ell} + e^{-\gamma \ell}}{2} \quad \text{and} \quad \sinh \gamma \ell = \frac{e^{\gamma \ell} - e^{-\gamma \ell}}{2}, \tag{32}$$

$$2\frac{E_i}{E_T}\left[1+\frac{Z_r}{Z_i}\right] = \left(1+\frac{k_r}{k_T}+\frac{1}{k_T}+k_r\right)e^{\gamma \ell} + \left(1+\frac{k_r}{k_T}-\frac{1}{k_T}-k_r\right)e^{-\gamma \ell} \tag{33}$$

$$= (1+k_r)\left(1+\frac{1}{k_T}\right)e^{\gamma \ell} + (1-k_r)\left(1-\frac{1}{k_T}\right)e^{-\gamma \ell}$$

$$\frac{E_i}{E_T} = \left[\frac{(1+k_r)\left(1+\frac{1}{k_T}\right)}{2\left(1+\frac{Z_r}{Z_i}\right)}\right] e^{\gamma \ell}\left[1 - \frac{(1-k_r)(1-k_T)}{(1+k_r)(1+k_T)}e^{-2\gamma \ell}\right]. \tag{34}$$

Also,

$$\frac{H_i}{H_T} = \frac{\frac{E_i}{Z_i}}{\frac{E_T}{Z_T}} = \left(\frac{E_i}{E_T}\right)\left(\frac{Z_r}{Z_i}\right)\frac{k_T}{k_r}. \tag{35}$$

For free space on both sides of the shield,

$$Z_r = Z_i = Z_W$$
$$k_r = k_T = k. \tag{36}$$

5.1.6 Non-Normal Incidence.

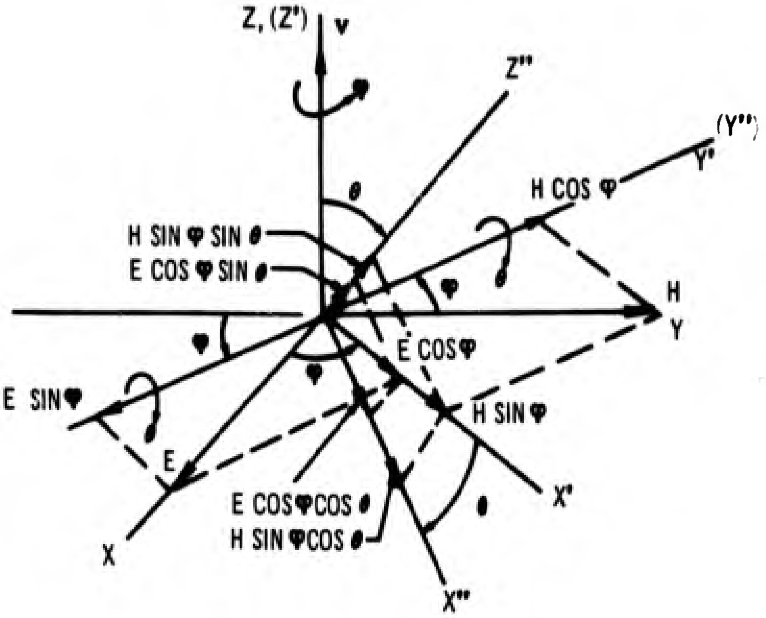

Fig. 5 Non-Normal Incidence

As in Fig. 5 , a coordinate system may be made to fit a traveling wave so that E is on the **X** coordinate, H on the **Y**, and propagation is along **Z**. This traveling wave can be assumed to be incident to the plane of the X'', Y' coordinates shown having its normal along Z''. The orientation of the X'', Y', Z'' coordinates with respect to the **X**, **Y**, **Z** can be expressed in terms of the spherical coordinates φ and θ, where θ is the angle of incidence of the wave impinging on the plane.

The fields on the X'', Y' coordinates can be assumed to be made up of two waves, each propagating in the Z'' direction:

$E_a = E \sin\varphi$	$E_b = E \cos\varphi \cos\theta$
$H_a = H \sin\varphi \cos\theta$	$H_b = H \cos\varphi$
$P_a = EH \sin^2\varphi \cos\theta$	$P_b = EH \cos^2\varphi \cos\theta$
$Z_{w_a} = \dfrac{E \sin\varphi}{H \sin\varphi \cos\theta} = \dfrac{\eta_o}{\cos\theta}$	$Z_{w_b} = \dfrac{E \cos\varphi \cos\theta}{H \cos\varphi} = \eta_o \cos\theta$ (37)

The power per unit area propagated in the Z'' direction is

$$P_a + P_b = EH\cos\theta \tag{38}$$

and the power per unit area propagated in the $-X''$ direction can be seen to be $EH \sin\theta$. Since the wave impedances are determined by the intrinsic impedances and geometry, then in terms of θ_1 (the angle of incidence) and θ_2 (the angle of refraction) in Fig. 4, they may be expressed as;

$$\begin{array}{l|l} Z_{wa} = \eta_o/\cos\theta_1 & Z_{wb} = \eta_o \cos\theta_1 \\ \eta_{wa} = \eta/\cos\theta_2 & \eta_{wb} = \eta\cos\theta_2 \end{array} \tag{39}$$

For the special case of free space on both sides of the shield, equation (34) becomes

$$\frac{E\sin\varphi}{E_{Ta}} = \frac{1}{4}\left(1+\frac{\eta_o\cos\theta_2}{\eta\cos\theta_1}\right)\left(1+\frac{\eta\cos\theta_1}{\eta_o\cos_2}\right)e^{\gamma\ell}\left[1-\frac{\left(1-\frac{\eta_o\cos\theta_2}{\eta\cos\theta_1}\right)^2}{\left(1+\frac{\eta_o\cos\theta_2}{\eta\cos\theta_1}\right)^2}e^{-2\gamma\ell}\right] \tag{40}$$

$$\frac{E\cos\varphi\cos\theta_1}{E_{Tb}\cos\theta_1} = \frac{1}{4}\left(1+\frac{\eta_o\cos\theta_1}{\eta\cos\theta_2}\right)\left(1+\frac{\eta\cos\theta_2}{\eta_o\cos\theta_1}\right)e^{\gamma\ell}\left[1-\frac{\left(1-\frac{\eta_o\cos\theta_1}{\eta\cos\theta_2}\right)^2}{\left(1+\frac{\eta_o\cos\theta_1}{\eta\cos\theta_2}\right)^2}e^{-2\gamma\ell}\right] \tag{41}$$

In emergence as shown in Fig. 6, E_{Tb} lies along the $+X'$ coordinate and E_{Ta} along the $-Y'$ coordinate. The vector sum of E_{Ta} and E_{Tb} will be rotated with respect to the incident E except at normal incidence. As a rule, the b fields will be attenuated more (usually by a factor of $1/\cos^2\theta_1$) than the a fields. The associated H fields are easily found from the wave impedances. Note that in the X', Y' coordinates the wave impedances of the T fields are again η_o.

Note that for most shields $\eta_o >> \eta$; $\cos\theta_2 \simeq 1$ even for $\theta_1 = \frac{\pi}{2}$ so that

$$1 \pm \frac{\eta_o\cos\theta_2}{\eta\cos\theta_1} \simeq \pm\frac{\eta_o}{\eta\cos\theta_1}, \qquad 1+\frac{\eta\cos\theta_1}{\eta_o\cos\theta_2} \simeq 1$$

$$1 \pm \frac{\eta_o\cos\theta_1}{\eta\cos\theta_2} \simeq \pm\frac{\eta_o\cos\theta_1}{\eta}^{*}, \qquad 1+\frac{\eta\cos\theta_2}{\eta_o\cos\theta_1}^{*} \simeq 1$$

*except for $\theta_1 \to \frac{\pi}{2}$

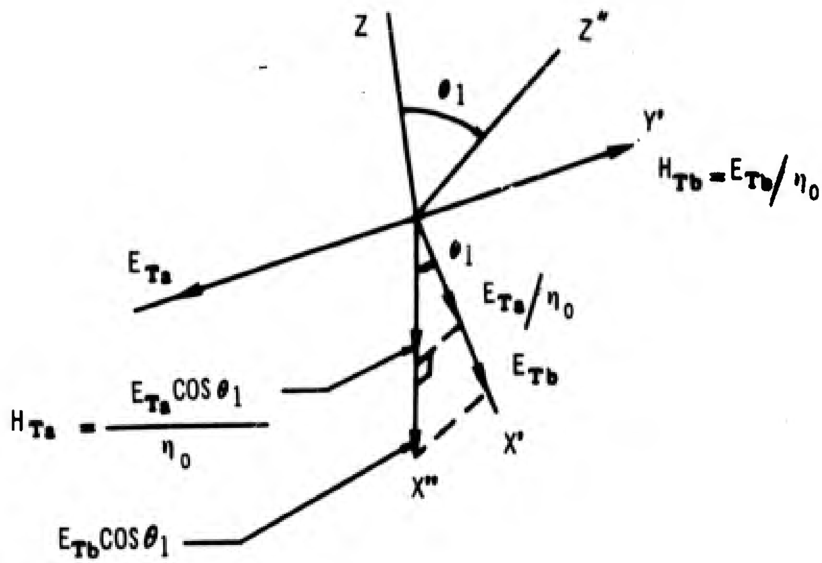

Fig. 6 Traveling Wave Emergence from a Plane

As in refraction,

$$\frac{\sin\theta_1}{\sin\theta_2} = \frac{\text{VELOCITY OF TRAVELING WAVE IN SHIELD}}{\text{VELOCITY OF TRAVELING WAVE IN AIR}} \tag{42}$$

Consideration of propagation in the $-X'$ direction is not necessary to solve the shielding problem and since energy flow is primarily normal to the shield, it is this flow that is considered.

5.1.7 Reflection Loss The term $\frac{(k+1)^2}{4k}$ can be attributed to the reflection that would occur if ℓ were infinite under conditions of equation (36) applied to equations (34) and(35). The reflection loss for R then becomes

$$R = 20\ \log_{10} \frac{|1+k|^2}{4\,|k|}\,. \quad \text{(db)} \tag{43}$$

When k is either small or large:

$$R \cong 20\ \log_{10} \frac{1}{4\,|k|}\ \text{ for }\ |k| = \left|\frac{Z_w}{\eta_w}\right| \ll 1,$$

$$R \cong 20\ \log_{10} \frac{|k|}{4}\ \text{ for }\ |k| = \left|\frac{Z_w}{\eta_w}\right| \gg 1. \tag{44}$$

For the shield material at normal incidence $\eta_W = \eta$ and from (1) $\eta = (1+j)\frac{|\eta|}{\sqrt{2}}$. Three important cases for the impedance ratio k and the reflection loss R can be considered as a result of low-impedance, free-space impedance, and high-impedance wave cases (see 5.1.4) at normal incidence. For a low-impedance wave, from equation (61)

$$Z_w \simeq j|Z_w| \quad \text{(ohms)} \tag{45}$$

so that

$$k = \frac{j|Z_w|}{(1+j)\frac{|\eta|}{\sqrt{2}}} = (1+j)\frac{|k|}{\sqrt{2}} . \tag{46}$$

Then the reflection loss R may be written from equation (43)

$$R = 20 \log_{10} \frac{\left|1+(1+j)\frac{|k|}{\sqrt{2}}\right|^2}{4|k|} = 20 \log_{10} \frac{1+\sqrt{2}|k|+|k|^2}{4|k|} . \quad \text{(db)} \tag{47}$$

For a free-space impedance,

$$Z_w = |Z_w| \text{(ohms)} \tag{48}$$

$$k = \frac{|Z_w|}{(1+j)\frac{|\eta|}{\sqrt{2}}} = (1-j)\frac{|k|}{\sqrt{2}} . \tag{49}$$

In this case,

$$R = 20 \log \frac{\left|1+(1-j)\frac{|k|}{\sqrt{2}}\right|^2}{4|k|} = 20 \log \frac{1+\sqrt{2}|k|+|k|^2}{4|k|} \tag{50}$$

as before.

For a high-impedance wave, from equation (55)

$$Z_w \simeq -j|Z_w| \text{ (ohms)} \tag{51}$$

$$k = \frac{-j|Z_w|}{(1+j)\frac{|\eta|}{\sqrt{2}}} = -(1+j)\frac{|k|}{\sqrt{2}} \tag{52}$$

and

$$R = 20 \log \frac{\left|1 - (1+j)\frac{|k|}{\sqrt{2}}\right|^2}{4|k|} = 20 \log \frac{1 - \sqrt{2}|k| + |k|^2}{4|k|}, \text{ (db)}$$

$$= 20 \log \frac{1}{4}\left[\frac{1}{|k|} - \sqrt{2} + |k|\right] \tag{53}$$

which is different from the other two cases where $R = 20 \log 1/4\left[\frac{1}{|k|} + \sqrt{2} + |k|\right]$

It will be necessary throughout this study for reflection loss calculations to utilize equations (47), (50) and (53). Special-case dipole formulas for reflection loss given in Pars. 5.1.8 through 5.1.10 cannot be directly applied even though they are commonly used (or mis-used).

5.1.8 Reflection Loss of Dipole High-Impedance Wave A high-impedance wave is obtained in the near field of an electric dipole (Ref. 1). Under normal incidence, where E_i and H_i are the components of the incident wave,

$$Z_w = \frac{E_i}{H_i} = \eta_o \frac{1 + \frac{1}{j\beta_o r} - \frac{1}{\beta_o^2 r^2}}{1 + \frac{1}{j\beta_o r}}, \text{ (ohms)} \tag{54}$$

where r is the distance from dipole source to shield in meters and $\eta_o = 120\pi$ ohms, the impedance of a free-space wave. In the near field where $\beta_o r \ll 1$,

$$Z_w \simeq \frac{\eta_o}{j\beta_o r}, \tag{55}$$

and using (1), (11), (12)

$$k = k_E = \frac{\eta_o}{\eta}\frac{1}{j\beta_o r} = -\frac{1+j}{\sqrt{2}}\frac{1}{\omega\epsilon_o r}\sqrt{\frac{\sigma}{\omega\mu}}. \tag{56}$$

Even at high frequencies, $|k| \gg 1$ and from (44)

$$R = R_E = \frac{|k_E|}{4} = 20 \log_{10} \frac{\sqrt{\frac{\sigma}{\omega\mu}}}{4\omega\epsilon_o r} \tag{57}$$

5.1.9 Reflection Loss of a Plane Wave. For a plane wave, under normal incidence,

$$Z_w = \eta_o = \sqrt{\frac{\mu_o}{\epsilon_o}} = 377 \text{ ohms}$$

and using (1), (11), (12)

$$k = k_\infty = \frac{\eta_o}{\eta} = \left[\frac{1}{1+j}\right]\sqrt{\frac{2\sigma\mu_o}{\varepsilon_o\omega\mu}}\ , \tag{58}$$

which is much greater than unity for the intrinsic impedance, η , of any metal. Thus from equation (44)

$$R = R_\infty \simeq 20\log_{10}\frac{1}{4}\sqrt{\frac{\sigma\mu_o}{\varepsilon_o\omega\mu}}\ , \tag{59}$$

5.1.10 Reflection Loss of a Dipole Low-Impedance Wave. A low-impedance wave may be obtained in the near field of a magnetic dipole. The wave impedance is

$$Z_w = \frac{E_t}{H_t} = \eta_o \frac{1+\dfrac{1}{j\beta_o r}}{1+\dfrac{1}{j\beta_o r}-\dfrac{1}{\beta_o^2 r^2}} \quad \text{(ohms)} \tag{60}$$

for normal incidence and, in the near field where $\beta_o r \ll 1$,

$$Z_w = j\eta_o\beta_o r \tag{61}$$

For this case, using (1), (11), (12)

$$k = k_H = \frac{\eta_o}{\eta}\cdot j\beta_o r = \frac{1+j}{\sqrt{2}}\ \mu_o r\sqrt{\frac{\sigma\omega}{\mu}} \tag{62}$$

and, at low frequencies, $|k|$ may be either greater than, equal to, or less than one. Hence, from equation (47)

$$R = R_H = 20\log_{10}\frac{1}{4}\left[\frac{1}{\mu_o r}\sqrt{\frac{\mu}{\omega\sigma}} + \sqrt{2} + \mu_o r\sqrt{\frac{\omega\sigma}{\mu}}\right] \tag{63}$$

5.1.11 Difference in Reflection Losses of Dipole High-Impedance and Low Impedance Waves. It is readily shown that it is much more difficult to shield against low-impedance waves than to shield against high-impedance waves at low frequencies. The difference of expressions (57) and (63) is $\Delta R = R_E - R_H$.

Note that

$$|k_E| \simeq |k_\infty| / \beta_o r, \qquad |k_H| \simeq |k_\infty| \beta_o r \tag{64}$$

and

$$\Delta R=20 \log_{10}\left[\frac{1}{|k_E||k_H|}+\frac{\sqrt{2}}{|k_E|}+\left|\frac{k_H}{k_E}\right|\right]$$

$$=20 \log_{10}\left[\frac{1}{|k_\infty|^2}+\frac{\sqrt{2}\,\beta_0 r}{|k_\infty|}+(\beta_0 r)^2\right] \tag{65}$$

Since

$$|k_\infty|\gg 1,$$

$$\beta_0 r\ll 1,$$

Then for all metals at low frequencies, ΔR is large and negative. Thus at low frequencies, only the low-impedance measurements have significance as a measure of shielding performance.

5.1.12 Shielding Effectiveness. By definition, the total shielding effectiveness is

$$S=A+R+B, \tag{66}$$

where

$$A=20 \log_{10} e^{\alpha \ell} \quad \text{(db)}$$

as in equation (8); and

$$R=20 \log_{10} \frac{|1+k|^2}{4|k|} \quad \text{(db)}$$

as in equation (43) (67)

and the remaining term under the conditions of equation (43)

$$B=20 \log_{10}\left|1-\frac{(k-1)^2}{(k+1)^2}\, e^{-2\gamma\ell}\right| \quad \text{(db)}$$

results from successive re-reflections within the shield. Expression (66) is the complete formula for shielding effectiveness of a single shield, and is the basic starting point for the material presented in Reference 2.

5.1.13 Re-Reflection Term B. For a metallic sheet, Paragraph 5.1.1 provides a formula for the propagation constant,

$$\gamma=\alpha+j\beta=(1+j)\alpha. \text{ (For all metals, } \alpha=\beta)$$

$$e^{-2\gamma\ell}=e^{-(1+j)2\alpha\ell}=e^{-2\alpha\ell}(\cos 2\alpha\ell-j\sin 2\alpha\ell) \tag{68}$$

Since

$$A = 20 \log_{10} e^{\alpha \ell} = 8.686 \, \alpha \ell \text{ db},$$

$$2\alpha \ell = .23A$$

$$e^{\alpha \ell} = 10^{\frac{A}{20}} \tag{69}$$

Then (70)

$$e^{-2\gamma \ell} = 10^{-0.1A}(\cos 0.23A - j \sin 0.23A). \text{ (A in db)}$$

If we put

$$\chi = \frac{(k-1)^2}{(k+1)^2} = \chi_{Re} + j\chi_{Im}, \tag{71}$$

then

$$B = 20 \log \left| 1 - \chi \cdot 10^{-0.1A}(\cos 0.23\,A - j \sin 0.23A) \right|. \text{ (db)} \tag{72}$$

For

$$|k| < 0.1 \text{ or } |k| > 10, \; \chi \cong 1 + j\,0$$

and

$$B = 10 \log \left[1 - 2 \times 10^{-0.1A} \cos 0.23A + 10^{-0.2A} \right]. \text{ (db)} \tag{73}$$

5.2 Other Concepts

The theory of shielding thus far developed may be called the transmission theory of shielding since attention has been focused on waves passing through the shield. A different physical picture of shielding is possible. The fields are produced by electric currents, the original field by currents in the generating source antenna and a secondary field by currents induced in the shield. The latter group of currents flow in directions such that their fields oppose and tend to cancel the original field on the side of the shield opposite from the source.

The principal weakness in application of this latter theory from the engineering viewpoint is that it is difficult to compute the induced currents without first solving the shielding problem itself. In order to find the induced currents, the tangential magnetic field strength must be calculated at both surfaces of the shield; but the shielding effectiveness is then determined. On the other hand, this theory presents a physical picture from which it can be readily concluded that a greater impairment in shielding will occur if the shield contains a seam or cut so as to interfere with the induced current flow than if it is cut along lines of flow. For example, if a plane wave is incident upon a perfectly conducting shield with an infinitely long slit, more power will be transmitted when the E vector is perpendicular to the slit than when it is parallel to it. The two physical analogues of shielding are complementary.

5.2.1 Transfer Impedance Analogy In the previous theoretical development, shielding effectiveness has been derived on the basis of incident-to-transmitted ratios of the E field or of the H field, the resulting expression (66) being the same for either case. (This result must be expected since the impedance of the transmitted wave is identical to the impedance of the incident wave.) The question arises whether a ratio of E_T to H_i or H_T to E_i might be a more sensitive indicator of shielding performance. To determine the answer, let the analogous transfer (mutual) impedance and admittance be

$$Z_{Ti} = \frac{E_T}{H_i}, \quad Y_{Ti} = \frac{H_T}{E_i}. \tag{74}$$

or

$$Z_{Ti} = \frac{E_T}{E_i}\frac{E_i}{H_i} = \frac{E_T}{E_i} Z_w \tag{75}$$

and

$$Y_{Ti} = \frac{H_T}{E_T}\frac{E_T}{E_i} = \frac{E_T}{E_i} \Big/ Z_w$$

Since the wave impedance Z_w is not dependent upon shielding properties, any sensitivity of indication resides in the E_T/E_i transmission ratio and is identical to the complete expression for shielding effectiveness already derived. There is no theoretical advantage in the crossed-field measurement of shielding performance. From the experimental viewpoint, there may be serious disadvantage since poorer signal-to-noise ratios should be expected in the E field measurement of a low-impedance wave or the H field measurement of a high-impedance wave.

5.3 Multi-Media Shielding Theory

To develop the theory for any number of multiple sheets or laminations of a single sheet, illustrated by Figs. 7, 8, 9, the approach beginning with equations (28) may be extended. Consider first only two sheets separated by an air gap, e.g., a double shield as in Fig. 9. Then the transmission coefficient is

$$T = \frac{E_{T3}}{E_i} = \frac{E_{T3}}{E_{T2}}\frac{E_{T2}}{E_{T1}}\frac{E_{T1}}{E_i} \tag{76}$$

where the subscripts 1, 2, and 3 refer successively to the first sheet, the air gap, and the second sheet. It is easy to write a general fomula for any number n of sheets (both metals and air gaps as in Fig. 7). Let the constants of a typical sheet be η_m, γ_m, ℓ_m, with parameters p and q. The general transmission coefficient is from Fig. 7 and equation (34),

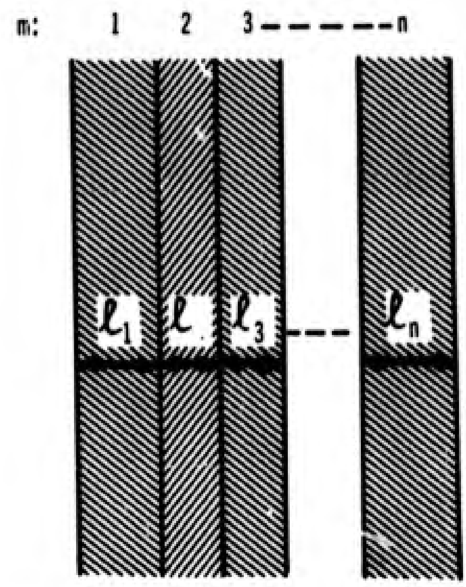

Fig. 7 Multi-Lamina Shielding

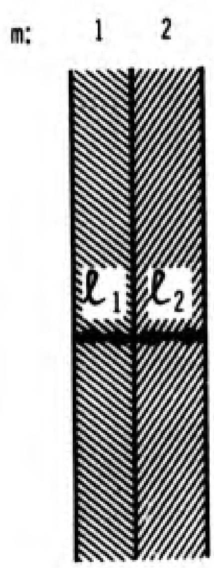

Fig. 8 Laminated Shield

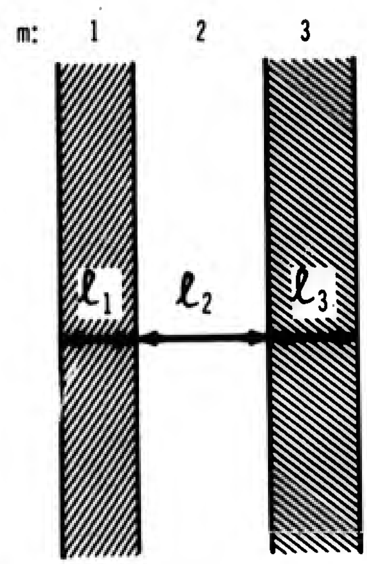

Fig. 9 Double Shield

$$T = p\left[\left(1-q_1 e^{-2\gamma_1\ell_1}\right)\left(1-q_2 e^{-2\gamma_2\ell_2}\right)\cdots\left(1-q_n e^{-2\gamma_n\ell_n}\right)\right]^{-1} \tag{77}$$
$$\times e^{-\gamma_1\ell_1-\gamma_2\ell_2-\cdots-\gamma_n\ell_n},$$

For the first shield (see Fig. 10a),

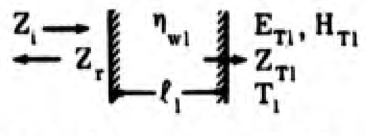

Fig. 10a Multi-Media Shielding: 1st Shield

equation (34) becomes

$$\frac{E_i}{E_{T1}} = \frac{1}{2\left[1+\frac{Z_r}{Z_i}\right]}\,\frac{(Z_r+\eta_{w1})(Z_{T1}+\eta_{w1})e^{\gamma\ell_1}}{\eta_{w1}\,Z_{T1}}\left[1-\frac{(\eta_{w1}-Z_r)(\eta_{w1}-Z_{T1})e^{-2\gamma\ell_1}}{(\eta_{w1}+Z_r)(\eta_{w1}+Z_{T1})}\right] \tag{78}$$

With shield #m (see Fig. 10b),

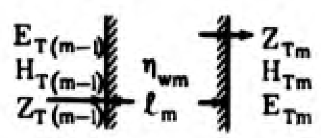

Fig. 10b Multi-Media Shielding: mth Shield

equation (28) becomes

$$E_{T(m-1)} = E_{Tm}\cosh\gamma\ell_m + \eta_{wm}\,H_{Tm}\,\sinh\gamma\ell_m$$

$$\frac{E_{T(m-1)}}{E_{Tm}} = \cosh\gamma\ell_m + \frac{\eta_{wm}}{Z_{Tm}}\,\sinh\gamma\ell_m$$

$$= \frac{1}{2}\left(\frac{Z_{Tm}+\eta_{wm}}{Z_{Tm}}\right)e^{\gamma\ell_m}\left[1-\frac{(\eta_{wm}-Z_{Tm})}{(\eta_{wm}+Z_{Tm})}e^{-2\gamma\ell_m}\right] \tag{79}$$

For the (last) shield, #n, (see Fig. 10c)

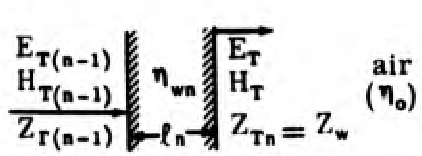

Fig. 10c Multi-Media Shielding: Last (nth) Shield

$$\frac{E_{T(n-1)}}{E_T} = \frac{1}{2}\left(\frac{Z_w+\eta_{wn}}{Z_w}\right)e^{\gamma\ell_n}\left[1-\frac{(\eta_{wn}-Z_w)}{(\eta_{wn}+Z_w)}e^{-\gamma\ell_n}\right] \quad (80)$$

Then

$$p=2^n\left(1+\frac{Z_r}{Z_i}\right)\left(\frac{\eta_{wi}}{Z_r+\eta_{wi}}\right)\prod_{m=1}^{m=n}\left[\frac{Z_{Tm}}{Z_{Tm}+\eta_{wm}}\right] \quad (81)$$

where

$$Z_{Tn} = Z_w \text{ and usually } Z_i = Z_r = Z_w$$

From equation (78),

$$q_1 = \frac{(\eta_{wi}-Z_r)\,(\eta_{wi}-Z_{Ti})}{(\eta_{wi}+Z_r)\,(\eta_{wi}+Z_{Ti})}\,. \quad (82)$$

From equation (79),

$$\underset{m\neq 1}{q_m} = \frac{(\eta_{wm}-Z_{Tm})}{(Z_{Tm}+\eta_{wm})}\,. \quad (83)$$

From equation (80),

$$q_n = \frac{(\eta_{wm}-Z_w)}{(Z_w+\eta_{wn})}\,. \quad (84)$$

where

$$Z_{Tn}=Z_W\,.$$

Also,

$$Z_{T(m-1)}=\frac{E_{shm}}{H_{shm}}=\frac{Z_{Tm}\cosh\gamma\ell_m+\eta_{wm}\sinh\gamma\ell_m}{\cosh\gamma\ell_m+\frac{Z_{Tm}}{\eta_{wm}}\sinh\gamma\ell_m}\,. \quad (85)$$

If each lamination is thick enough and $Z_r=Z_i=Z_{Tn}=Z_w$,

$$p=2^{n+1}\left(\frac{\eta_{wi}}{Z_w+\eta_{wi}}\right)\left(\frac{Z_w}{\eta_{wn}+Z_w}\right)\prod_{m=1}^{m=n-1}\left(\frac{\eta_{w(m+1)}}{\eta_{wm}+\eta_{w(m+1)}}\right), \quad (86)$$

$$\underset{\substack{m\neq 1\\ m\neq n}}{q_m}=\frac{\eta_{wm}-\eta_{w(m+1)}}{\eta_{w(m+1)}+\eta_{wm}},\quad q_n=\frac{\eta_{wn}-Z_w}{\eta_{wn}+Z_w}\,, \quad (87)$$

and

$$q_1=\left(\frac{\eta_{wi}-Z_w}{\eta_{wi}+Z_w}\right)\left(\frac{\eta_{wi}-\eta_{w2}}{\eta_{wi}+\eta_{w2}}\right). \quad (88)$$

5.4 Laminated Shielding

For a laminated sheet of two different materials as in Fig. 8, n = 2 and the penetration loss of the laminated sheet is simply the sum of those for the two lamina,

$$A_{\ell 2} = 20 \log_{10} \left| e^{\gamma_1 \ell_1 + \gamma_2 \ell_2} \right| = 8.686 \; (\alpha_1 \ell_1 + \alpha_2 \ell_2). \text{ (db)} \tag{89}$$

The corresponding reflection loss is (for thick laminations)

$$R_{\ell 2} = -20 \log_{10} |p| = 20 \log_{10} \left[\frac{1}{8} \left(1 + \frac{\eta_{w1}}{Z_w}\right) \left(1 + \frac{\eta_{w2}}{\eta_{w1}}\right) \left(1 + \frac{Z_w}{\eta_{w2}}\right) \right]$$

$$= 20 \log_{10} \frac{1 + \frac{\eta_{w1}}{Z_w}}{2} + 20 \log_{10} \frac{1 + \frac{\eta_{w2}}{\eta_{w1}}}{2} + 20 \log_{10} \frac{1 + \frac{Z_w}{\eta_{w2}}}{2}, \text{ (db)} \tag{90}$$

or the sum of the reflection losses at each interface. It should be noted that η_{w1} and η_{w2} both vary as $\sqrt{f}$; hence, reflection loss at the metal-to-metal interface is independent of frequency, whereas it is a function of frequency for metal-air interfaces. This property is particularly important in low-frequency shielding.

The correction term due to successive re-reflections is

$$B_{\ell 2} = 20 \log_{10} \left| \left(1 - q_1 e^{-2\gamma_1 \ell_1}\right) \left(1 - q_2 e^{-2\gamma_2 \ell_2}\right) \right|$$

$$= 20 \log_{10} \left| \left(1 - q_1 e^{-2\gamma_1 \ell_1}\right) \right| + 20 \log_{10} \left| \left(1 - q_2 e^{-2\gamma_2 \ell_2}\right) \right|, \text{ (db)} \tag{91}$$

which is not simply the sum of correction factors for the individual lamina (unless the laminations are very thick) since q_1 involves the impedance looking into the second sheet.

5.5 Double Shielding

Of considerable importance is the case of two shielding sheets separated by an air space (Fig. 9): $n=3$, $\eta_{w2} = Z_w$, $\alpha_2 = 0$, $\gamma_2 = j\beta_o = j2\pi/\lambda_o$. and $Z_r = Z_1 = Z_w$. Then,

$$p = 16 \left(\frac{\eta_{w1}}{Z_w + \eta_{w1}}\right) \left(\frac{Z_{T1}}{Z_{T1} + \eta_{w1}}\right) \left(\frac{Z_{T2}}{Z_{T2} + Z_w}\right) \left(\frac{Z_w}{Z_w + \eta_{w3}}\right). \tag{92}$$

Even if the air gap is thick, $Z_{T1} \neq Z_w$ because there is no attenuation. If the shields are thick,

$$p = 16\left(\frac{\eta_{w1}}{Z_w + \eta_{w1}}\right)\left(\frac{Z_{T1}}{Z_{T1} + \eta_{w1}}\right)\left(\frac{\eta_{w3}}{\eta_{w3} + Z_w}\right)\left(\frac{Z_w}{\eta_{w3} + Z_w}\right). \tag{93}$$

If $\eta_{w3} = \eta_{w1} = \eta_w$,

$$p = 16\left(\frac{\eta_w}{Z_w + \eta_w}\right)^2\left(\frac{Z_{T1}}{Z_{T1} + \eta_w}\right)\left(\frac{Z_w}{Z_w + \eta_w}\right). \tag{94}$$

The transmission coefficient for this case is

$$T_{m2} = p\left[\left(1 - q_1 e^{-2\gamma_1 \ell_1}\right)\left(1 - q_2 e^{-j2\beta_0 \ell_2}\right)\left(1 - q_3 e^{-2\gamma_3 \ell_3}\right)\right]^{-1} \cdot \exp\left(-\gamma_1 \ell_1 - j\beta_0 \ell_2 - \gamma_3 \ell_3\right), \tag{95}$$

where the subscript m2 denotes multiplicity of 2. Components of the shielding expression become, for the conditions of equation (92),

$$A_{m2} = 8.686\,(\alpha_1 \ell_1 + \alpha_3 \ell_3),$$

$$R_{m2} = 20 \log_{10} \frac{\left|1 + \frac{Z_w}{\eta_{w1}}\right|}{2} + 20 \log_{10} \frac{\left|1 + \frac{\eta_{w1}}{Z_{T1}}\right|}{2} + 20 \log_{10} \frac{\left|1 + \frac{Z_w}{Z_{T2}}\right|}{2} + 20 \log_{10} \frac{\left|1 + \frac{\eta_{w3}}{Z_w}\right|}{2} \quad \text{(db)} \tag{96}$$

$$B_{m2} = 20 \log_{10}\left|1 - q_1 e^{-2\gamma_1 \ell_1}\right| + 20 \log_{10}\left|1 - q_2 e^{-j2\beta_0 \ell_2}\right| + 20 \log_{10}\left|1 - q_3 e^{-2\gamma_3 \ell_3}\right|. \quad \text{(db)}$$

It should be noted that $\beta_0 \ell_2$ is a phase term while $\gamma_1 \ell_1$ and $\gamma_3 \ell_3$ are loss terms, hence, the middle term of B_{m2} may be significant when the other two are negligible.

For the special case where both metallic sheets are of the same material and thickness, $\gamma_1\ell_1 = \gamma_3\ell_3 = \gamma\ell$ and for thick sheets,

$$A_{m2} = 2 \times 8.686\alpha\ell \quad \text{(db)}$$

$$R_{m2} = 20\log_{10}\frac{\left|1+\frac{\eta}{Z_w}\right|}{2} + 20\log_{10}\frac{\left|1+\frac{\eta}{Z_{T1}}\right|}{2} + 40\log_{10}\frac{\left|1+\frac{Z_w}{\eta}\right|}{2}$$

$$B_{m2} = 20\log_{10}\left|1-q_1e^{-2\gamma\ell}\right| + 20\log_{10}\left|1-q_2e^{-j2\beta_0\ell_2}\right|$$

$$+ 20\log_{10}\left|1-q_3e^{-2\gamma\ell}\right| \quad \text{(db)} \qquad (97)$$

The penetration loss is double that of a single sheet. The middle term of B_{m2} may be rewritten as:

$$20\log_{10}\left|1-q_2\left(\cos 4\pi\frac{\ell_2}{\lambda_0} - j\sin 4\pi\frac{\ell_2}{\lambda_0}\right)\right| \quad \text{(db)} \qquad (98)$$

5.5.1 **Electrically-Thick Materials.** ($\eta_{w1} = \eta_{w3} = \eta_w$) For the common case of metals sufficiently thick that re-reflections within the metal may be neglected due to their high penetration loss, $Z_{T2} \simeq \eta_{w3}$; and from equation (83)

$$q_2 = \frac{Z_w - \eta_{w3}}{Z_w + \eta_{w3}} = \frac{1-\frac{\eta_w}{Z_w}}{1+\frac{\eta_w}{Z_w}} \qquad (99)$$

Normally, $\eta_w \ll Z_w$, and $\eta_w \ll Z_{T1}$, $R_{m2} \simeq -40\log_{10}\left|4\frac{\eta_w}{Z_w}\right|$, and

$$q_2 \simeq 1-4\frac{\eta_w}{Z_w} \qquad (100)$$

The middle term of B_{m2} becomes the entire expression

$$B_{m2} \simeq 20\log_{10}\left|1-\left(1-4\frac{\eta_w}{Z_w}\right)\left(\cos 4\pi\frac{\ell_2}{\lambda_0} - j\sin 4\pi\frac{\ell_2}{\lambda_0}\right)\right| \quad \text{(db)} \qquad (101)$$

For much of the frequency range where $\frac{\ell_2}{\lambda_0} \ll \frac{1}{8}$ (also see Par. 8.2),

$$B_{m2} \simeq 20\log_{10}\left|4\frac{\eta}{Z_w} + j4\pi\frac{\ell_2}{\lambda_0}\right| \quad \text{(db)} \qquad (102)$$

Since $\left| 4\frac{\eta}{Z_w} + j4\pi\frac{\ell_2}{\lambda_0} \right|$ is much less than one, B_{m2} is negative over a considerable portion of the frequency spectrum.

For example, consider a double copper shield with an air spacing of 1 inch (= 2.54 cm), a free-space wave of normal incidence with a wave impedance Z_w of η_0 at a frequency of 1 mc. From Par. 5.1.2),

$$4\frac{\eta}{Z_w} = 4\frac{(1+j)\ 2.61\times 10^{-7}\sqrt{10^6}}{377} = (1+j)\,2.77\times 10^{-6}\ ,$$

$$4\pi\frac{\ell_2}{\lambda_0} = 4\pi\ \frac{2.54\times 10^{-2}}{300} = 1.06\times 10^{-3}\ ,$$

$$B_{m2} \simeq 20\ \log_{10}\left|\ 2.77\times 10^{-6} + j(2.77\times 10^{-6} + 1.06\times 10^{-3})\right|$$

$$\simeq 20\ \log_{10}\left|\ 1.06\times 10^{-3}\right| \simeq -60\,\text{db}. \tag{103}$$

This result need not always be the case. For instance, at frequencies high enough such that

$$\ell_2 = (2k-1)\frac{\lambda_0}{4}, \qquad k = 1,2,3,\cdots,$$

$$B_{m2} = 20\ \log_{10}\left|\ 1 + q_2\right| \simeq 20\ \log_{10} 2 = 6\,\text{db}. \tag{104}$$

At shielding resonances, the B_{m2} of the double shield can be as much as 6 db better or at 1 mc 60 db worse than with an air gap; however, R_{m2} must also be considered.

5.5.2 Comparison of Double and Single Shields Let us compare the double shield with a single shield of the same total metal thickness. For a single shield, A is the same, the middle term of B disappears. By expressing R as $R = 20\ \log_{10}\left|\frac{1}{p}\right|$, the difference in shielding effectiveness Δ may be written

$$\Delta = S_{double} - S_{single} = 20\ \log_{10}\left|\frac{\text{p without gap}}{\text{p with gap}}\right|$$

$$+ 20\ \log_{10}\left|\frac{\text{re-reflection with gap}}{\text{re-reflection without gap}}\right| \tag{105}$$

For sufficiently thick laminations and a sufficient air gap, the additional factors in equation (81) with the air gaps are

$$\frac{2\,\eta_{w1}}{(\eta_{w1}+\eta_{w3})} \quad \text{(deletion of term for no gap)} \tag{106a}$$

$$\frac{Z_{T1}}{Z_{T1}+\eta_{W1}} \simeq 1 \quad \text{Since } Z_{T1} \gg \eta_{W}, \quad (\text{Par. } 8.2), \tag{106b}$$

$$\frac{Z_{T2}}{Z_w + Z_{T2}} = \frac{\eta_{W3}}{Z_W + \eta_{W3}} \sim \frac{\eta_{W3}}{Z_W},$$

and $2^2 = 4.$

So that, as in Par. 5.5.1

$$\left|\frac{\text{p with gap}}{\text{p without gap}}\right| = 4\left|\frac{\eta_{W3}}{Z_W}\right| = 27.7 \times 10^{-7}\sqrt{\frac{f}{mc}}$$

$$20 \log_{10}\left|\frac{\text{p without gap}}{\text{p with gap}}\right| \quad 111.2 \text{ db} - 10 \log \frac{f}{mc} \tag{107}$$

for $Z_W = \eta_0$ and $\eta_{W1} = \eta_{W3} = \eta_W$.

Since for the same conditions and for $\ell_2 \ll \frac{\lambda_0}{8}$

$$\left|\frac{\text{re-reflection with gap}}{\text{re-reflection without gap} \simeq 1}\right| = \left|\frac{2\eta_w}{Z_w} + j\,\frac{4\pi\ell_2}{\lambda_0}\right| \tag{108}$$

Equation (23), where $\gamma\eta = j\omega\mu$, can be applied so that at normal incidence (Note: from equation (99), η_w is η_{w3})

$$\frac{2\eta_w}{Z_w}\left|1 + \frac{j2\pi\ell_2 Z_w}{\lambda_o \eta_w}\right| = \frac{2\eta_w}{Z_w}\left|1 + j\beta_0\ell_2(\eta_0)\left(\frac{1}{\eta_w}\right)\right|$$

where

$$\eta_o = \frac{j\omega\mu_o}{j\beta_o} \quad \text{and} \quad \frac{1}{\eta_w} = \frac{\gamma}{j\omega\mu}$$

Then from equation (105),

$$\Delta = 20 \log_{10} \frac{1}{2}\left|1 + \frac{\mu_0}{\mu}\gamma \ell_2\right| \tag{109}$$

At $\Delta \geq 0$:

$$\left|1 + \frac{\mu_0}{\mu}\gamma \ell_2\right| \geq 2 \tag{110}$$

Let

$$\frac{\mu_0}{\mu}\gamma \ell_2 = \frac{\mu_0}{\mu}(1+j)\beta \ell_2 = a$$

Then at $\Delta = 0$

$$\left|1+(1+j)a\right| = \sqrt{(1+a)^2 + a^2} = \sqrt{1+2a^2+2a} = 2$$

$$a = -\frac{1}{2} \pm \sqrt{7/4}, \qquad \text{or } a = 0.825$$

For copper where $\mu = \mu_0$, and for $\ell_2 = 2.54$ cm

$$\beta \ell_2 = .825 = \frac{\omega}{v}\ell_2 = \left[2.54 \times 10^{-2} \mathrm{m}(2\pi f)\right] \Big/ \left[.415 \frac{\mathrm{m}}{\mathrm{sec}} \sqrt{f/\mathrm{cps}}\right] \tag{111}$$

Then $\Delta \geq 0$ for

$$f \geq \left[(.825 \times .415 \times 10^2) / (2.54 \times 2\pi)\right]^2 = 4.7 \,\mathrm{cps} \tag{112}$$

A second assumption here is that the penetration loss is high enough to avoid re-reflections in the metal; therefore, for thinner shields, the lower frequency limit for validity of that assumption is set by

$$A \geq (8.686 \text{ db/neper})\, \alpha \ell \geq 15 \text{ db from equation (8)}$$

Since $\alpha = 15.1 \dfrac{\text{nepers}}{\text{m}} \sqrt{\dfrac{f}{\text{cps}} \mu_r \sigma_r}$ equation (18), for copper,

$$\sqrt{f} = \frac{15m\ \sqrt{cps}}{8.686 \times 15.1\ell} \simeq \frac{1\,\text{meter}\sqrt{cps}}{8.69\ell} \qquad (113)$$

With $\ell = 2.4 \times 10^{-2}$ inch $= 6.1 \times 10^{-4}$ meter, a commonly encountered thickness, the assumption is valid at frequencies above

$$f \simeq \frac{1}{(8.69 \times 6.1 \times 10^{-4})^2} = 3.6 \times 10^4 \text{ cps} \qquad (114)$$

For $f \geq 4.7$ cps, ℓ must be 6-2/3 inches of copper. Since the lower frequency limit is proportional to μ and the upper proportional to $1/\mu$, a μ_r of 75 would have made both frequencies 475 cps for $\ell = 24$ mils.

At 1 mc, from equations (103) and (108

$$\Delta = 111.2 \text{ db} - 60 \text{ db} = 51.2 \text{ db} \qquad (115)$$

6.0 FACTUAL DATA - NONUNIFORM SHIELDING THEORY

The viewpoint taken in this program is that any nonuniform shield may be treated as a uniform shield with one or more discontinuities or imperfections. That is, each imperfection is simply another path for the transmission of RF energy in parallel with energy transmitted through the uniform shield. With each such path is associated an effective shielding factor. These factors can be combined in various combinations to represent a variety of shielding arrangements.

Since total shielding effectiveness, S, may be expressed in terms of the shielding effectiveness due to each variable, the approach throughout this study program has been to perform laboratory measurements in such a manner that the effect of each variable may be readily isolated. With the resulting knowledge of each variable, it is possible to determine the shielding effectiveness of any combination of variables constituting a shielding situation. It was intended to isolate and measure the variable factors listed in Table A, which determine total measured effectiveness of shielding.

Table A Shielding Variables

Variables	Shielding Symbol	Remarks
Independent		
Frequency of incident field		f
Impedance of incident field		Z_w
Measurement technique employed		Consistent with theory
Dependent		
Shield material, including change due to:	S_1	Permeability; conductivity; thickness
No. of layers comprising shields	ΔS_m	Multiple shields
Laminated shields	ΔS_ℓ	Plated, clad metals
Material Configuration	S_2	Solid, perforated, etc.
Shape	S_3	Box, tube, etc.
Size	S_4	Enclosed volume
Fixed-seam joint construction	S_5	Soldered, brazed, etc.
Access-seam joint construction	S_6	Contact fingers, gaskets, etc.
Nonuniform shield construction	S_7	Combinations of materials
Metallic conductors projecting into a shielded region	S_8	Antenna effect
Electrical filters	S_9	Conductive coupling

6.1 Separation of Shielding Effectiveness Factors

The two conditions depicted in Figs. 11 and 12 show RF energy emanating from Point 1 and received at Point 2 with and without a shield discontinuity between the signal source and the receptor. Basically, the problem is one of determining the difference in transmission between the two points for a wide variety of "imperfections" in shielding configurations.

As an approach to the separation of variables let us consider, first, an ideal shield of uniform, continuous material (Fig. 11). Let the shielding effectiveness for this case equal S_1 (the material factor symbol), where:

$$S_1 = 20 \log_{10} \frac{|H_0|}{|H_1|} \quad \text{(db)} \tag{116}$$

$|H_0|$ is the absolute magnitude of the magnetic field without the shield, and $|H_1|$ is the absolute magnitude of the magnetic field beyond the interposed shield. It is readily apparent that the signal level at the receptor is produced solely by the phasor field H_1 ($= |H_1| e^{j\theta_1}$) ; therefore H_1 and H (the total field at the receptor) are one and the same tield. Consider next an identical situation, except that the shielding material is imperfect, having a discontinuity or defect such as a seam or hole (Fig. 12).

Some additional signal will be coupled to the receptor through this defect. Transmission through the defect may be considered to be in parallel with that transmitted through the original ideal shield. Let the additional field which results from the defect be designated as H_5 ($= |H_5| e^{j\theta_5}$) so that the total field at the receptor, H ($= |H| e^{j\theta}$) equals $H_1 + H_5$. The total shielding effectiveness, S, is now:

$$S = 20 \log_{10} \frac{|H_0|}{|H_1 + H_5|} \quad \text{(db)}$$

$$= 20 \log_{10} \frac{|H_0|}{\left| |H_1| e^{j\theta_1} + |H_5| e^{j\theta_5} \right|} \tag{117}$$

$$= 10 \log_{10} \frac{|H_0|^2}{(|H_1| \cos\theta_1 + |H_5| \cos\theta_5)^2 + (|H_1| \sin\theta_1 + |H_5| \sin\theta_5)^2}$$

$$= -10 \log_{10} \frac{|H_1|^2 + |H_5|^2 + 2|H_1||H_5| \cos(\theta_1 - \theta_5)}{|H_0|^2} \quad \text{(db)}$$

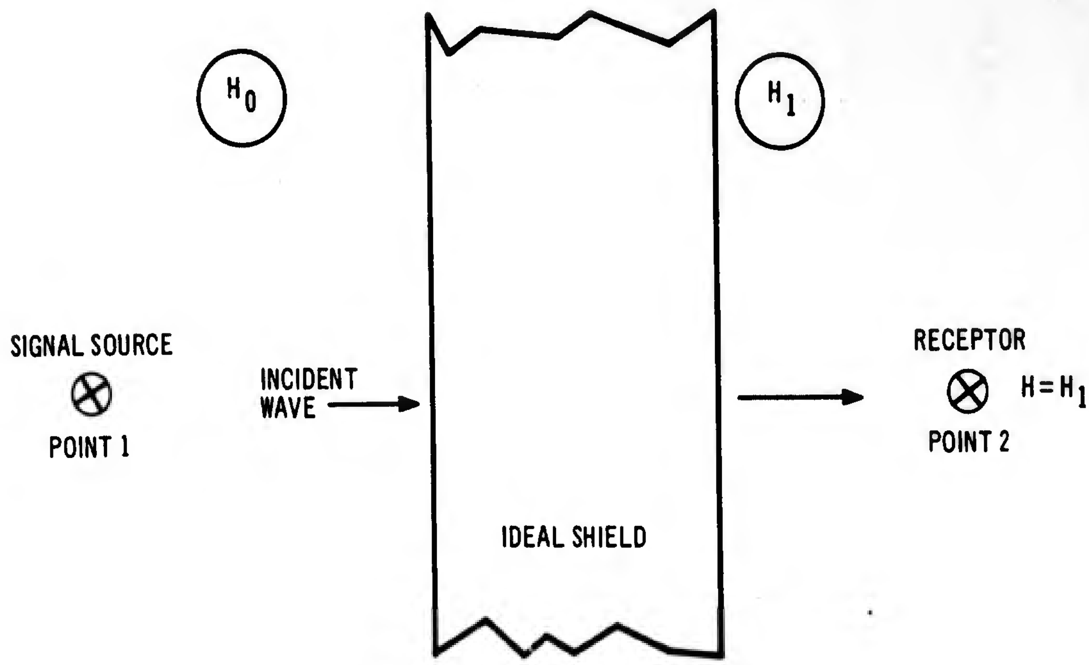

Fig. 11 Shielding Test Arrangement; Ideal Shield

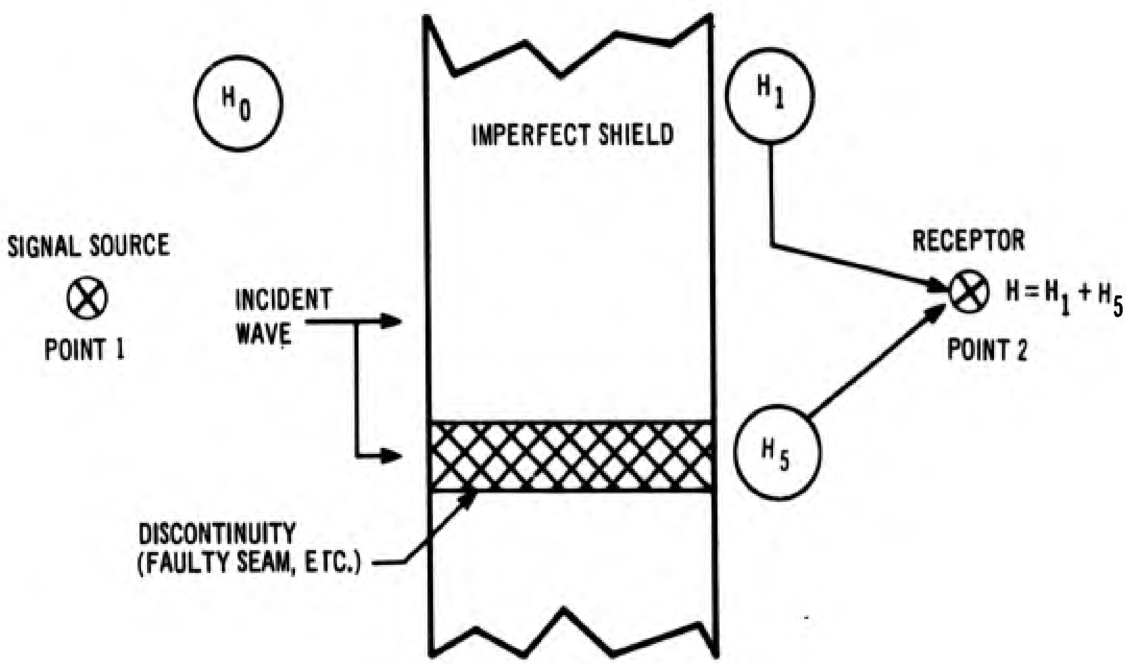

Fig. 12 Shielding Test Arrangement; Imperfect Shield

In general,

$$\frac{H_p}{H_0} = 10^{-\frac{S_p}{20}} \tag{118}$$

and, by writing ${}_1\theta_5 = \theta_1 - \theta_5$,

the total shielding effectiveness may be written

$$S = -10 \log_{10}\left[10^{-\frac{S_1}{10}} + 10^{-\frac{S_5}{10}} + (2)\, 10^{-\frac{S_1+S_5}{20}} \cos\ {}_1\theta_5\right] \text{ (db)} \tag{119}$$

The shielding effectiveness of the defect is S_5 where

$$S_5 = 20 \log_{10} \frac{|H_0|}{|H_5|} \text{ (db)} \tag{120}$$

Since

$$H_5 = H - H_1, \tag{121}$$

substitution in equation (120) yields

$$S_5 = 20 \log_{10} \frac{|H_0|}{|H - H_1|}$$

$$= -20 \log_{10} \frac{\left|\,|H|(\cos\theta + j \sin\theta) - |H_1|(\cos\theta_1 + j \sin\theta_1)\right|}{|H_0|}$$

$$= -10 \log_{10} \frac{\left(|H|\cos\theta - |H_1|\cos\theta_1\right)^2 + \left(|H|\sin\theta - |H_1|\sin\theta_1\right)^2}{|H_0|^2}$$

$$= -10 \log_{10} \frac{|H|^2 + |H_1|^2 - 2|H||H_1| \cos(\theta_1 - \theta)}{|H_0|^2} \text{ (db)} \tag{122}$$

Use equation (118) to obtain

$$S_5 = -10 \log_{10} \left[10^{-\frac{S}{10}} + 10^{-\frac{S_1}{10}} - 2 \cdot 10^{-\frac{S+S_1}{20}} \cos(\theta_1 - \theta) \right]. \quad \text{(db)} \tag{123}$$

An alternate useful expression may be obtained by expressing S_5 in terms of S, S_1, θ_1, θ_5 by first taking the antilogarithm of equation (119).

$$10^{-\frac{S}{10}} = 10^{-\frac{S_1}{10}} + 10^{-\frac{S_5}{10}} + 2 \times 10^{-\frac{S_1+S_5}{20}} \cos {}_1\theta_5 \tag{124}$$

Complete the square of the last 2 terms.

$$10^{-\frac{S}{10}} - 10^{-\frac{S_1}{10}} \sin^2 {}_1\theta_5 = \left[10^{-\frac{S_5}{20}} + 10^{-\frac{S_1}{20}} \cos {}_1\theta_5 \right]^2 \tag{125}$$

Take the square root.

$$10^{-\frac{S_5}{20}} + 10^{-\frac{S_1}{20}} \cos {}_1\theta_5 =$$

$$+\left[10^{-\frac{S}{10}} - 10^{-\frac{S_1}{10}} \sin^2 {}_1\theta_5 \right]^{\frac{1}{2}}, \quad \text{for } \left[10^{-\frac{S_5}{20}} + 10^{-\frac{S_1}{20}} \cos {}_1\theta_5 \right] \geq 0,$$

or (126)

$$-\left[10^{-\frac{S}{10}} - 10^{-\frac{S_1}{10}} \sin^2 {}_1\theta_5 \right]^{\frac{1}{2}}, \quad \text{for } \left[10^{-\frac{S_5}{20}} + 10^{-\frac{S_1}{20}} \cos {}_1\theta_5 \right] \leq 0,$$

A change in branches of the expression occurs at the changeover points:

$$10^{-\frac{S_5}{20}} = -10^{-\frac{S_1}{20}} \cos {}_1\theta_5$$

$$10^{-\frac{S}{10}} = 10^{-\frac{S_1}{10}} \sin^2 {}_1\theta_5 \tag{127}$$

or

$$10^{-\frac{S_5}{10}} = 10^{-\frac{S_1}{10}} - 10^{-\frac{S}{10}}, \tag{128}$$

$$10^{-\frac{S_5}{20}} = \pm\left[10^{-\frac{S}{10}} - 10^{-\frac{S_1}{10}} \sin^2 {}_1\theta_5\right]^{\frac{1}{2}} - 10^{-\frac{S_1}{20}} \cos {}_1\theta_5, \tag{129}$$

The logarithm of this expression yields

$$S_5 = -20 \log_{10}\left\{\pm\left[10^{-\frac{S}{10}} - 10^{-\frac{S_1}{10}} \sin^2 ({}_1\theta_5)\right]^{\frac{1}{2}} - 10^{-\frac{S_1}{10}} \cos ({}_1\theta_5)\right\}$$

$$= S_1 - 20 \log_{10}\left\{\pm\left[10^{\frac{S_1 - S}{10}} - \sin^2 ({}_1\theta_5)\right]^{\frac{1}{2}} - \cos ({}_1\theta_5)\right\}. \tag{130}$$

In the more general case, where there are n transmission paths or (n-1) defects with respect to a perfect shield, we have:

$$S = 20 \log_{10} \frac{|H_0|}{\left|\sum_{p=1}^{n} H_p\right|} \text{ (db)} \tag{131}$$

Since

$$H_p = |H_p| (\cos \theta_p + j \sin \theta_p) \tag{132}$$

where θ_p is the phase angle of H_p with respect to H_0.

$$S = -20 \log_{10} \frac{\left| \sum_{p=1}^{n} |H_p| (\cos\theta_p + \sin\theta_p) \right|}{|H_0|}$$

$$= -10 \log_{10} \frac{\left(\sum_{p=1}^{n} |H_p| (\cos\theta_p)\right)^2 + \left(\sum_{p=1}^{n} |H_p| \sin\theta_p\right)^2}{|H_0|^2}$$

$$= -10 \log_{10} \frac{\sum_{p=1}^{n} |H_p|^2 + 2 \sum_{p=1}^{n-1} \sum_{q=1}^{n-p} |H_p|\,|H_{p+q}| (\cos\theta_p \cos\theta_{(p+q)} + \sin\theta_p \sin\theta_{(p+q)})}{|H_0|^2}$$

$$= -10 \log_{10} \frac{\sum_{p=1}^{n} |H_p|^2 + 2 \sum_{p=1}^{n-1} \sum_{q=1}^{n-p} |H_p|\,|H_{p+q}| \cos(\theta_p - \theta_{(p+q)})}{|H_0|^2} \text{ (db)} \quad (133)$$

But $\frac{H_p}{H_0} = 10^{-\frac{S_p}{20}}$;

hence,

$$S = -10 \log_{10} \left\{ \sum_{p=1}^{n} 10^{-\frac{S_p}{10}} + 2 \sum_{p=1}^{n-1} \sum_{q=1}^{n-p} 10^{-\frac{S_p + S_{p+q}}{20}} \cos(\theta_p - \theta_{(p+q)}) \right\} \text{ (db)} \quad (134)$$

6.2 Magnetic Permeability at Extremely Low Frequencies

For magnetic materials, measurements show that overall shielding effectiveness S becomes asymptotic to some nonzero value as the frequency approaches zero. This situation is illustrated by Fig. A35 of Appendix A, which represents experimental data obtained on a shielding enclosure of high permeability material (box 53). The same statement is presumably true for S_1, and for S_5 also, if the leakage path is metallic.

6.3 Relationships for S Equal to S_1

The magnitude of the total magnetic field $|H|$ is

$$|H| = \left||H_1|e^{j\theta_1} + |H_5|e^{j\theta_5}\right| = \left|\left(|H_1|\cos\theta_1 + |H_5|\cos\theta_5\right)\right.$$

$$\left. + j\left(|H_1|\sin\theta_1 + |H_5|\sin\theta_5\right)\right| \cdot \text{(amp/meter)} \tag{135}$$

By squaring the equation,

$$|H|^2 = |H_1|^2 + |H_5|^2 + 2|H_1||H_5|(\cos\theta_1 \cos\theta_5 + \sin\theta_1 \sin\theta_5)$$

$$= |H_1|^2 + |H_5|^2 + 2|H_1||H_5|\cos{}_1\theta_5 \cdot \text{(amp/meter)}^2 \tag{136}$$

From Fig. 13 where the dashed curve S_1 intersects the solid curve S, the fields H and H_1 are equal in magnitude so that

$$0 = |H_5|^2 + 2|H_1||H_5|\cos{}_1\theta_5$$

and

$$\cos{}_1\theta_5 = -\frac{|H_5|}{2|H_1|} \cdot (\text{for } S = S_1,) \tag{137}$$

where from the minus sign ${}_1\theta_5$ must be in the second or third quadrants

or

$$H \approx H_1 \quad \text{because } H_5 \ll H_1 \tag{138}$$

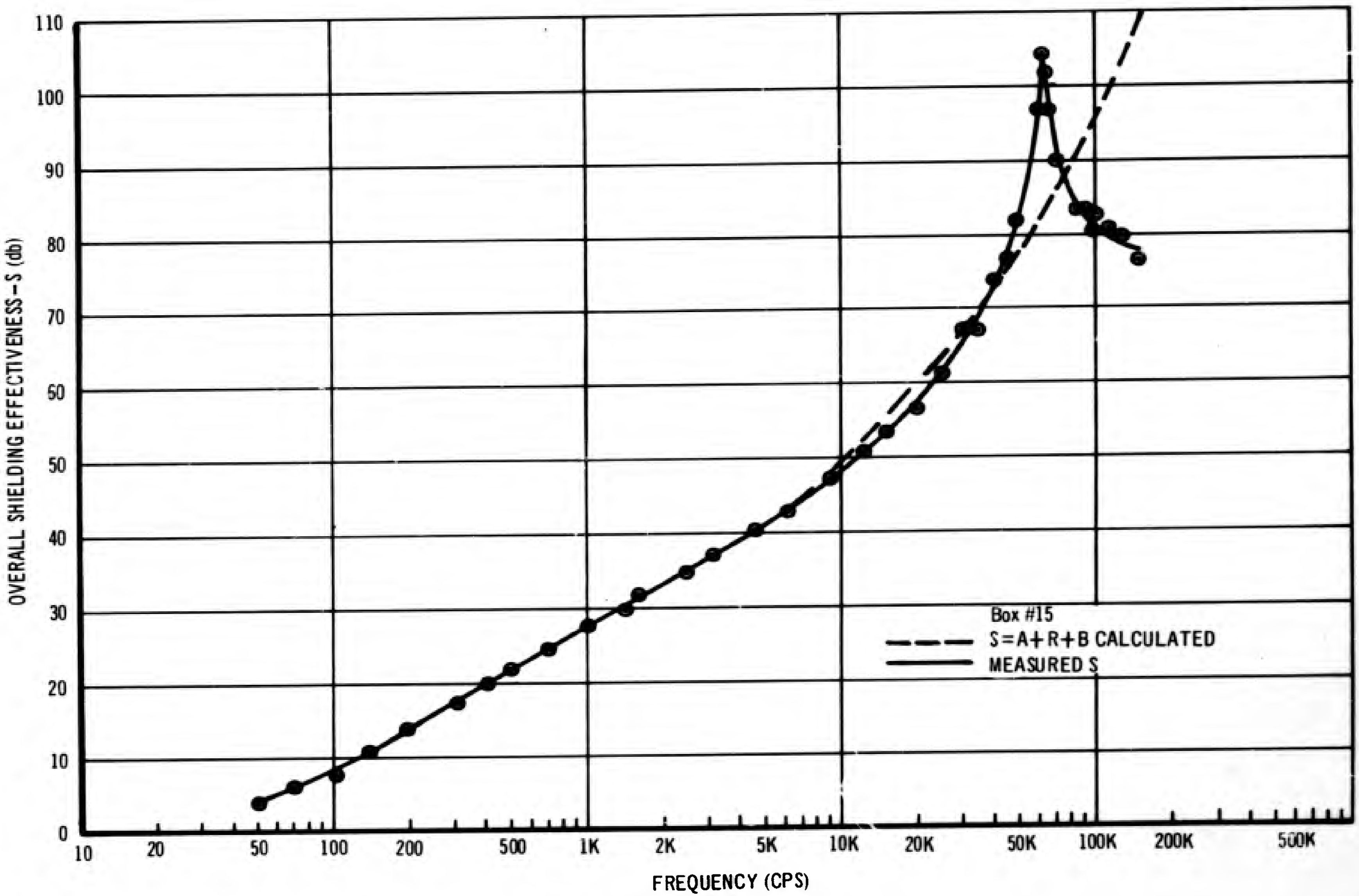

Fig. 13 Low Frequency Shielding Effectiveness – Copper, Box 15 with Soldered Lid

7.0 FACTUAL DATA - EXPERIMENTAL APPROACH

7.1 Problem Areas

7.1.1 Initial Problem Definition Initial effort on the Study was confined to attempts at defining problems which required immediate solution to initiate the study. In general, the desired approach for determining the shielding effectiveness of various metals and enclosures was known. A standard test enclosure design was required.

7.1.1.1 Since it was decided that the largest test enclosure or box would have dimensions eight times that of the smallest, the dimensions selected were: 1.5" x 2" x 2.5"; 3" x 4" x 5"; 6" x 8" x 10"; and 12" x 16" x 20". It was realized that a Standard Reference Box was required immediately so that preliminary assessment of the approach to determining shielding effectiveness could be made. It was necessary that the Standard Reference Box represent as nearly as possible a seamless enclosure; hence construction methods as well as the overall box design had to be evaluated. Amounts and kind of material to be ordered were dependent upon box design and quantities required. Lead time for procurement of materials was known to be considerable.

7.1.1.2 Three major problems relative to design of the test enclosures had to be resolved:

(1) The method of inserting probe antennas into the boxes without compromising their effectiveness as shields.
(2) In addition to needing a sensor lead-in, access to the interior of the box was required. Maintaining shielding integrity at this access seam was recognized as a critical problem and one which was never fully resolved.
(3) Since it was not known how data might vary with the position of the probe antenna within the box, an effective method of orienting and of maintaining orientation of the probe within the boxes during measurements had to be established.

7.1.1.3 Once the problem of test enclosure basic design was resolved, development of test methods could proceed concurrently with development of the test boxes. Aspects of test philosophy had to be resolved; determination of the number and location of measurement points within the boxes was necessary; and a suitable probe antenna positioning method had to be determined, since conceivably data might vary for each point within the enclosure about which the probe antenna could be rotated. Further, decision was required whether to monitor multitudinous points or a relatively few predetermined positions.

7.1.2 Problems Associated with Test Setups and Measurement. It had been proposed that measurement techniques used during this Study would be basically those developed by Richard B. Schulz, D. P. Kanellakos, and others at Armour Research Foundation, and which have been proposed for adoption as IEEE Standards (Ref. 5). This approach at first seemed logical because the test boxes in a sense were miniature shield rooms. However, for greater simplicity in correlating measured data relative to the various factors which were to be evaluated, it was considered most desirable that the boxes be immersed in a uniform field at frequencies from 50 cps to 200 kc. The means for creating such a field then became a problem to be solved. It should be mentioned that a decision had been reached to place the excitation antennas exterior to the test enclosures throughout the Study, for greater flexibility in the design of test setups.

7.1.2.1 As soon as a Standard Reference Box could be obtained, a loop sensor antenna had to be designed. Antenna access to the first box was by means of a split, shaft-lock bushing, which permitted the loop to be located in any position within the box and any excess lead-in to be withdrawn before securely clamping the access bushing. This arrangement was not entirely satisfactory because constant movement of the lead-in cable through the bushing eventually resulted in severe damage to its outer braid. A new means of access had to be devised. (Paragraph 7.2.1)

7.1.2.2 The first group of low-frequency tests utilized a simple single turn, two-inch diameter loop, formed from RG-59/U coaxial cable by removing one-fourth inch of braid from one end of the cable, then completing a loop by soldering the inner conductor to the external braid. In addition to mechanical difficulties which were discussed above, the uniformity of preliminary measurements made of the field inside the test box aroused a suspicion that this loop was too large to detect incremental variations of the field. Accordingly, two more loops were designed to resolve this problem. (Paragraph 7.3.1)

7.1.2.3 Considerable effort was expended in developing test setups which would assure a high degree of confidence in the accuracy and repeatability of shielding effectiveness measurements. At the very low frequencies it was at first considered that the external excitation coil produced an essentially magnetic field. At the first indication of receiver susceptibility to this field, the NM-40A and the NF-105 receivers were moved outside of the screen room in which the test setup was located. The normal 30-foot coaxial cable between the receiver and the probe antenna was replaced with a twisted, shielded pair when receiver background levels indicated considerable leakage into the standard cable. Noise levels increased. The grounding system was investigated to asoertain that no ground loop existed. Next, the twisted pair cable was replaced with coaxial cable which penetrated the screen room wall by means of a feed-through UHF connector, grounding the external braid to the wall. The two receivers were then bonded directly to the external screen room wall. No improvement was noticed. It became apparent that the leakage problem was due to an intense electric field component surrounding the excitation coil.

A continuing problem was that of generating a sufficiently strong external field to enable the determination of shielding effectiveness of all metals and thicknesses included in the Study. Contributing to this problem was the desirability of using generators which were continuously tunable rather than fixed in frequency.

7.1.2.4 It was calculated (Section 7.3.3.6) that at approximately 944 mc the signal input to the NF-112 in the absence of a test box was 110 db above 1 μ volt. The loss in 30 feet of RG-5B/U at 944 mc is 3.3 db. Therefore, the maximum signal calculated to have been seen by the receiver was approximately 107 dbμ v.

The receiver indicated a level of only 101 dbμv. It is believed that the 6 db discrepancy between calculated and indicated levels was due to the cumulative effect of errors in the test setup: (1) The power output of the generator was not precisely defined; (2) The distance between the transmitting antenna and the probe antenna was measured from the monopole to the element having the highest current in the transmitting array. This distance was not equal to that of the isotropic center; (3) The monopole had no ground plane.

Problems encountered in making measurements at approximately 1 Gc were numerous. Repeatability of measured data was initially difficult to achieve because of introduction of reflection and phasing errors. Physical placement of the enclosure for which S was being determined was extremely critical. Insertion and removal of the test enclosure pickup probe caused slight displacement of the enclosure which in turn resulted in variations in the reinforcement and cancellation effects of the field in the vicinity of the probe antenna. Considerable radio frequency leakage was noted in the NF-105 receiver which introduced errors in measurements of highly effective shields. BNC type connectors were found to provide inadequate RF seals at UHF. It was noted that, as the mode of operation of the power oscillator was changed, the output was reduced or became erratic. This difficulty was identified as a critical maintenance problem.

7.1.2.5 One objective of this Study was to measure shielding effectiveness at the lowest resonant frequency of the test enclosures (approximately 944 mc for the TE_{101} mode for a 6 x 8 x 10 inch box). Due to the high Q (approximately 30,000) of the boxes, minor deviations produced major problems: (1) Normal oscillator drift became excessive, since the frequency was determined by three dependent variables; plate tuning, cathode tuning, and coupling. (2) Normal incremental, generator-dial frequency change proved excessive and was calculated to be approximately 40 kc. Backlash of the tuning gears produced a frequency change of several megacycles. (3) The actual cavity resonant frequency was extremely difficult to establish precisely at a given time. Because the wall thickness of the test boxes was relatively thin, normal building vibration and air circulation continuously altered the cavity's dimensions and consequently its natural resonant frequency. If the wall thickness were increased for mechanical stability, it is doubtful that shielding effectiveness values could be measured.

7.1.2.6 At approximately 10 Gc, problems first encountered at 1 Gc became more acute. It had been planned to use a very small horn antenna as a pickup inside the test boxes, but the multiplicity of reflections and distortion of the field within the boxes produced very ambiguous shielding effectiveness data. Another problem was that of attenuating the signal input to the receiver; but from a leakage standpoint, no satisfactory variable or step-type microwave attenuator was found. Since S values were expected to be very large, high peak power radar pulses literally splattered in all directions as they reflected from a rotating enclosure then re-radiated from walls and metal structures. These extraneous signals passed through openings in the receiver case, bypassing the signal input attenuator and producing erroneous indications.

7.1.3 Procurement and Fabrication Problems. Many problems associated with this Study have been non-technical in nature. For simplicity in reducing data associated with the various shielding effectiveness factors it was desired that all sheet metal be procured in thicknesses of 1, 2, 5, 10, 25, and 50 thousandths of an

60

inch. Unfortunately, commercially available thicknesses of metals are not to a common standard. Even when a nominal thickness was procurable permissible tolerances were as great as 60 percent. For a given metal, all desired nominal thicknesses or sheet widths in a common grade or alloy could not always be obtained. (Table B)

Another procurement problem was the difficulty of obtaining plated, clad, perforated, patterned, and expanded metals conforming to desired specifications. Some forms of metal were not available for fabricating boxes.

It was decided that an enclosure fabricated with a specially welded seam would most closely simulate a "seamless" structure. It has been found a practical impossibility as of the date of this Study to produce electron-beam welded seams of metals thinner than ten mils. The beamwidth of the welding device is only 0.003-inch; known cutting and bending techniques, and clamping methods cannot produce a butt joint of thin metals to the required accuracy. Another limitation was the inability to control the beam intensity with sufficient accuracy and stability to prevent burn-through. Several other problems which arose because of the relative thinness of metals used for this Study and the resultant mechanical instability of the test enclosures were: (1) Uniform pressure of the lid and spring fingers could not be maintained. Variations occurred each time the box was handled or the lid removed. (2) Lids did not fit precisely, causing occasional gaps between lid and fingers and splitting at the corners. (3) Soldering of finger stock and of feed-through connectors caused warpage. (4) It was very difficult to achieve sufficient contact with the gasket which provided a seal at microwave frequencies since only very limited pressure could be applied to the boxes. (5) Some boxes could not support their own weight.

7.2 Preparation for Investigation of Shielding Effectiveness

7.2.1 Test Enclosure Fabrication.

This Study required the isolation of variable factors which would ultimately determine the shielding effectiveness of a structure or enclosure. Control over these factors had to be established and maintained throughout the Study. The test items chosen to facilitate the desired factor isolation was a box which resembled a miniature, solid-wall, shield room. The complete list of fabricated enclosures for test is shown in Table C. A standard size of 6 x 8 x 10 inches was adopted. A fold-over lid was fitted to the 6 x 8 inch open end. Since it was necessary to gain repeated access to the interior of the test enclosures, the box opening and closing method was of considerable technical importance. The method chosen consisted of two rows of beryllium copper fingers surrounding the outer periphery of the box and two rows around the inner periphery. The lid was designed with a U-channel to make full contact with all four rows of fingers (Fig. 14). In addition, a woven metal gasket could be inserted to establish contact with the edge of the enclosure if needed. This type of construction was intended to compensate for non-uniformity of box contour, especially around the open end. Theoretical considerations indicated that the boxes would resonate in the TE_{101} mode at a frequency determined by the two largest dimensions. Thus, it was thought that an antenna lead-in entry at the center of an 8 x 10 inch side would least disturb the normal field pattern within the box (Figs. 15 and 16).

Table B Materials Procured For Study

Material	Form	Type	Condition	Thickness (inches)	Notes
Copper	Sheet	ETP		.0016	(Also .0030, .0124, .0243 and .0503)
Copper	Perforated Sheet	ETP		.0243	Perforations approximately 0.125 inches diameter on 0.250 inch centers.
Copper	Dimple Embossed Sheet	ETP		.0243	Dimples approximately 0.125 inches diameter on 0.250-inch centers.
Aluminum	Sheet	6061-0		.0251 .0500	
Aluminum	Sheet	1100		.0058 .0078 .0117	
Aluminum	Expanded Sheet	6061-0		.0510	.250 inch openings, .060 inch strands.
Brass	Sheet	SAE 70 C Yellow	Annealed	.0020 .0057 .0260	
Magnesium	Sheet	AZ31B	"0"	.0100 .0244 .0436	
Monel	Sheet	QQ-N-281 Class A	Annealed	.0087 .0246 .0480	
Steel	Sheet	SAE 1020	Annealed	.0099 .0244 .0480	
Netic Steel	Sheet	S3-6		.0136 .0507	
Netic Steel	Sheet	S3		.0241	
Titanium	Sheet	TIMET HTD TI-8A1IM		.0286 .0618	
Aluminum	Dimple Embossed Sheet	6061-0		.0251	Dimples approximately 0.125 inches diameter on 0.250-inch centers.

Table B Materials Procured For Study (Continued)

Material	Form	Type	Condition	Thickness (inches)	Notes
Steel	Dimple Embossed Sheet	SAE 1020	Annealed	.0244	Dimples approximately 0.125 inches diameter on 0.250 inch centers.
Tape	Electrically Conductive			.016	
Aluminum	Woven Mesh Fly Screen				
Copper	Woven Mesh Fly Screen				
Copper	Expanded Sheet	ETP		.0243	0.250-inch openings, approximately 0.050-inch strands.
Ferrite Tape	Ferotron	03-14-222		0.016	
Hardware Cloth	Zinc-dipped	No. 23 gauge No. 4 mesh			
Aluminum	Woven Tubing	1 inch I.D.			
Epoxy	Conductive	Series 8000, No. 360-18 Silver Series, No. 581-29			
Pipe	1 inch I.D.	Copper Aluminum Black Iron Galvanized Iron			
Tinned Copper	Braid	Low Picks High Picks			

Simulated Shield Rooms, 12 x 16 x 20 inches:

- Galvannealed Steel, H-joint, Type BC
- Galvannealed Steel, Lindsay Structural Joint
- Copper Screen, Cell Type, Butt Joint
- Copper Screen, Single Type, Butt Joint

Beryllium Copper Spring Fingers:

- .005 x .125 inches
- .010 x .281 inches

Table C Description of Shielding Boxes

Test Enclosure Number	Composition	Thickness (inches)	Inside * Dimensions (inches)	Seam Construction	Lid Contact	Remarks
1	Copper	.0243	1.5x2.0 x2.5	EB Welded	4 rows fingers	
2	Copper	.0243	3 x 4 x 5	EB Welded	4 rows fingers	
3	Copper	.0243	6 x 8 x 10	EB Welded	4 rows fingers	Convert to 60
3S	Copper	.0243	6 x 8 x 10	EB Welded	Soldered on	
4	Copper	.0243	12x16x20	Soldered	4 rows fingers	
5	Copper	.0243	6 x 8 x 10	Soldered	4 rows fingers	Convert to 5A
5A	Copper	.0243	6 x 8 x 10	Soldered	2 rows fingers	
5S	Copper	.0243	6 x 8 x 10	Soldered	Soldered on	
6	Copper	.0243	6 x 8 x 10	Brazed	4 rows fingers	Convert to 6A
6A	Copper	.0243	6 x 8 x 10	Brazed	2 rows fingers	
6S	Copper	.0243	6 x 8 x 10	Brazed	Soldered on	
7	Copper	.0243	6 x 8 x 10	Screw-held	2 rows fingers Screw-held	Convert to 7A
7A	Copper	.0243	6 x 8 x 10	Soldered	2 rows fingers Screw-held	Convert to 7B
7B	Copper	.0243	6 x 8 x 10	Soldered	fingers removed Screw-held	Convert to 7C
7C	Copper	.0243	6 x 8 x 10	Soldered	Technit Gasket	Convert to 7D
7D	Copper	.0243	6 x 8 x 10	Soldered	Polastrip Gasket	Convert to 7E
7E	Copper	.0243	6 x 8 x 10	Soldered	Silver epoxy sealed	Convert to 7F

*Last dimension is height

Table C Description of Shielding Boxes (Continued)

Test Enclosure Number	Composition	Thickness (inches)	Inside Dimensions (inches)	Seam Construction	Lid Contact	Remarks
7F	Copper	.0243	6 x 8 x 10	Soldered	Conductive epoxy sealed	Convert to 7G
7G	Copper	.0243	6 x 8 x 10	Soldered	Metex RF Gasket	
8	Copper	.0243	8 x 8 x 8	Soldered	2 rows fingers	
9	Copper	.0243	8 x 8 x 10	Soldered	2 rows fingers	L-Shaped
10	Copper	.0243	10x7 13/16	Soldered	2 rows fingers	Cylindrical
11S	Copper	.0016	3 x 4 x 5	Soldered	Soldered on	
12S	Copper	.0030	3 x 4 x 5	Soldered	Soldered on	
13S	Copper	.0053	3 x 4 x 5	Soldered	Soldered on	
14	Copper	.0124	6 x 8 x 10	EB Welded	4 rows fingers	
15	Copper	.0503	6 x 8 x 10	EB Welded	4 rows fingers	
15S	Copper	.0503	6 x 8 x 10	EB Welded	Soldered on	
16A	Copper	.0243	6 x 8 x 10	Soldered	2 rows fingers	Externally embossed
16B	Copper	.0243	6 x 8 x 10	Soldered	2 rows fingers	Reversed embossing
17	Copper	.0243	6 x 8 x 10	Soldered	2 rows fingers	Perforated 1/8" holes on 1/4" ctrs
18	Aluminum	.051	3 x 4 x 5	Soldered	2 rows fingers	Expanded
21	Copper	18 x 24 Mesh	12x16x20	Simple butt	Bolted butt	Single layer Screening
22	Copper	18 x 24 Mesh	12x16x20	ACE Engr. Butt Joint	Bolted butt	Cell Type Screening

Table C Description of Shielding Boxes (Continued)

Test Enclosure Number	Composition	Thickness (inches)	Inside Dimensions (inches)	Seam Construction	Lid Contact	Remarks
23S	Aluminum	.0058	6 x 8 x 10	Soldered	Soldered on	
24S	Aluminum	.0078	6 x 8 x 10	Soldered	Soldered on	
25S	Aluminum	.0117	6 x 8 x 10	EB Welded	Soldered on	
26	Aluminum	.0251	6 x 8 x 10	EB Welded	4 rows fingers	
27	Aluminum	.050	6 x 8 x 10	EB Welded	4 rows fingers	
27A	Aluminum	.050	6 x 8 x 10	EB Welded	4 rows fingers	Added seam
27T*	Aluminum	.050	6 x 8 x 10	EB Welded	4 rows fingers	Temperature Shock
28	Aluminum	.0251	6 x 8 x 10	Dip Brazed	2 rows fingers	
29	Aluminum	.0251	6 x 8 x 10	Screw-held	2 rows fingers	
30	Aluminum	.0251	6 x 8 x 10	Spot-welded	2 rows fingers	
31	Aluminum	.0251	6 x 8 x 10	Continuous Weld	2 rows fingers	
33	Magnesium	.025	6 x 8 x 10	Screw-held	2 rows fingers	
34	Magnesium	.050	6 x 8 x 10	Screw-held	2 rows fingers	
35	Magnesium	.025	6 x 8 x 10	EB Welded	2 rows fingers	
36	Magnesium	.050	6 x 8 x 10	EB Welded	2 rows fingers	
37	Brass	.0260	6 x 8 x 10	Soldered	2 rows fingers	
38	Brass	.0260	6 x 8 x 10	Screw-held	2 rows fingers	Convert to 39

*T denotes temperature shock tested.

Table C Description of Shielding Boxes (Continued)

Test Enclosure Number	Composition	Thickness (inches)	Inside Dimensions (inches)	Seam Construction	Lid Contact	Remarks
40	Monel	.0246	3 x 4 x 5	Soldered	2 rows fingers	Convert to 41
42	Monel	.0246	3 x 4 x 5	Continuous Weld	2 rows fingers	
43	Monel	.0246	3 x 4 x 5	Screw-held	2 rows fingers	
44	Monel	.0246	3 x 4 x 5	Brazed	2 rows fingers	
45	Monel	.0087	3 x 4 x 5	Continuous Weld	2 rows fingers	
46	Monel	.0480	6 x 8 x 10	Continuous Weld	2 rows fingers	
47	Steel	.0244	6 x 8 x 10	Screw-held	2 rows fingers	Convert to 49
47T*	Steel	.0244	6 x 8 x 10	Screw-held	2 rows fingers	
47TS*	Steel	.0244	6 x 8 x 10	Screw-held	Soldered on	
48	Steel	.0244	6 x 8 x 10	Brazed	2 rows fingers	
48T*	Steel	.0244	6 x 8 x 10	Brazed	2 rows fingers	
48TS*	Steel	.0244	6 x 8 x 10	Brazed	Soldered on	
50	Steel	.0244	6 x 8 x 10	Continuous Weld	2 rows fingers	Convert to 64
50S	Steel	.0244	6 x 8 x 10	Continuous Weld	Soldered on	
51	Steel	.0099	3 x 4 x 5	Continuous Weld	2 rows fingers	

*T denotes temperature shock tested.

Table C Description of Shielding Boxes (Continued)

Test Enclosure Number	Composition	Thickness (inches)	Inside Dimensions (inches)	Seam Construction	Lid Contact	Remarks
52	Steel	.0480	6 x 8 x 10	Continuous Weld	2 rows fingers	
53	S3 Netic	.0219	6 x 8 x 10	Screw-held	Screw-held	
54	S3 Netic	.0219	6 x 8 x 10	Spot-welded	Screw-held	
54A	S3 Netic	.0219	6 x 8 x 10	Continuous Weld	Screw-held	
55	S3 Netic	.0507	6 x 8 x 10	Continuous Weld	Screw-held	
56	S3-6 Netic	.0136	6 x 8 x 10	Continuous Weld	Screw-held	
57	Chomeric #581-29	Cannot be Controlled	6 x 8 x 10	Seamless	2 rows fingers	Used as coating inside surface of Plexiglas box.
58	Chomeric #360-18	As uniformly thin as practicable	6 x 8 x 10	Seamless	2 rows fingers	
63	Steel Aluminum Plated	.0251 w/ .005 aluminum, both sides	6 x 8 x 10	Soldered	4 rows fingers	
67	Steel, Gal vannealed	.0244 w/ .001 zinc both sides	6 x 8 x 10	Soldered	4 rows fingers	
68	Brass	.002	3 x 4 x 5	Soldered	2 rows fingers	
69	Brass	.005	6 x 8 x 10	Soldered	2 rows fingers	
70	Copper	.0243	10" Diameter	Seamless	2 rows fingers	Spherical

Table C Description of Shielding Boxes (Continued)

Test Enclosure Number	Composition	Thickness (inches)	Inside Dimensions (inches)	Seam Construction	Lid Contact	Remarks
71	Galvannealed Steel		12x16x20	Lindsay Structural Joint	Inter-locked	Miniature Shield room External Frame
72	Steel Galvannealed		12x16x20	H-Joint, Type BC	Inter-locked	Miniature Shield Room
74	Titanium	.0286	3 x 4 x 5	Gas Welded	2 rows fingers	
75	Titanium	.0618	3 x 4 x 5	Gas Welded	2 rows fingers	

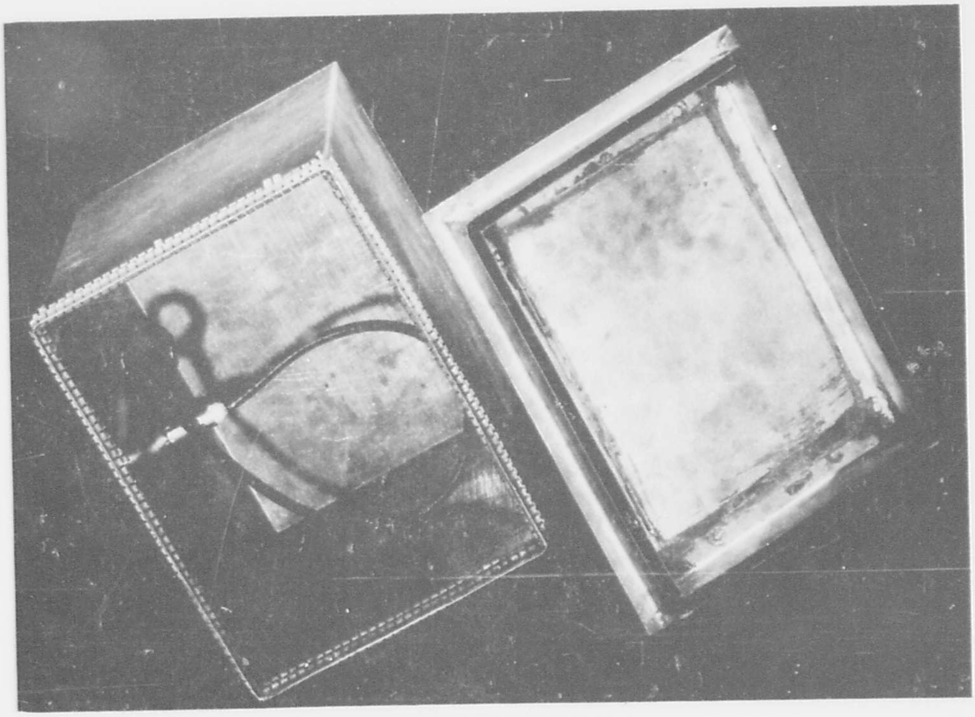

Fig. 14 Standard Reference. Box and 2-inch Loop Antenna

Originally, entry was through a split, shaft-lock bushing which was replaced with a UG-414/U BNC type adapter (Fig. 17) and finally with a UG-201A/U adapter for UHF and microwave measurements.

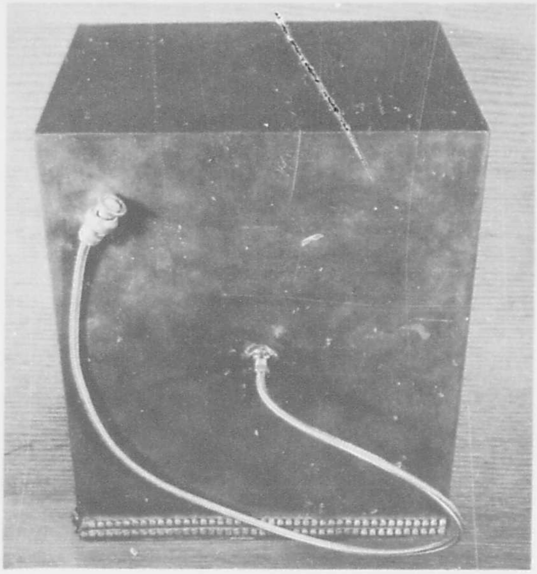

Fig. 15 Standard Reference Box (Probe Penetration Detail)

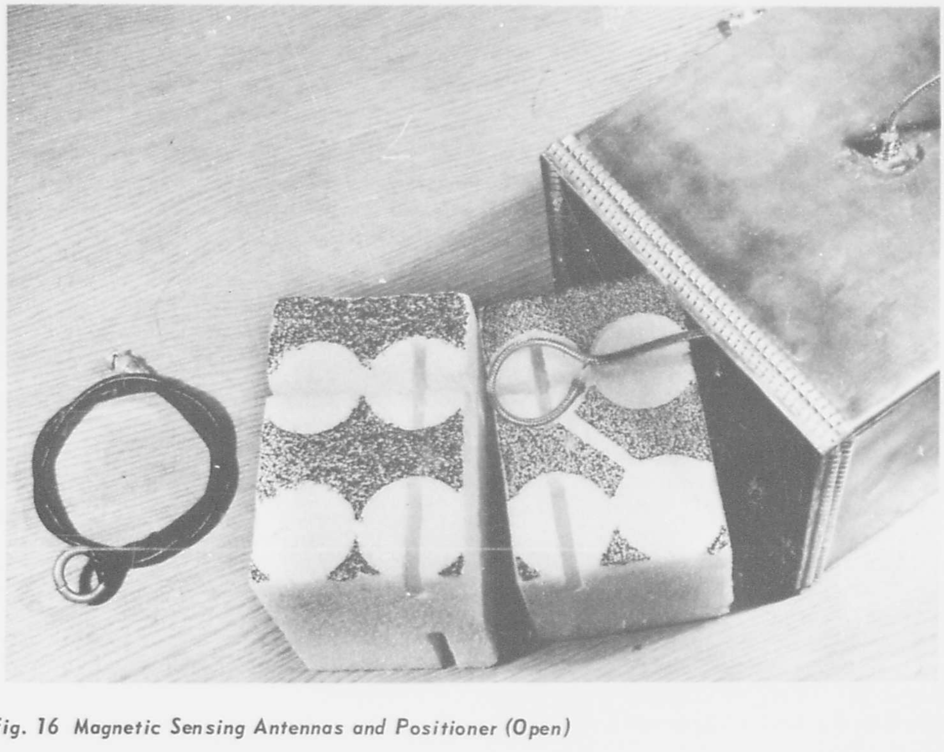

Fig. 16 Magnetic Sensing Antennas and Positioner (Open)

7.2.1.1 Standard Reference Enclosure. Data from the first box fabricated, after the general design was established, was to be used as a standard of reference (Box No. 3). The prime requisite for a standard reference enclosure was that it be essentially seamless as well as uniform in wall thickness. If possible, it was desired that no chemical composition or crystal structure alteration occur as the result of the seam-forming process selected. Drawn and explosive-formed boxes were considered but material thickness could not be accurately controlled. The Boeing electron-beam welding process was selected because it was anticipated that a box so fabricated would closely represent the ideal seamless shield concept (Fig. 18). The closure and lead-in entry were as described above (Figs. 14 and 16). The box was fabricated of pure (ETP) copper, 24.3 thousandths of an inch thick.

7.2.1.2 Materials Requisitioned. Because long lead times were required for many materials, requisitions were prepared immediately after test enclosure dimensions were established. Table B describes materials which were procured for this Study. It is to be noted that indicated thicknesses are the average of actual measured thicknesses of material used in the fabrication of the test enclosures.

7.2.2 Antenna Positioner for Magnetic Sensor Loop. The greatest number of test enclosures were opaque, therefore it was required that a method be devised for orienting, and maintaining the orientation of, the magnetic sensing loop which was to be placed inside the enclosures. The original design was a fairly elaborate tracking and positioning mechanism which would facilitate the plotting of an infinite number of points within the boxes with a great degree of repeatable accuracy. It was suspected though that its bulk and composition would create reflection problems at the higher test frequencies. Also, it appeared impractical for use in the small and thin-wall boxes. A less sophisticated positioning device was constructed of a split block of styrofoam by machining coil-holding slots in desired discrete positions. This device provided twenty-seven fixed positions for data collection. Styrofoam is extremely stable dimensionally, has very low moisture absorbent characteristics and low dielectric loss.

7.2.3 Very-Low and Low Frequency Field Measurements Technique The VLF-LF field measurements technique used throughout this Study was an adaptation of a proposed IEEE Standard for the determination of shielding effectiveness of enclosures. Measurements were to be made at several positions within the test boxes in addition to that at the geometrical center. By surrounding the test enclosures with a uniform magnetic field, any differences in measured data as the antenna location within a box was varied provided an indication of anomalies in shielding effectiveness of the enclosure.

7.2.3.1 A modified Helmholtz coil (Fig. 19) was wound on a polystyrene structure which was double the dimensions of the largest test enclosure to be immersed therein. Test enclosures were oriented within the coils to minimize effects of the lid closure joint. Also, the axis of the interior sensing loop antenna was maintained parallel to the axis of the exterior excitation coils (Figs. 20 and 21). The uniformity of the magnetic field within the test jig was determined in the following manner:

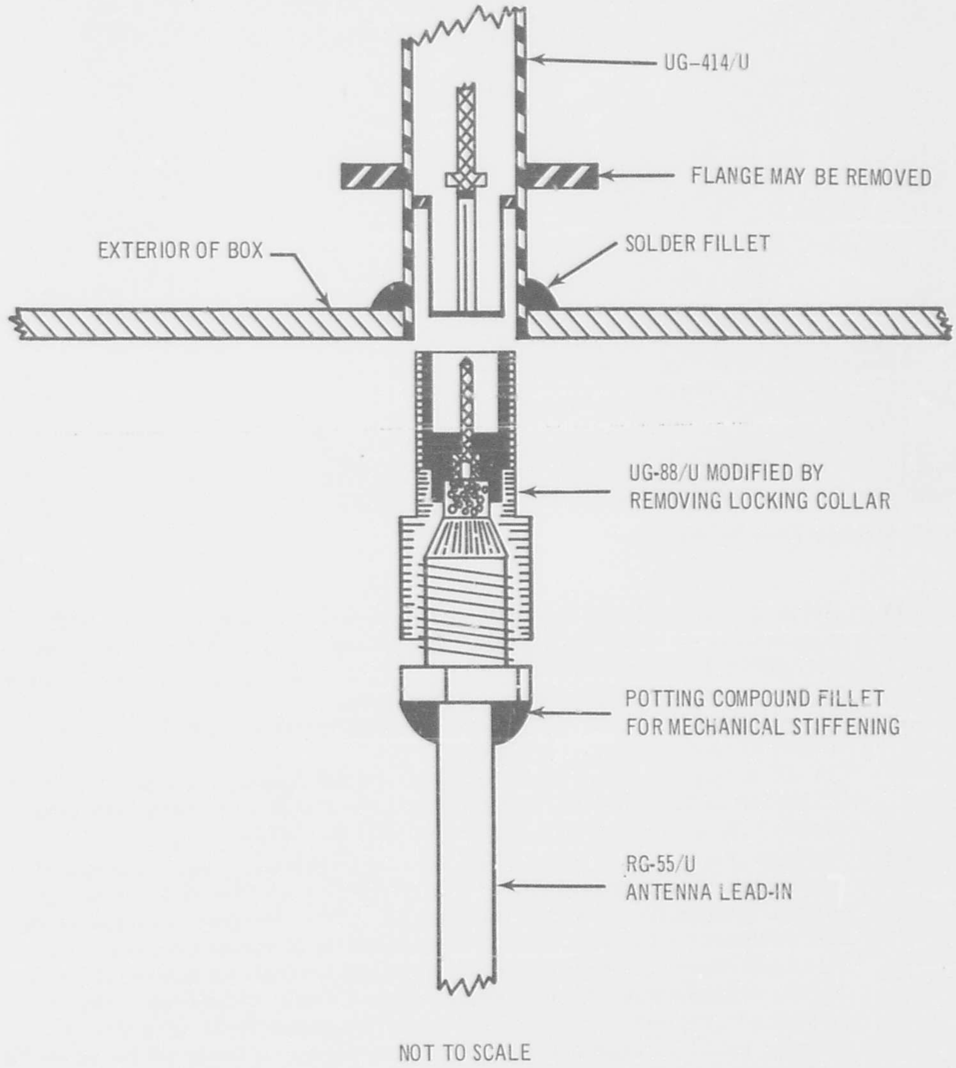

Fig. 17 Major Details of Test-Enclosure Penetration & Antenna Lead Connection

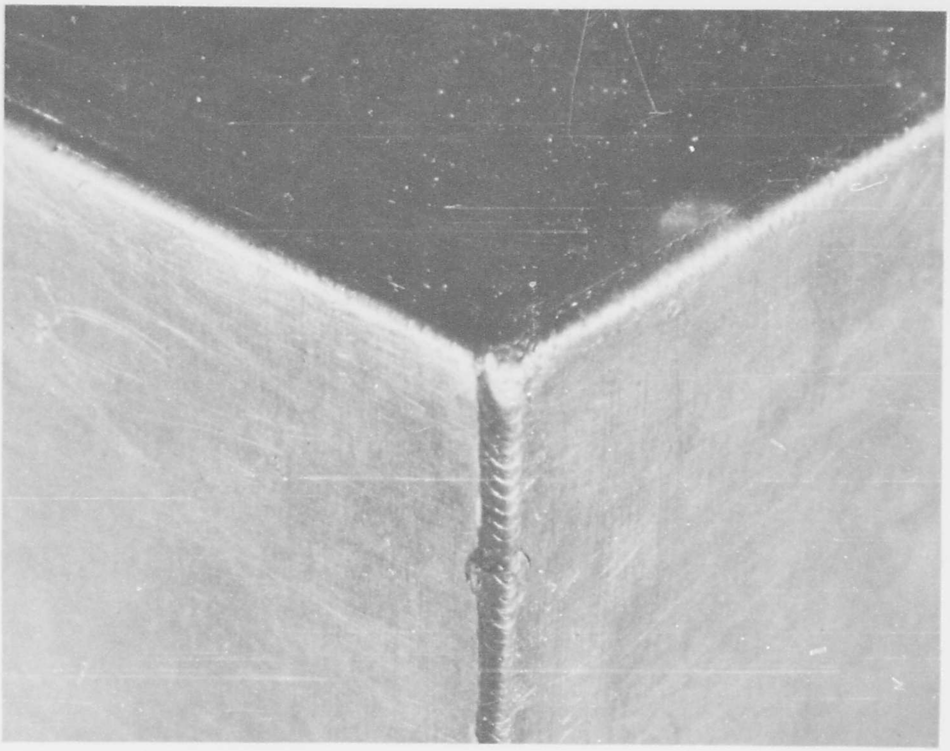

Fig. 18 Electron-Beam Welded Seams

(1) Nylon guide laces were strung between centers of each side, and diagonally, at three levels: six inches above, coincident with, and six inches below the midpoint of the coils. The guides were marked at two-inch intervals from the structure.

(2) An audio oscillator was adjusted for maximum undistorted signal output at each selected frequency.

(3) An AC magnetic-field evaluator was moved point-by-point along each guideline in turn and the detected voltage at each interval was measured with a vacuum tube voltmeter and recorded.

(4) Voltage measurements were expressed in terms of decibels deviation from that voltage measured at the geometric center of the coils and plotted (Appendix A, Figs. A1 through A15). Proper orientation of the evaluator was maintained for each point of measurement. Point-by-point measurements were made in but a single quadrant at each level, because spot-checks verified the field's symmetry. Superposing of graphed data revealed that a magnetic field of uniform density (±1 db) existed in a rectangular region at least 12 by 16 by 20 inches (Fig. 22).

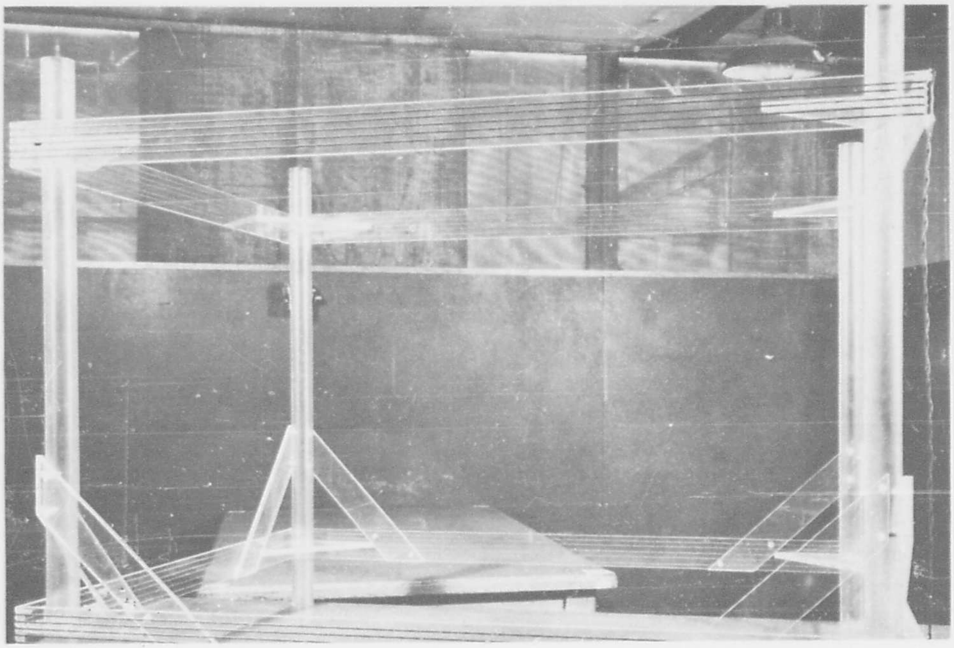

Fig. 19 Magnetic-Field Test Jig

7.2.3.2 Interior Magnetic-Sensing Antennas. Three different designs of loop antennas have been used during this Study. First experiments were conducted with the simple loop described in Section 7.1.2.2.

7.3 Test Setups

Shielding effectiveness data was obtained using three distinct test setups: VLF-LF, VHF, and microwave. In addition, attempts were made to measure S at resonance; measurements were made of electrical conductivity, initial magnetic permeability, and phase angle, requiring setups as described below.

7.3.1. VLF-LF Field Test Setup In this Study, shielding effectiveness measurements were made by placing enclosures of various materials and sizes in a uniform field. The field was produced by a Helmholtz coil devised especially for this Study. Design details and frequency limitations of the coil are given in a later section. The basic setup and instrumentation as pictured (Fig. 20) provided a means for measuring shielding effectiveness values as high as approximately 100 db over a range of 50 cps to 200 kc. One of the signal generators was used to drive the power amplifier which was connected to the modified Helmholtz coil. One VTVM monitored the input voltage to the amplifier (the oscilloscope was monitored to minimize distortion of the amplifier's output) and the other VTVM monitored the current into the excitation coil to assure a constant 1-ampere

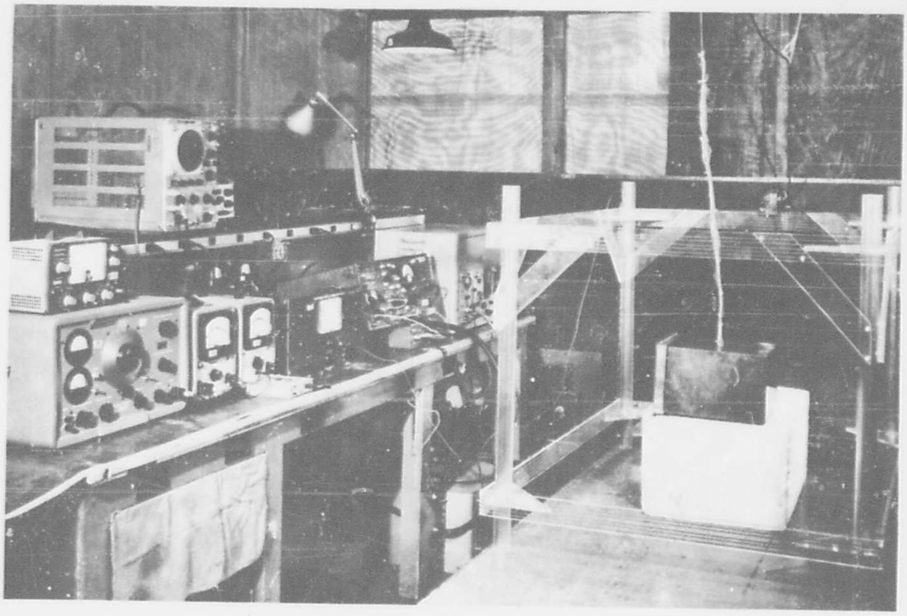

TEST EQUIPMENT

1. Hewlett Packard Audio Signal Generator, 20 cps to 20 kc, Model 205AG, Serial No. 7023
2. Heathkit Audio Generator, 1 cps to 200 kcps, Model AG-9A, BAC No. TLX 01578
3. Tektronix Oscilloscope, Type 515A, Serial No. 2761
4. Hewlett Packard Vacuum Tube Voltmeter, Model 400H, Serial No. 4771
5. Hewlett Packard Vacuum Tube Voltmeter, Model 400H, Serial No. 001-08541
6. Hewlett Packard AC Probe, Model 456A, Serial No. 103-01258
7. McIntosh 60 Watt Power Amplifier, Model MC-60, BAC No. TL-03057
8. Empire Devices Tuning Unit, Model TX/NF-105, 14 kc to 150 kc, Serial No. 1896
9. Empire Devices Noise and Field Intensity Meter, Model NF-105, Serial No. 1948
10. Stoddart Aircraft Radio Co. Radio Interference Field Intensity Meter and Power Supply, Model NM-40A, 30 to 15,000 cps, Serial No. 246-4.

Fig. 20 VLF–LF Field Test Setup

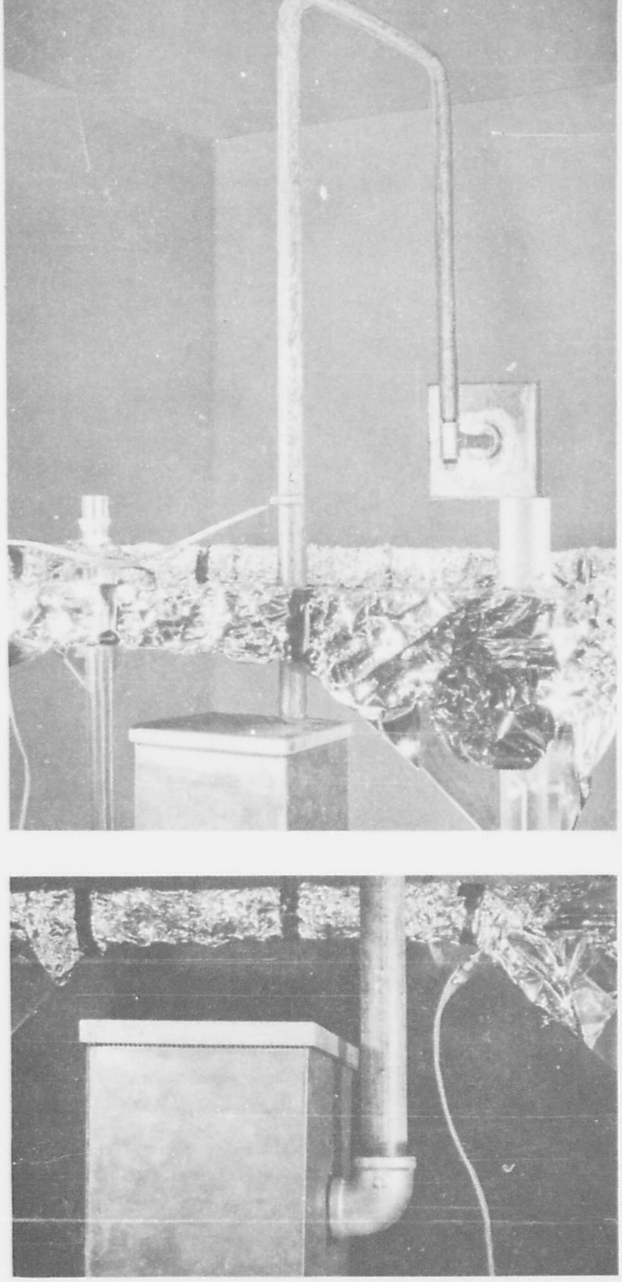

Fig. 21 Test Setup - 50 Cps to 200 Kc.

FIELD UNIFORMITY:

Single Hatched Area = 1 db Variation from Value at Geometric Center of Magnetic Field Test Jig.

Double Hatched Area = 1 db Total Variation Between any Two Points.

Depth of Uniform Field = 12 inches minimum.

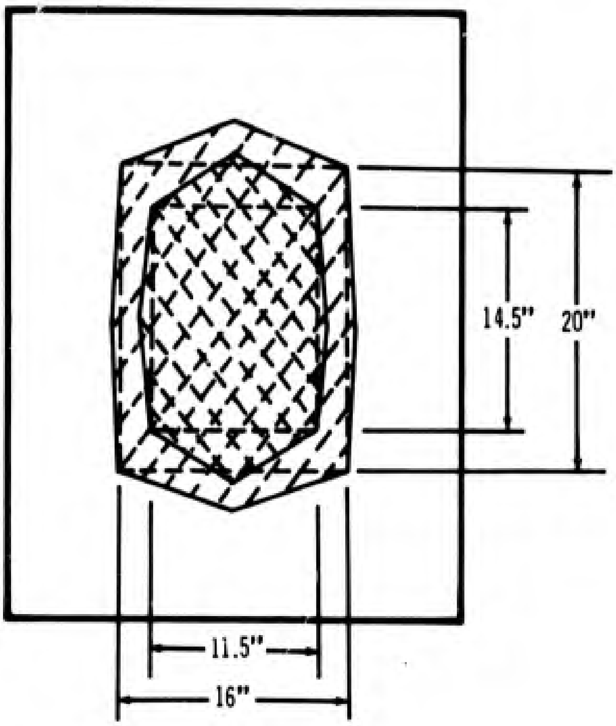

Fig. 22 View of Magnetic Field (Looking into Coil)

level. Above 20 kc, a Cornell-Dubilier Capacitance Decade Box provided neutralization of the coils' reactance. Two magnetic-sensing loop antennas were used to obtain all the low-impedance field data reported herein :

(1) A one-inch-diameter loop; five turns of 24-gauge enameled wire, wound inside a split loop of 0.156-inch ID brass tubing; 15-inch lead of RG-55/U coaxial cable terminated in a modified UG-88/U connector as shown in Fig. 17.

(2) A second loop was required for Test Enclosure No. 1 and both were one-of-a-kind. The extremely small dimensions of this box (1.5 x 2.0 x 2.5 inches) limited loop dimensions to a maximum of one-half inch diameter. Fabrication of such an antenna posed problems of obtaining usable tubing, fabrication skill, and finding a connector small enough to permit the loop to be centered. Since data obtained from Box No. 1 would be used only in establishing the "size factor", it was decided that flexibility was not needed. The antenna,

constructed as shown in Fig. 23 could be rotated about the geometric center of the enclosure in two planes.

The magnetic-sensing loop was connected to one of two field intensity meters by 30 feet of RG-59/U coaxial cable. This cable was brought through a 1.5-inch galvanized steel pipe projected through the screen room wall which provided approximately 16 db protection to the shorted cable at 100 cps. The extremely large electric field near the coils was considerably reduced by wrapping with household aluminum foil and grounding to the conduit. A gap was provided in these wrappings to prevent shorted-turn transformer effects. It was necessary further to add an elbow to shield the approximately four inches of lead exposed between the conduit and test box. This elbow permitted the boxes to be placed within a few thousandths of an inch of the conduit; tape was applied to avoid accidental grounding of the boxes since grounding was desired only at the receiver input connector.

7.3.2 UHF Test Setup at Approximately 1Gc. Power output was the paramount requirement in the selection of a generator. Two were available; the AN/APT-5, which is a World War II jamming transmitter; the Airborne Instruments Labs (AIL) type 124A signal generator. The latter was chosen; it was tunable from 300 to 2500 Mc and provided approximately 10 watts of A1 (CW) emission (similar to the APT-5). A log periodic antenna having a nominal 7-db gain from 400 to 1200 Mc was used to illuminate the test enclosures. The interior sensing antenna was a simple 2-inch monopole probe; it was not top loaded nor did it include a ground plane. It was fabricated of RG-59/U cable surrounded by a copper tube so that only a 2-inch length was exposed at the center of the enclosure.

Within the screen room it was necessary to be constantly alert to reflection problems. Physical placement of the test enclosures was extremely critical. Experimental measurements indicated that use of an available indoor antenna range was feasible and results were more satisfactory than for the screen room setup. Also, measurements made at the antenna range were equivalent to free-space measurement. The latter was insured by the liberal use of RF absorbent material and non-reflective walls. Susceptibility problems were avoided by replacing the NF-105 receiver with the NF-112 which is much better shielded.

The BNC type connector selected for energy transfer through the enclosure wall required extra shielding around it to reduce leakage to below the background noise level of the NF-112. The oscillator cavity of the AIL 124A required periodic removal of dirt, grease, and other foreign matter to assure high signal output power at all frequencies.

7.3.3 Enclosure Resonance Test Setup. The above setup was modified somewhat for direct attempts to measure shielding effectiveness at resonance. A Hewlett-Packard slotted line, Model 805A was inserted between the log periodic antenna and the AIL 124A generator. A 1N23A crystal detector and HP415B standing wave indicator were conventionally connected (Fig. 24).

To establish shielding effectiveness adequately, it is desirable to perform shielding effectiveness measurements at the lowest natural resonant frequency of the enclosure (Ref. 5). Initial work has been accomplished on the standard 6 x 8 x 10 - inch copper enclosure of 24-mil thickness.

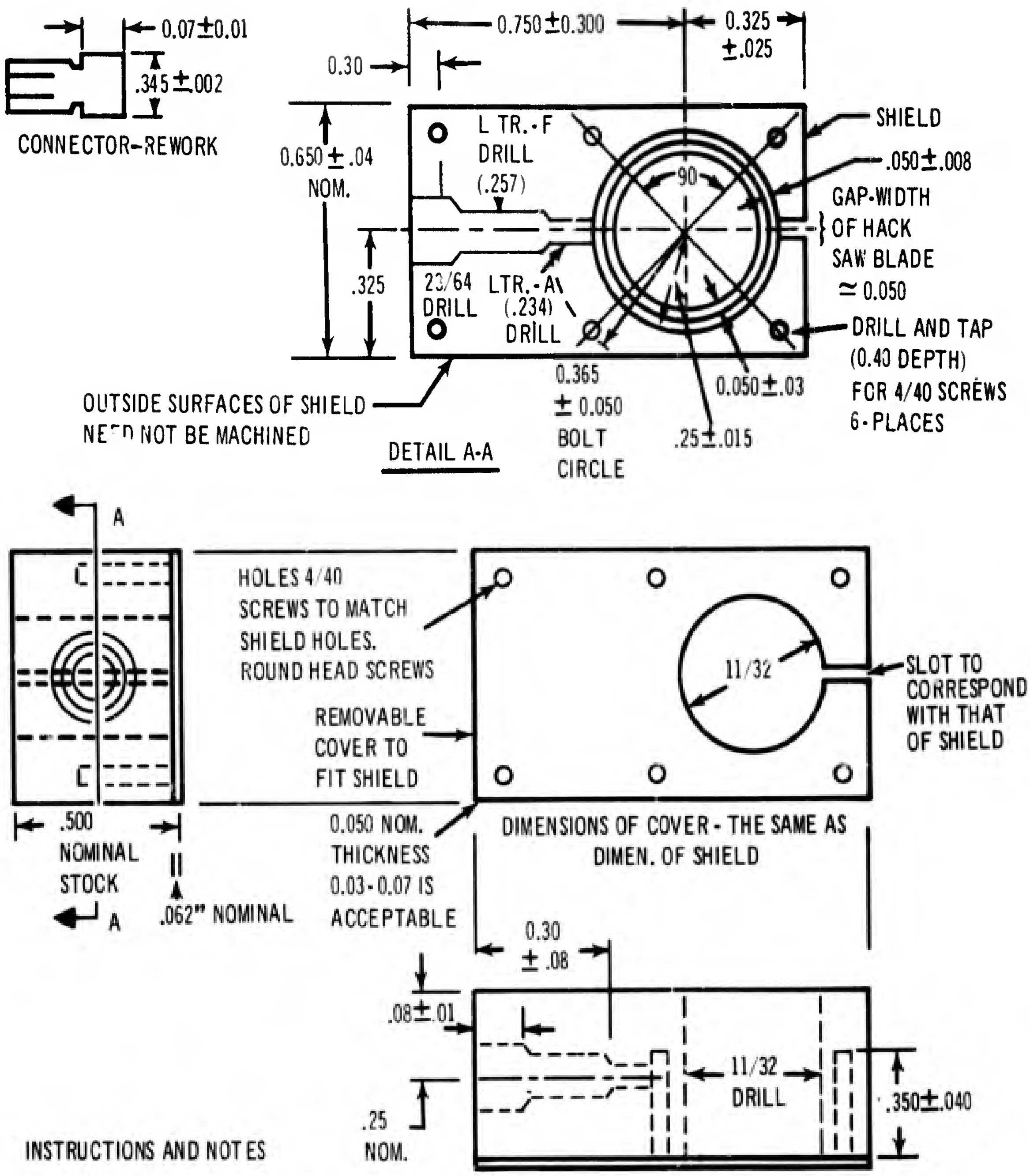

INSTRUCTIONS AND NOTES

1. CHUCK SHIELD BLOCK IN LATHE AND BORE 11/32 HOLE OFF CENTER THEN CUT 0.05 CIRCULAR TROUGH(GROOVE).
2. MATERIAL-BRASS, SHIELD AND COVER
3. REQUIREMENT-PIECES: ONE COVER
   ONE SHIELD
   ONE CONNECTOR
   (REWORK CONNECTOR SUBMITTED) CONNECTOR TO BE SOLDERED INTO 23/64" HOLE.
4. PURPOSE-SHIELD THE TEN TURNS OF #24 ENAM. WIRE WHICH FIT IN GROOVE.
5. HOLES FOR SCREWS NOT SHOWN IN ALL VIEWS-THESE HOLES NEED NOT BE ON BOLT CIRCLE.

Fig. 23 One-Half-Inch Magnetic-Sensing Antenna

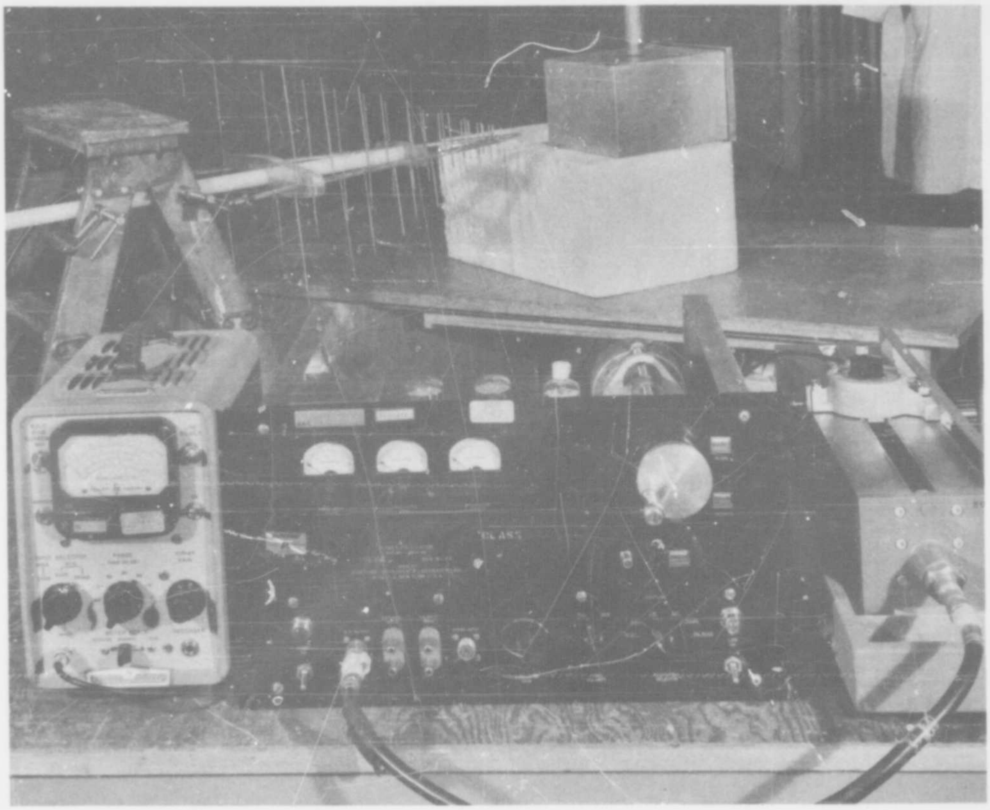

Fig. 24 UHF Setup (at Resonance Below 1Gc)

7.3.3.1 Coordinate System — Wavelength. To analyze this enclosure, it is first necessary to establish a coordinate system as in Fig. 25.

The air-space resonant wavelengths of the rectangular prism cavity are given by:

$$\lambda_o = \frac{2}{\sqrt{\left(\frac{\ell}{a}\right)^2 + \left(\frac{m}{b}\right)^2 + \left(\frac{n}{c}\right)^2}} , \tag{139}$$

where a, b, and c are the x, y, z dimensions respectively of the cavity. Since resonance is in the UHF region, the predominant electric field will be considered.

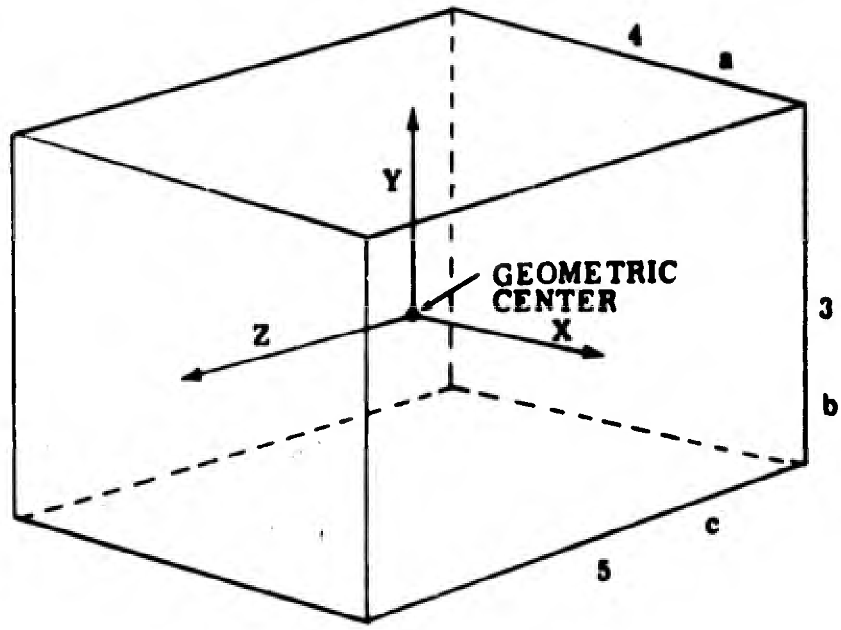

Fig. 25 Coordinate System Relative to Enclosures

7.3.3.2 Mode of Operation. No field variation occurs in the Y direction so the $TE_{\ell 0n}$ mode is significant. As shown in Fig. 25, b is the shortest dimension and c the longest. Since the field is constant in the Y direction and the lowest natural resonant frequency is required, the consideration may be limited to the TE_{101} mode.

7.3.3.3 Frequency of Resonance. For the standard enclosure, expressed in MKS units,

a = 0.153 meters,
b = 0.204 meters, and
c = 0.254 meters.

NOTE: With any internal conductors enclosure will resonate like a line.

For $\ell=1, m=0$, and $n=1$,

$$\lambda_0 = \frac{2}{\sqrt{24.18 + 15.45}} = 0.318 \text{ meters} = 12.5 \text{ inches} \tag{140}$$

The resonant frequency in megacycles is therefore

$$f_0 = \frac{300}{0.318} = 944 \text{ mc} \tag{141}$$

7.3.3.4 Figure of Merit — Q. For the $TE_{\ell on}$ mode, the figure of merit (Ref. 6) is given by

$$Q = \frac{\lambda_0}{\delta} \frac{(abc)}{2} \frac{(p^2+r^2)^{3/2}}{p^2c(a+2b)+r^2a(c+2b)}, \tag{142}$$

where

$$\delta = \text{skin depth} = \frac{0.066}{\sqrt{f}} = \frac{0.066}{\sqrt{9.44\times10^8}} = 2.15 \cdot 10^{-6} \text{ meters}$$

$$p = \frac{\ell}{a} = \sqrt{24.18} \text{ meter}^{-1}, \tag{143}$$

$$r = \frac{n}{c} = \sqrt{15.45} \text{ meter}^{-1}.$$

Therefore,

$$Q = \left(\frac{0.318}{2.15\times10^{-6}}\right)\left[\frac{0.5\times0.153\times0.204\times0.254(24.2+15.5)^{3/2}}{24.2\times0.254\times0.509+15.5\times0.20\times0.559}\right] \tag{144}$$

$$= 29{,}600.$$

It is apparent that the theoretical unloaded Q is extremely high in the region of resonance.

7.3.3.5 Half-Power Point. The bandwidth of the one-half power point at resonance is

$$B = 2\Delta f_{(1/2\,\text{pwr.})} = \frac{f}{Q} = \frac{10^9}{3\cdot10^4} = 33\,\text{kc}. \tag{145}$$

7.3.3.6 Radiated Power — Latitude of Instrumentation. In the vicinity of resonance, 944 Mc, far-field measurements were taken. For accurate far-field data, the antenna under test should be illuminated with a plane wavefront. Since plane wavefronts are obtainable only at infinite distances, some limits must be designated.

The test distance of 22 inches which was used is almost twice the wavelength of 12.5 inches. Using $R > \lambda/2\pi$ criterion this is sufficient. Using $2D^2/\lambda$ considerations an aperture of D=11.7 inches can be accomodated.

The minimum power delivered to the log periodic antenna is 10 watts. For a nominal 7-db gain over an isotrope, the effective radiated power (ERP) is 50 watts and at the receiving antenna, a distance of 22 inches, the received power density is:

$$\Phi = \frac{P_t}{4\pi R^2} = \frac{50}{4\pi}\left(\frac{39.37}{22}\right)^2 = 12.9 \text{ watts/meter}^2. \tag{146}$$

At the receiving antenna, the electric field is:

$$E = \sqrt{120\pi\, \mathcal{P}} = \sqrt{120\pi\,(12.9)} = 69.3 \text{ volts/meter} \tag{147}$$

and the open-circuit voltage is:

$$V_{oc} = E h_e = 69.3 \times 2.54 \times 10^{-2} = 1.76 \text{ volts}, \tag{148}$$

where h_e = 1 inch = 0.0254 meter is the effective height of the 2 inch monopole antenna.

The pickup monopole radiation resistance, Ref. 9, at 944 Mc is

$$R_a = 40\pi^2 \left(\frac{\ell}{\lambda}\right)^2 = 40\pi^2 \left(\frac{2}{12.5}\right)^2 = 9.9 \text{ ohms}; \tag{149}$$

the loss resistance may be neglected.

Antenna reactance is given by

$$X_{ant} = -\frac{1}{\omega C_{ant}} = \frac{-1/\omega}{2\pi\epsilon\ell}\left[\ln\frac{\ell}{a} - 1\right],$$

where a=.0253/2 inches is the radius of its cross section of #22 AWG copper-weld center conductor of RG-59/U

$$X_{ant} = \frac{36\pi \times 10^9\left[2.3\log_{10}\left(2/.0127\right) - 1\right]}{2\pi \times 944 \times 10^8 \times 2\pi \times .051} \text{ ohms} = -253 \text{ ohms}$$

is the antenna reactance. The equivalent circuit loop impedance is

$$|Z| = |60 - j253| = 265 \text{ ohms} \tag{150}$$

and the receiver input voltage is

$$V_R = \frac{1.76 \times 50}{265} = 0.33 \text{ volts} \tag{151}$$

or 110.4 db above one microvolt

7.3.4 Microwave Test Setup at Approximately 10 Gc. Essentially two test setups were made at approximately 10 Gc:

(1) When shielding effectiveness of an enclosure was expected not to exceed 50 db, a Sperry 2K39 Klystron was used as an X-band generator. It provided 300 milliwatts average output power in association with a frequency meter, power supply, and laboratory attenuators (Fig. 26).

(2) For measurements of higher shielding effectiveness, a converted RT-15A/APS-15 radar set (Fig. 27) supplied energy for tests.

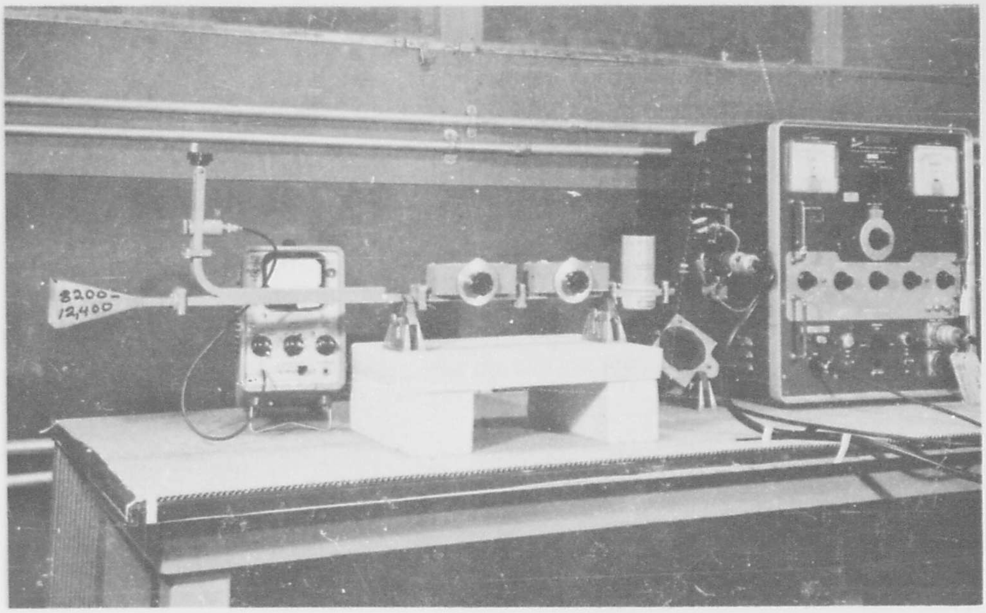

Fig. 26 Klystron Transmitting Test Setup (Shown in Screen Room)

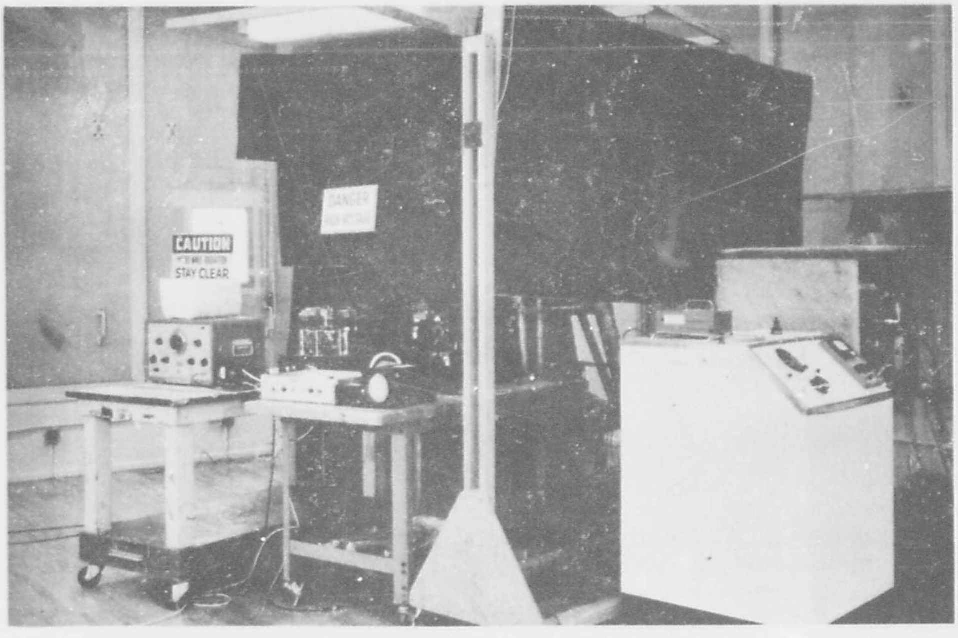

Fig. 27 10 Gigacycle Test Setup – Exterior View

The original magnetron was replaced with a 4J52 magnetron operating at 9.4 Gc. The radar set was triggered with a two-microsecond pulse from a Hewlett-Packard Pulse Generator Model 212-A which also varied the pulse repetition rate. An X-band waveguide carried the signal into an anechoic chamber. Peak power generated was approximately 45 kilowatts. The transmitting antenna was an E-H plane pyramidal horn which provided a calculated E-plane beamwidth of 10.7 degrees. The interior sensing antenna was a monopole approximately one-twelfth wavelength long at 9.4 Gc. It was made of Sub-Minax coaxial cable which produced far less field distortion within the test enclosures than even the lowest gain horn antenna. Also, the circular radiation pattern of the monopole permitted a 360-degree rotation of the test enclosure about the antenna's longitudinal axis. The pickup monopole was located for maximum E-field interception as calculated for the enclosures when considered as high-Q cavities. The antenna was connected to the NF-112 by two lengths of double shielded coaxial cable, RG-9A/U.

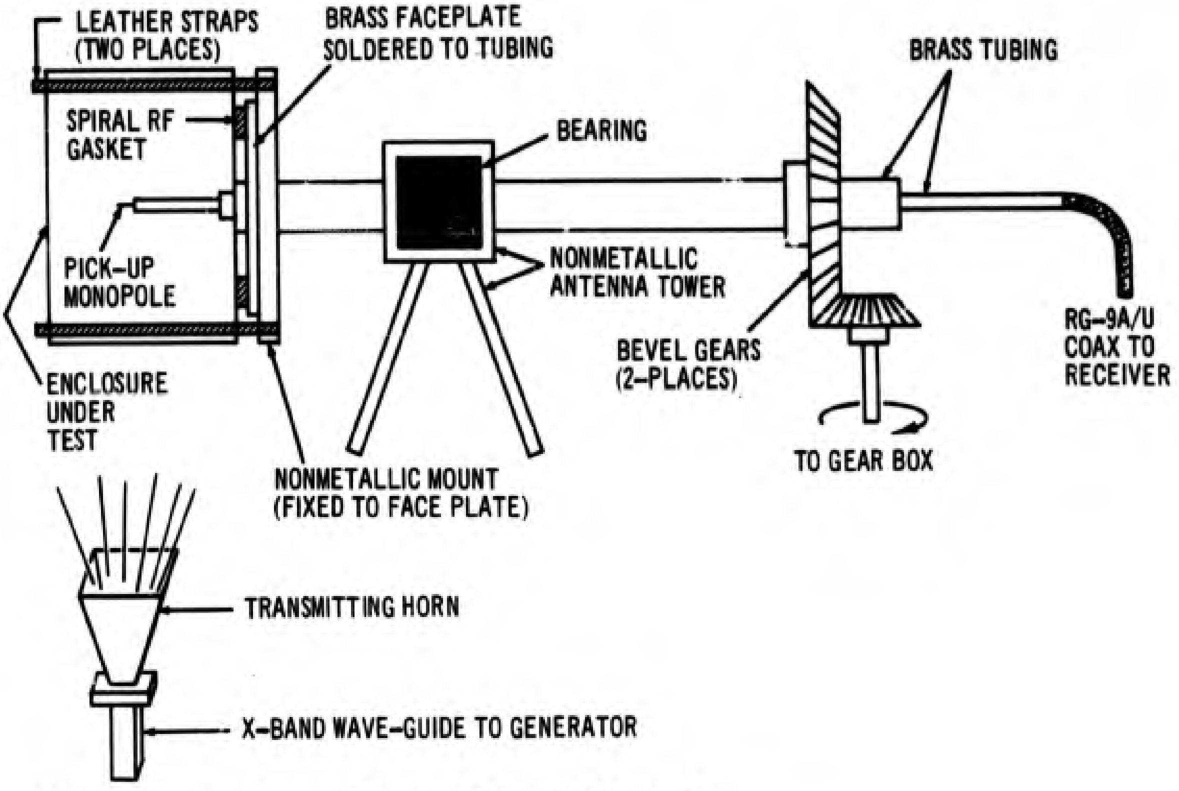

Fig. 28 Antenna Tower – Rotational Scheme (Side View)

The high field intensity required elaborate precautions to avoid undesired signal entry at several points in the setup. The RG-9A/U cable was routed through a brass tube which in turn was fitted with a faceplate which could contact one side of the enclosure under test. An RF gasket was required between the faceplate and the enclosure (Fig. 28). A Scientific-Atlanta Rotary Joint, type RJ-2, was placed within a larger diameter brass tube. Several layers of household foil were tightly wrapped around the rotary joint and N-type entry connector.

Cable leakage was reduced below receiver background noise level. When signal input to the receiver needed to be reduced, well shielded, fixed-type attenuators only were found to be satisfactory. X-band absorbent material was placed around the NF-112 receiver and the VIDEO and IF output connectors on its front panel were capped to further reduce undesired signal pickup. A Varian Associates Servo Plotter Model G-10 was connected to the EXTERNAL METER connector of the NF-112 receiver to plot directly the received signal as the test enclosure was rotated.

7.3.5 **Microwave Transmitting – Horn Considerations.** When selecting a suitable transmitting horn for the microwave frequencies, it is advantageous to determine the half-power beam width and power gain of the horn being considered. The distance between the horn and the boundary of the far field region should also be determined. Theoretical calculations are given for a horn used in this study.

7.3.5.1 Beamwidth. The selected transmitting horn has H and E plane aperture dimensions, a and b respectively, of 9.02 cm and 7.75 cm. The H and E plane slant heights, ℓ_h and ℓ_e respectively, are 11.43 cm and 9.40 cm and the wave length λ at the operating frequency of 9.4 Gc is 3.19 cm.

From Ref. 8, the half-power beamwidth in the E plane is given by

$$\theta_E \simeq \frac{25.5\lambda}{b} \text{ degrees} \tag{152}$$

where θ_E is measured from the horn's longitudinal axis

Therefore,

$$\theta_E \simeq \frac{2.25(3.19\text{cm})}{7.75\text{cm}} = 10.5\,(\text{degrees}) \tag{153}$$

In the H plane, the half-power beamwidth measured from the longitudinal axis is

$$\theta_H \simeq \frac{35\lambda}{a} = \frac{35(3.19\text{cm})}{9.02\text{cm}} = 12.4\,(\text{degrees}) \tag{154}$$

7.3.5.2 Gain. From Ref. 1, the pyramidal horn gain in decibels over an isotropic radiator is

$$\begin{aligned} G &\simeq 10\log_{10}\left[\frac{10ab}{\lambda^2}\right] \\ &\simeq 10\log_{10}\left[\frac{10(9.02\text{cm})(7.75\text{cm})}{(3.19\text{cm})^2}\right] \\ &\simeq 18.4\,(\text{db}) \end{aligned} \tag{155}$$

A more comprehensive analysis, where the phase deviations show E and H plane loss figures of 1.5 db (total), yields a gain of 16.9 db (Ref. 7, Section 10.3).

Due to the high flare angle of the horn employed, the above gain equation is approximate. D. R. Rhodes (Ref. 10) has shown that for high flare angles, E plane horn pattern break-up does not occur until the horn reaches a length of approximately 7λ. No problem of break-up exists in the H plane.

7.3.5.2.1 Phase Deviation. In the E plane the maximum phase deviation s in wavelengths is

$$s = \ell_e - r, \quad \text{(wavelengths)}$$

where r is the axial distance between the horn's apex and aperture. Geometrically the representation is shown in Fig. 29.

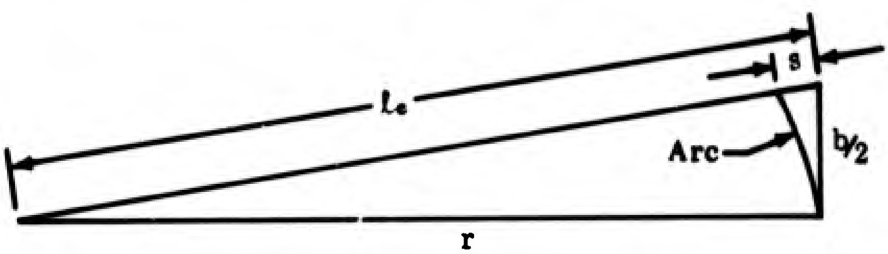

Fig. 29 E Plane of Pyramidal Horn; Geometric Representation

Since

$$r = \sqrt{\ell_e^2 - \left(\frac{b}{2}\right)^2},$$

by substitution,

$$s = \ell_e - \sqrt{\ell_e^2 - \left(\frac{b}{2}\right)^2} \simeq \ell_e - \ell_e\sqrt{1 - \left(\frac{b}{2\ell_e}\right)^2} \simeq \frac{b^2}{8\ell_e} \tag{156}$$

or, expressed in wavelengths,

$$\frac{s}{\lambda} \simeq \frac{b^2}{8\lambda\ell_e} \simeq \frac{(7.75\text{cm})^2}{8(3.19\text{cm})(9.4\text{cm})} = 0.25 \text{ wavelength} \tag{157}$$

In the H plane the maximum aperture phase deviation t in wave lengths is

$$t = \ell_h - r. \quad \text{(wavelengths)} \tag{158}$$

Similarly,

$$r = \sqrt{\ell_h^2 - \left(\frac{a}{2}\right)^2} \tag{159}$$

or,

$$t = \ell_h - \sqrt{\ell_h^2 - \left(\frac{a}{2}\right)^2} \text{ (cm)}$$

$$t/\lambda \simeq \frac{a^2}{8\lambda \ell_h} \text{ wavelengths}$$

$$\simeq \frac{(9.02\text{cm})^2}{8(3.19\text{cm})(11.43\text{cm})} = 0.28 \quad \text{(wavelengths)} \tag{160}$$

7.3.5.3 Figs. 30 and 31 are pictorial representations of the horn and measurement technique.

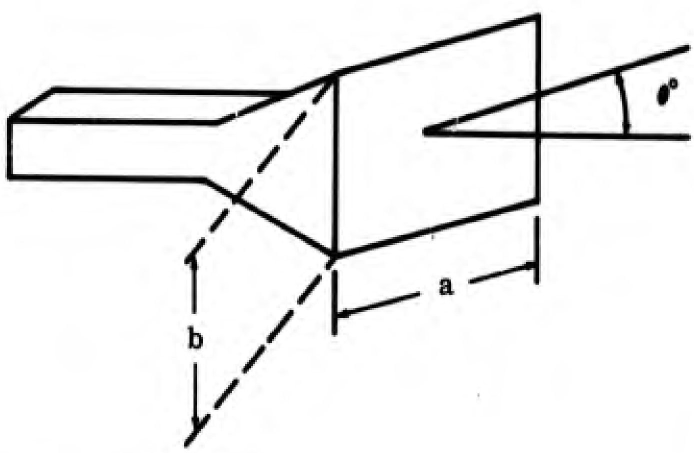

Fig. 30 Transmitting Horn

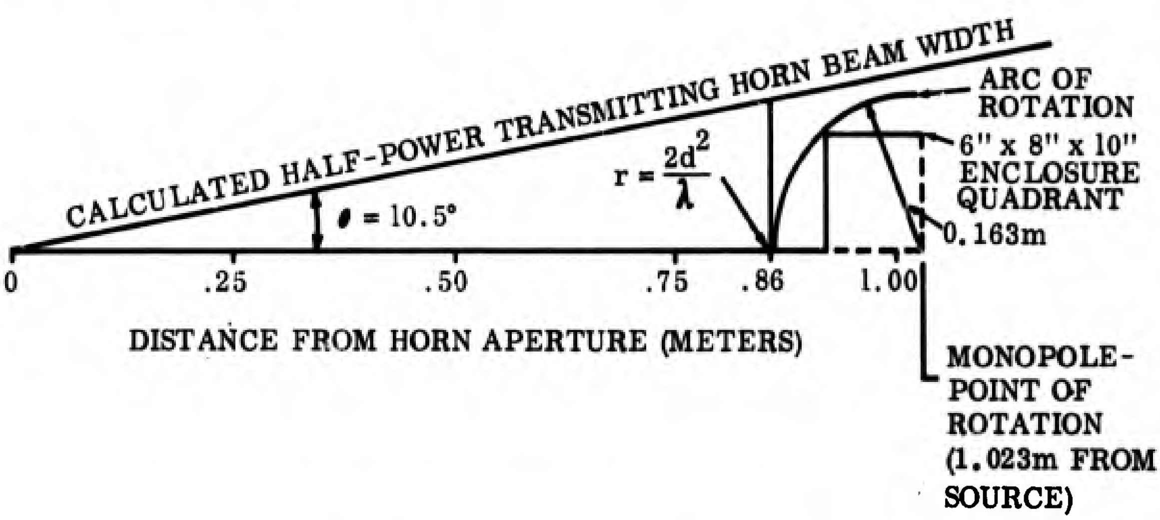

Fig. 31 Transmitting Horn Beam Width Representation: E Plane

7.3.5.3.1 Far-Field Calculation. The pickup monopole is placed in the transmitting horn's far-field to assure that in free space the monopole will see a plane wave transmitted by the horn. The distance from the horn aperture to the near boundary of the far-field region is (Ref. 11)

$$r = \frac{2d^2}{\lambda} \text{ (meters)} \tag{161}$$

where d is taken as the diagonal distance of the horn aperture.
Then,

$$r = \frac{2(11.7\,\text{cm})^2}{3.19\,\text{cm}} \times 10^{-2}\,\frac{\text{m}}{\text{cm}} = 0.86 \text{ meters} \tag{162}$$

$$.86\text{m} \sin 10.5° = 0.157\text{m}$$

7.3.5.3.2 Enclosure. The maximum diagonal distance from the axis of enclosure rotation to the corner of the enclosure is calculated to be 6.4 inches (0.163 meters) for the case of the 6 by 8 by 10 inch boxes. Therefore, for the test enclosure to be in the horn's far-field, the separation distance between the transmitting horn aperture and the axis of rotation is 0.86 plus 0.163, or 1.023 meters. The clearance to the half-power beam-width for the E and H field vectors is calculated to be 0.187 and 0.22 meters respectively as shown in Fig. 32. Thus the far-field condition is the limiting factor in how close the test enclosure can be placed to the transmitting horn.

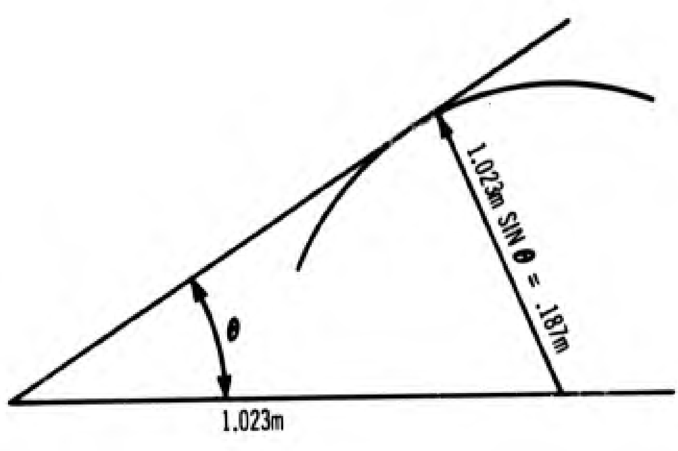

Fig. 32. Transmitting Horn; Beam Clearance

7.3.6 Determination of Permeability, μ, of Composition. To determine experimentally the permeability of a given material at various frequencies, two loops may be spaced a fixed distance of n material thicknesses apart with the two coils aligned coaxially. The material separating the loops should approximate an infinite sheet, i.e., negligible fringing of fields should exist around edges. One coil is excited and the resultant field in the second loop is recorded. The measurement is taken for the case when n = 2 and repeated for a single thickness of material and for an airgap equal to a single thickness; a total of three measurements per frequency. Use of measured data is given in Paragraph 8.1.

7.3.7 Determination of Net Phase Angle. As suggested by theory, a phase differential may be measured between the incident magnetic field and the field in the center of the illuminated test enclosure due to variable material and seam shielding factors. Two separate techniques used to observe this phase shift phenomenon are presented.

7.3.7.1 Amplitude Comparison Method. Two 10-turn sampling coils were inserted within the uniform field of the Helmholtz Inductor and excited by the current source shown in Fig. 33. One of the sampling coils (H) is in the center of the enclosure under test and a second (H_{sh}) pickup coil outside the enclosure receives the incident field with both coils coaxially aligned with the Helmholtz coil. The method consists of measuring the signal amplitudes in the two pickup coils as a function of frequency with a standard Radio Frequency Field Intensity

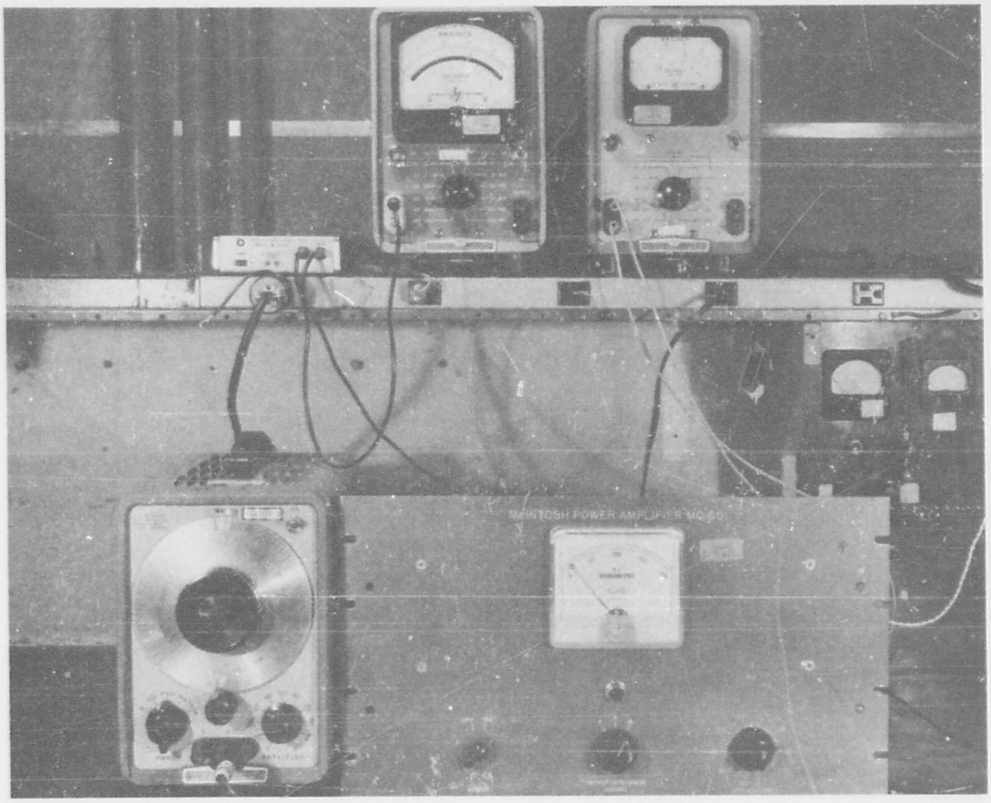

Fig. 33 Helmholtz Indicator Current Source, Generator Amplifier Equipment

Meter; Stoddart Co. Model NM-40, or Empire Devices Co. Model NF-105, Fig. 34. With the aid of a junction box fitted with BNC connectors, the coils are connected in series and the resultant signal amplitude measured. By use of the law of cosines, the phase angle $\Delta\theta$ between H and H_{sh} is computed as

$$\text{Arccos} \left[\frac{|H_{sh}|^2 + |H|^2 - |H_s|^2}{2\ |H_{sh}|\ |H|} \right] \quad \text{(degrees)} \qquad (163)$$

where the magnetic field intensity is measured in terms of received microvolts. $|H_s|$ is the equivalent resultant field magnitude when the two pickup coils are series connected. Note that H_{sh} actually includes both the reflected and incident fields (see 5.1.5).

It is necessary to balance lead capacity to ground on the H_{sh} coil for the series connection. Presumably a twisted and shielded cable pair would be satisfactory; however, two RG-55A/U coaxial cables with the shields of each cable grounded at one extremity and with the center conductors connected to the pickup coil were employed.

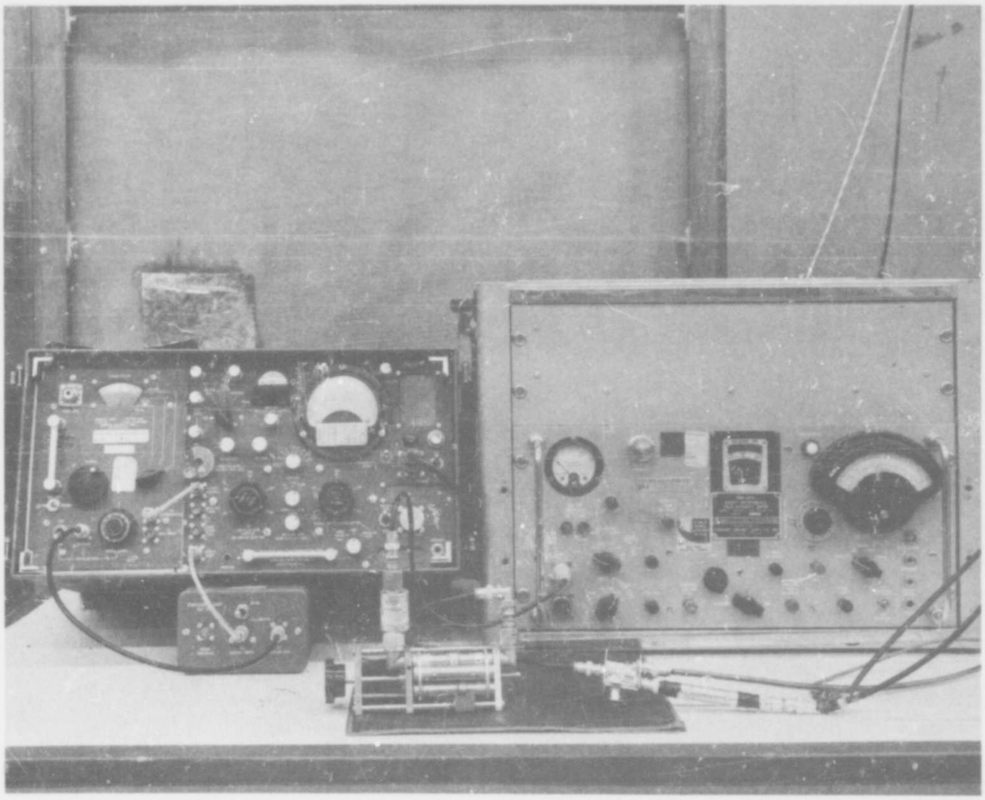

Fig. 34 Phase Angle Determination Equipment Amplitude Comparison Techniques

Although good results have been obtained with this technique certain precautions are required. For greater accuracy an attenuator should be inserted in the incident or both pickup loop cables so that at the receiver

$$|H_{sh}| \simeq |H|$$

Fixed and step attenuators of 50 ohms impedance have been employed.

Prior to conducting additional measurements using this technique, theoretical analyses and experimentation should be performed to enable an increase in the measured signal level from the H pickup loop when testing at frequencies near resonance. Also, when increasing H coil turns it should be remembered that loop and attenuator impedances are critical, since any loading of the pickup loop by the receiver input or attenuator impedances will introduce errors when the coils are series connected. These errors are not normally obvious when testing and in some cases are greater than anticipated. It is wise therefore to monitor this loading effect as the frequency of test is varied. Further, it should be noted that the Stoddart Model NM-40 receiver has high impedance inputs, while the Empire Devices Model NF-105 receiver does not. A measurement technique was developed which circumvents this problem and is described in Paragraph 7.3.7.2.

It is important to monitor the signal-plus-noise to noise ratio near the resonant frequency of the enclosure since normally low signal amplitudes are obtained. It is well to employ noise correction curves, Fig. 35, and to perform the calculations of phase differential at each frequency before proceeding with the data, as it is not difficult to incur errors in measurement with large errors resulting in the phase angle calculation near resonance. When removed from resonance, particularly on the low frequency side, this "signal-to-noise" ratio problem is less severe.

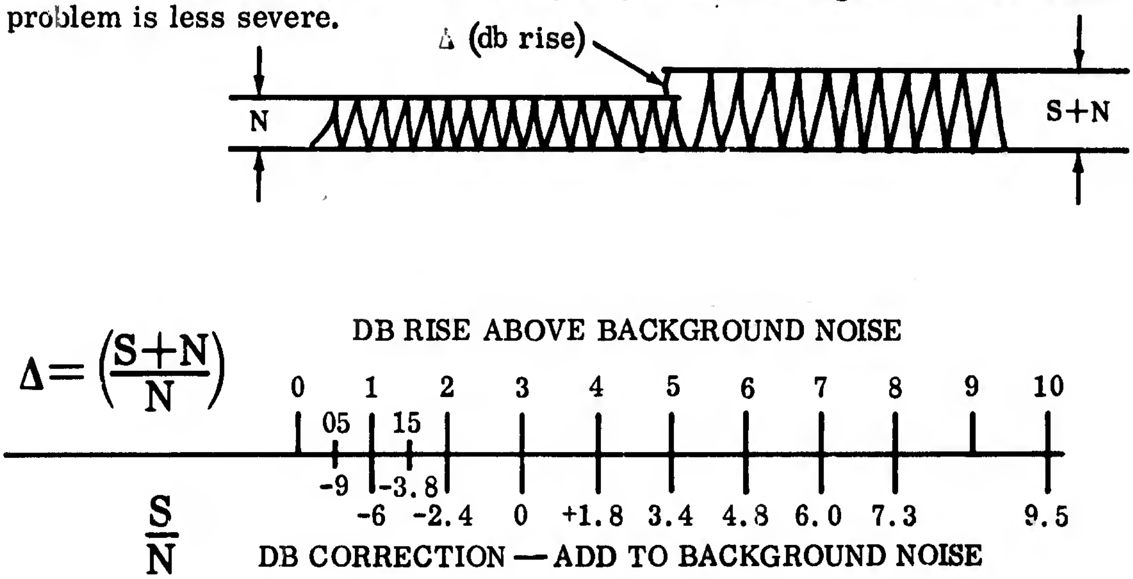

CORRECTION NOMOGRAPH FOR LOW SIGNAL-TO-NOISE RATIOS.
(See "Adding Decibel Expressed Quantities" A. L. DiMattia and L. R. Jones, Audio Engineering Magazine, July 1951, page 15.)

Fig. 35 Correction Nomograph – Low Signal-To-Noise Ratio

7.3.7.2 Direct-Reading Method. Phase determination was simplified at audio and low frequencies by the employment of a commercial type phase meter. This measurement technique improved the accuracy, repeatability, and ease of measurement while significantly increasing the rapidity of signal phase comparisons. Semi-direct readout of phase became possible with a conventional phase meter coupled to suitable wide band amplifiers of controllable frequency response. Data were plotted as collected without further mathematical manipulation as an aid in determining θ.

The basic measurement unit employed was an Acton Laboratories Phase Meter of ±1 percent, ±3 degrees accuracy from 20 cps to 20 kcs with an approximate 3 degree accuracy degradation to 100 kcs. A complete description of test equipment is presented in Table D.

The phase angle is read directly on a 7-inch square meter with mirrored scale, Figs. 36 and 37. Quadrant ambiguity is eliminated since the phase angle, as indicated by the instrument, is the result of comparing zero axis crossings of the two applied signals. The average zero-axes correspond to the average value of the AC component of the applied signals. Therefore, to obtain the greatest accuracy when comparing sinusoidal signals, the amplitude and waveform to each channel of the phase-meter was monitored to insure waveform symmetry each side of the zero-voltage axis. Low distortion is not necessarily required as clipping circuits transform the input signals to fast-rise-time square waves.

Once the phase angle is approximated, it is possible to transfer this angle, as read on the meter, to other quadrants by polarity and lead-lag reversal switches. Since four meter ranges are available, zero to 36, 90, 180, and 360 degrees, and since accuracy is based on the full scale meter range, it is possible to reduce measurement error to less than ±4 degrees, particularly below 20 kc.

Wide-band amplifiers are used to supply the required 2 volts minimum peak-to-peak to each channel of the phase meter. A Tektronix preamplifier with voltage gains of 100 and 1000 is cascaded with an Infrared Standards Laboratory amplifier with variable and step gain adjustments. Both amplifiers incorporate step-switches to control the low and high frequency response and adequate control of unwanted 60, 120, and 400 cps signals is possible. Signal-plus-noise to noise ratio has not been a problem even at enclosure resonance as a 175 turn pickup coil (H) within the enclosure has provided more than ample signal for measurements thus far obtained. Pickup coil impedance does not introduce error since the preamplifier input impedance is much higher.

In operation, the frequency response of the two amplifiers is adjusted in keeping with the frequency of test. Each amplifier has step response switches labeled by frequency. External attenuators, Fig. 38, and amplifier gains are adjusted for ample signal amplitude and waveform conditions in the sampling H_{sh} and test enclosure (H) coils. The two loops are then individually switched to the Tektronix preamplifier and the phase difference between the two readings noted without disturbance of the amplifier gain and response controls. It should be noted that a phase shifter could be inserted directly before or behind the cascaded amplifiers. By adjustment of the phase shifter to zero on the phase

Table D Laboratory Equipment List For θ Phase Angle Determination

1. Phase Meter, Acton Laboratories, Acton, Mass., Type 320-AB, Ser. No. 968.

2. Low Level Preamplifier, Tektronix Inc., Beaverton, Oregon, Type 122, Ser. No. 05281 with Type 125 Power Supply, Ser. No. 404.

3. Low Noise Amplifier, Infrared Standards Laboratory, Santa Barbara, Calif., Model ISL-603.

4. Oscilloscope, Tektronix Model 536, Ser. No. 001642, with Type 53/54C Dual Trace Plug-In Unit.

5. Turret Attenuator, Stoddart Aircraft Co., Hollywood, Calif., Model 40506-3, 50 ohm, 0-50 db in 10 db steps.

6. Step Attenuator, Microlab Co., Livingston, N. J., Model AV-20N, 0-10 db in 2 db steps.

7. Wide Range Oscillator, Hewlett-Packard, Palo Alto, Calif., Model 200-CD, Ser. No. 21146.

8. Current Probe, Hewlett-Packard, Model 456A, Ser. No. 103-02556.

9. VTVM, Hewlett-Packard Model 400H, Ser. No. 313.

10. Power Amplifier, McIntosh Laboratory Inc., Binghamton, N. Y., Model MC-60, Type A121.

11. Decade Capacitor, Cornell-Dubilier Electric Co., So. Plainfield, N. J., Model CDB-3, Ser. No. 24110 and Model CDA-J, Ser. No. 20379.

12. Pickup Coil, 2 Inch Nominal Diameter, 500 Turns No. 30 Enameled Wire, Shielded, Laboratory Constructed.

13. Pickup Coil, 2 Inch Nominal Diameter, 175 Turns, No. 27 Enameled Wire, Shielded, Laboratory Constructed.

14. Noise and Field-Intensity Meter, Empire Devices, Inc., Amsterdam, N. Y., Model NF-105, Ser. No. 1948.

15. Radio Interference Field Intensity Meter, Stoddart Aircraft Radio Co., Hollywood 38, Calif., Model NM-40A, Ser. No. 310-33.

16. Pickup Coil, 1 Inch Nominal Diameter, 10 Turns, No. 27 Enameled Wire, Shielded, Laboratory Constructed.

17. Pickup Coil, One-Half Inch Nominal Diameter, 10 Turns, No. 27 Enameled Wire, Laboratory Constructed.

18. Helmholtz Coil, 32 x 40 inch, 5 Turns Each Solenoid, Laboratory Constructed.

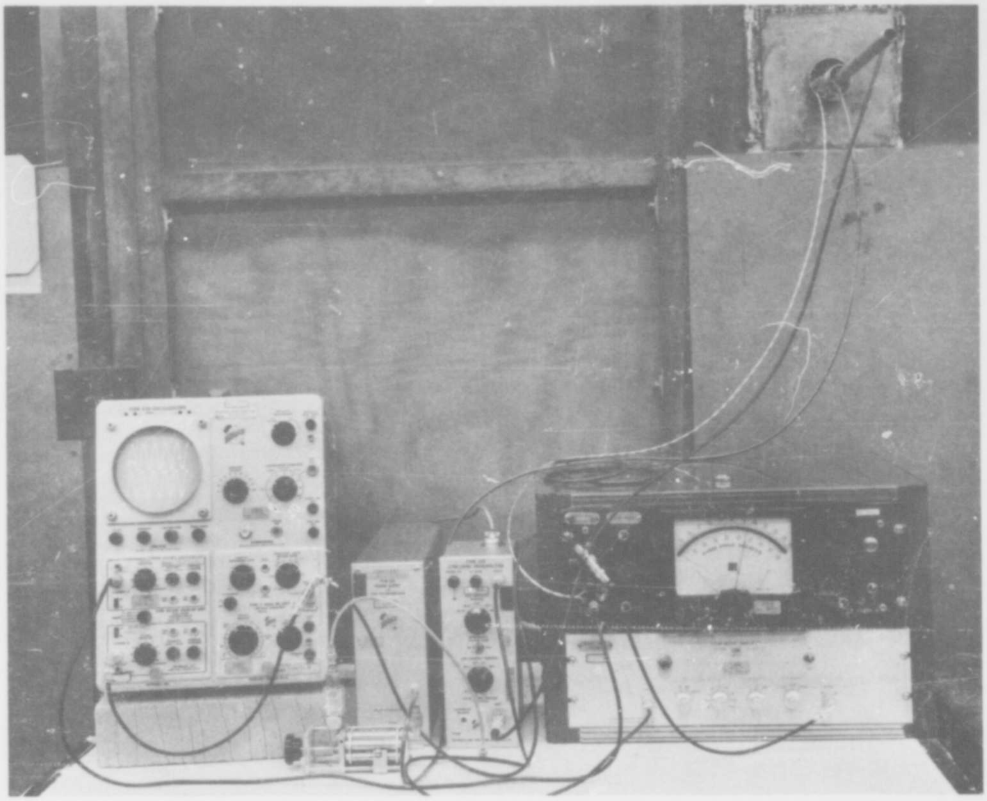

Fig. 36 Phase Angle Determination Equipment, Direct Reading Method

meter, with the sampling coil, it would be possible to read-out the phase angle directly. A phase shifter was not constructed, due mainly to the wide range of test frequencies; the substraction process effectively cancels all amplifier phase shift. A connection to the Helmholtz coil current source provides sufficient reference signal for the phase meter at each frequency to 100 kcs. Figs. 38 and 39 show sample phase-versus-frequency plots for enclosures numbered 15 and 53 respectively, using the "direct-reading" technique. When the sampling coil is rotated 180 degrees in the field, data for transposed plots are obtained.

7.4 Measurement Techniques

The basic technique used in making measurements of shielding effectiveness at all frequencies was that of determining the decibel level of an electromagnetic field at a point in space but surrounded by a shielding enclosure, then comparing that level with one obtained in the absence of a shielding enclosure. The difference represents the measure of the effectiveness of the shield in the presence of an electromagnetic field at a given frequency.

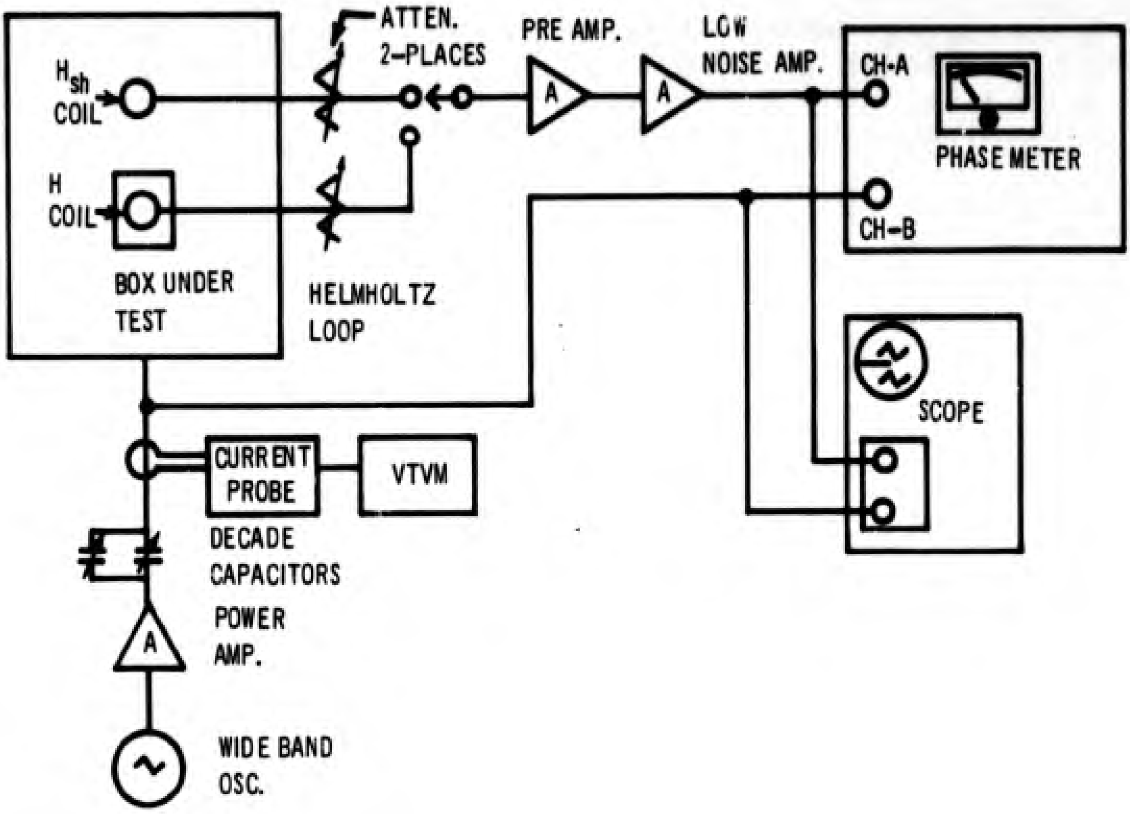

Fig. 37 Phase Comparator Block Hook-Up Diagram

7.4.1 VLF–LF Field Measurements (50 cps–200 kc). All measurements of shielding effectiveness, up to 200 kc, were accomplished within a modified Helmholtz coil (Figs. 20 and 21). The field within the coil was produced by a constant 1-ampere current at all frequencies; the latter required adjustment to compensate for the presence or absence of the box. Without a test enclosure, the magnetic-sensing loop was located at the geometric center of the exterior excitation coil and coaxial to it. Field strength was measured at each frequency. Background noise level was determined by first removing the pickup loop and shorting the coaxial cable. Unusually high background levels were usually the result of inadequacy of the setup or an indication that the field intensity receivers required maintenance. Next, the sensing loop was placed at the geometric center of a test enclosure and so oriented that it would be coaxial with the excitation coils when the longitudinal axis of the enclosure was parallel to the magnetic field of the external excitation coils. This relationship of antennas-to-enclosure provided maximum sensitivity while it minimized the effect of the access seam on shielding effectiveness data.

7.4.1.1 Reflection Loss. Even though the magnetic field is uniform within the test region, the wave impedance is not uniform. Therefore, a shielding surface at one location in the test setup will exhibit an apparent different value of shielding effectiveness than the same surface at another location. This is due to a change in reflection loss. At any location, and for all but the lowest frequencies, the reflection-loss term R in the expression for shielding effectiveness is given by equation (44). Because the wave impedance could double from one size box to a box of the next larger size, an increase in R of 6 db could result. A correction is then necessary, to compensate for the effect of the test setup, when a test specimen is compared with one of the next larger size.

7.4.2 UHF Measurements at Approximately 1Gc. As is shown in Fig. 24, the log periodic antenna and the interior 2-inch monopole were so located that a 22-inch spacing existed between the monopole and that element of the transmitting array which carried the greatest current. The monopole was in the far field and parallel to the elements of the transmitting array. Data was taken both with and without the test enclosure; also, with the antenna pointed at both the top and bottom of the enclosure. The latter technique proved to be valuable in assessing the integrity of the lid closure. Primarily because the enclosure access seam and the bottom seams were dissimilar, a variation in measured shielding effectiveness of 1, 2, or even greater than 6 db was detected between cover and bottom illumination.

7.4.2.1 Measurements at Enclosure Resonance. Resonance of the 6 x 8 x 10 inch test enclosures was calculated to be 944 Mc. Considered as a high-Q cavity, there should have been a radical change in shielding effectiveness or a change in VSWR of the received signal at or near this frequency. Neither could be detected in this first trial. Later, actual resonant frequency of the enclosures was established by directly exciting the cavity with the 2-inch monopole connected to a pulse modulated HP-614A UHF Signal Generator. A one-turn loop was placed in the cavity at the point of maximum magnetic field. The detected signal was rectified by a crystal detector and fed to a standing wave indicator. The lowest resonant frequency noted was 912 Mc (within 4 percent of that previously calculated). Measurements of S values were never accomplished for reasons presented in Section 7.1.2.5.

7.4.3 Measurements at Approximately 10 Gc. Time economies in the collection of data were achieved by the direct plotting of measured field inside the test enclosure as the enclosure was rotated 360 degrees. Test frequency was 9.4 Gc. The X-band instrumentation configuration used in obtaining antenna-pattern type field plots of Appendix C is shown in Fig. 27. The zero-angle rotational reference for the test enclosure is shown at the top center of each field plot. Fig. 40 shows that, at the reference, energy from the transmitting horn was incident to the bottom of the test enclosure. As an enclosure was rotated clockwise (looking into the anechoic chamber as in Fig. 41) the polar recording chart was rotated clockwise beneath the plotter thereby producing the field plots as shown in Appendix C. Generally, maximum energy penetrated an enclosure having "airtight" fixed seams, through the access seam. Maximum signal level within the enclosure then was generally measured at the zero-angle reference position due to such leakage through the lid-closure gaps.

7.4.3.1 Computing Minimum Shielding Effectiveness. Since the field level within a test enclosure varied as the enclosure was rotated about the axis of the sensing monopole, the angle of maximum signal representing minimum shielding effectiveness is the worst case; thus, shielding effectiveness (minimum S) is calculated at that angle. Minimum values of S were thought to result from closure leakage for most enclosures tested and is primarily a measure of the integrity of both the fixed and access seams at 9.4 Gc. Computation of S was

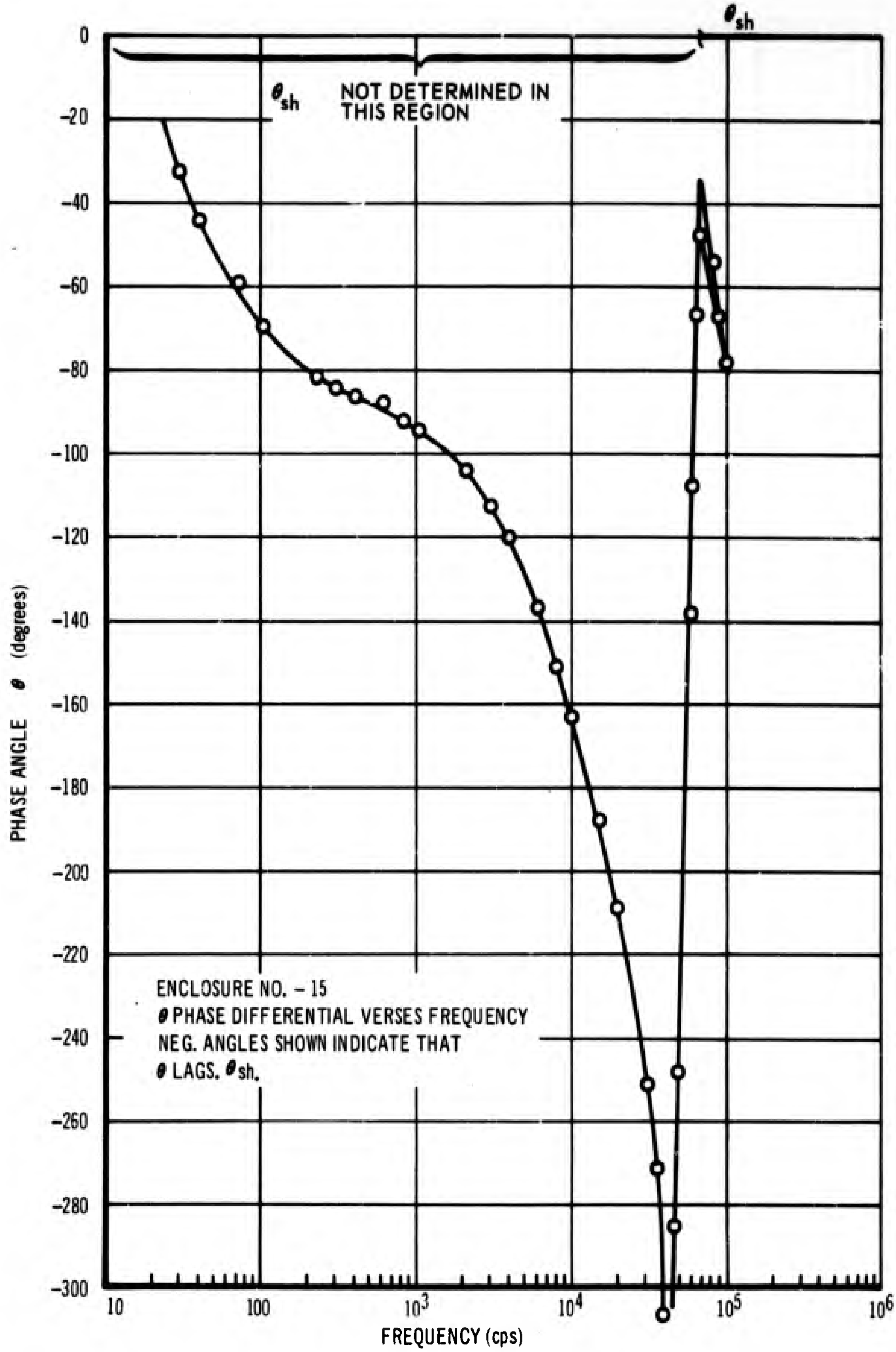

Fig. 38 **Enclosure No. – 15** ***θ PHASE DIFFERENTIAL VERSES FREQUENCY***

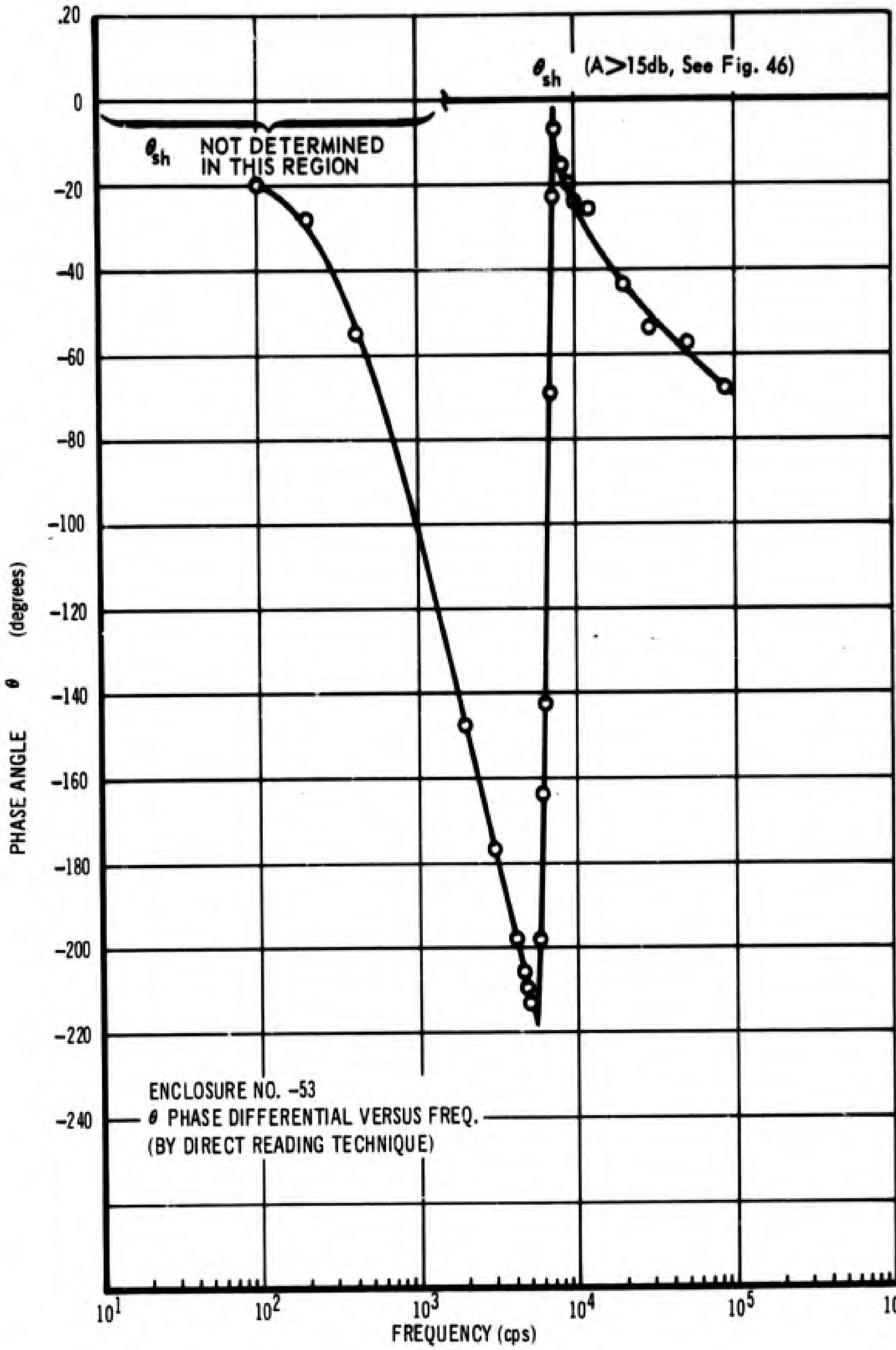

Fig. 39 Enclosure No. −53 θ PHASE DIFFERENTIAL VERSUS FREQUENCY

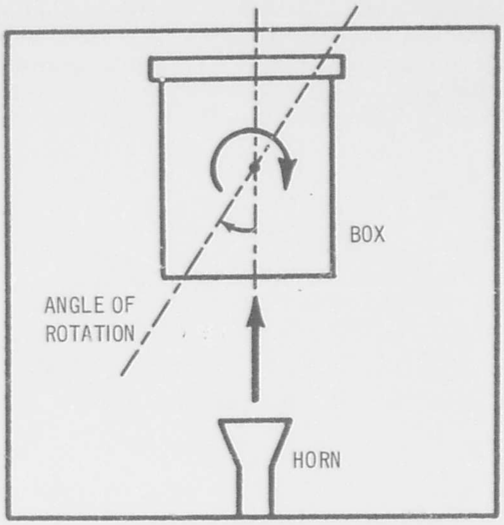

Fig. 40 Transmitting Horn, Test Enclosure Relationship At The Zero–Angle Rotational Reference

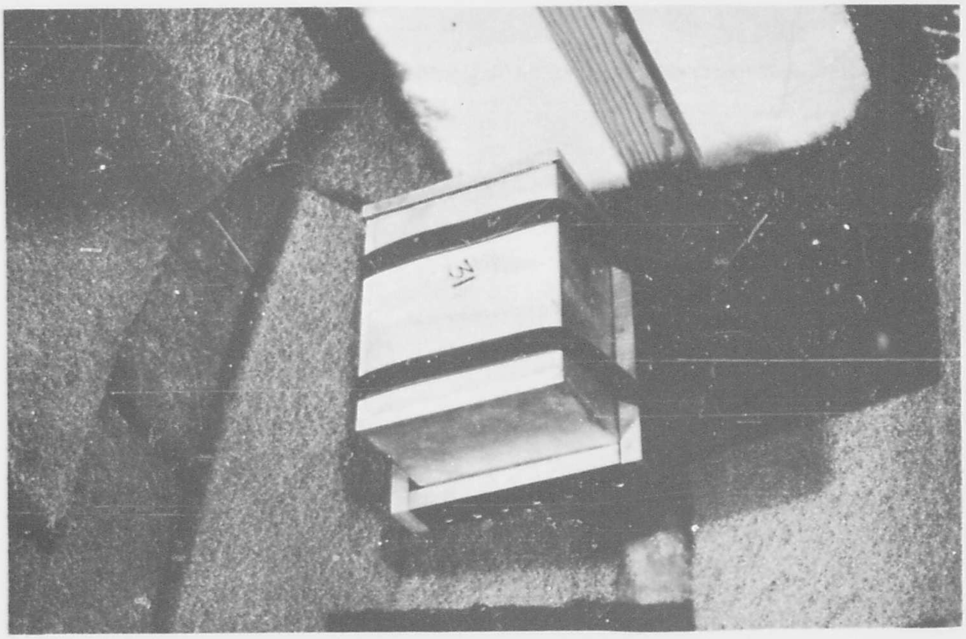

Fig. 41 10 Gigacycle Test Setup – Interior View accomplished by adding the receiver input attenuation value to the maximum signal level picked up inside the shielded enclosure recorded on the field plot shown in Fig. 42. Subtract the sum from the field level measured in the absence of the test enclosure: the difference is the measure of minimum shielding effectiveness of the enclosure. Unless specifically stated otherwise, figures used in further discussions of measurements made at 9.4 Gc, are relative to minimum S.

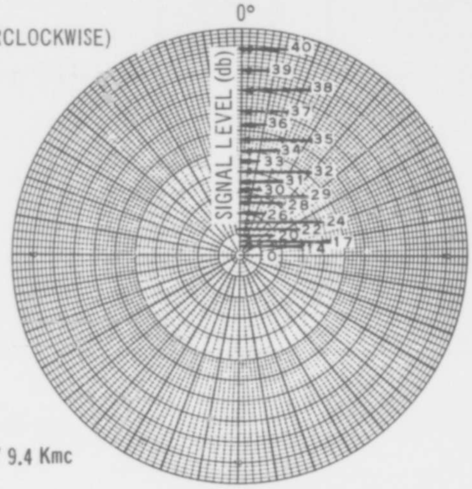

Fig. 42 X–Band Field Pattern Data Interpolation Chart

7.5 Establishing Experimental Reference Standards

7.5.1 Standard Box. At the beginning of the Study program, one test enclosure was designated as a reference standard, against which the performance of all other enclosures could be compared. Box No. 3 was selected. It has been described in Paragraph 7.2.1.1.

7.5.2 Antenna Locations. First tests made with this box were for the purpose of determining how and where to locate the magnetic sensing antennas inside the enclosures for future measurements; it seemed reasonable to expect that measured shielding effectiveness would vary somewhat with the location of the loop within the enclosure. To minimize the multitude of possible antenna locations and the corresponding amount of measurement effort which conceivably would be required, five representative antenna locations were selected for investigation: (Fig. 43)

Position No. 1, the geometric center of a test enclosure, was expected to provide data indicative of the maximum shielding effectiveness and to yield the most stable and repeatable test readings.

Position No. 2, the center of a side, was expected to prove somewhat less satisfactory than No. 1. All data presented in this report for Position No. 2 was measured at the center of the 8 x 10 inch side opposite the penetration (or entry) point.

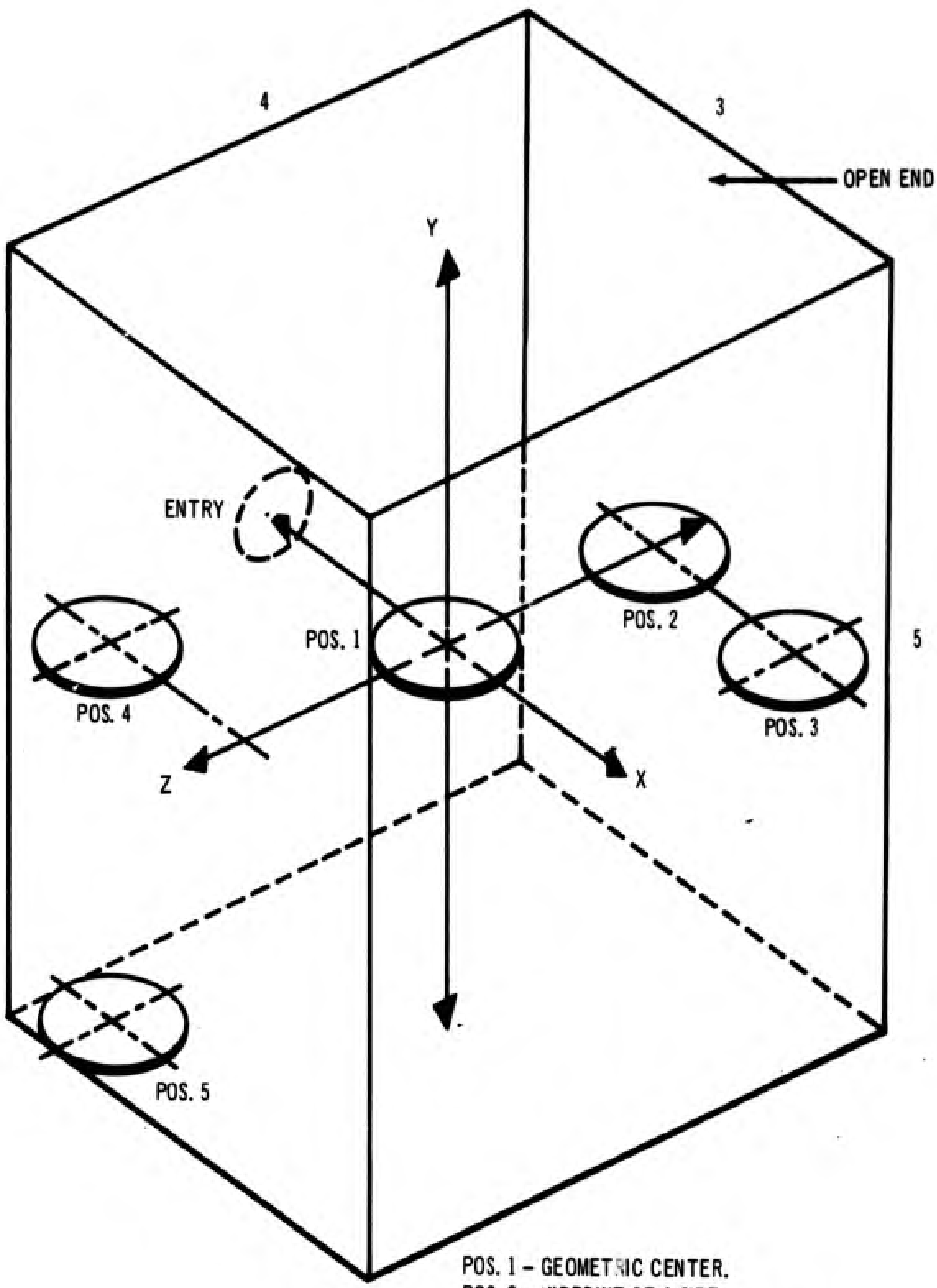

POS. 1 – GEOMETRIC CENTER.
POS. 2 – MIDPOINT OF A SIDE.
POS. 3 – SEAMLESS DIHEDRAL CORNER.
POS. 4 – DIHEDRAL CORNER SEAM.
POS. 5 – TRIHEDRAL CORNER SEAM.

Fig. 43 Standardized Magnetic-Sensing Antenna Locations

Position No. 3 designates the midpoint of a seamless dihedral edge.

Position No. 4 identifies a location similar to No. 3 except at a dihedral edge seam.

Position No. 5 is at a trihedral corner seam; the loop antenna is laid flush against the side which is oriented at right angles to the magnetic field of the exterior excitation coil.

7.5.3 Derivation of Standard Reference Data. Shielding effectiveness data were obtained for each of the five antenna locations described above over a frequency range of 50 cycles to 200 kilocycles. A typical data sheet for Position No. 1 (Table E) describes how the indicated effective shielding of Box No. 3, at that antenna location, was determined. A side-by-side tabulation of data obtained for all five antenna positions (Table F) provided comparative proof that the shielding effectiveness within an enclosure is essentially constant at a given frequency except in trihedral corners (Position No. 5). Measured data indicated no variance of more than ±1 decibel in shielding effectiveness among the other four positions. The Reference-Standard Data column of Table F was established by taking the average value of data obtained in the first four antenna positions, adjusted to the nearest 0.5 db. (Note: As measurements techniques were refined, the accuracy of collected data improved over that shown.)

The field inside a test enclosure was found to be essentially uniform except as noted. Accordingly shielding effectiveness data were obtained with the magnetic sensing antenna located in Position No. 1 (Fig. 43) throughout the Study program. Evaluation of shielding effectiveness factors is presented in the sequence in which they were studied.

7.5.3.1 Shielding Deterioration at Trihedral Corners. Shielding deterioration at trihedral corners had not been considered a "shielding effectiveness factor." Theory indicates that such deterioration does occur but that it is negligible. However, review of data (Table G) shows that shielding effectiveness measured at Position 5 was generally 10 db less than that for the enclosure as a whole and is therefore of considerable consequence. Theory was developed only for the purpose of showing that indicated variations in shielding effectiveness attributable to variations in wave impedance, over a shielding surface of 6 x 8 x 10 inches dimensions, would be minor. However, penetration loss is probably the significant factor and may be explained qualitatively as follows: In Detail A-A, Fig 44, it can be seen that current in those walls of an enclosure which are parallel to the excitation magnetic field flows uniformly around the corners of the enclosure.

As shown in Detail B-B however, the current in those walls of an enclosure which are perpendicular to the excitation magnetic field does not flow uniformly in lines parallel to the extreme edges of the wall but in fact tends to flow across the corners rather than go around them. Since the shield is a conductor penetration is actually by current (covered by field equations) which sets up the field inside the box. Proximity to the increased penetration at the top and bottom (plus alteration of current paths) produces a different shielding effectiveness in position #5.

Table E Typical Measured Data, Box No. 3, Antenna Position No. 1

FREQUENCY	FIELD WITHIN COIL *	MEASURING SYSTEM BACKGROUND NOISE LEVEL		RECEIVER ATTENUATER SETTING db.	INDICATED SIGNAL LEVEL*	CORRECTION FACTOR db.	RECEIVED SIGNAL LEVEL*	EFFECTIVE SHIELDING Decibels db.
		Sig. Gen. OFF*	Sig. Gen ON*					
50 cps.	16	2	2	0	35	-20	15	1
100 cps.	22	-13	-13	20	18	-20	18	4
200 cps.	28	-15	-15	20	20	-20	20	8
400 cps.	34	-5	-5	20	20	-20	20	14
800 cps.	39.5	-14	-14	20	20	-20	20	19.5
1000 cps.	41	-13	-13	20	19.5	-20	19.5	21.5
1.6 kc	46	-16	-15	20	20	-20	20	26
2.4 kc.	49	-17	-15	20	20	-20	20	29
3.2 kc.	52	-17	-15	20	20	-20	20	32
4.5 kc.	55	-17	-15	20	20	-20	20	35
6.4 kc.	57	-17	-15	20	20	-20	20	37
9.0 kc.	61	-18	-14	20	20	-20	20	11
12 kc.	63.5	-18	-14	20	20	-20	20	43.5
25 kc.	65.5	-5	-4	20	0.5	none	20.5	45
55 kc.	68	-5	-5	20	0.5	none	20.5	47.5
45 kc.	69.5	-5	-5	0	17	none	17	52.5
50 kc.	76	-6	-4	0	16	none	16	60
60 kc.	73	-6	-4	0	15	none	15	58
100 kc.	80	-6	-5	0	11	none	11	69
150 kc.	83	-21	-6	0	7	none	7	76
200 kc.	85	-21	-6	0	3	none	3	82

*All data are referenced to decibels above 1 μ volt.

Table F **Derivation of Reference – Standard Data**

FREQUENCY	ANTENNA POSITION					REFERENCE-STANDARD DATA*	TOLERANCE
	NO. 1	NO. 2	NO. 3	NO. 4	NO. 5		
50 cps.	1 db.	1 db.	1 db.	1 db.	0 db.	1 db.	0
100 cps.	4	3.5	3	4	2	3.5	± 1/2 db.
200 cps.	8	8	7.5	8	4	8	± 1/2
400 cps.	14	13	12.5	13	6	13	± 1
800 cps.	19.5	18.5	18.5	19	10	19	± 1/2
1600 cps.	26	25.5	25	25.5	15.5	25.5	± 1/2
3200 cps.	32	31.5	31	31.5	21.5	31.5	± 1/2
6400 cps.	37	37	36.5	37	27	37	± 1/2
12 kc.	43.5	43	42	43	33	43	± 1
25 kc.	45	45	45	44.5	35.5	45	± 1/2
50 kc.	60	60.5	59.5	60.5	48.5	60	± 1/2
100 kc.	69	69	68.5	70	58.5	69	± 1
200 kc.	82	82	81.5	83	73	82	± 1

*Data from Pos. 1 thru 4 adjusted.

All data obtained from Test Enclosure No. 3.

Table G **Deterioration in Shielding Effectiveness of an Enclosure at Trihedral Corners**

FREQUENCY	ANTENNA POSITION NO.5 BOX 3	REFERENCE STANDARD DATA	COMPARABLE SHIELDING EFFECTIVENESS OF POS. 5
50 cps.	0 db.	1 db.	-1 db.
100 cps.	2	3.5	-1.5
200 cps.	4	8	-4
400 cps.	6	13	-7
800 cps.	10	19	-9
1600 cps.	15.5	25.5	-10
3200 cps.	21.5	31.5	-10
6400 cps.	27	37	-10
12 kc.	33	43	-10
25 kc.	35.5	45	-9.5
50 kc.	48.5	60	-11.5
100 kc.	58.5	69	-11.5
200 kc.	73	82	-9

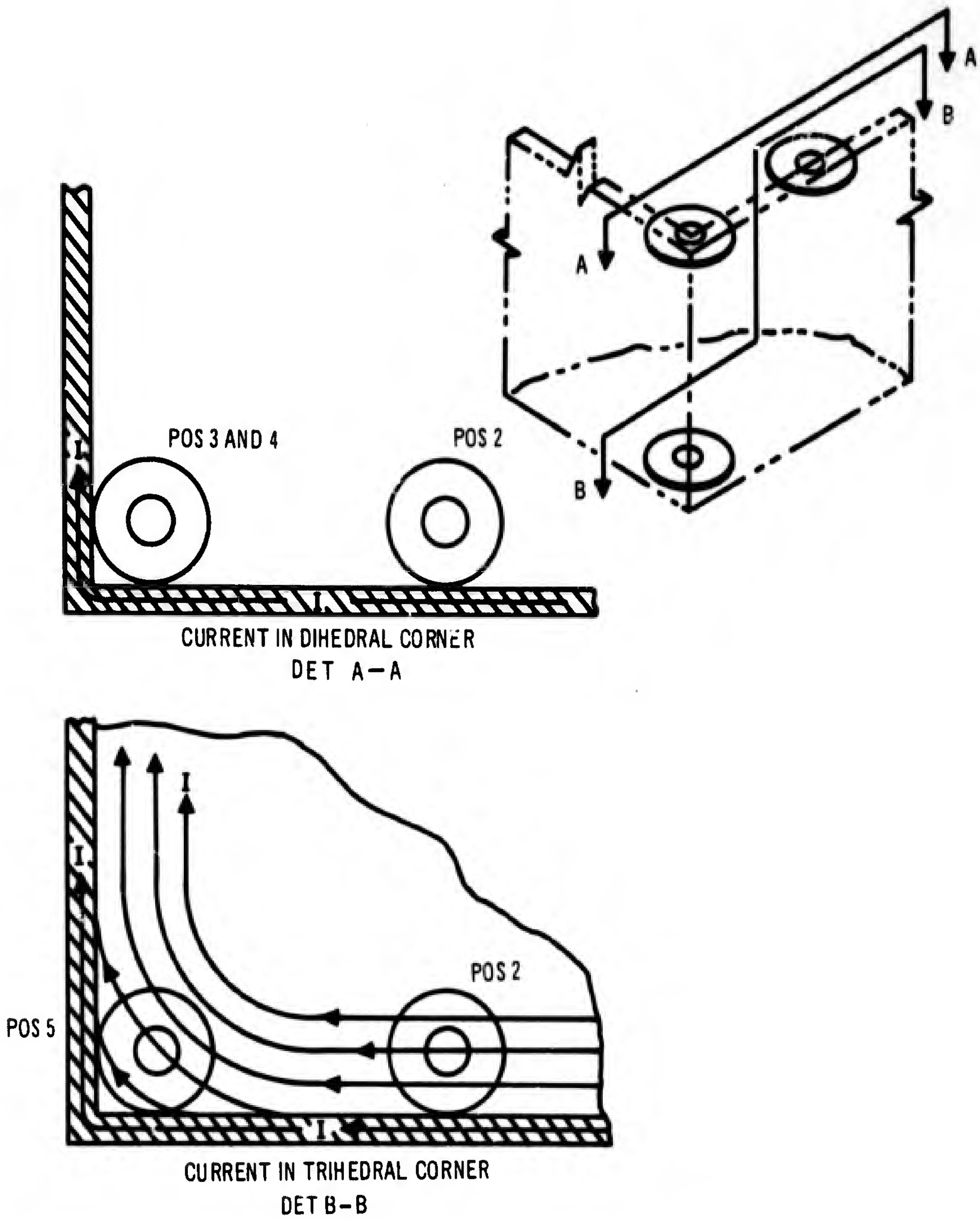

Fig. 44 Comparison of Induced Flow About Dihedral and Triheadral Corners

8.0 FACTUAL DATA - DERIVATION OF RESULTS

This section of the report details how the theoretical considerations of Sections 5.0 and 6.0 are applied to the experimental data of Appendices A through C in order to obtain the shielding parameters of use in design.

8.1 Material Factor S_1

From Section 5.0, $S_1 = A_1 + R_1 + B_1$ where the subscript 1 applies to material (See Table A Section 6.0), ℓ to laminated material, and ℓ_n to n laminations of material. It is convenient to consider A, R and B separately in the derivation process and to combine them later by simple addition in order to obtain the material factor S_1.

8.1.1 General Term Separation Technique A general technique for separation of shielding terms A_1, R_1, B_1, uses a lamination of n shielding layers, where n is any number greater than one. The technique is illustrated in Fig. 45.

The measurement steps are:

(1) Measure the effectiveness, S_1, of a single sheet at some frequency, f_1, at which its penetration-loss term, A_1, is known to be greater than 15 db.

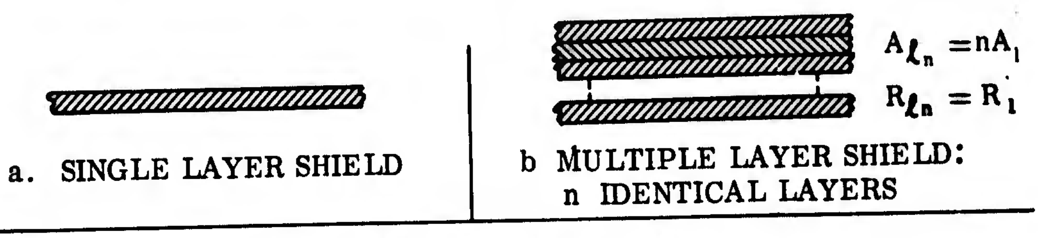

At f_1, $B \approx 0$ FOR $A_1 > 15$db

$$S_1 = R_1 + A_1$$

$$S_{\ell_n} = R_1 + nA_1$$

At f_2 For $A_1 < 15$db, $B_1 \neq 0$: $S_1 = R_1 + A_1 + B_1$

For $nA_{\ell_n} > 15$db, $B_{\ell_n} = 0$: $S_{\ell_n} = R_1 + nA_1$

Fig. 45 Experimental Separation of A + R + B Parameters

(2) At the same frequency, measure the shielding effectiveness, S_n, of n thicknesses of the shielding barrier in intimate contact (or a single sheet n times as thick as the original single sheet). Under this condition, the total reflection loss will be the same as for step (1) since there are only two shielding interfaces, see (eq. 86). $R_1 = R_{\ell n}$

(3) Calculate the penetration loss, A_1 of a single sheet and the reflection loss from both interfaces, R_1. Note that $A_{\ell n} = nA_1$

$$\left.\begin{array}{l} A_1 = \dfrac{S_{\ell n} - S_1}{n-1} \\ \\ R_1 = \dfrac{nS_1 - S_{\ell n}}{n-1} \end{array}\right\} \text{ at } f_1 \qquad (164)$$

(4) At a lower frequency, f_2, at which the penetration loss for a single shield is less than 15 db, but for n multiple layers is greater than 15 db, again measure the shielding effectiveness, $S_{\ell n}$ of this combination as well as S_1 for a single sheet.

(5) Perform the following calculations for the single-sheet values at frequency f_2.

$$A_1(\text{at } f_2) = A_1(\text{at } f_1)\sqrt{\frac{f_2}{f_1}}$$

$$R_1(\text{at } f_2) = R_{\ell n}(\text{at } f_2) = S_{\ell n}(\text{at } f_2) - nA_1(\text{at } f_1)\sqrt{\frac{f_2}{f_1}} \qquad (165)$$

$$B_1(\text{at } f_2) = S_1(\text{at } f_2) - A_1(\text{at } f_2) - R_1(\text{at } f_2)$$

$$= S_1(\text{at } f_2) + (n+1)A_1(\text{at } f_1)\sqrt{\frac{f_2}{f_1}} - S_{\ell n}(\text{at } f_2)$$

8.1.2 Use of Term Separation to Obtain Permeability The permeability μ_1, of S3-Netic material was determined using Box #53. Two 10-turn coils were coaxially aligned one on each side of the material under test and centered with it. The three measurements were conducted as described above and in Par. 7.3.6. For the airgap measurement, fiberglass was substituted as a separator; for the double thickness condition, the enclosure cover was rigidly clamped to the enclosure side surface so that no airgaps existed. Measurements for a frequency of 10 kc are shown in Table H. From the previous paragraph, and paragraph 5.1,

$$A_1 = \frac{S_2 - S_1}{2-1} = \ell\sqrt{f}\cdot\sqrt{\mu_r\,\sigma_r}\left(131\ \frac{\text{db}}{\text{m}}\frac{1}{\sqrt{\text{cps}}}\right), \qquad (166)$$

where A_1 is the penetration loss of composition and 2 is the number of material thicknesses in the test. To apply the relationship, it is necessary that

$$A_1 \geqq 15\,\text{db}.$$

Table H Permeability Determination, Signal Measurements of Enclosure Number 53, S3-Netic Material

Frequency	10 kcs
*Airgap	81.5 dbμv
Single Thickness	38 dbμv
Double Thickness	-0.3 dbμv
S_1 = 81.5 - 38 = 43.5 db	
$S_{\ell 2}$ = 81.5 + 0.3 = 81.8 db	

*This measurement for information only.

The other quantities are defined by convention. Then,

$$\mu_r = \left[\frac{(S_2 - S_1)}{131 \text{ db } \ell\sqrt{f\sigma_r}}\right]^2 \text{ henries/meter} \tag{167}$$

For the Netic material at a frequency f of 10 kc, S_1 and $S_{\ell 2}$ were calculated to be 43.5 db and 81.8 db respectively. The conductivity σ_r from previous laboratory measurements was determined to be 0.14487 referenced to the material copper. Therefore,

$$\mu_r = \left[\frac{(81.8 - 43.5)\ \text{m}\sqrt{\text{cps}}\ 39.7\,\text{in}}{(131.)(21.9)\,10^{-3}\,\text{in}\sqrt{10^4\,\text{cps}}\sqrt{0.145\,\text{m}}}\right]^2$$

$$= [13.76]^2. \tag{168}$$

NOTE: As mentioned in 7.3.7.1, a coil measuring the field entering the shield, actually measures the incident plus reflected fields and not simply the incident value for which S is defined. However for A $\geq$ 15db, the resultant reflected field is negligible because of cancellation and the result is as shown.

8.1.3 Penetration Loss A_1 Various techniques are available for determining the penetration loss A_1 of which one is given in Paragraph 8.1.1. Another approach is one wherein two curves of shielding effectiveness as a function of frequency are obtained for any given material, one for a single thickness and another for a double thickness of that material. Such curves were obtained by means of the experimental techniques of the previous paragraph for Netic material only, but

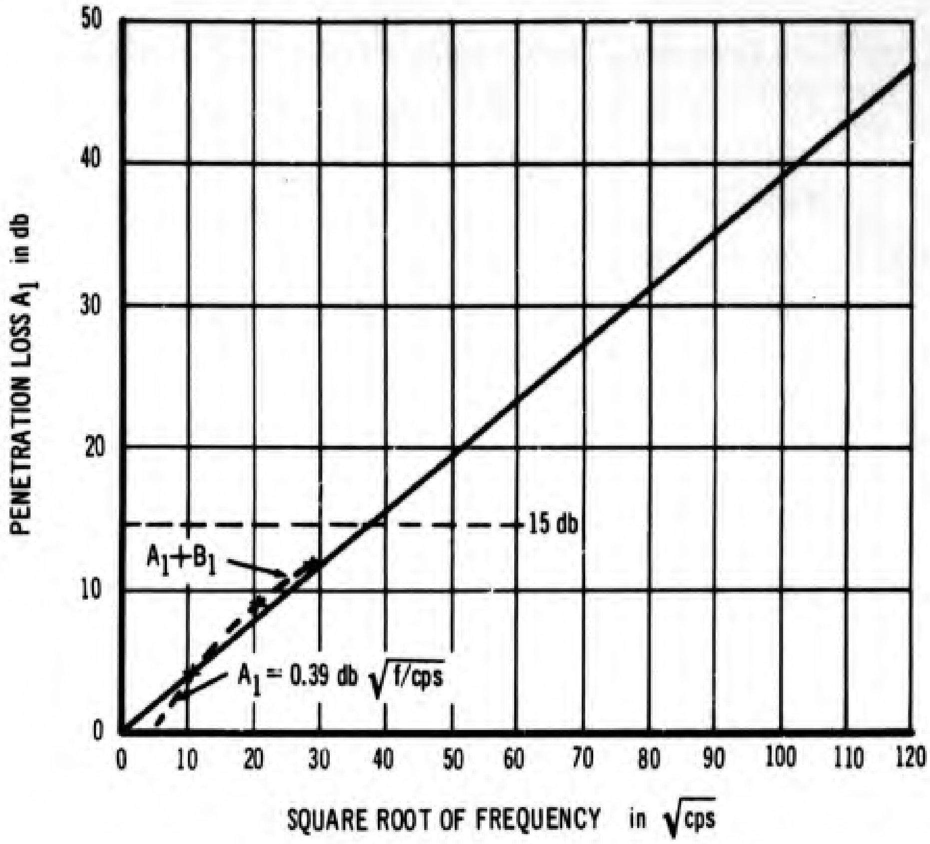

Fig. 46 Penetration Loss and Penetration Loss Plus Correction Term For Netic Material of Box # 53

the same approach would be required for any high permeability shielding material. Data obtained by this approach for the Netic material are given in Appendix A, Fig. A16. In order to obtain the penetration loss A_1 from these data, it is necessary to subtract one curve from the other. When this is done and the result is plotted as a function of square root of frequency, Fig. 46 results. The straight line portion of this curve which passes through the origin is the desired penetration loss A_1.

This same technique may be used to obtain a penetration loss for nonmagnetic materials. For nonmagnetic materials the initial magnetic permeability is the same as that of air and the penetration loss factor may be readily calculated from a knowledge of material electrical conductivity. The expressions used in this case are simply equations (5) and (8) of the theoretical derivation. This approach has been used to calculate the design parameters for nonmagnetic materials given in Paragraph 9. 1.

8.1.4 Reflection Loss R_1 It might appear upon first consideration that the reflection loss term R_1 could be obtained by simple subtraction of A_1 already obtained from the material factor S_1, the single-thickness curve of Fig. A16, Appendix A. Such is not the case since as has been pointed out, a true S_1 has not been measured. Also S_1 depends on the incident, reflected and emerging wave impedances which vary with the measurement setup used. If the wave impedance of any setup is known it is necessary only to determine the intrinsic impedance η_w of the shielding material in order to obtain the impedance ratio k_1 and, from this, the reflection loss factor R_1.

For magnetic materials, it is necessary to obtain $\sqrt{\mu_r \sigma_r}$. The value of $\sqrt{\mu_r \sigma_r}$ is obtainable from the penetration loss factor A_1 by means of equations (5) and (8) and (18). Hence, measured values of electrical conductivity may be used to yield $\frac{1}{\sigma_r}\sqrt{\mu_r \sigma_r} = \sqrt{\frac{\mu_r}{\sigma_r}}$ from which k_1 may then be calculated, and then R_1.

8.1.4.1 A second approach for nonmagnetic materials is basically similar except that the initial magnetic permeability μ is already known to be the same as that of air and need not be determined from a measurement of A_1. The electrical conductivity σ is known from either measurement or handbook data and, consequently, successive calculations of A_1, k_1, and R_1 can proceed directly.

Intrinsic impedances η of the various materials measured in the program were obtained in this manner and are plotted in Figs. 47 and 48 for presentation in Paragraph 9.1. The impedance ratio k_1 is also plotted vs η for low impedance values of Z_W in Fig. 48 and for $Z_W = \eta_0$ in Fig. 49. The value of R_1 calculated from Eq.(47) is plotted in Fig. 48 and from Eq.(44) is plotted in Fig. 49. An example of how to find R_1 using Cu and $|Z_W| = 0.1$ ohm is shown in Fig. 48.

8.1.5 Correction Term B_1

The correction term B_1 is, for most applications, of minor significance and yet it is the most difficult of all to obtain since it depends upon both A_1 and k_1. If A_1 is greater than approximately 15 db, the correction factor B_1, as obtained from expression (72) is negligible. For A_1 less than 15 db, two different cases may be distinguished for obtaining B_1. In both of these, cases it is necessary first to obtain the value of the impedance ratio k_1. If k_1 is either very much larger than one or very much less than one, then B_1 is independent of k_1 and may be determined directly from A_1 in accordance with equation (73).

It is this case which has been plotted in Section 9.1 for the material factor. For the rare case where k_1 is of the order of one, the expanded equation (65) must be utilized in order to obtain B_1. As an aid to this calculation, a χ factor has been plotted on Fig. 7 of Reference 2 to express the variation with k_1 for a dipole source.

8.2 Shielding Multiplicity Term ΔS_m

It has been shown from the theoretical section that the shielding effectiveness for multiple shields is the sum of the separate penetration loss terms, the incident and emerging reflection loss terms and a correction term called the shielding multiplicity term ΔS_m represented by Eq.(105).

In the low frequency region below 200 kc, the quantity $\beta_0 \ell_2$ is much less than one and, provided A_1 and A_3 are each greater than 10 db, equation (103) is valid for a double shield.

Note: It is important to note that equation (109) is not valid for $\beta_0 \ell_2 Z_w/\eta_{w3} \rightarrow O$:

as $\beta_0 \ell_2 \rightarrow O$, $\Delta S_m \rightarrow 20 \log_{10} \left(\frac{\eta_{w1} + \eta_{w3}}{2\eta_{w3}} \right)$ and ΔS_m is determined by

p alone since in expression (106b) $Z_{T1} \rightarrow \eta_{w3}$ as $\beta_0 \ell_2 \rightarrow O$; including equation (106a), $\Delta S_m \rightarrow O$.

In the higher frequency region where $\beta_0 \ell_2$ is not negligible, and from expression (83),

$$q_2 \simeq 1 \text{ for } \eta_{w3} < .1 \, Z_w,$$

so that

$$\Delta S_{m2} = 10 \log 2. \left(1 - \cos 4\pi \frac{\ell_2}{\lambda_0}\right) \text{(db)}$$

and from (105), (107)

$$\Delta S_{m2} = 115\,\text{db} - 10 \log_{10} f/_{Mc} + 10 \log_{10} \left(1 - \cos \frac{4\pi \ell_2}{\lambda_0}\right) \text{(db)} \tag{169}$$

The last term of this relationship is plotted on Fig. 49.

8.3 Lamination Term S_ℓ, ΔS_ℓ

For laminated materials it was shown in the theoretical Section 5.4 that the total shielding effectiveness is the sum of the separate penetration losses and reflection losses at each interface of the individual lamina plus re-reflection terms. Laminated shielding is considered to be the same as multiple shielding in which the air spaces have been shrunk to zero. The total shielding effectiveness of the laminations is $S_\ell = A_\ell + R_\ell + B_\ell$ (see 5.3, 5.4), but the $\Delta S_\ell = S_\ell - S_1$ comparison to a single shield is of greater interest.

8.4 Material Configuration Factor S_2

The material configuration factor accounts for bypassing energy in much the same manner as the fixed-seam factor S_5. It is obtained from the same expression as in Par. 6.1 if the subscript 5 is replaced by 2. Because of the lack lack of experimental data, these relationships are given in Fig. 50 on the basis of assumptions discussed in Par. 9.4.

8.5 Shape Factor S_3

It was anticipated that the shape of an enclosure would influence, to some extent, its shielding effectiveness. Five test enclosures were designed to aid in the isolation of a "shape" factor, numbers 5, 8, 9, 10, and 70. All were made of 0.0243 inch thick ETP copper and were rectangular, cubic, "L", cylindrical, and spherical in shape. All seams were soldered and all enclosures except the sphere had four rows of fingerstock at the lid closure seam. Dimensions were selected so that all boxes were roughly equal in size varying only 17 percent maximum in volume and total surface area from the standard reference, Box No. 3 (Table J). Therefore all test enclosures in this group were exposed to electromagnetic waves of approximately equal impedances at the surfaces of the enclosures. Data tabulated in Table K indicate that the measured shielding effectivenesses of these boxes were equal within ±1 db and their adjusted average value differed only ±0.5 db maximum from Standard-Reference Data. Shape of an enclosure then has no effect on shielding effectiveness.

8.6 Size Factor S

The simplest variable factor which might be expected to affect the shielding effectiveness of an enclosure was thought to be that of physical dimensions. To isolate such factor, a comparison of data obtained from Test Enclosures No. 1, 2, 3, and 4 was initiated. It can be seen in Table L that much of the data taken between 1 kc and 200 kc indicates that shielding effectiveness doubled as the physical dimensions of the test boxes were doubled (6 ± 1 db). It would be a false conclusion that size, of itself, is responsible for variations in shielding effectiveness. Actually, variation of low-frequency data with variation in physical size has proved to result only from differences in impedance of the magnetic wave front present at the faces of enclosures of various sizes. Simply stated, the shielding effectiveness of an enclosure below 200 kc is generally independent of its physical dimensions. However, at higher frequencies the dimensions of an enclosure do determine its resonant frequency as a cavity and, although not experimentally proved in this program, it is believed that shielding effectiveness is considerably reduced at and very near the resonant frequencies (TE_{101} mode and higher).

8.7 Fixed-Seam Factor S_5

From theoretical equations (123) and (130), it is apparent that the determination of the fixed-seam factor S_5 is dependent upon knowledge of the material phase angle θ_1 and either the net phase angle θ or the fixed-seam phase angle θ_5. Once these phase angles have been determined, it is a simple matter of substitution in one of these equations in order to obtain the fixed-seam factor S_5. Consequently, the discussion of the following paragraphs is with respect to obtaining the required phase angles.

8.7.1 Net Phase Angle The net phase angle θ is determined directly from measured data obtained in accordance with Paragraph 7.3.7 and with values for several materials given in Figs. 38 and 39. In the two experimental techniques presented, the technique involving direct phase measurement by means of a phase angle meter apparently yields superior results and also provides direct results. However, where a phase angle meter is not available, the other approach uses a direct measurement of the field components and makes possible a determination of the net phase angle θ by use of the law of cosines, equation (163).

8.7.2 Material Phase Angle θ_1 The material phase angle θ_1 is a function of both the penetration loss A_1 (= $8.686\, \alpha_1 \ell_1$) and the impedance ratio k_1. From a knowledge of these quantities previously determined, θ_1 may be calculated directly. (Since in 7.3.7 θ is measured for incident plus reflected fields and not just incident, θ must be calculated accordingly).

Table J Dimensional Relationships of Antennas and Test Enclosures Used in Determination of "Shape" Factor

PARAMETER	BOX NO. 5	BOX NO. 8	BOX NO. 9	BOX NO. 10	BOX NO. 70	MAXIMUM VARIATION FROM NO. 5	VARIATION EXPRESSED IN DECIBELS
Antenna Dia. to Smallest Dim.	1:6	1:6	1:6	1:7.8	1:10	+67%	4.4db.
Vertical Dim. to Geo. Ctr.	5"	4"	4"	5"	5"	-20%	-1.9
Nearest Side							
to Antenna Rim	2.5"	3.5"	2.5"	3.4"	4.5"	+80%	5.1
to Antenna Ctr.	3.0"	4.0"	3.0"	3.9"	5.0"	+67%	4.4
Farthest Side							
to Antenna Rim	3.5"	3.5"	4.5"	3.4"	uniform	+28%	2.1
to Antenna Ctr.	4.0"	4.0"	5.0"	3.9"	distance	+25%	1.9
Surface Area Parallel to Field	280 sq.in.	256 sq.in.	288 sq.in.	245 sq.in.		-22.5%	-2.2
Total Surface Area	367 sq.in.	384 sq.in.	424 sq.in.	341 sq.in.	314 sq.in.	-16.6%	-1.6
Volume	480 cu.in.	512 cu.in.	544 cu.in.	478 cu.in.	512 cu.in.	+17%	1.4

Table K Relation of Enclosure Shape to Shielding Effectiveness

FREQUENCY	STANDARD REFERENCE DATA	RECTANGULAR BOX NO. 5	SQUARE BOX NO. 8	L-SHAPED BOX NO. 9	CYLINDRICAL BOX NO. 10	SPHERICAL BOX NO. 70	BOX DATA SUMMARY	VARIATION FROM REFERENCE DATA
50 cps.	1 db.	1 db.	1 db.	2 db.	1 db.	0 db.	1 db. ± 1	0 db.
100 cps.	3.5	3	4	4.5	3.5	3.5	3.5 ± 1	0
1000 cps.	21	20	22	21	21.5	21.5	21 ± 1	0
12 Kc.	43	42	43	43	42.5	43.5	42.5 ± 1	+ 1/2
200 Kc.	82	80.5	81	82.5	82.5	82.5	81.5 ± 1	-1/2

Table L Relation of Enclosure Size to Shielding Effectiveness

Frequency	Box No. 1, Pos. No. 1	Box No. 2, Pos. No. 1	Box No. 3, Pos. No. 1	Box No. 4, Pos. No. 1
50 cps	0 db	0 db	1 db	2 db
100 cps	1	2	3.5	6.5
1000 cps	10	15	21	26
12 kc	30	36.5	43	49
200 kc	68	74	82	82.5

8.7.3 Path-Difference Phase Angle $_1\phi_5$ The path-difference phase angle $_1\phi_5$ has been expressed in Paragraph 6.1 as a function of both ϕ and ϕ_1. This relationship is used to calculate $_1\phi_5$ directly.

8.7.4 Fixed-Seam Phase Angle ϕ_5 Since the fixed-seam phase angle ϕ_5 is simple, the difference between ϕ_1 and $_1\phi_5$ it may be calculated directly. (Correction from incident-plus-reflected to incident fields can be made from theoretical considerations or experimental results.)

8.7.5 Use of Phase Angles From these phase angles, an uncorrected fixed-seam factor S_5 is calculated for an experimental setup but must be corrected for more general use in design data. The correction Sa is for the total lineal length of fixed seams exposed to the exciting field in order to obtain a fixed-seam factor for a one-inch length of seam.

$$S_a = 10 \log a, \quad (a = \text{seam length}) \tag{170}$$

which for the 10 inch seams in the particular boxes measured is equal to 10 db. The correction assumes that power (current through the seam at a fixed voltage) is proportional to seam length.

This correction applies to S_5 only and not to S.

The general expression (170) has also been plotted and presented in Paragraph 9.7 for design use with any total length of fixed seams.

8.8 Access-Seam Factor S_6

The determination of the access-seam factor S_6 is quite similar to that for the fixed-seam factor S_5. Since the only type of seam involved is that of spring contact fingers against the metal shielding surface, the curves are plotted for each one of the shielding surfaces. It should also be noted that the data obtained from Appendix A are for either 1, 2 or 4 rows of fingers. When more than 1 row of contact fingers is involved, 20 log m (db) has been subtracted from S where m is the number of rows. There is no theoretical justification for this, especially at VLF and LF where S_1 predominates; however it does permit separation of the curves on the graph. When applying S_6, the quantity 20 log m must be re-inserted.

8.9 Nonuniformity Factor S_7

Insufficient data was obtained in order to plot a curve for a nonuniformity factor; hence, the few data obtainable from Appendix A are presented in tabular form.

8.10 Protrusions Factor S_8 and Filter Factor S_9

No data is available to evaluate these factors although they are required for any complete shielding design.

9.0 FACTUAL DATA - DESIGN PARAMETERS

This section presents parameters derived in accordance with the last section and presented in a form useful for the design of shielding enclosures. It is intended that the various parameters be combined in accordance with equation (134) in order to obtain the overall shielding effectiveness of an enclosure. Each one of the separate S_p factors represents a parallel path for the transmission of electromagnetic energy from the source through the shielding enclosure to a receiving device. One of the shielding effectiveness factors, the material factor S_1, is expressed differently depending upon whether the shielding involved is a single shield, a multiple shield, or a laminated shield. Basic to the expression for this parameter are expressions which enter into S_1 for a single shield. When multiple shields are involved, the form of the single shield data is still useful when combined with a correction term ΔS_m. In the case of laminated shields, the penetration loss and reflection loss terms for single shield materials are again useful when combined with the correction term ΔS_ℓ (Para. 8.2, 8.3).

9.1 Material Factor S_1

The information presented in Figs. 47 and 51 is for a single shielding layer.

9.1.1 Arrangement of Data Fig. 51 has plotted on the right hand side both penetration loss curves for various materials and penetration loss plus correction or re-reflection loss values for these materials as functions of the product of material thickness and square root of frequency. In this method of plotting, all of the penetration loss curves are straight lines passing through the origin. Any deviation of the solid lines from this straight line is caused by the re-reflection loss term B, and, in these instances, it is the sum of $A_1 + B_1$ that is plotted.

Reflection loss curves of Fig. 47 present, in the upper right-hand quadrant, the reflection loss R_1 for low-impedance waves as a function of the absolute value of the impedance ratio k_1. Since this impedance ratio is a function of both the wave impedance Z_w and the metal intrinsic impedance η, the absolute value of k_1 has been plotted as a function of η for various wave impedances Z_w in the lower right-hand quadrant. Also, since η is in turn a function of square root of frequency, these relationships have been plotted for various metals in the lower left-hand quadrant. The wave impedance Z_w also is a function of $\sqrt{f}$ for the Helmholtz coil test setup and this relationship has been plotted for reference purposes in the upper left-hand quadrant.

Similar curves are presented for plane waves in Fig. 48.

9.1.2 Assumptions In Fig. 51, the straight line portions of the quantity $A_1 + B_1$ are valid for all values of the impedance ratio k_1 since B_1 is negligible in this region. However, for the nonlinear portions of this curve, the values have been plotted on the assumption that the absolute value of k_1 is either less than 0.1 or greater than 10. The left-hand portion of Fig. 51 - Penetration Phase Angle- is a presentation of data for a case investigated in the study.

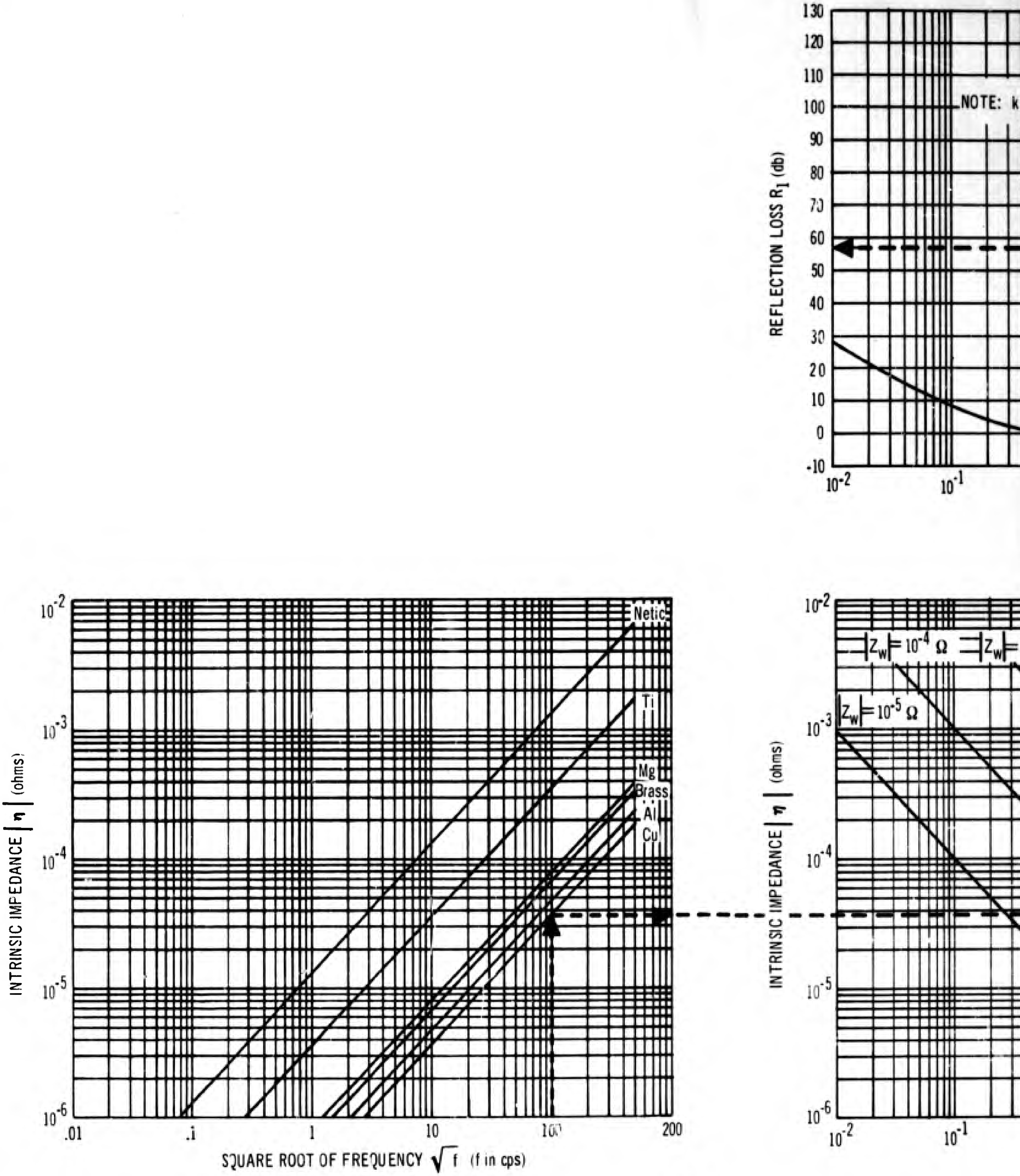

130
120
110
100
NOTE: k
90
80
70
60
50
40
30
20
10
0
-10
REFLECTION LOSS R_1 (db)
10^{-2}
10^{-1}
10^{-2}
10^{-3}
10^{-4}
10^{-5}
10^{-6}
INTRINSIC IMPEDANCE $|\eta|$ (ohms)
Netic
Ti
Mg
Brass
Al
Cu
.01
.1
1
10
100
200
SQUARE ROOT OF FREQUENCY $\sqrt{f}$ (f in cps)
$|Z_w| = 10^{-4}\ \Omega$
$|Z_w| = 10^{-5}\ \Omega$

1

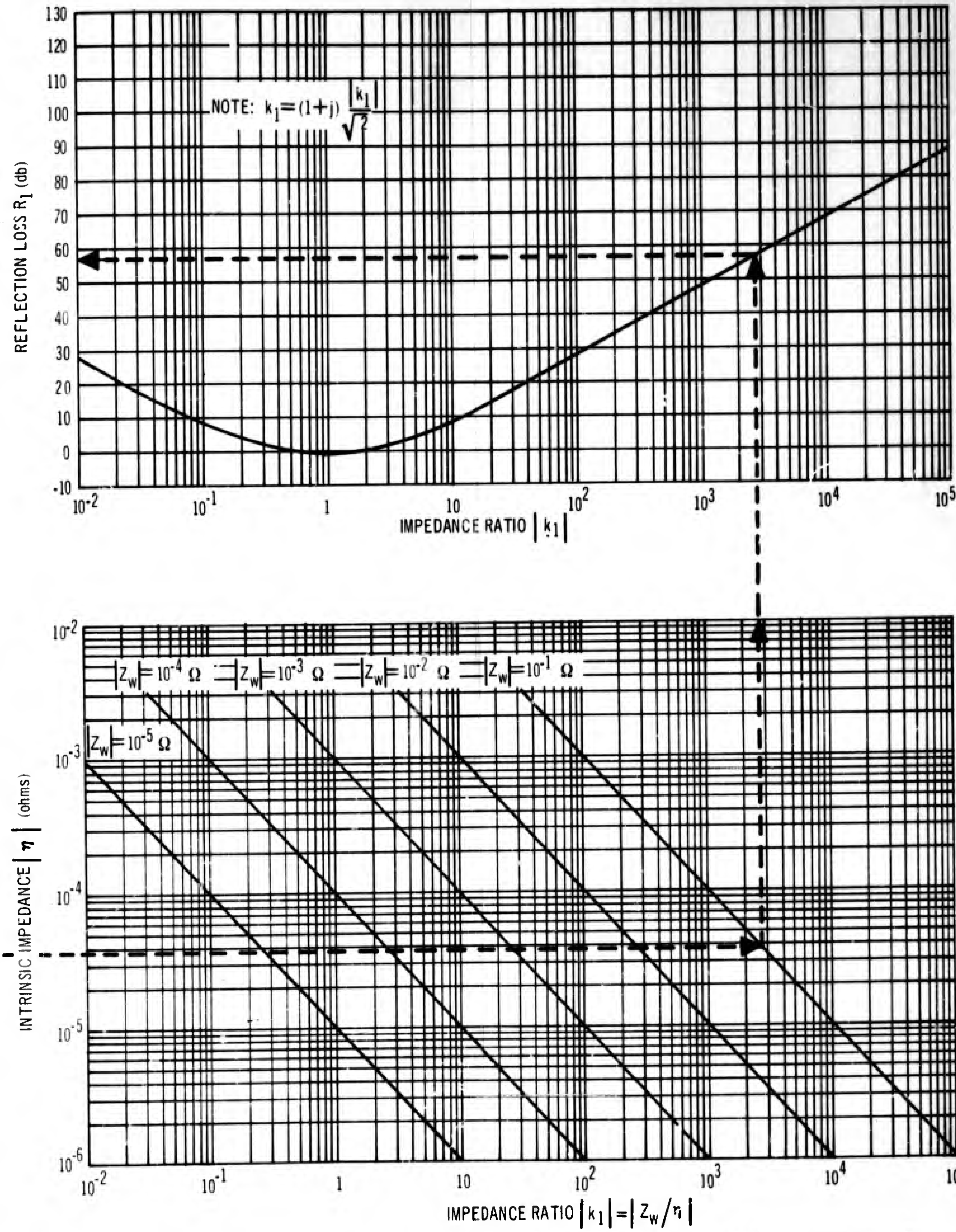

Fig. 47. Reflection Loss R_1 For Low-Impedance Wave

2

1

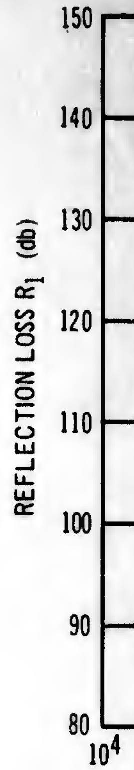
150
140
130
120
110
100
90
80
10^4
REFLECTION LOSS R_1 (db)

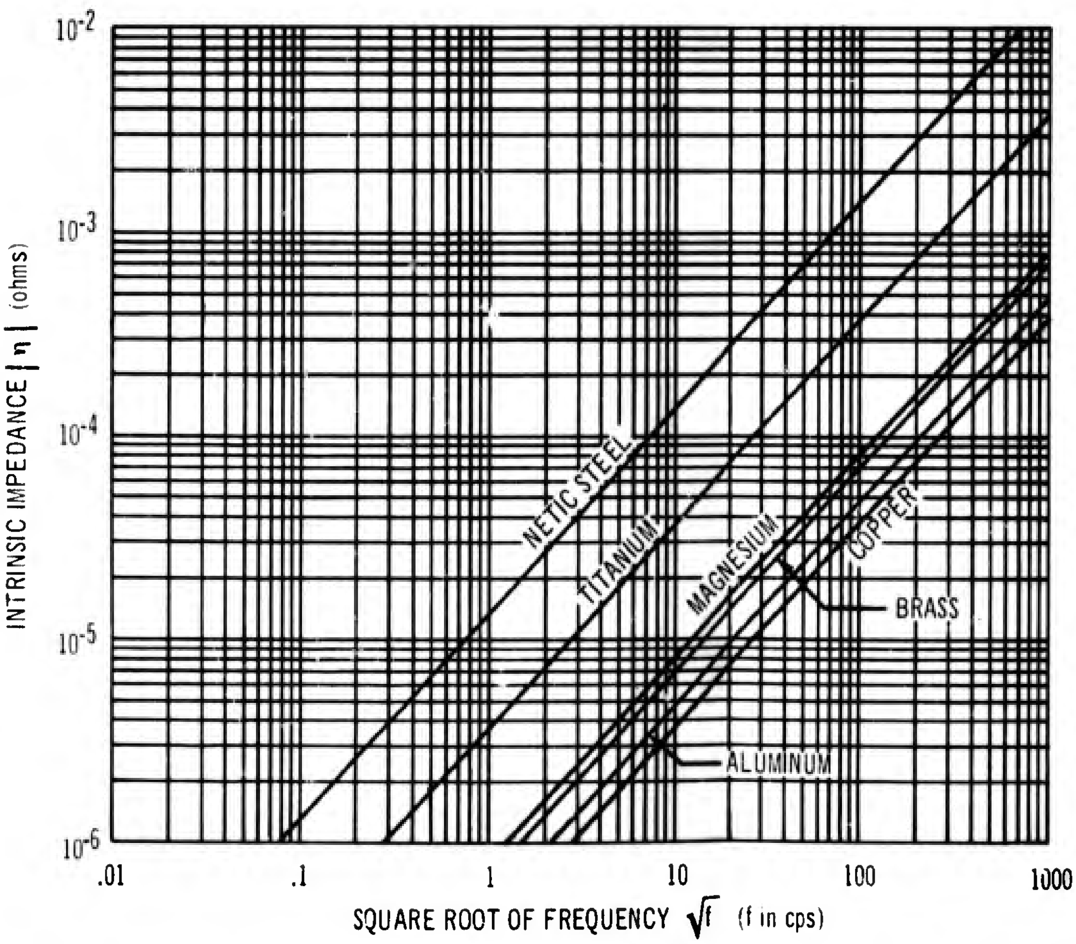
10^{-2}
10^{-3}
10^{-4}
10^{-5}
10^{-6}
INTRINSIC IMPEDANCE $|\eta|$ (ohms)
NETIC STEEL
TITANIUM
MAGNESIUM
COPPER
BRASS
ALUMINUM
.01
.1
1
10
100
1000
SQUARE ROOT OF FREQUENCY $\sqrt{f}$ (f in cps)

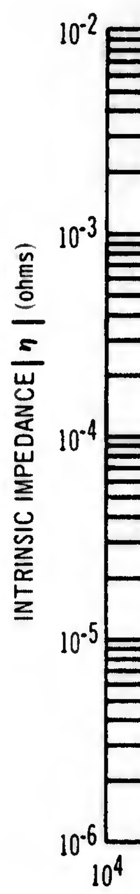
10^{-2}
10^{-3}
10^{-4}
10^{-5}
10^{-6}
10^4
INTRINSIC IMPEDANCE $|\eta|$ (ohms)

2

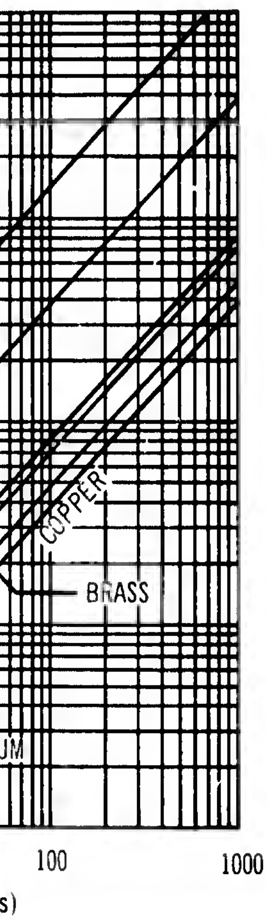

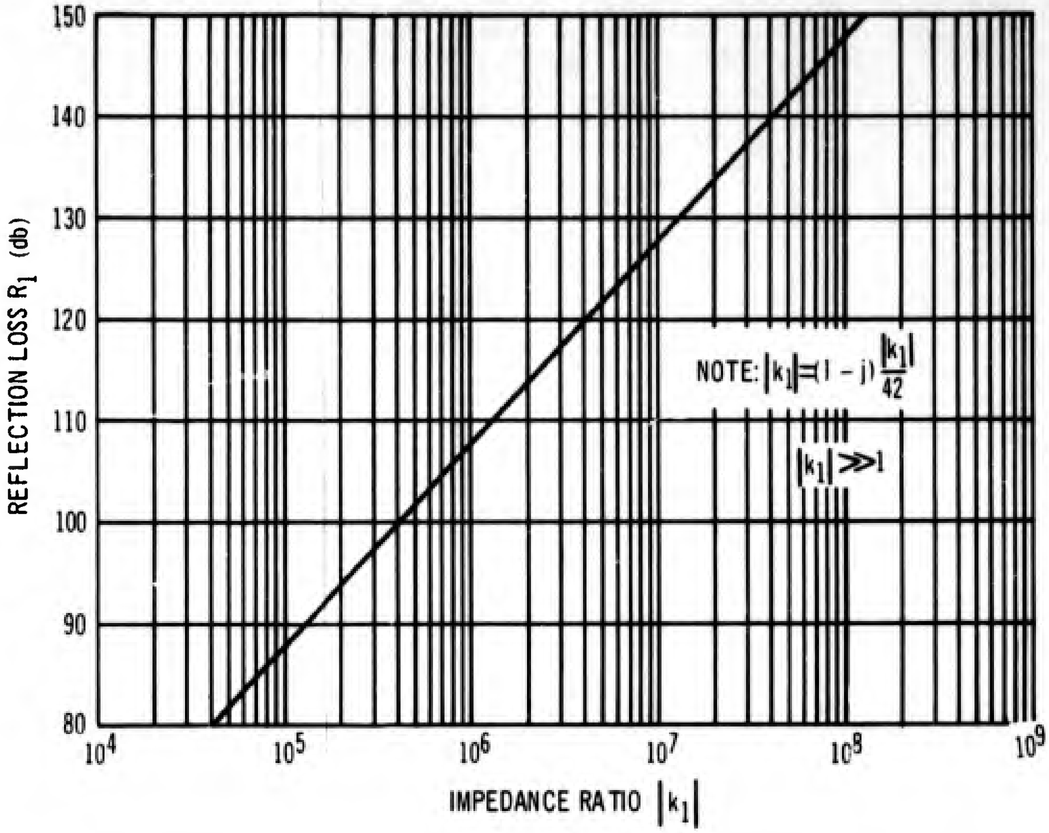

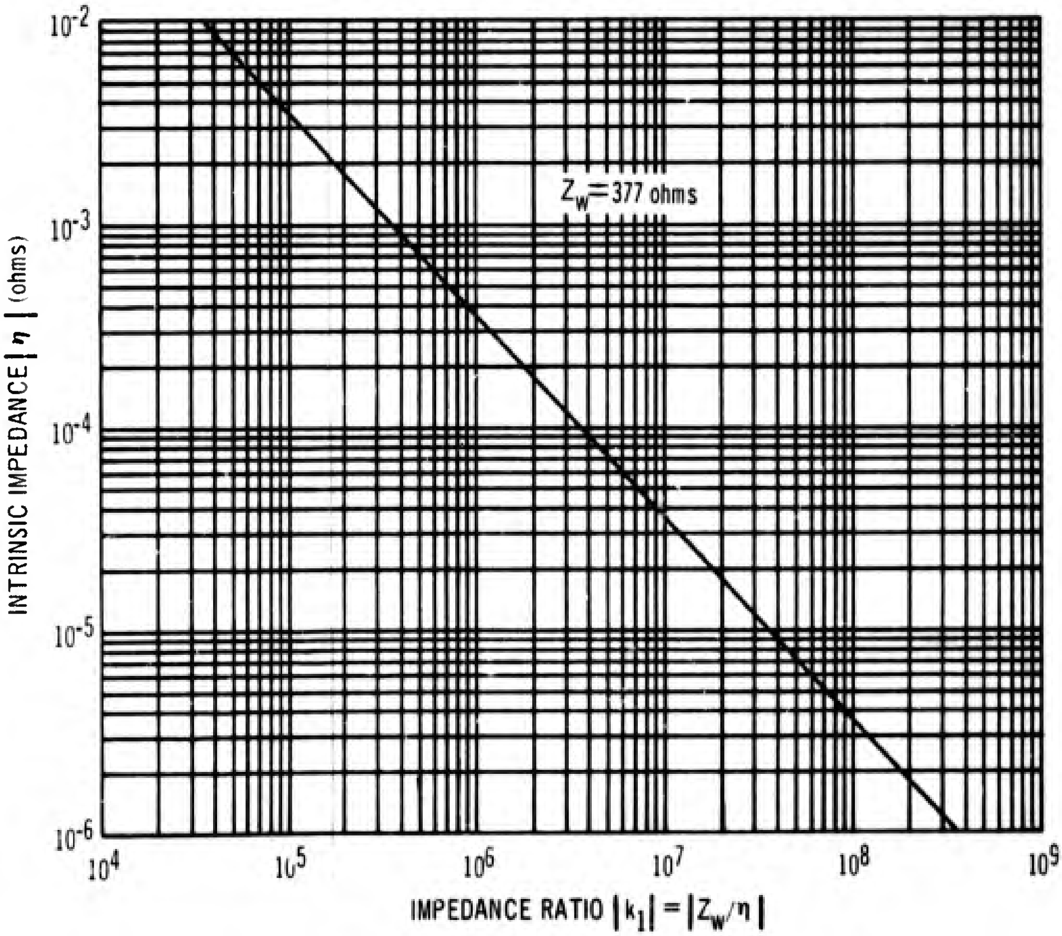

Fig. 48 Reflection Loss R_1 For Plane Wave

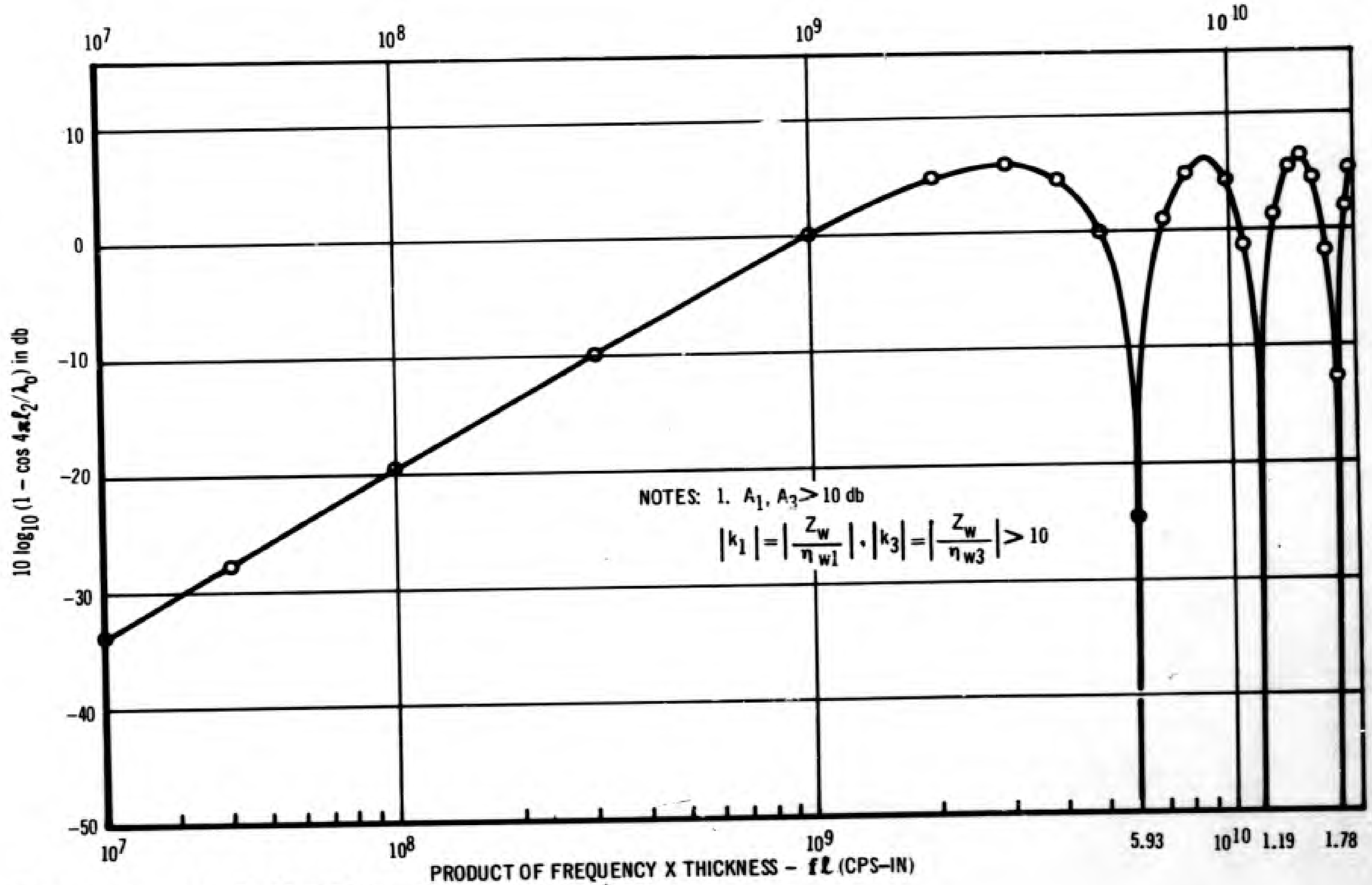

Fig. 49 Resonance in Double Shielding at High Frequencies

If these conditions are not met, the correction term B_1 may be obtained from equation (72) or by the use of Figs. 2 and 7 of Reference 2 for a dipole source.

No assumptions have been made for the information presented on Figs. 47 and 48.

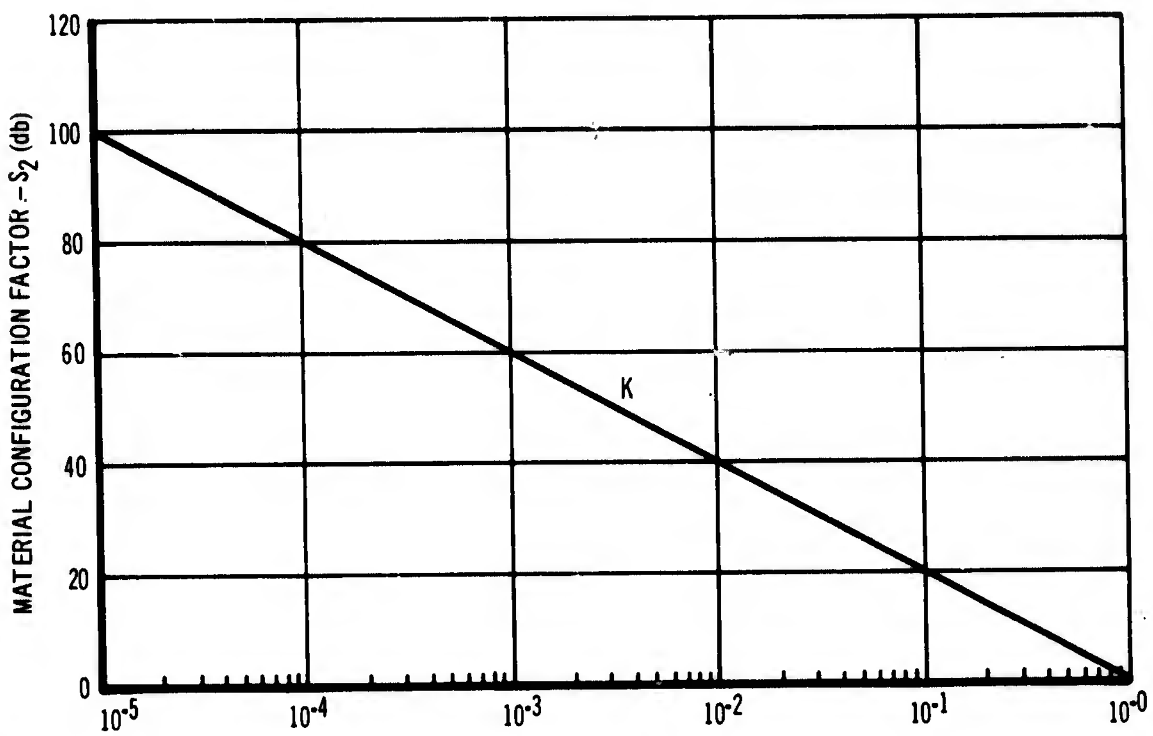

Fig. 50 Material Configuration Factor – S_2; Fraction – Open Area

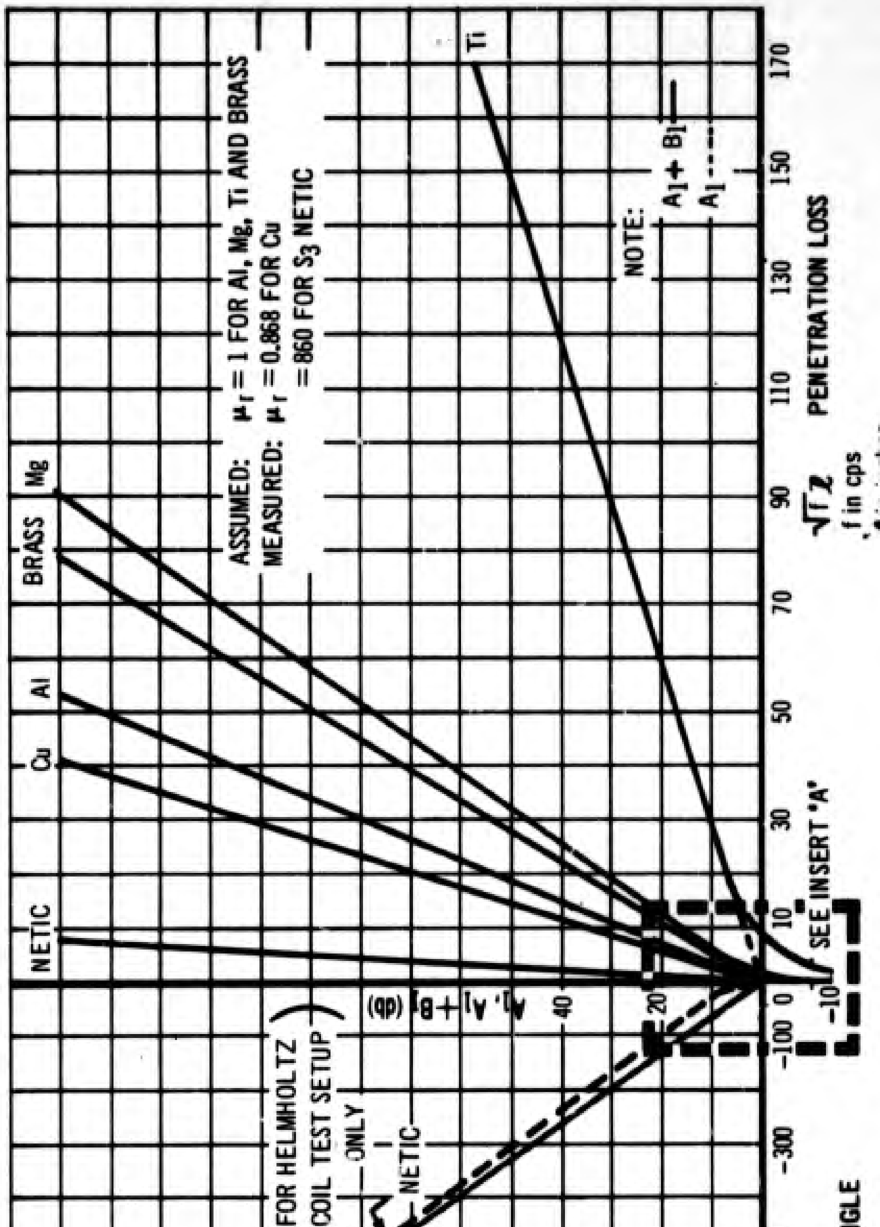

Fig. 51. Penetration Parameters

9.1.3 **Usage** . To obtain the material factor S_1 at any given frequency f, first calculate the product of the thickness in inches times the square root of this frequency in $\sqrt{cps}$. Enter the abscissa of this figure for the value calculated, project a vertical line to the curve representing the material of the shield as illustrated by the dashed arrow. From the intersection of this line with the curve, project the horizontal line to the ordinate to obtain the magnitude of $A_1 + B_1$. For the same value of square root of frequency, project a vertical line downward from the abscissa in the lower left-hand quadrant until it intersects with the curve for the same material, again as indicated by the dashed arrow. From this intersection proceed horizontally to the right until a curve representing the actual incident wave impedance is reached in the lower right hand quadrant. At this intersection, proceed vertically into the upper right hand quandrant until intersection with the reflection loss curve. Proceed from there horizontally to the left until intersection with the ordinate to obtain the value of the reflection loss for that material at that frequency. The sum of the $A_1 + B_1$ and the R_1 values is the total value for the material factor S_1.

9.2 Multiplicity Correction Term B_m $(\equiv \Delta S_m)$

When multiple shielding is employed, the total penetration loss is simply the sum of the separate penetration losses of the individual shields (illustrated for double shielding by equation (97)) and the reflection loss is similarly the sum of the separate reflection losses of the individual shields. However, there is a correction term for multiple shielding which is unique. The data presented here are for the special but common case of only two shields which need not be identical.

9.2.1 **Arrangement of Data** The multiplicity correction term for a double shield B_{m2} is plotted as a function of absolute value of impedance ratio $|k_3|$ for various absolute values of the impedance ratio $|k_1|$. In this form, Fig. 52 is useful in the fairly low frequency range, although not so close to zero that A_1 or A_3 is less than 10 db. At higher frequencies, Fig. 49 is more useful and exhibits resonance conditions existing between the shielding layers. With this figure, the multiplicity correction term is plotted as a function of the product of the frequency in cycles per second and spacing between shields in inches. Note that for shielding by materials identical with respect to both composition and thickness, it is not necessary to use Fig. 52 in the low frequency range since B_{m2} is equal to the negative of R_1 (See Paragraphs 5.5, 8.1, 8.2).

9.2.2 **Assumptions** The complete multiplicity correction term B_{m2} given in equation (97) is quite complicated for the general case. However, most design applications are covered under some simplifying assumptions. For both figures, it is assumed that both A_1 and A_3 are greater than 10 db. For Fig. 52 only, it is assumed that the spacing between shields is a very small part of the wave length, specifically ℓ_2 is much less than $\lambda/4\pi$. In Fig. 49 only, it is assumed that both the absolute values of k_1 and k_3 are greater than 10.

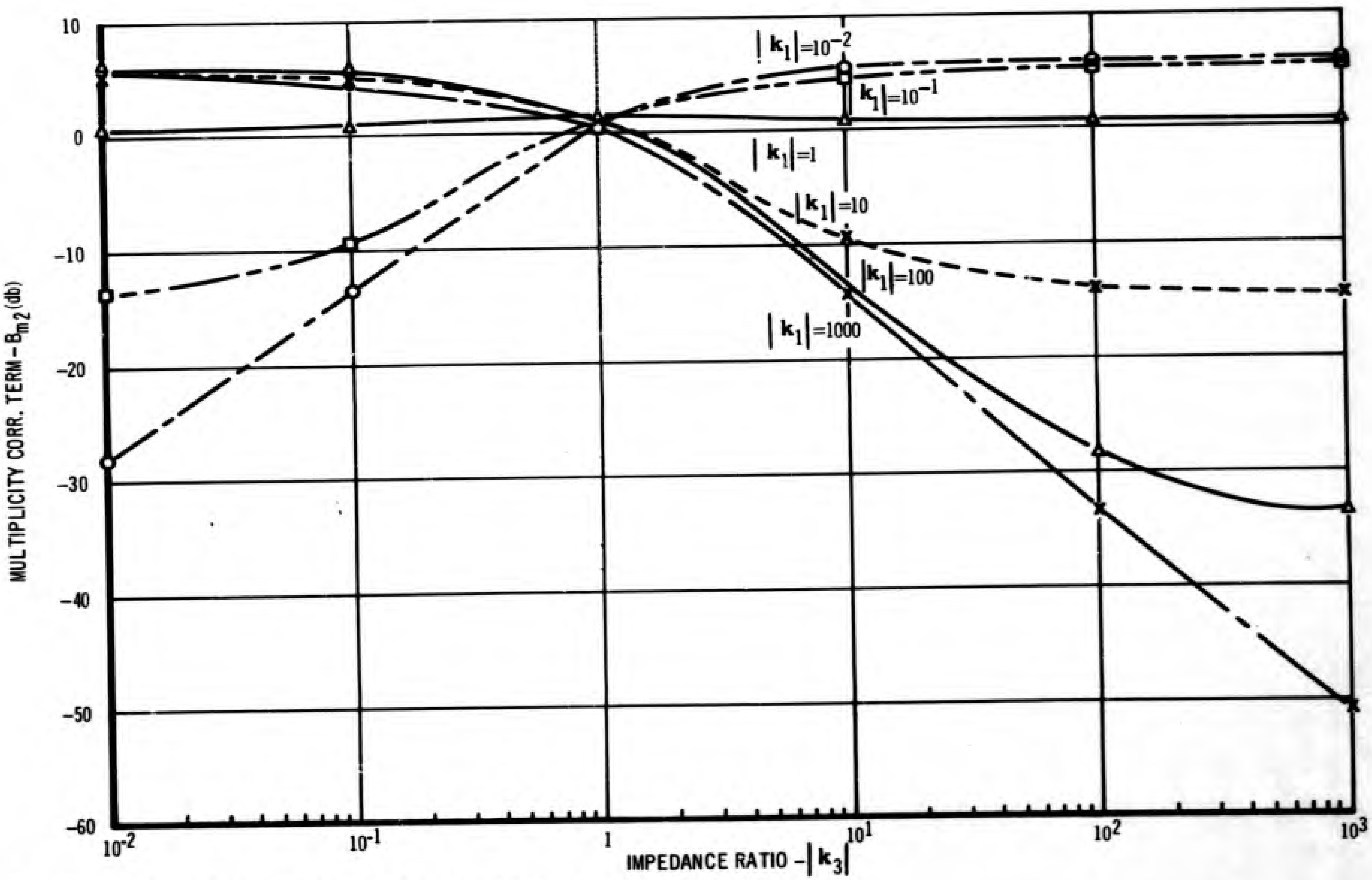

Fig. 52. Multiplicity Correction Term for Double Shielding at Low Frequencies

9.2.3 Usage Subject to the assumptions already mentioned, Fig. 52 is entered for low frequencies at a given value of the impedance ratio $|k_3|$ projected vertically down to a given value of $|k_1|$ and horizontally thence to the ordinate in order to find the value of the correction term B_{m2}.

For the higher frequency values of B_{m2} involving a free-space wave, Fig. 49 may be used subject to the normally valid assumptions already noted. This figure is entered on the abscissa for a given product of frequency in cycles per second times spacing in inches, projected vertically downward to intersection with the curve, and thence horizontally to the left to the ordinate in order to obtain the value of the multiplicity correction term B_{m2}.

9.4 Material Configuration Factor S_2

The material configuration factor accounts for any deviation in performance of material from that of a plain sheet of the same thickness. Such deviation may occur due to perforations in the material, due to a woven type of construction rather than a sheet construction, etc.

9.4.1 Arrangement of Data Inadequate experimental data are available in order to present this parameter with any high degree of confidence. The intention of the arrangements shown is simply to illustrate the general form in which the data are expected to be arranged. It is anticipated that actual data will be sensitive primarily to percent of open area for solid type sheets (Ref. 12) and to a similar different function of open area for woven or knitted type materials. It is anticipated that curves will be presented for the material configuration factor S_2 as a function of frequency f for different percentages of open area of solid sheets and that a similar figure will be presented for woven and knitted type sheets. It is further anticipated that the percent of open area curves will be generally similar for all compositions of materials and may be presented very readily as functions of frequency in the manner shown in Fig. 50. This curve is based upon the assumption that the leakage field H_2 is proportional to the decimal open area K or

$$S_2 = -20 \log K, \quad 0 \leq K < 1. \quad \text{(db)} \tag{171}$$

9.5 Shape Factor S_3

Experimental data indicates that the size factor S_4 also is infinite over the S_3 has no effect upon the shielding performance in the low frequency range. It is anticipated that similar results will hold for the entire radio frequency range, but experimental confirmation has not been obtained for this report.

9.6 Size Factor S_4

Experimental data indicate that the size factor S_4 also is infinite over the low frequency range. However, it is anticipated that the situation will be far different in the vicinity of cavity resonance of the enclosure. It has not been possible to obtain experimental data to support or deny this assumption, but the anticipated effect is illustrated conceptually by Fig. 53.

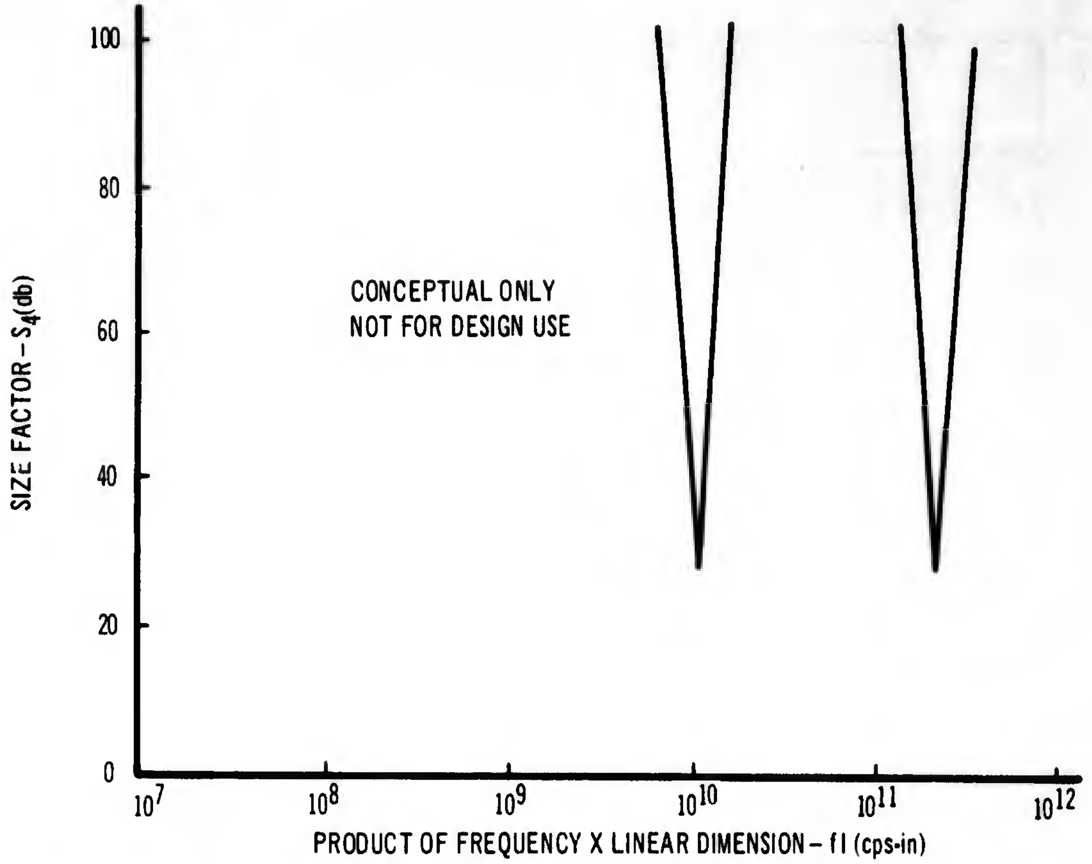

Fig. 53 Size Factor – S_4

9.7 Fixed-Seam Factor S_5

The fixed-seam factor S_5 and the access seam factor S_6 both constitute most important limitations to shielding performance, even more important than the shielding material itself in many applications. Because of the experimental difficulty in determining how to obtain the required data, only several experimental cases are presented for the fixed-seam factor S_5.

9.7.1 Arrangement of Data The fixed-seam factor is presented for a one-inch length of seam as a function of frequency on the upper right hand side of Fig. 54 for each of the several combinations measured. Associated with each seam is a phase retardation of the magnetic field associated with it and this negative phase angle θ_5 is plotted on the lower right-hand portion of Fig. 54 for the various combinations measured. In order to account for any given total length of seam subjected to the incident field, a seam length term S_a has been plotted in Fig. 55 and is to be added to the values obtained from Fig. 54 in order to represent a given shielding situation. A seam length term S_a of Fig. 55 is also applicable to determination of the access seam factor S_6. It is intended that for more available data, a separate representation of Fig. 54 would be used for each type of material.

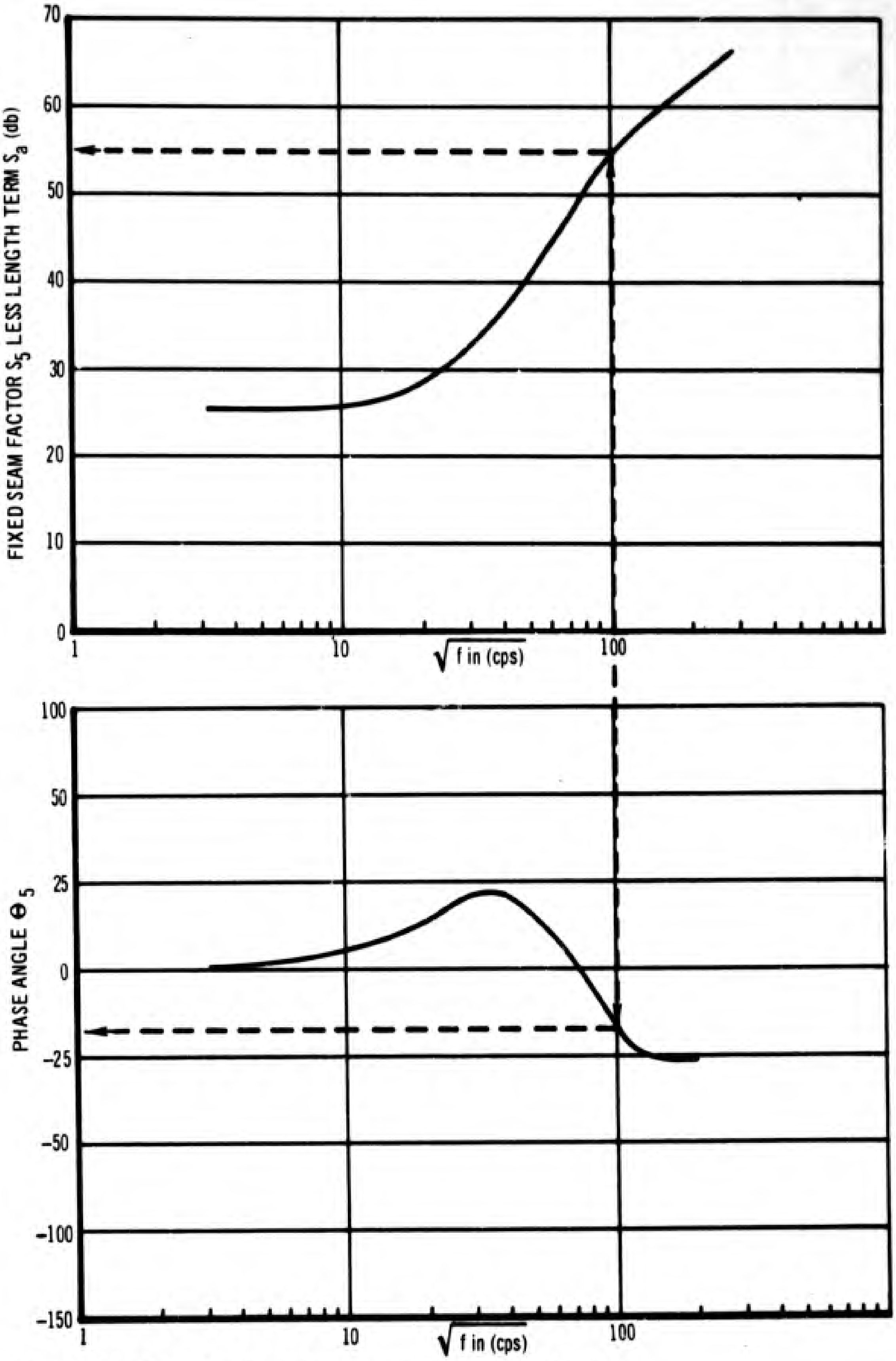

Fig. 54. Fixed Seam Factor S_5 Less Length Term S_a (For Copper)

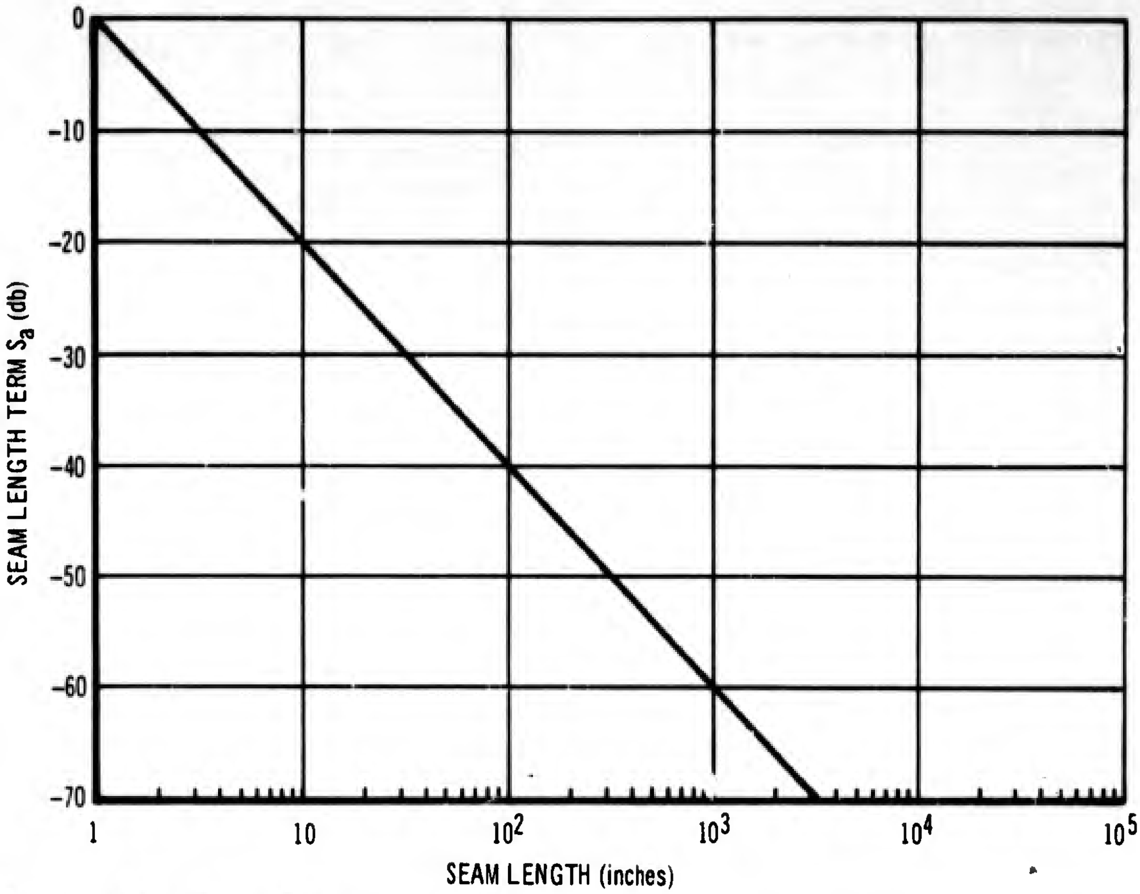

Fig. 55. Seam Length Term S_a

9.7.2 Assumptions It has been assumed that the total field from the leakage path through a fixed seam is directly proportional to the total length of that seam subjected to the incident wave and that wave impedance Z_W remains constant. Relationship between the coordinate values given in Fig. 55 are predicated on this assumption. While this assumption appears to be quite reasonable, it has yet to be verified by experiment. Since the curves of Fig. 54 represent calculations performed upon measured data (such calculations involving the small difference of two large quantities in certain regions), it can be assumed that the overall accuracy has been degraded from that of the original data. The engineering estimate of accuracy of the resulting curves given in Fig. 54 is ±4 db. However, this accuracy is for the particular cases measured. It can be expected that there will be a considerable variation among different boxes of the same type of construction; statistical data to give a measure of the confidence level is not available.

9.7.3 Usage For any given value of square root of frequency which has already been applied to the determination of the material factor S_1, Fig. 54 is entered on the abscissa and a vertical line extended upward to the curve for the particular type of seam to be considered. At the intersection with this curve, a horizontal line to the ordinate is the value of S_5 for a one-inch length of seam. In order to obtain the value of S_5 for a given shielding enclosure, this value must be corrected for the seam length by application of Fig. 55. It is entered with the same value of square root of frequency on the abscissa and extended vertically downward to the intersection with the curve and from thence horizontally to the left to the intersection with the ordinate in order to give the value of the correction term which is algebraically added (the correction term is negative) to the value just determined.

In order to make use of this information in expression (119), phase angle information is obtained from two places. For the given value of the square root of frequency used in Fig. 54, the vertical line is extended downward for intersection with the curve representing a particular seam desired, and from that point horizontally to the left to the intersection with the ordinate. From the ordinate is read the phase lag due to passage of the wave through the fixed seam. Also required is a phase angle due to passage of the wave through material itself and this is obtained from the left hand portion of Fig. 51 by extending the previously determined horizontal dashed line to intersection with the phase angle curve and thence vertically to intersection with the ordinate in order to obtain the phase delay through the shielding material. The required phase angle $_1\theta_5$ is simply the algebraic difference of θ_1 minus θ_5.

9.8 Access Seam Factor S_6

This factor enters into the shielding performance calculations in the same manner as the fixed-seam factor S_5. However, the seams themselves are of quite a different nature and, for this reason, the parameters for them are presented in a different manner.

9.8.1 Arrangement of Data Although data for the access seam factor S_6 are used in a manner similar to those for the fixed seam factor S_5, they are somewhat differently arranged since there is only one type of seam contact involved, although this may be either single or multiple. In Fig. 56, the access seam factor S_6 has been plotted as a function of frequency for the contact of a single row of phosphor bronze spring fingers against the given shielding materials. For a total length of seam other than one inch, the seam correction term S_a already given in Fig. 55 must be algebraically added. In addition, if more than one row of contact fingers is involved at the access seam, then an additional seam multiplicity term S_{6m} must be added and this term is obtained from Fig. 57.

For the access seam, its phase angle θ_6 enters into the overall shielding expression for S_6 in the same manner that the phase angle θ_5 enters into the expression for S_5. Values of θ_6 are presented on the lower portion of Fig. 56.

9.8.2 Assumptions In addition to the seam length assumption discussed under paragraph 9.7.2, an assumption is made as to the effect of seam multiplicity. The assumption is that every doubling of the row of contact fingers increases the shielding effectiveness by 6 db. This assumption remains to be verified by experimental results.

9.8.3 Usage Usage of these data is similar to those for the fixed-seam factor S_5 but with the addition of one extra term to account for seam multiplicity.

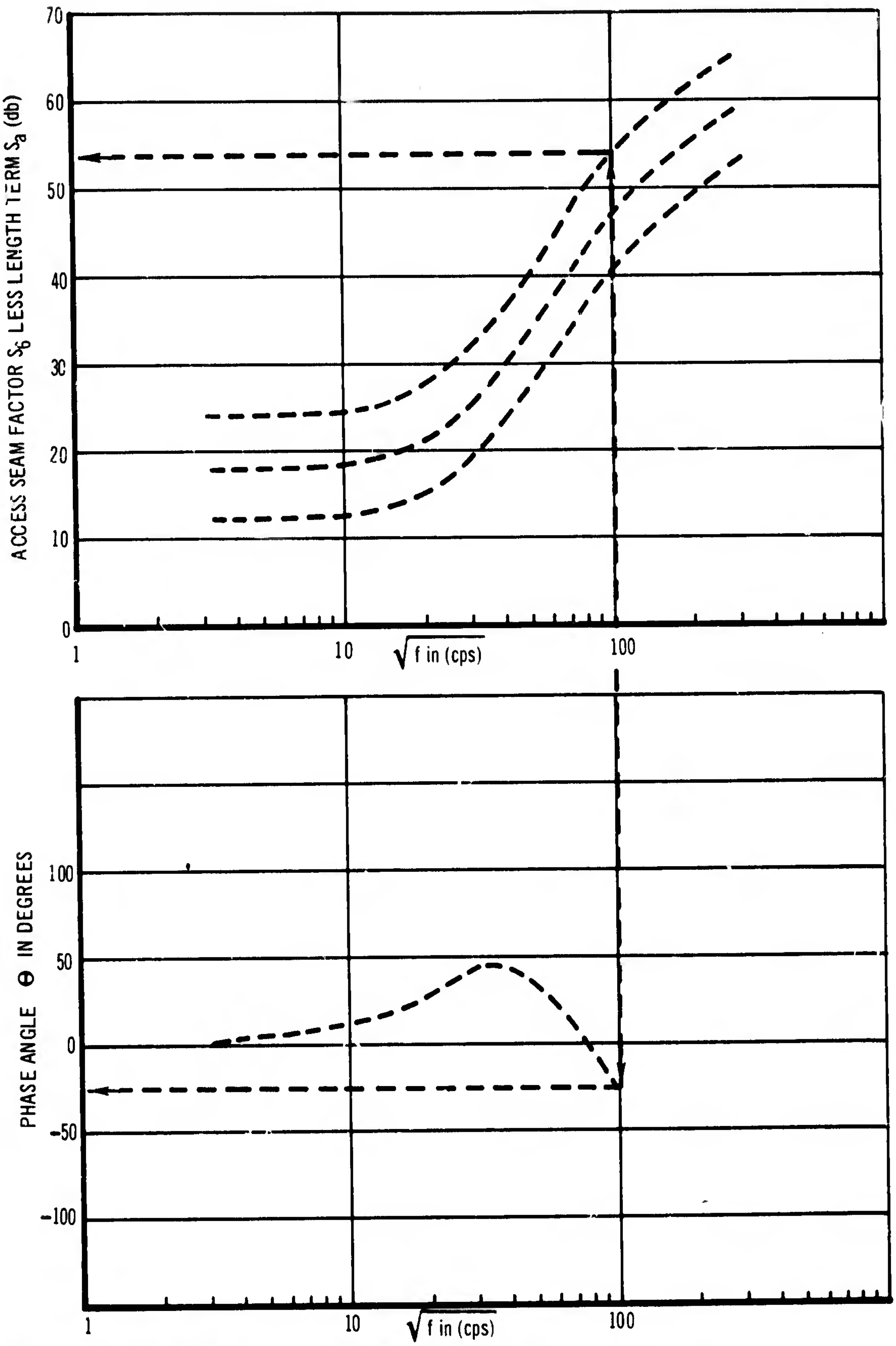

Fig. 56. Access Seam Factor S_6 Less Length Term S_a For Single Seam

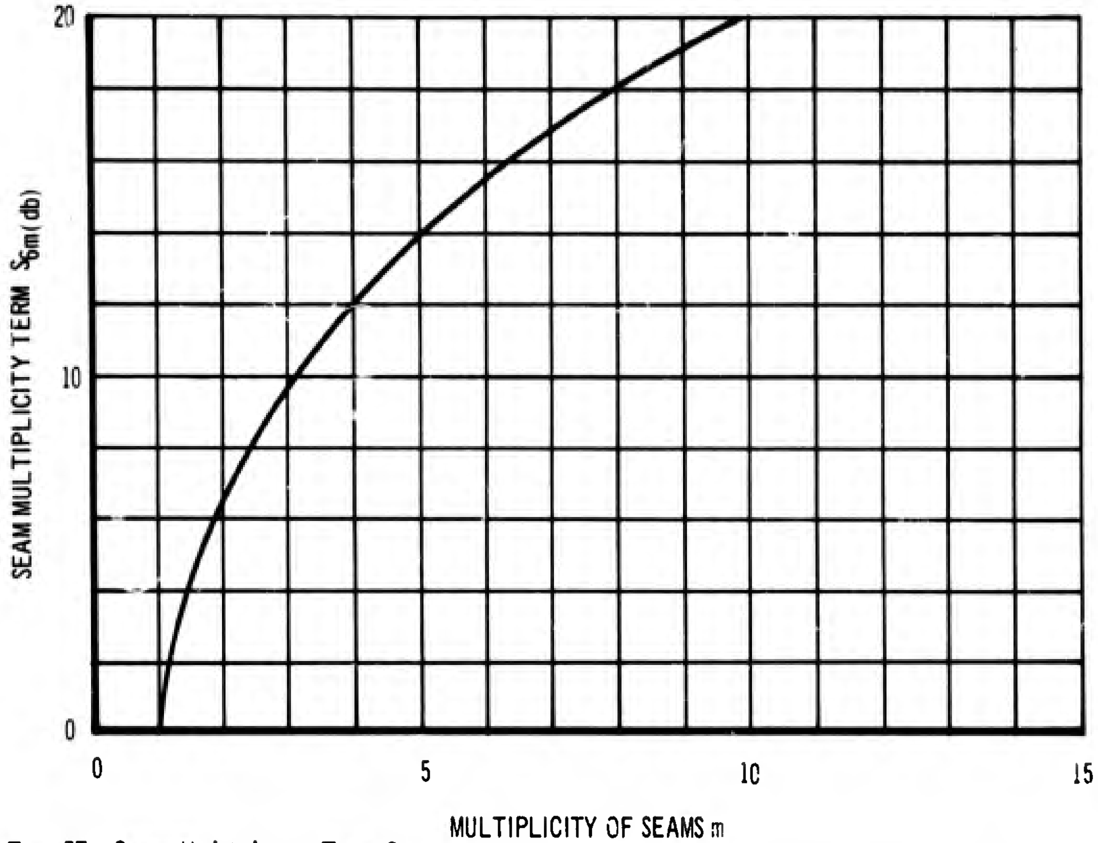

Fig. 57. Seam Multiplicity Term S_{6m}

9.9 Other Shielding Factors S_7 through S_9

No experimental information is available on the following factors:

1. Nonuniformity factor S_7 which relates the effect on shielding performance utilizing different materials and/or material configurations in different parts of the shielding construction. (One common need for this factor is in enclosures using waveguide-below-cutoff air inlets.)

2. Protrusions factor S_8 which accounts for the degradation in performance due to protrusions from the shield which may act as stub type antennas.

3. Filter factor S_9 which accounts for leakage through the shield due to insertion of the filter in the shield.

10.0 FACTUAL DATA – DESIGN EXAMPLES

In order to illustrate how the design data of Section 9.0 might be used, three examples are given, each with a different end objective. The objectives are:

1. Use of the parameters of Section 9.0 in order to determine performance of an enclosure already designed.
2. Design of an enclosure to achieve some desired performance.
3. Determination of degradation in performance due to some design limitation.

10.1 Performance of a Given Design

Assume a shielding enclosure with the following features:

1. Material - copper 0.023-inch thick
2. Multiplicity - single enclosure
3. Laminations - none
4. Material Configuration - solid sheet
5. Shape - rectangular parallelopiped (box shaped)
6. Size - 9 x 12 x 15 inches
7. Fixed Seams - 4 twelve-inch soldered seams
8. Access Seams - 2 fifteen-inch seams and 2 nine-inch seams with double rows of phosphor-bronze contact fingers
9. Other characteristics such as the effect of filters, air inlets, etc., are assumed to be immaterial. Let it be desired to obtain the performance of this enclosure at a frequency of 10 kc against a low impedance wave having a wave impedance given by the expression Z_W equals $j10^{-5}.f$ ohms where f is expressed in cps.

The following steps are outlined in order to derive the overall shielding effectiveness S:

1. Material Factor S_1
   The square root of f is 10^2 and Fig. 51 (insert) is entered with this value, $(\sqrt{f}.\ell)$ following the dashed arrows in order to determine the value of $A_1 + B_1$ equal to 10 db.

   For the square root of f equal to 10^2 enter Fig. 47 with this value and follow the dashed arrows to determine the reflection loss R_1 equal to 57 db.
2. Multiplicity Term ΔS_m
   This term is zero since only a single shield is involved.
3. Lamination Term ΔS_ℓ
   This term also is zero since there are no laminations. Thus $S_1 = 10 + 57 = 67$ db.
4. Material Configuration Factor S_2
   Since the configuration is a solid sheet, there is no leakage path due to configuration and S_2 is infinite.
5. Shape Factor S_3
   This factor is infinite.

6. Size Factor S_4
This factor is also infinite at the given frequency.

7. Fixed-Seam Factor S_5
For the square root of f equal to 10^2, Fig. 54 is entered with a line projected upward to the soldered-seam curve (screw-held Netic seam used in illustration) and thence over to ordinate to determine that the fixed seam factor for a one-inch seam is 54.5 db. For four twelve-inch seams, the total seam length is 48 inches and it is determined from Fig. 55 that the seam-length term S_a is -33.6 db, which must be algebraically added to the previous figure $S_5 = 20.9$ db.

In order to use this information in the final calculations, it is appropriate to determine the phase-difference angle $_1\theta_5$ which is simply θ_1 minus θ_5. The angle θ_1 is determined by projecting the horizontal dashed line of Fig. 51 leftward for intersection with the θ_1 curve and thence vertically to the abscissa. For the given case, θ_1 equals -70 degrees. Similarly, the vertical dashed line of Fig. 54 is projected downward until it intersects with the soldered-seam curve (screw-held Netic seam used in illustration) and thence horizontally to the left to the ordinate in order to determine a phase angle θ_5 equal to -35 degrees. Thus, $_1\theta_5$ is equal to -35 degrees.

8. Access-Seam Factor S_6
For the square root of f equal to 10^2, Fig. 56 (a conceptual illustration only) is entered at that value of the abscissa and the dashed line projected vertically upward is followed until intersection with the curve for a copper surface. A horizontal dashed line projected to the left indicates the access seam factor for a one-inch seam length to be 54 db. To this factor must be added the seam length term S_a. For access seams along each of the 15 and 9-inch sides, the total seam length is 48 inches. For this case, the seam length term S_a has already been determined for 48 inches to be -33.6 db. Also to be added is a term for multiplicity of seams, in this case double seams. The seam multiplicity term S_{6m} is determined from Fig. 57 to be 6.0 db. $S_6 = 54 - 33.6 + 6.0 = 26.4$ db.

It is again appropriate at this point to determine the phase angle resulting from seam penetration. From Fig. 56, the vertical dashed line is projected downward to intersection with the curve for a copper surface and then horizontally to the left to the ordinate in order to obtain the phase angle θ_6 equal to -26 degrees. The phase difference angle $_1\theta_6$ is θ_1 minus θ_6 and, since θ_1 already has been determined, this is -44 degrees.

9. Shielding Effectiveness S
All of the quantities so far determined are entered in equation (134) in order to determine the overall shielding effectiveness of the enclosure at a frequency of 10 kc.

$$S = -10 \log \left\{ \left[10^{-\frac{67}{10}} + 10^{-\frac{20.9}{10}} + 10^{-\frac{26.4}{10}} \right] + 2 \left[10^{-\frac{67+20.9}{20}} \cos\left(-35^\circ\right) \right. \right.$$

$$\left. \left. + 10^{-\frac{67+26.4}{20}} \cos\left(-44^\circ\right) + 10^{-\frac{20.9+26.4}{20}} \cos\left(-35^\circ + 26^\circ\right) \right] \right\}$$

$$= -10 \log \left[1.04 \times 10^{-2} + 2 \left(3.82 \times 10^{-5} + 1.54 \times 10^{-5} + 4.25 \times 10^{-3} \right) \right]$$

$$= 17.2 \text{ db}.$$

Thus, the overall shielding effectiveness S of the enclosure is 17.2 db at a frequency of 10 kc.

10.2 Design to a Desired Performance

Design to meet a desired performance is basically a process of synthesis of the various parameters to be considered. In order to meet some desired performance, it is necessary that every one of the factors S_1 through S_9 be greater than the performance desired unless such performance is desired in a region of low-frequency shielding resonance. For a given frequency of interest then, it is possible to enter each one of the design parameter curves Figs. 47 through 57 to determine each separate factor that will meet these criteria. Indeed, it is good practice to allow for some degradation due to combination of the various factors to the extent that any one given factor should be at least 10 db above the required final result. Even additional safety factors might be desirable for any variations in actual construction. With these considerations as guidelines, the design is then basically a process of successive evaluations of performance for various combinations which meet the separate basic criteria, of which each calculation is similar to that illustrated in paragraph 10.1.

10.3 Degradation Due to a Design Limitation

In some cases, one or more structural requirements may limit the performance to values less than would otherwise have been obtained. Examples of such limitations might be a requirement that the shielding material be of one kind rather than another, that it be made of several different types of materials for a given application, that the access seam may have no more than 2 rows of contact fingers, that the seams have to be screwed together instead of soldered, etc. Whatever the particular limitation imposed, it is generally necessary to calculate the performance in accordance with paragraph 9.1 under both sets of conditions: where the design limitation is imposed, and where it is lifted. There is obviously no effective degradation if the change in a given design parameter is such that the smallest value of the parameter is 20 db or more greater than any other parameter. When the lowest value is under this figure, it is frequently possible to obtain a first approximation of the degradation effect by comparing the very lowest parameter value of one case with the very lowest value of all the parameters for the other case. The difference between the two would be a first approximation to the degradation.

Previous page was blank, therefore not filmed.

11.0 CONCLUSIONS

11.1 Major Conclusions

11.1.1 The feasibility of designing shielding upon sound engineering principles has been demonstrated and methodology therefor has been established.

11.1.2 Techniques for obtaining the data required have been established and some of the data have been obtained.

11.1.3 A phenomenon of low-frequency shielding resonance has been discovered and explained upon a theoretical basis.

11.1.4 This phenomenon of low-frequency resonance is a useful effect which can be utilized to obtain improved shielding performance at some selected low frequency and may be used as the basis for detecting flaws in metals and metallic seams. Both applications have formed the bases of patent disclosures.

11.2 Specific Shielding Factors

11.2.1 Overall Shielding Effectiveness S

1. There is no theoretical advantage in measuring cross-field transfer impedances, such as incident E to transmitted H or incident H to transmitted E. Actually, there would be an experimental disadvantage because of greater noise-to-signal ratios (paragraph 5.2). However, when the field is setup by a known current and measured by an induced voltage, a transfer impedance is in actuality being measured.
2. Shielding effectiveness against high-impedance waves at low frequencies is much greater than against low-impedance waves at the same frequencies. Consequently it is necessary and most practical to measure shielding effectiveness against H fields, to provide a measure of minimum shielding performance at low frequencies (paragraph 5.1.11).
3. Magnetically susceptible components may be located almost anywhere within a "seamless" enclosure, except in the trihedral corners, without fear of reducing the effective shielding of those components.

11.2.2 Material Factor S_1

1. The shielding effectiveness of double shields is generally better than that of single shields having the same total thickness of metal; although at a very low frequencies this difference approaches zero, along with shielding effectiveness.

2. Normally, the shielding effectiveness of a double shield will be much less than that of the sum of both when considered as two single shields because the air gap cannot be infinite. If the shields are spaced an odd multiple of 1/4 wavelengths apart, shielding effectiveness can be slightly increased or considerably decreased.
3. For multiple shields the total penetration loss is the sum of the penetration losses for each medium and the total reflection loss is the sum of the reflection losses at each interface. The total correction term for re-reflection loss is the sum of the individual correction terms, including the air gap, which dominates.
4. At the metal-to-metal interfaces of laminated sheets, reflection loss R is independent of frequency because the ratio of the intrinsic impedances of the lamina remains constant.

11.2.3 Shape Factor S_3 The shape of an enclosure, as such, does not contribute to its shielding effectiveness, except as noted in paragraph 11.2.4.2 and 11.3.

11.2.4 Size Factor S_4

1. Within a uniform electromagnetic field, the size of an enclosure bears no significant relation to its shielding effectiveness, except in the vicinity of cavity resonance as noted in paragraph 2 below.
2. The resonant frequency of an enclosure, considered as a cavity, is determined by its size and shape. At and very near resonance there is expected to occur a considerable deviation in shielding effectiveness which is, of course, related to size and shape of the enclosure.

11.2.5 Fixed Seam Factor S_5 The closest practical approach to a perfect permanent seam or joint was thought to be that formed by electron beam welding. The entire operation is accomplished in a high vacuum chamber which practically eliminates air as a contaminant; nothing in the process can alter the chemical composition. However, there is some evidence (No. 26 of Fig. A18 and No's. 30, 31 of A32) to indicate that this supposedly perfect seam construction is very little better, if at all, than several other types. It is probable that the crystal structure, paralleling each side of the bead, has been altered in a manner resembling a "cold" solder joint and that inclusions of voids reduces the effective electrical conductivity required for superior performance.

11.2.6 Access Seam Factor S_6 In any otherwise effective shielding enclosure, the design of points of entry and access present major design problems in efforts to maintain the shielding integrity of the enclosure. It is practically impossible to design an access joint which will provide as much shielding effectiveness as a good seamless enclosure. Although it has long been recognized that all openings in enclosures are undesirable, it remained for this study to provide a means for quantitatively evaluating the deterioration of shielding effectiveness which results.

11.3 Notes on Overall Study:

The following general notes and comments apply to the totality of research, theoretical development and numerical calculations performed in this study. They embody the constraints and limitations inherent in the application and extrapolation of the results contained herein to the analysis or design of shielding structures.

1. The impedance of the impinging field is a determining factor in R_1 and B_1 (although A_1 depends only on the material). (Paragraph 8.0)

2. The wave impedance inside of a conductor will in nearly every case be its intrinsic impedance.

3. The field theory applied herein states that the energy flow inside the conductor is in the form of a current. There are the following implications of using a circuit analysis:

   (a) Approximations, such as of shield thickness and of impedance, are not usually compatible. Use of simpler, more readily visualized basic concepts will help overcome this problem.

   (b) A box acting as a shield is an inductor and has a configuration which fits that of a low impedance field. If the field is set up by another inductor, such as a Helmholtz coil, there is a mutual inductance between the generator coil and the box; however, whether the field is furnished by the coil or by a free space wave, the effect on a pickup coil inside the box will be much the same since the self inductance of the box predominates over the mutual inductance. It appears that the impedance of the impinging field is determined more by the configurations S_3 and S_4 of the shield than of the field source.

   (c) Since the inside of the shield acts as a waveguide below cut-off, the validity of assuming the emerging and impinging waves to have the same impedance is questionable. Resolution of this problem is, however, not difficult if it is treated on a circuit basis.

   (d) Both circuit and field theory must be considered in the application (as well as in the development) of shielding theory.

4. The effect of the shield on H is not quite the same as on E. If $\eta \ll Z_r$ and $\eta_W \ll Z_T$, in the R term of (34) E_i/E_T is influenced by K_r but not by K_T and H_i/H_T, using (35), is influenced by K_T but not by K_r. In other words E but not H is affected by the abrupt

decrease of impedance when entering the shield while H but not E is affected by the abrupt increase of impedance on emergence. Considering H as a current and E as a voltage, this would be expected. Also an abrupt impedance change means an abrupt change in the ratio E/H and thus an abrupt change in one but not necessarily the other field.

12.0 RECOMMENDATIONS FOR FUTURE RESEARCH

12.1 Additional Experimental Data

More experimental data are required to make full use of the techniques developed. These should include:

1. Data on additional combinations for the types of shielding factors measured.
2. Data on shielding factors not measured.
3. Extended frequency measurements.
4. For each shielding factor, a statistical number of measurements should be obtained to establish a confidence level.

12.2 Low-Frequency Shielding

The phenomenon of low-frequency resonance in shielding should be used in the development of economical low-frequency shielding enclosures.

12.3 Design Reference

Combine shielding data obtained in the above programs into a design reference using the material of Section 9.0 of this report as a guide.

13.0 IDENTIFICATION OF PERSONNEL

PROGRAM MANAGER — RICHARD B. SCHULZ

Mr. Schulz received a Bachelor of Science degree in Electrical Engineering from the University of Pennsylvania in 1942 and a Master of Science degree in Electrical Engineering in 1951. He has completed graduate courses equivalent to Ph. D. requirements.

Prior to joining Boeing, he developed a laboratory standard RFI meter at the University of Pennsylvania. Later, he was a consultant engineer in electrointerference research, development, design, and specification testing. His company, known as Electro-Search, under various government contracts, designed shielding installations, tested shielding, and made field surveys of electrointerference at Naval establishments.

In 1955 he joined the Armour Research Foundation (now IIT Research Institute) as program development coordinator for electrical engineering research. His technical efforts include development of a thermistor-bridge voltmeter for accurate, low-level, direct-amplitude calibration of electrointerference measuring equipment and Hall effect magnetic-field pickup devices for electrointerference field intensity instrumentation. This also included efforts as a project engineer on development of satellite RFI instrumentation.

He joined the United Control Corporation in 1961 as Chief of the Electro-Interference Section, where he was directly engaged in the electrointerference aspects of the Minuteman weapon system. Mr. Schulz joined The Boeing Company in 1962 as a staff engineer in Aero-Systems Technology, where he was engaged in microelectronics and electromagnetic compatibility activities. He is now Chief of Electrocompatibility and Microavionics Unit in the Airplane Division.

He is a registered professional engineer and has been active in both national and local technical organizations. Presently he is treasurer of the Seattle Section of the Institute of Electrical and Electronics Engineers and has been active in the group on electromagnetic compatibility, both as past chairman of the Seattle chapter and as a former member of national administrative committee. He was a member of the IRE Subcommittee 27.5 on standards for measuring shielded enclosures, 1958 to 1963, and the American Standards Committee C63 on radio interference, 1960 to 1961. He is a member of Tau Beta Pi, Eta Kappa Nu, and Sigma Tau honorary societies.

Mr. Schulz is the author or coauthor of 30 technical papers on electrocompatibility topics and has a text book on this subject in preparation.

PROGRAM LEAD ENGINEER — VELLAR C. PLANTZ

Mr. Plantz is employed as a research engineer in the Boeing Electrocompatibility Unit. For the past year he has been responsible for the Electrointerference Test Integration Group in the Minuteman Engineering Department.

During that time he directed the development of electrointerference test methods and procedures. His educational background includes more than 500 hours in specialized electronic engineering courses.

Before coming to Boeing, Mr. Plantz was a Design Unit Supervisor for United Control Corporation Engineering Department. In this capacity he directed the electrointerference minimization service from design review to MIL Specs for customer equipment and subsystems.

From March 1953 to April 1961, Mr. Plantz was employed by the Martin Company. Here his assignments included design specialist for the GBSD Laboratory and design support group and senior engineer, GBSD Electrointerference Minimization Group. During the latter assignment, he directed electrointerference design studies. He also aided in development of the GPL Electrointerference Group, contributing to the TITAN system functional compatibility test philosophy, test plans, and tests.

Mr. Plantz is a member of the Institute of Electrical and Electronic Engineers (Seattle Chapter Chairman, Group on Electromagnetic Compatibility). His papers include: "Interference Suppression of B-57 Aircraft," presented during and published in the Proceedings of the Second Conference on Radio Frequency Interference Reduction, Armour Research Foundation; "Electrointerference," distributed as a supplement to "Quasies and Peaks"; "Are Rivet Structures 'Inherently' Bonded?" published in Aviation Age; and "Electrointerference and Missile Systems," published in the Engineers Bulletin by the Colorado Society of Engineers and many others.

TEST ENGINEER — DAVID R. BRUSH

Mr. Brush received a Bachelor of Electrical Engineering degree from the University of Minnesota in 1958, with a major in electronics.

From May 1949 to June 1958, Mr. Brush was employed by the Network for Mid America at KTIS. During this time he was responsible for design of custom communication equipment. In 1955, he was appointed Chief Engineer of KTIS Minneapolis, master control headquarters for the network.

In July 1958, Mr. Brush joined Boeing as an associate engineer. He worked at this time on preparation of test outlines for the evaluation of electronic systems on the 707 airplane.

After a year of engineering with United Control, Mr. Brush rejoined The Boeing Company as associate research engineer and has since been providing research support for the Electronics Project Design Group. In this work he has been concerned with laboratory verification of theoretical analyses and system testing.

Mr. Brush is a member of the Institute of Electrical and Electronics Engineers and the Group on Electromagnetic Compatibility.

REFERENCES

1. S. A. Schelkunoff, Electromagnetic Waves, D. Van Nostrand Co., 1943.

2. R. B. Schulz, V. C. Plantz and D. R. Brush "Shielding Theory and Practice," Proceedings, Ninth Tri-Service Conference on Electromagnetic Compatibility, 1963.

3. C. S. Vasaka, Theory, Design and Engineering Evaluation of Radio-Frequency Shielded Rooms, Report No. NADC-EL-54129 of USNADC, Aug. 1956.

4. E. Weber, Electromagnetic Fields, Vol. I, John Wiley, 1950.

5. R. B. Schulz and D. P. Kanellakos, Shielding Enclosure Performance Utilizing New Techniques, IRE Convention Record, 1961.

6. The Microwave Engineers Handbook and Buyer Guide, Horizon House, Inc., 1963.

7. H. Sasek, Antenna Engineering Handbook, McGraw-Hill Co., 1961.

8. Reference Data for Engineers, Fourth Edition, Federal Telephone and Radio Corp., 1949.

9. S. A. Schelkunoff, H. T. Friis, Antennas; Theory and Practice, John Wiley and Son, 1952.

10. D. R. Rhodes, An Experimental Investigation of the Radiation Patterns of Electromagnetic Horn Antennas, Proc. IRE, Sept. 1948.

11. J. D. Kraus, Antennas, McGraw-Hill, 1950.

12. R. B. Schulz, Solving ELF Shielding Problems with High Permeability Materials, National Aerospace Electronic Conference, Dayton, May, 1964.

ADDITIONAL INFORMATION

1.	First Quarterly Report:	Appendix
2.	Second Quarterly Report:	Sections 5.5.1 and 5.6
3.	Third Quarterly Report:	Sections 4.6, 5.0 - 5.7
4.	Fourth Quarterly Report	Sections 5.2 - 5.2.4

APPENDIX A MEASURED DATA 50 cps to 200

Appendix A1 Helmholtz Coil

To determine the uniformity of the magnetic field within the Helmholtz coil a three-dimensional grid of nylon lacing was constructed and comparative measurements were made at two inch spacing on each of three levels within the coil. The results of these field measurements are plotted in Figs. A1 through A15.

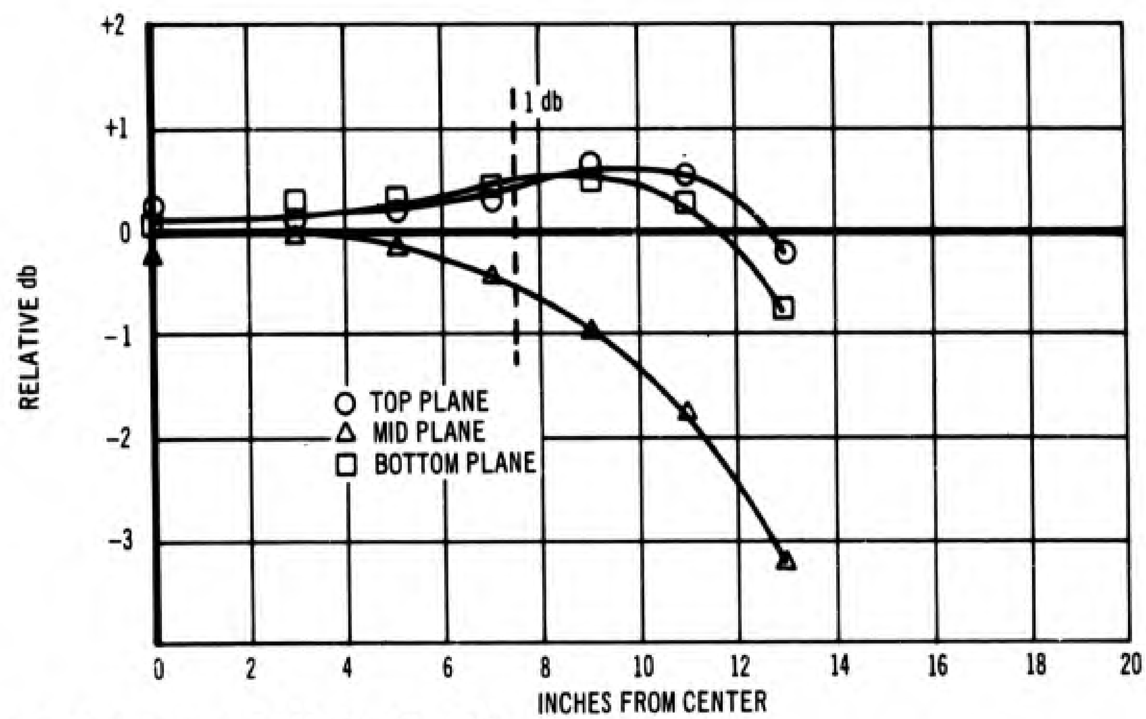

Fig. A-1 Magnetic Field Plot: Short Side - 50 cps

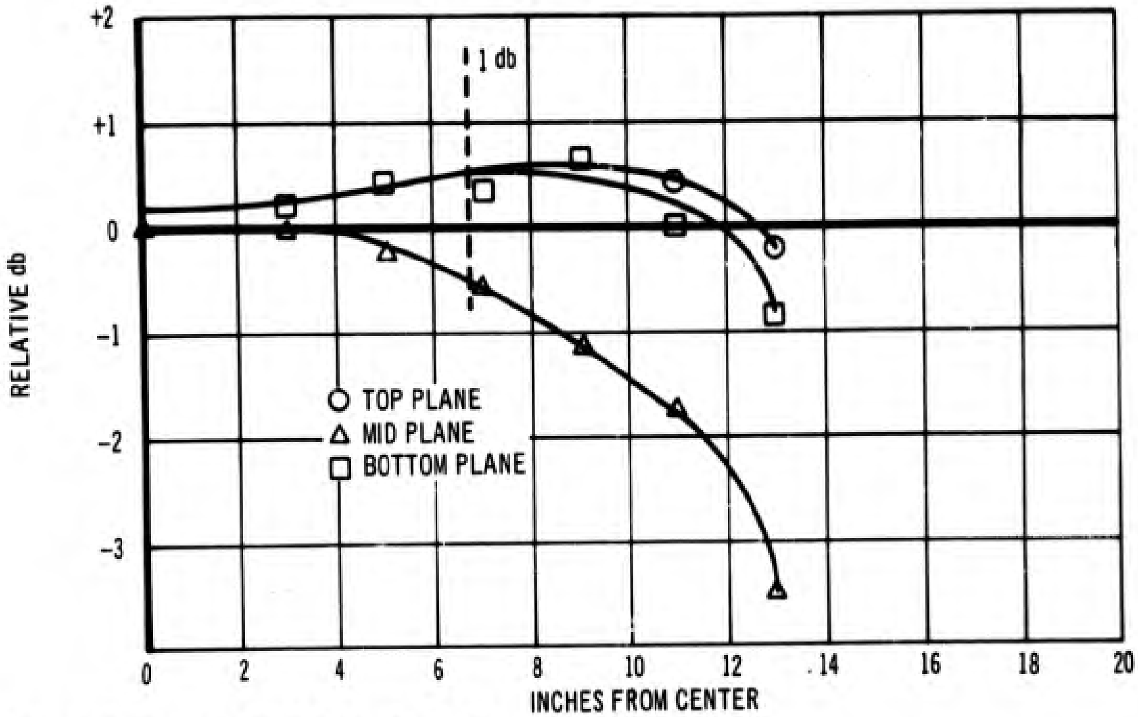

Fig. A-2 Magnetic Field Plot: Short Side – 500 cps

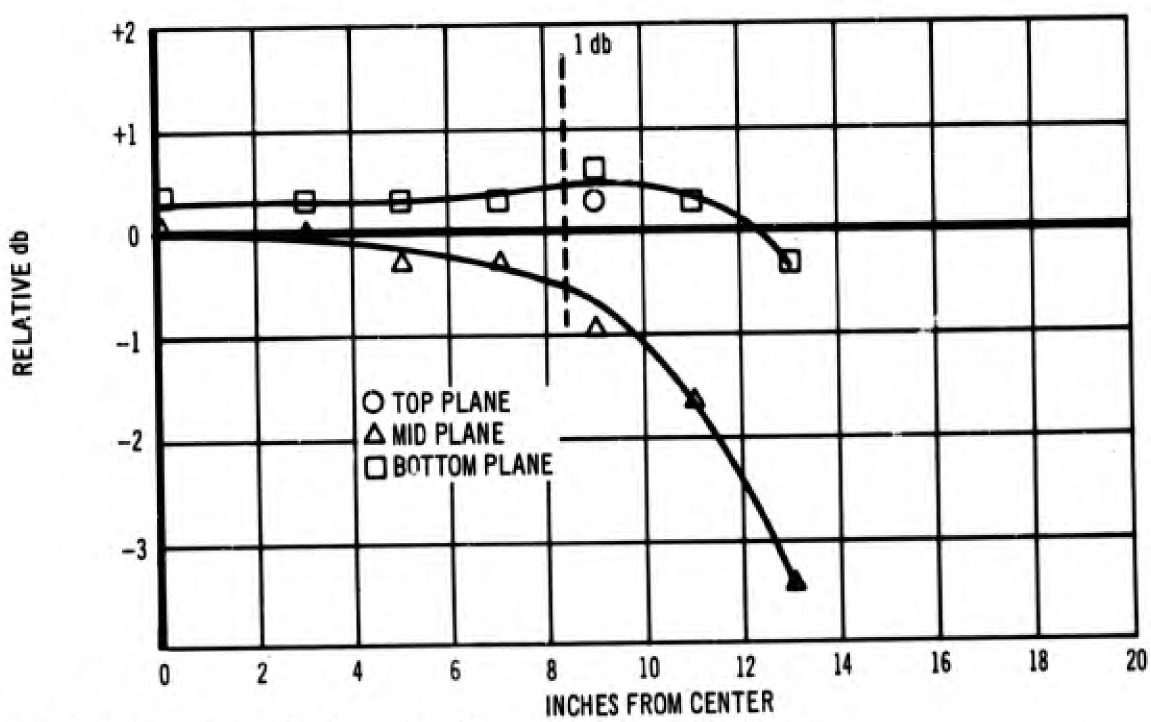

Fig. A-3 Magnetic Field Plot: Short Side – 1500 cps

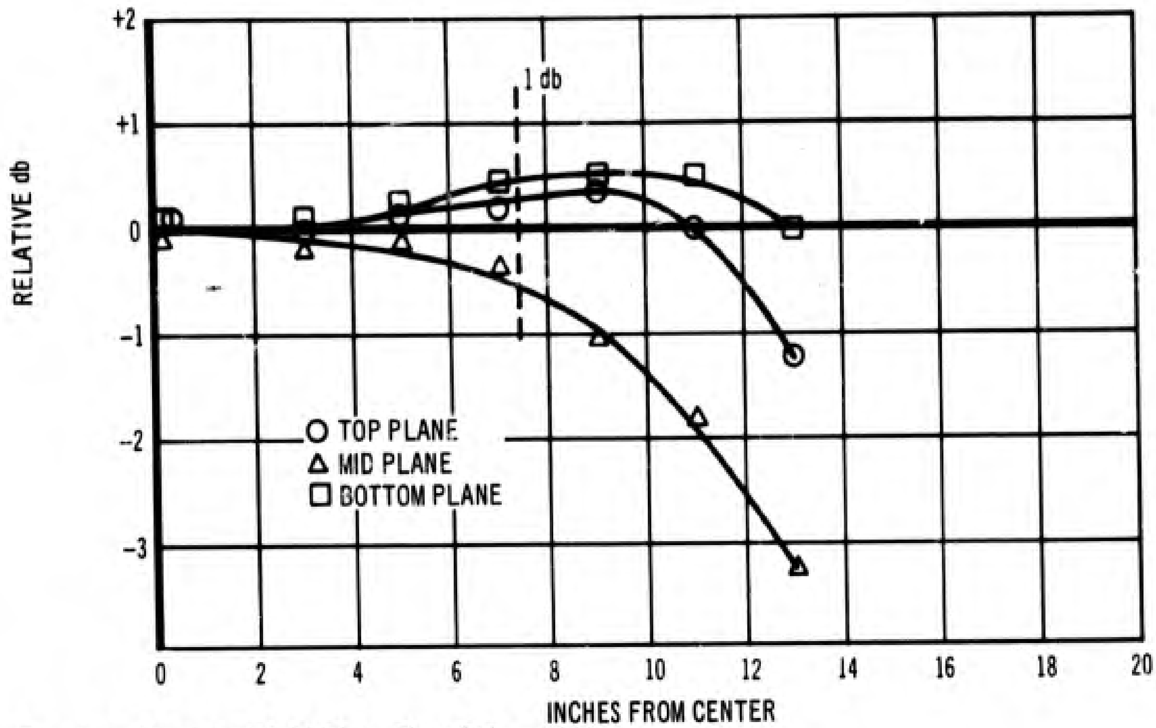

Fig. A–4 Magnetic Field Plot: Short Side – 5000 cps

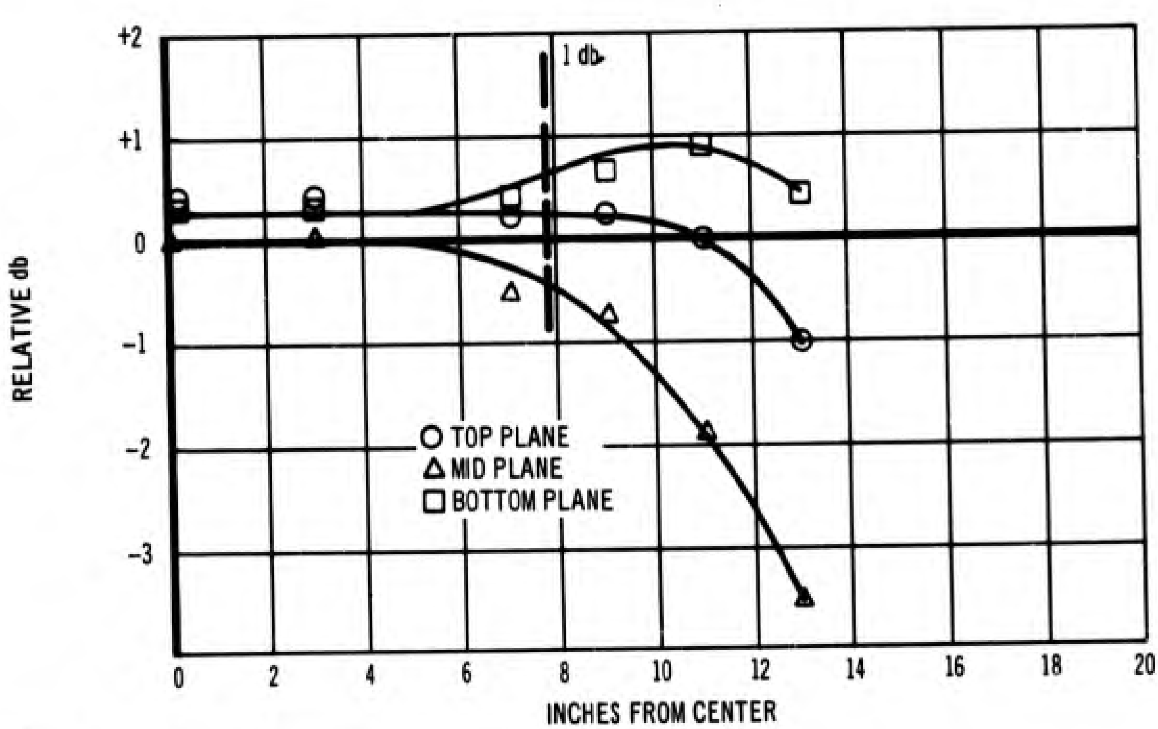

Fig. A–5 Magnetic Field Plot: Short Side – 15000 cps

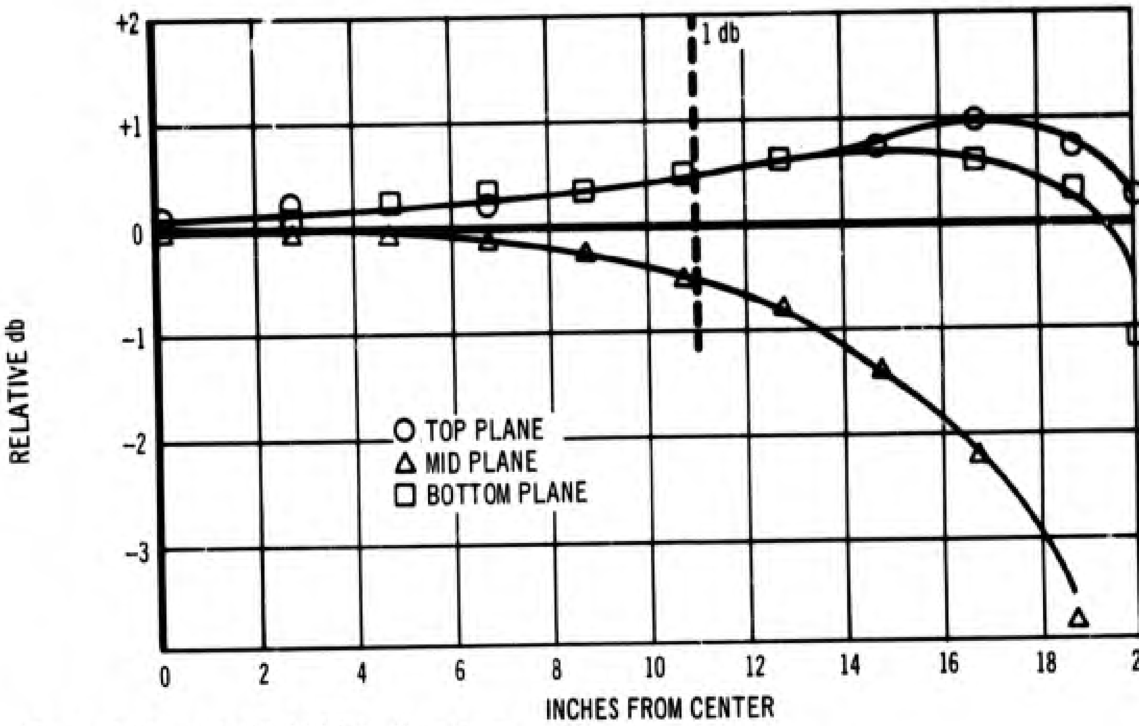

Fig. A-6 Magnetic Field Plot: Hypotenuse – 50 cps

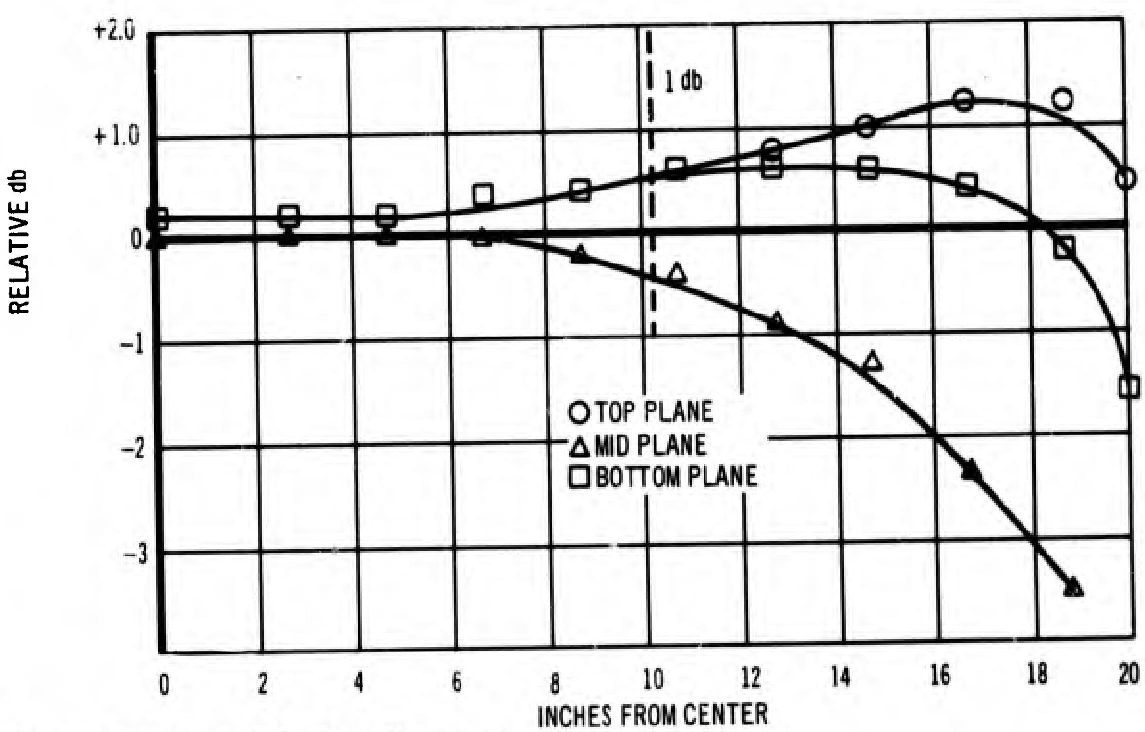

Fig. A-7 Magnetic Field Plot: Hypotenuse – 500 cps

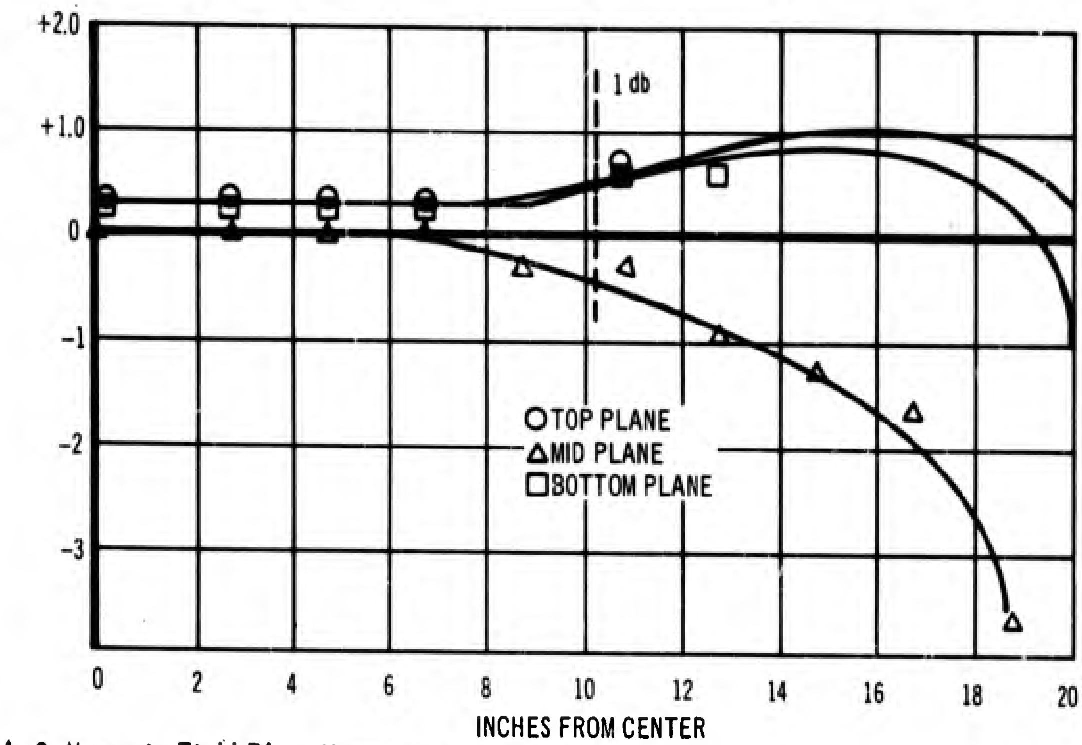

Fig. A-8 Magnetic Field Plot: Hypotenuse – 1500 cps

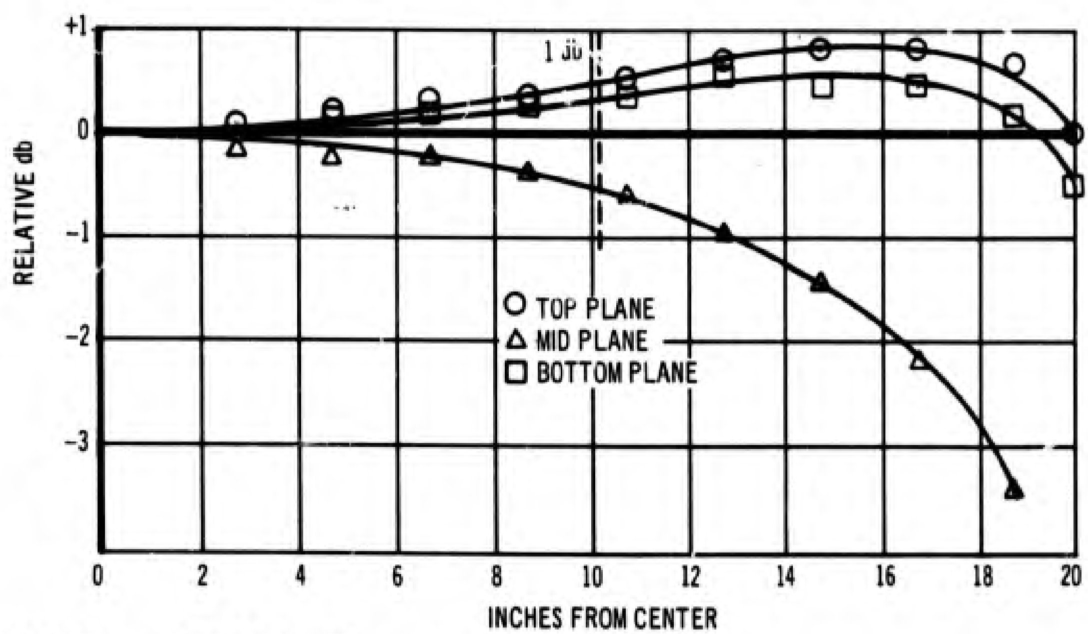

Fig. A-9 Magnetic Field Plot: Hypotenuse – 5000 cps

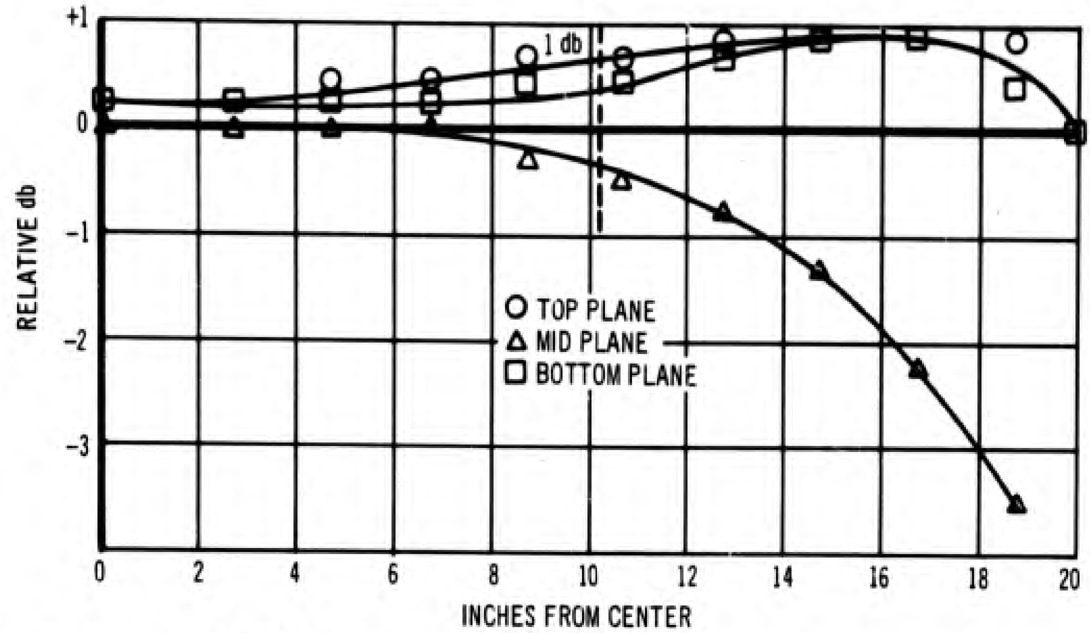

Fig. A-10 Magnetic Field Plot: Hypotenuse – 15000 cps

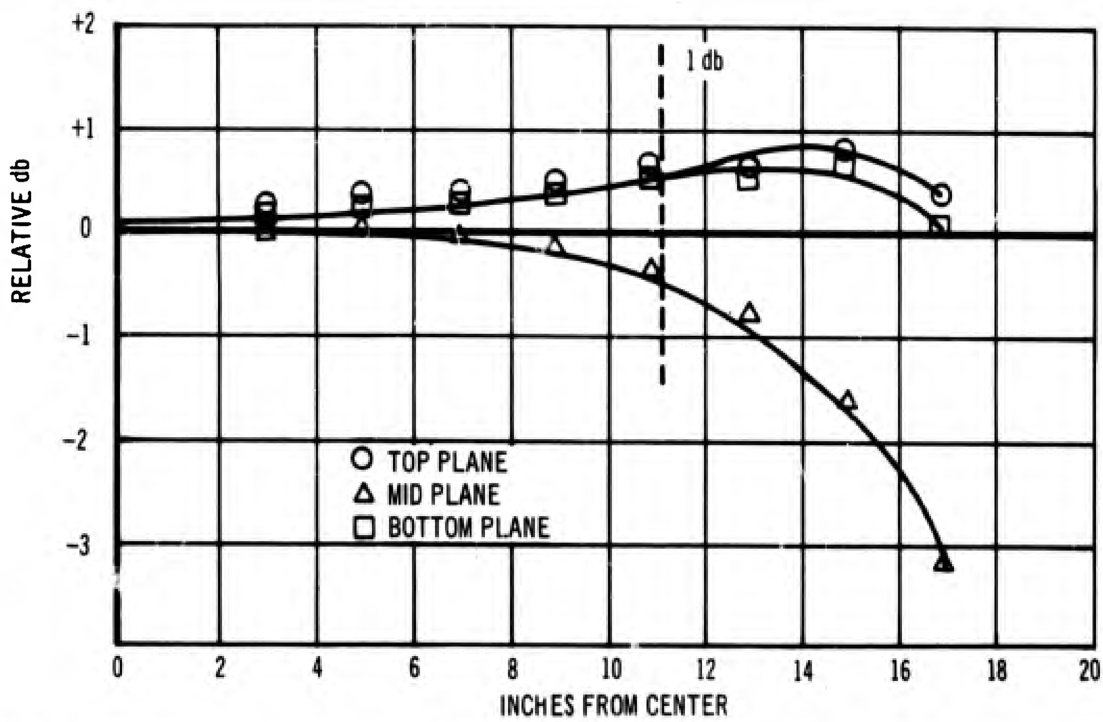

Fig. A-11 Magnetic Field Plot: Long Side – 50 cps

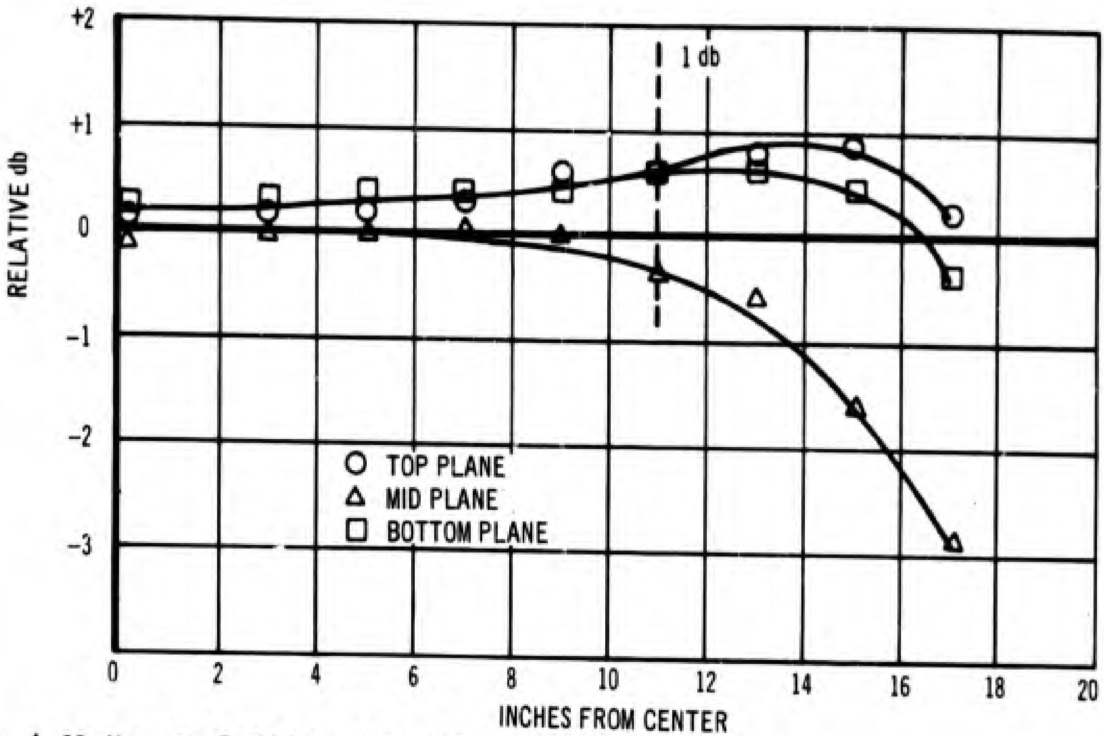

Fig. A-12 Magnetic Field Plot: Long Side – 500 cps

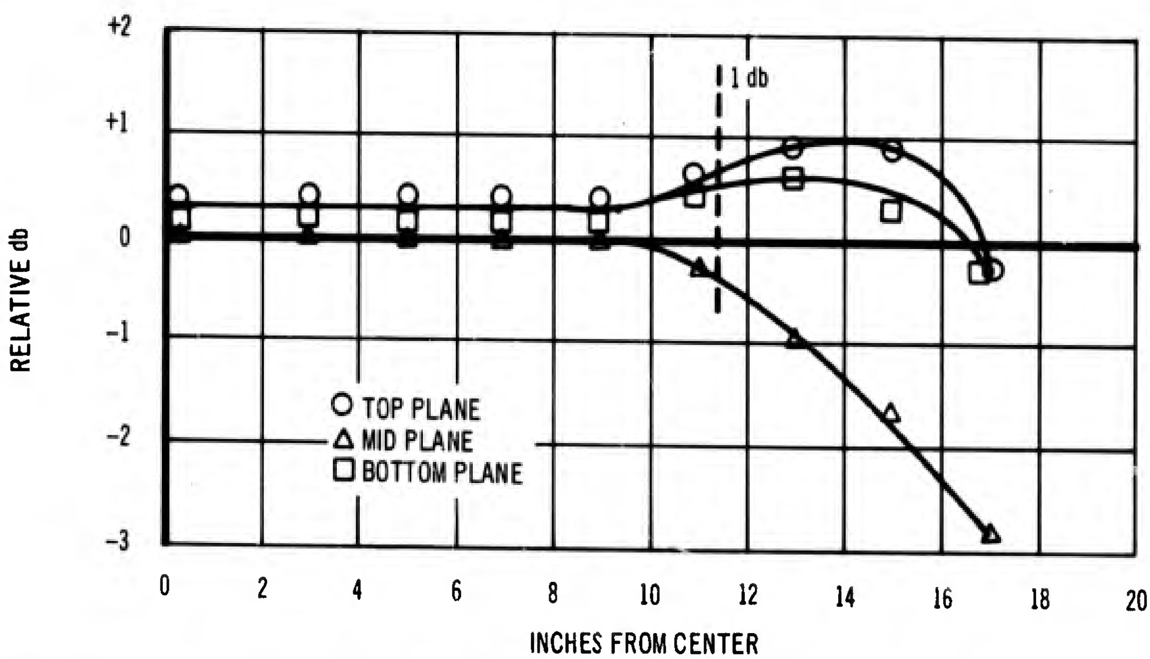

Fig. A-13 Magnetic Field Plot: Long Side – 1500 cps

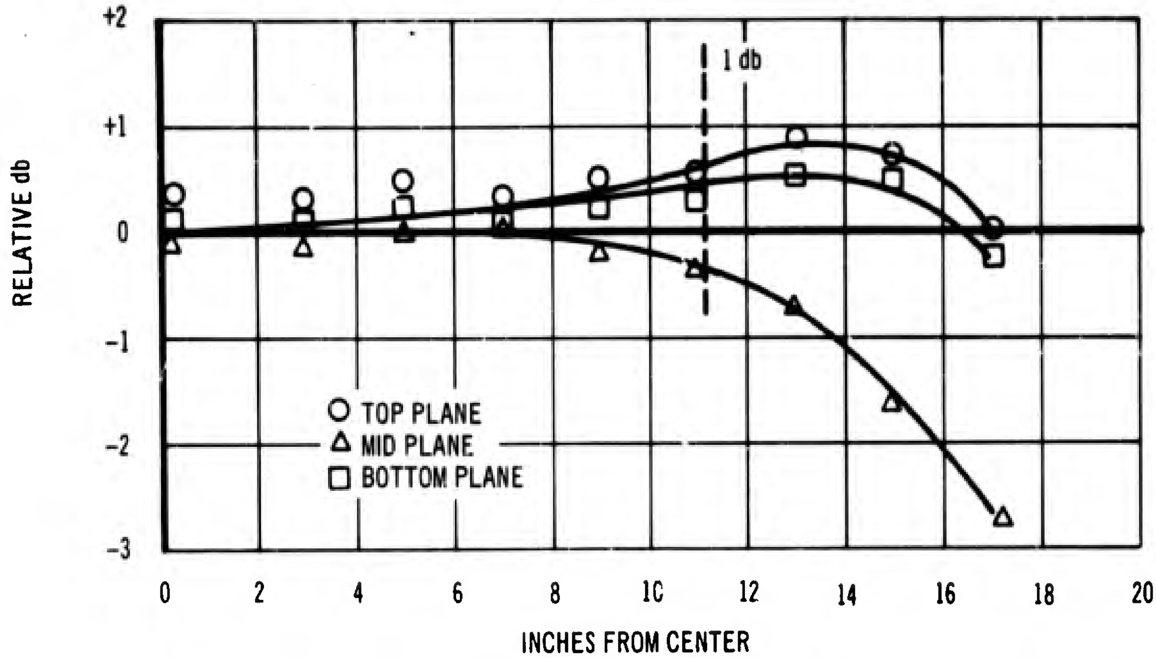

Fig. A-14 Magnetic Field Plot: Long Side – 5000 cps

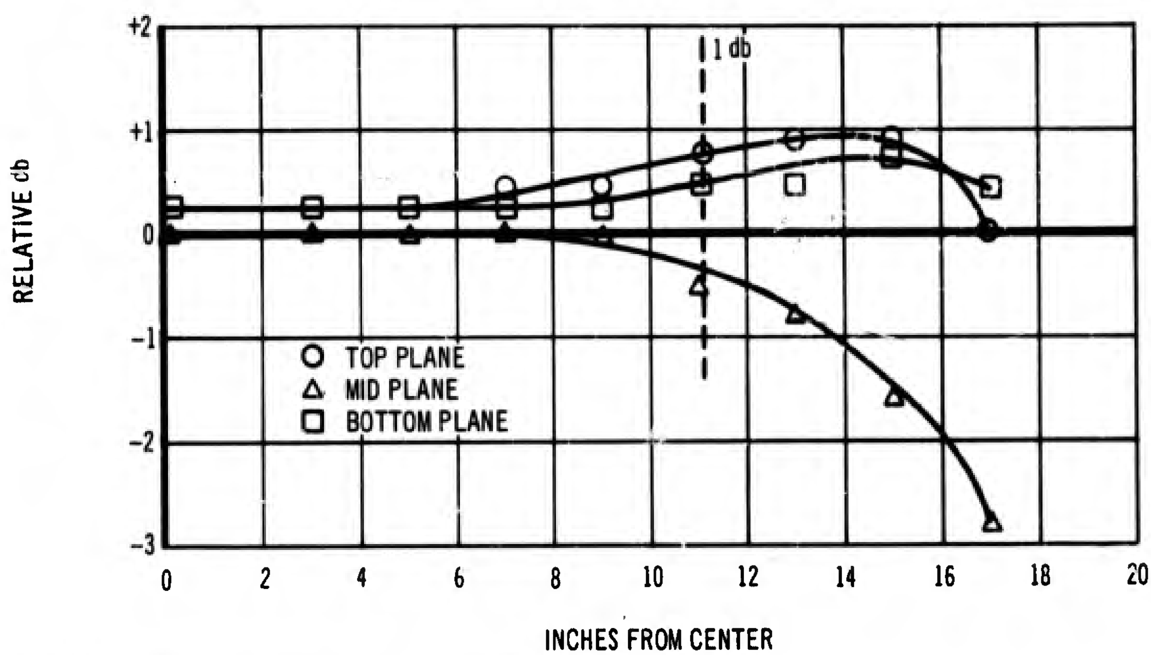

Fig. A-15 Magnetic Field Plot: Long Side – 15000 cps

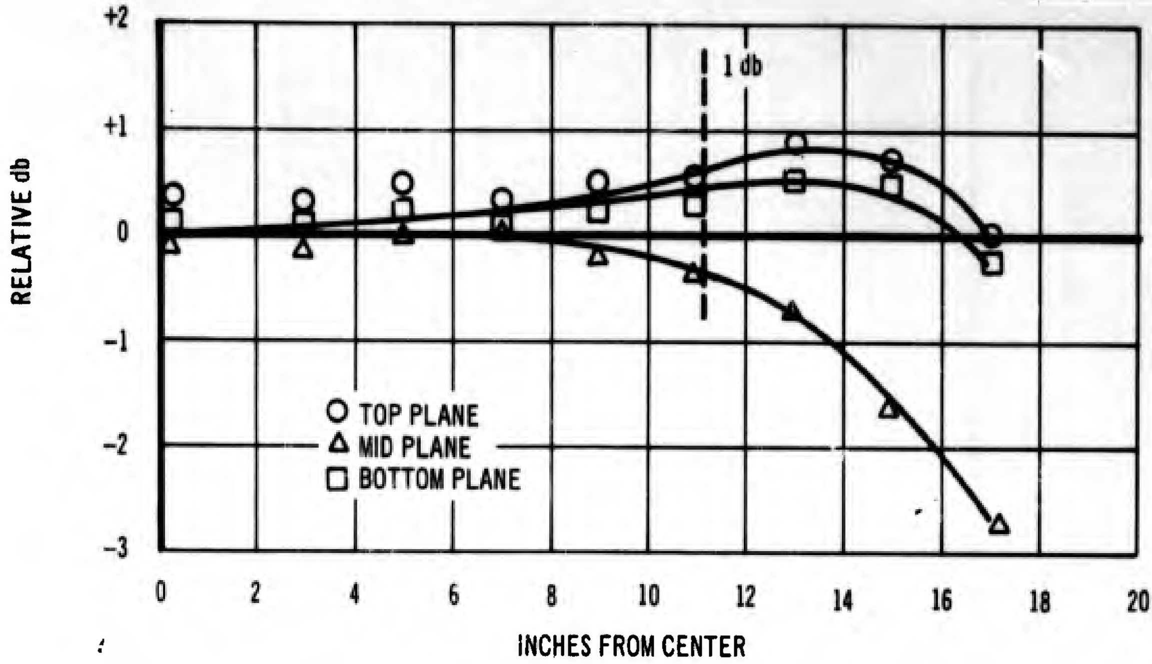

Fig. A-14 Magnetic Field Plot: Long Side – 5000 cps

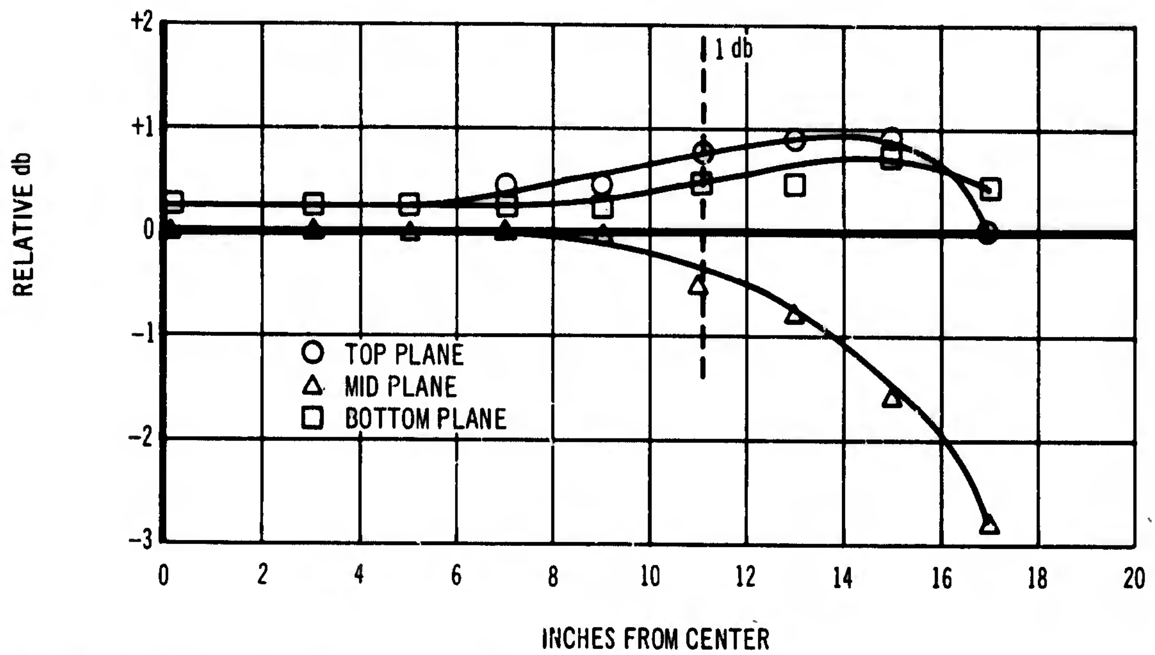

Fig. A-15 Magnetic Field Plot: Long Side – 15000 cps

Appendix A2 Shielding Effectiveness of Netic Steel

The results of measurements of shielding effectiveness of Netic steel, using a two-coil method rather than the Helmholtz coil, is presented in Fig. A16. Data for two versus one thickness was desired for comparison purposes and is also depicted on Fig. A16.

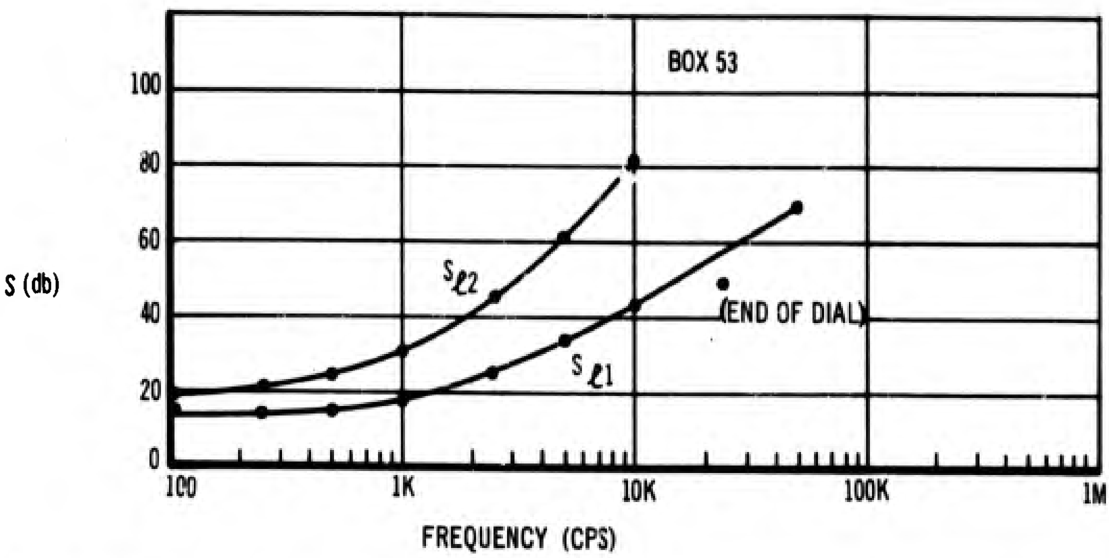

Fig. A-16 Shielding Effectiveness of One and Two Thicknesses of Netic Material Using Two Small Coil Test Setup.

Appendix A3 Measured Shielding Effectiveness 50 cps to 200 kc

All data below 200 kc., which was obtained by measuring the shielding effectiveness of various test enclosures, is presented in graphical form in Figs. A17 through A41. Data has generally been grouped as pertinent to the isolation of specific shielding effectiveness factors, Table A1. Most data has been adjusted for an impedance value equal to that of a wave front present at the broad face of a 6 x 8 x 10 inch box. Data for the SIZE factor and the SHAPE factor are presented as measured.

It is anticipated that objections may be directed, in several instances, at the graphic interpretation of data. The necessity for taking closely-spaced measurements was not recognized in the early part of the Study. Subsequently many early test boxes were modified or submitted to environmental tests before "fill-in" could be obtained. Therefore the shape of the graphs, as presented, corresponds to the shape of detailed data obtained more recently. Box No. 47 data, for example, has been substantiated by data obtained from the same box following temperature shock (# 47T).

Two sets of data exhibit double peaks, for which no explanation is offered (Boxes # 52 and # 67).

The effect of adjusting measured data to compensate for wave front impedance at boxes smaller than 6 x 8 x 10 inches is apparent in Fig. A21, Box # 45. Between 1250 cycles and 9 kc., data points are as measured. The approximately 6 db difference is not fully realized until 30 kc. resulting in a discontinuity between 9 and 12 kc.

TABLE A1 ENCLOSURES ALLOCATED FOR ISOLATION OF SHIELDING EFFECTIVENESS FACTORS

Figure	Box Number	Metal
Material Factor S_1		
Variation with Thickness		
A 17	11, 12, 13, 14, 3, 15	(copper)
A 18	23, 24, 25, 26, 27	(aluminum)
A 19	35, 36	(magnesium)
A 20	37, 56, 69	(brass)
A 21	42, 45, 46	(monel)
A 22	50, 51, 52	(steel)
A 23	54A, 55, 56	(netic steel)
A 24	74, 75	(titanium)
Variation with Composition		
A 25	3, 26, 35, 42, 50, 54A, 37, 57, 58, 74	
Variation with Multiplicity and Laminations		
A 26	22, 63, 67	
A 27	71, 72	
Material Configuration Factor S_2		
A 28	3, 16A, 16B, 17, 18	
A 29	21	
Shape Factor S_3		
A 30	5, 8, 9, 10, 70	
Size Factor S_4		
A 31	1, 2, 3, 4	

TABLE A1 ENCLOSURES ALLOCATED FOR ISOLATION OF SHIELDING EFFECTIVENESS FACTORS (Cont.)

*Fixed Seam Factor S_5		
Figure	Box Number	Metal
A 32	28, 29, 30, 31	(aluminum)
A 33	33, 34, 38	(magnesium & brass)
A 34	40, 43, 44	(monel)
A 35	47, 48, 53, 54	(steel & netic steel)
A 36	27A, 27T	(seam length)
A 20	37	(brass)
A 17	3	(copper)
A 37	5	(copper)
A 38	6	(copper)
A 39	7	(copper)
A 18	26, 27	(aluminum)
A 36	27A	(aluminum)
A 21	42	(monel)
A 22	50	(steel)
A 23	54A	(netic steel)
A 27	22, 71, 72	
*Access Seam Factor S_6		
A 37	5, 5A	
A 38	6, 6A	
A 39	7, 7A, 7B	
A 40	7C, 7D, 7G	
A 41	7E, 7F	

* To assure that the effect of seams only were being measured, several sets of data were taken after soldering the lids on. Such boxes have been assigned an "S", e.g. Box #5S.

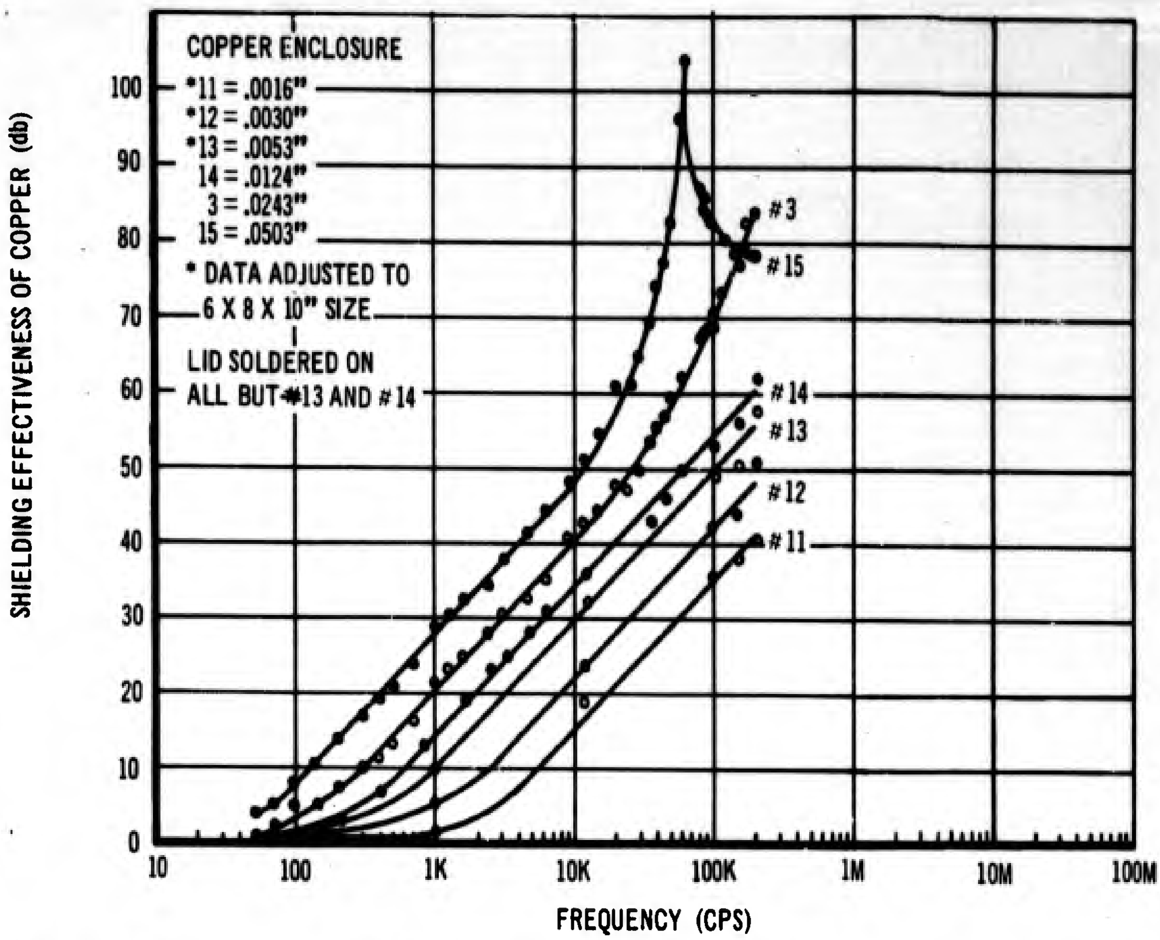

Fig. A-17 Measured Shielding Effectiveness (Variation with Thickness)

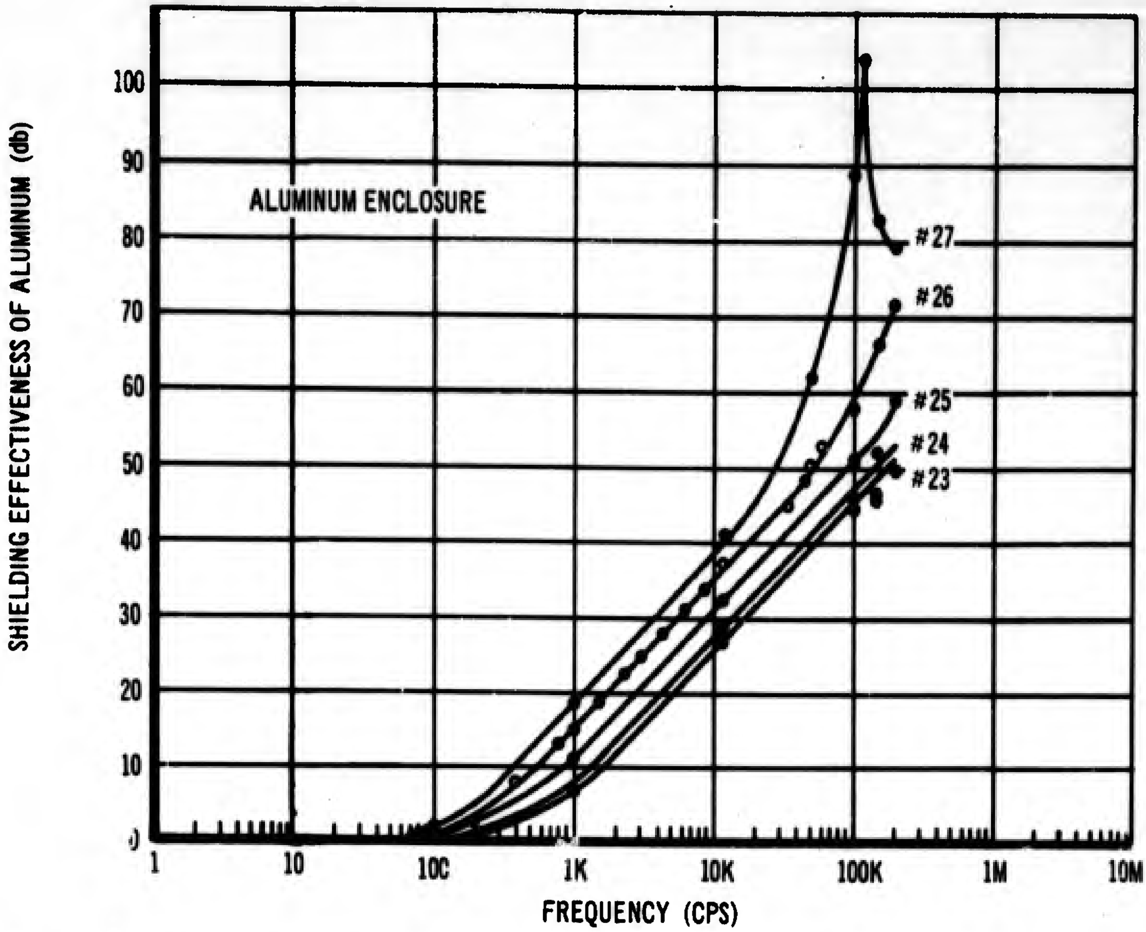

Fig. A-18 Measured Shielding Effectiveness (Variation with Thickness)

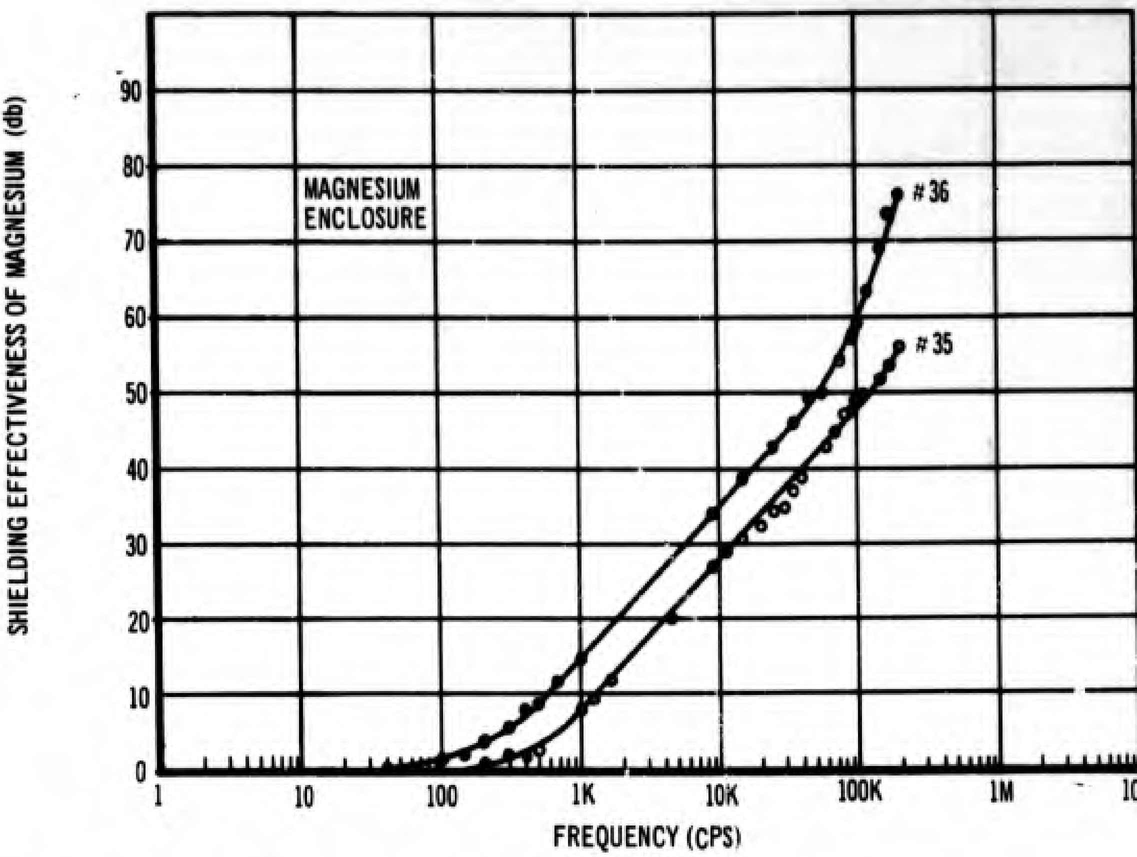

Fig. A-19 Measured Shielding Effectiveness (Variation with Thickness)

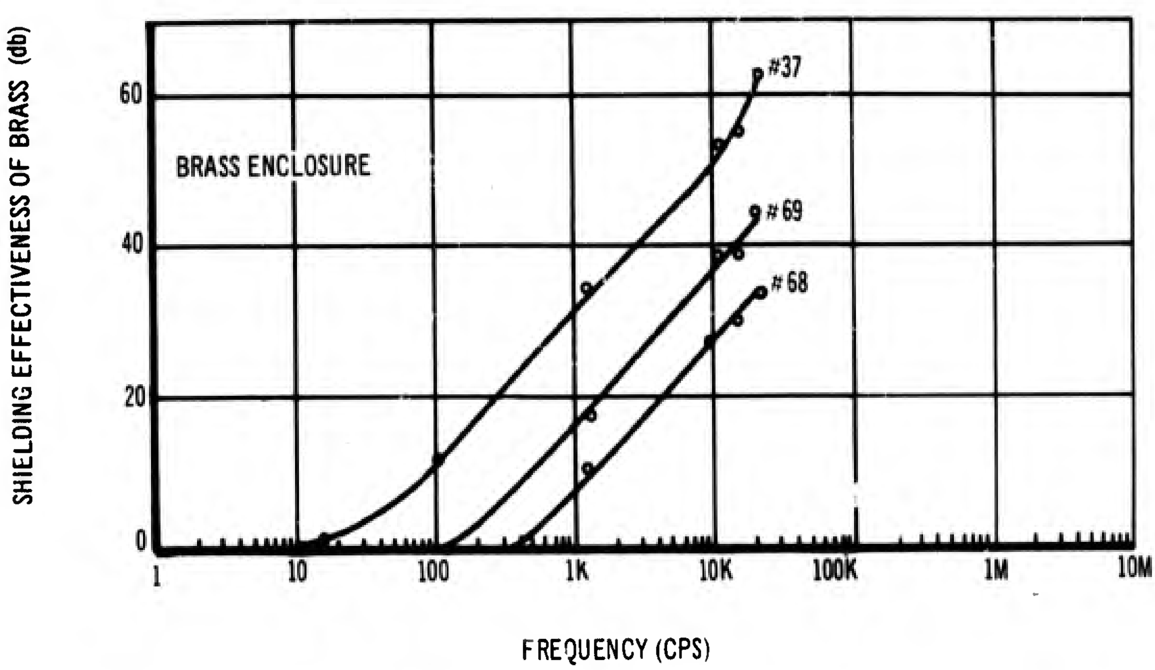

Fig. A-20 Measured Shielding Effectiveness (Variation with Thickness)

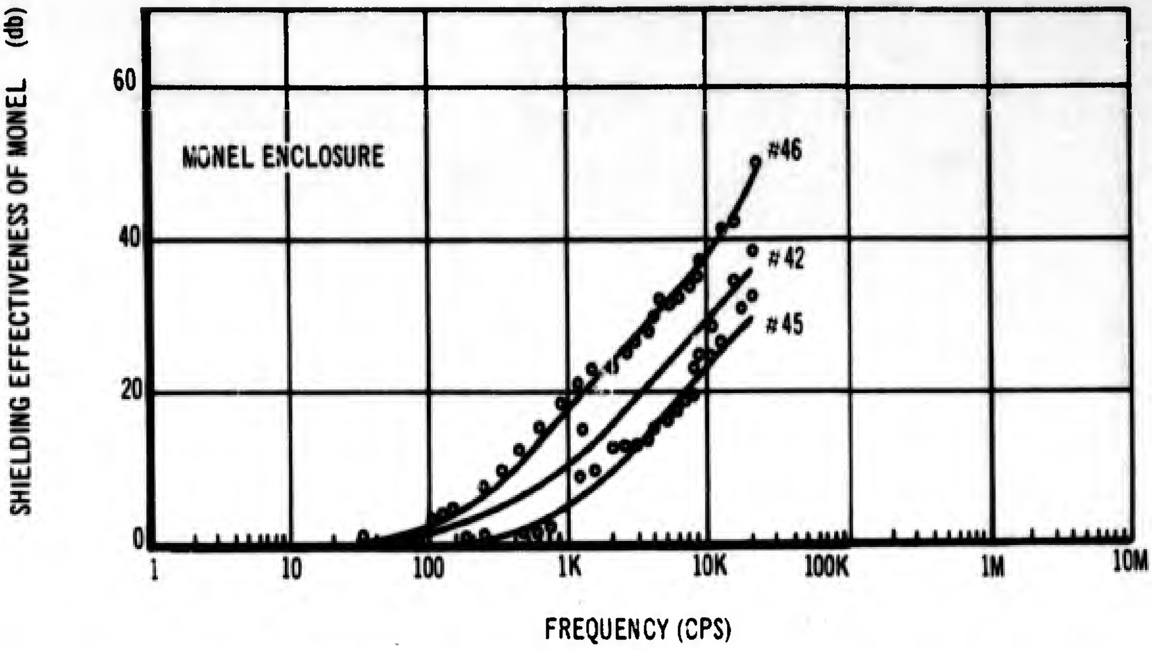

Fig. A-21 Measured Shielding Effectiveness (Variation with Thickness)

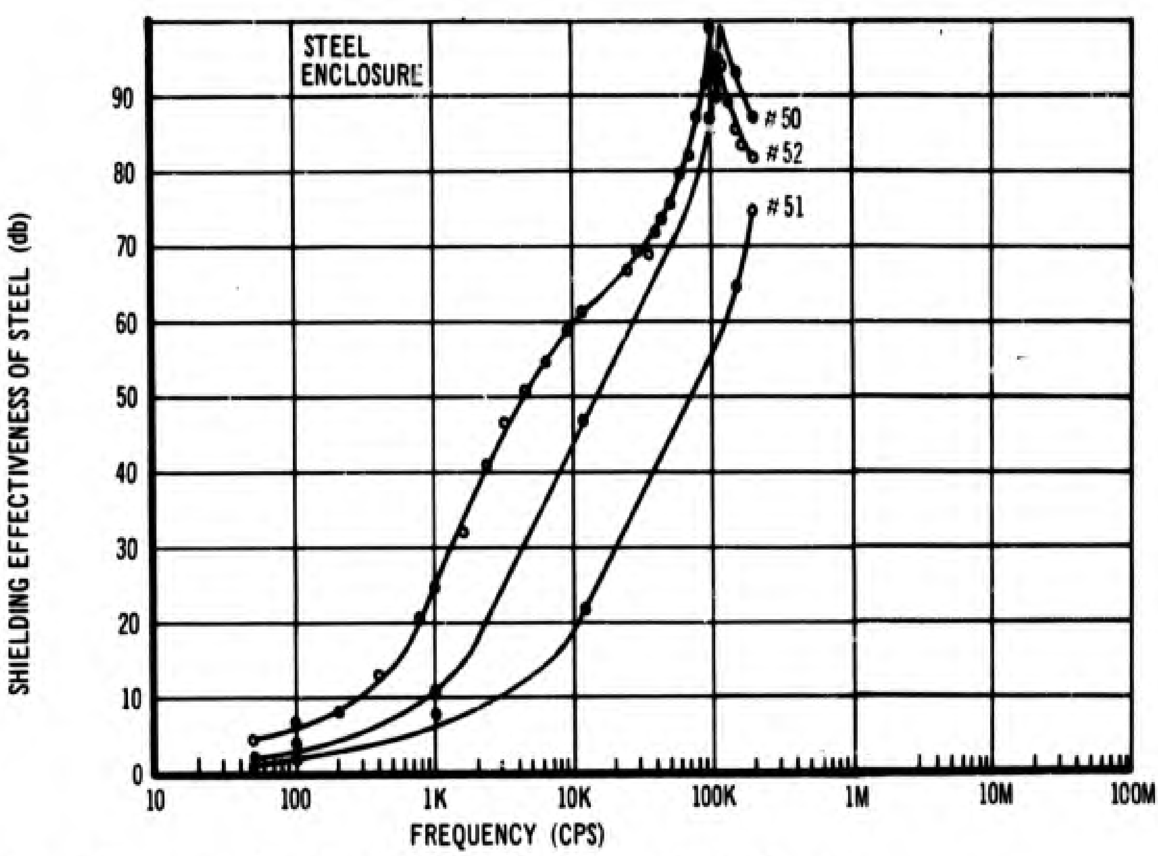

Fig. A-22 Measured Shielding Effectiveness (Variation with Thickness)

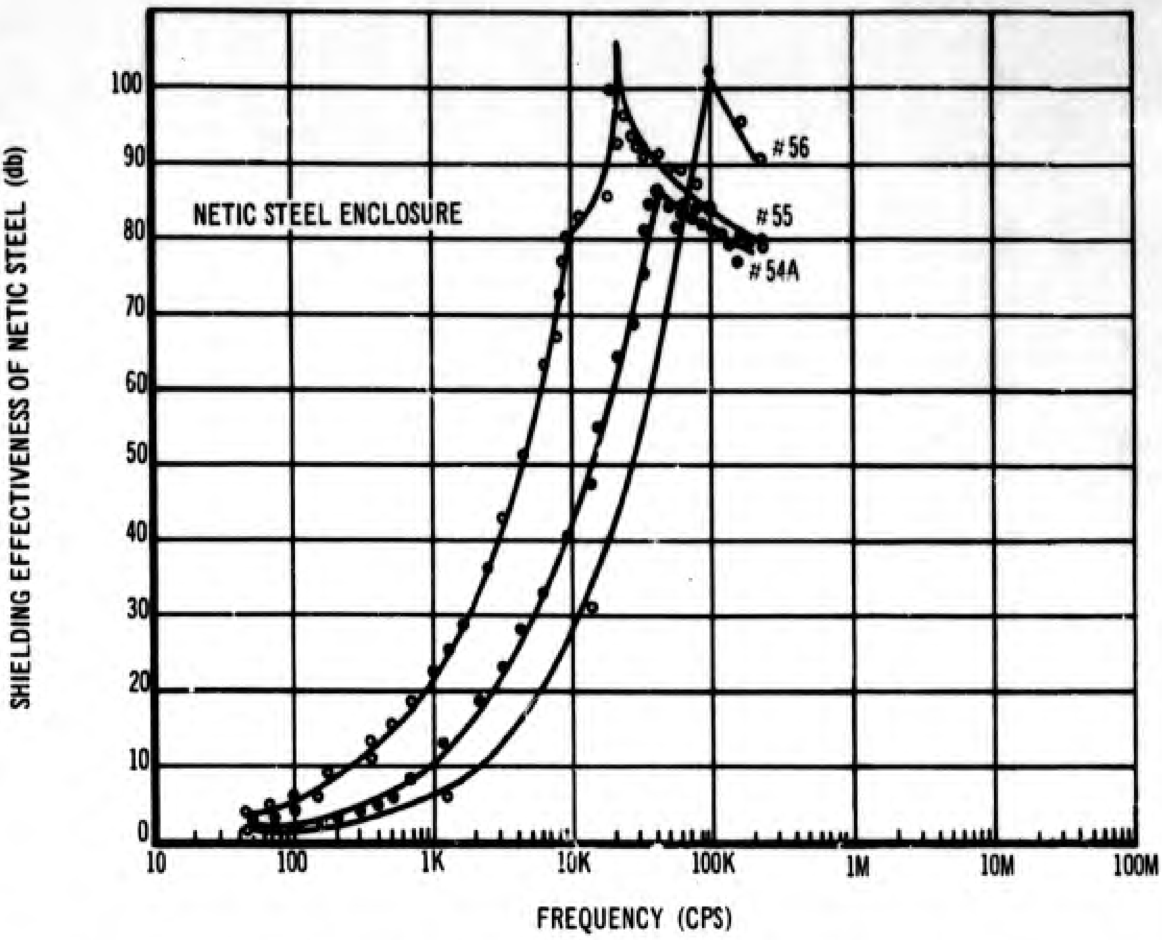

Fig. A-23 Measured Shielding Effectiveness (Variation with Thickness)

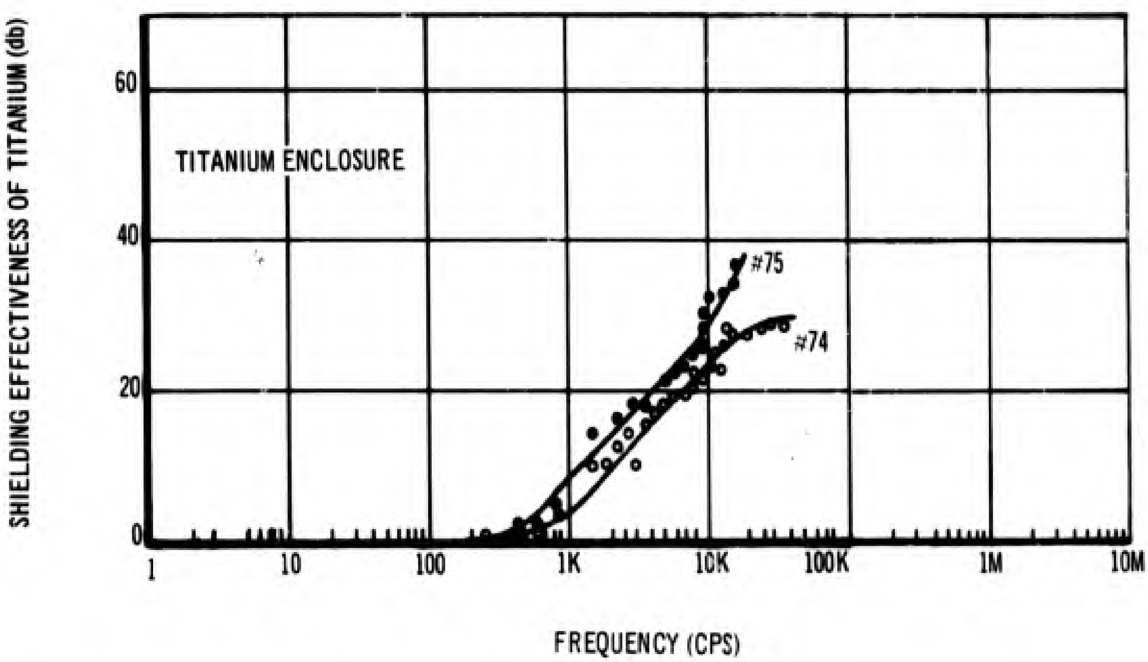

Fig. A-24 Measured Shielding Effectiveness (Variation with Thickness)

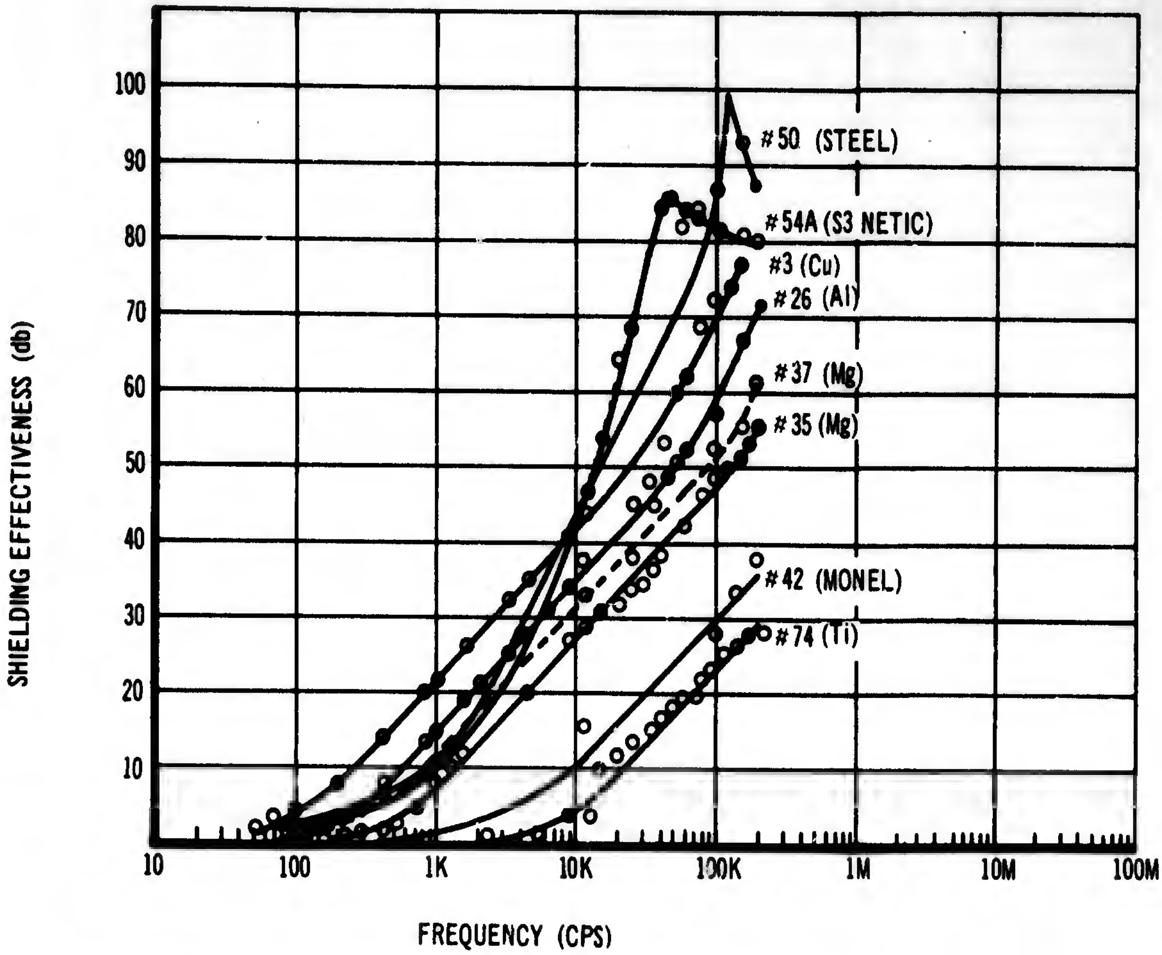

Fig. A–25 Measured Shielding Effectiveness (Composition Factor)

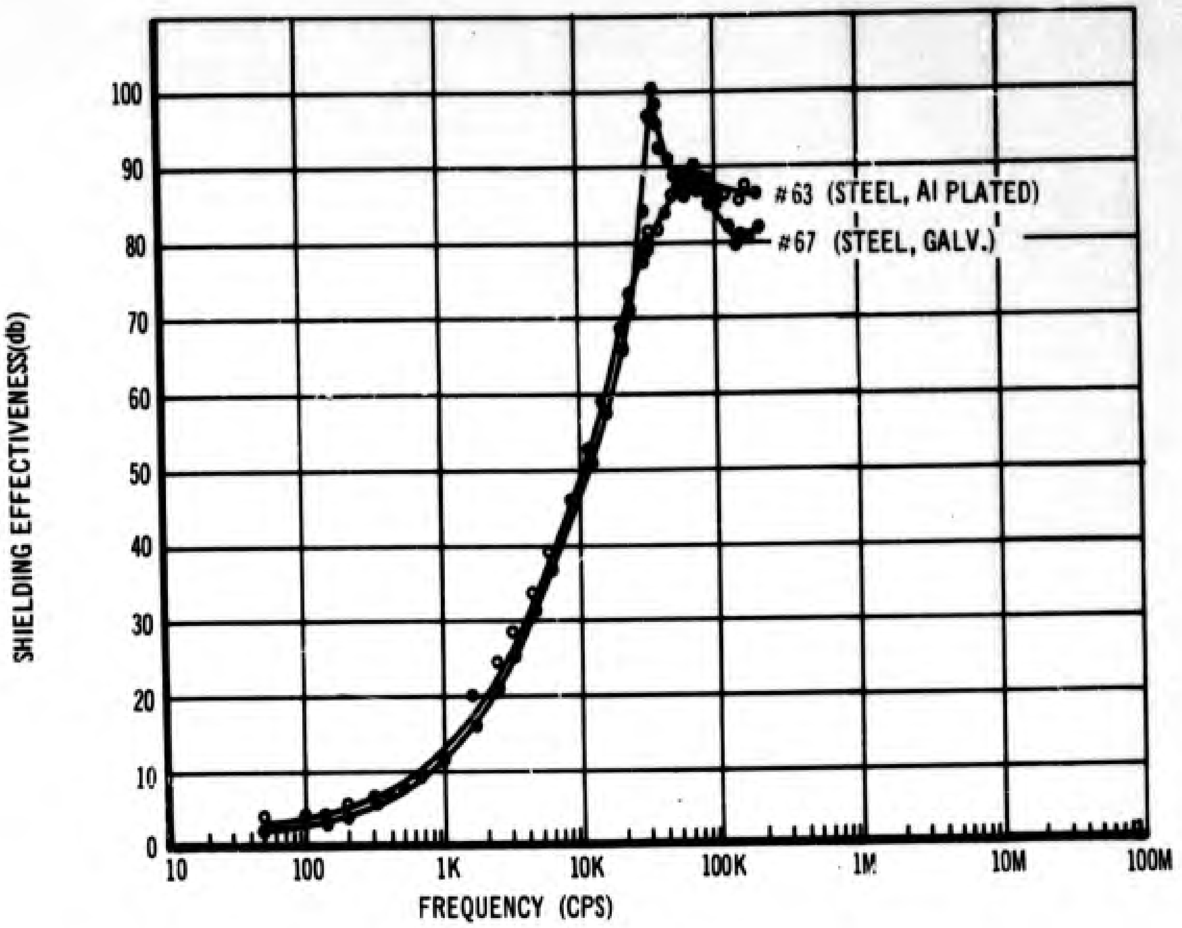

Fig. A-26 Measured Shielding Effectiveness (Laminated Shields)

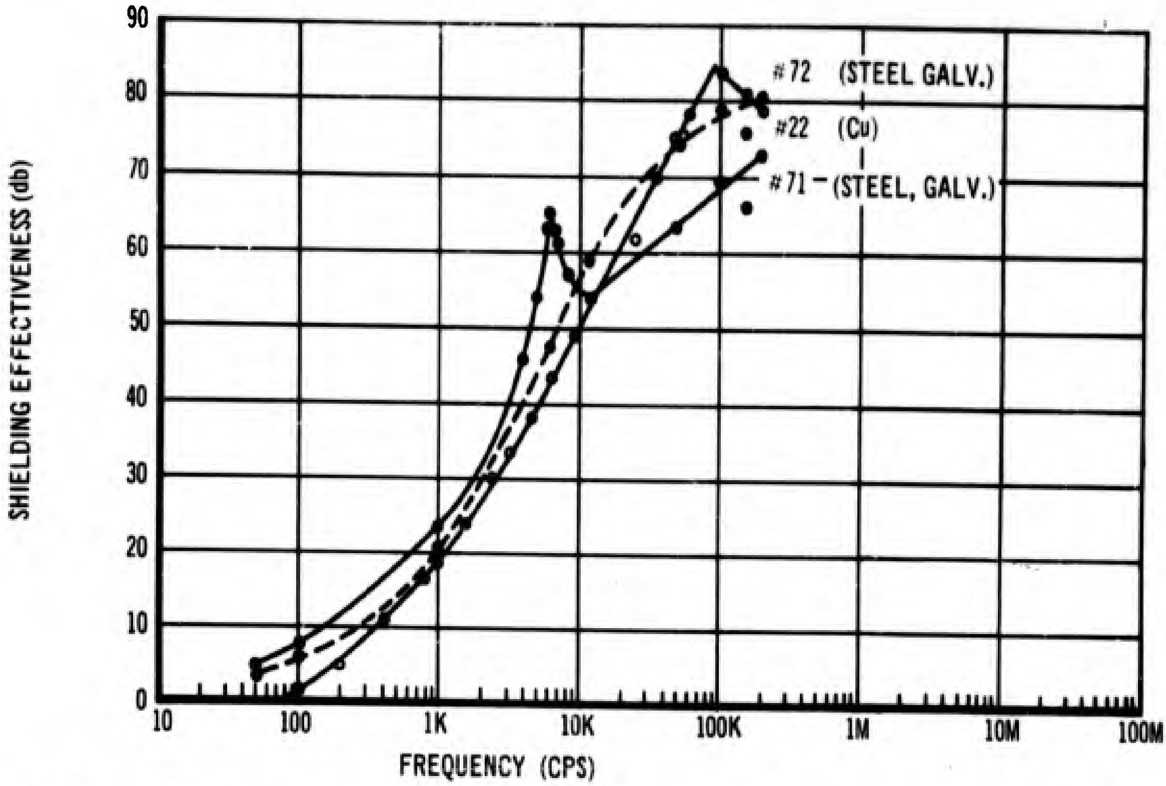

Fig. A–27 Measured Shielding Effectiveness (Multiple Shields)

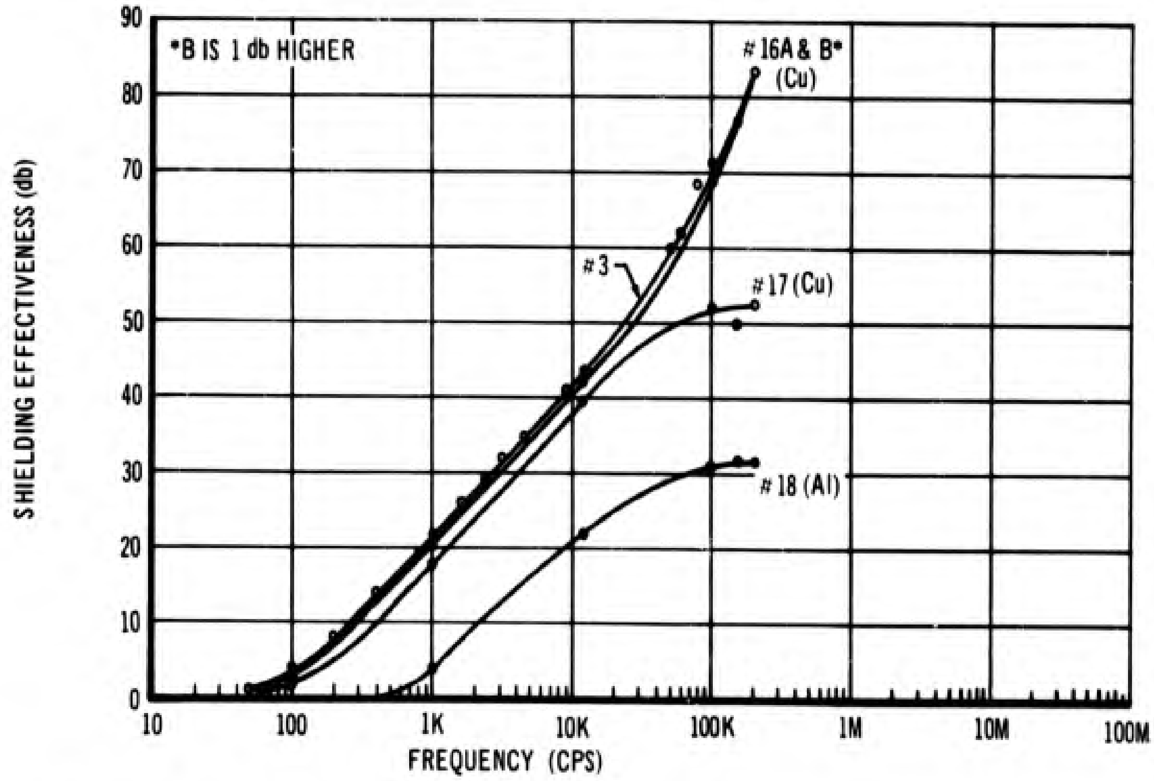

Fig. A–28 Measured Shielding Effectiveness (Material Form Factor)

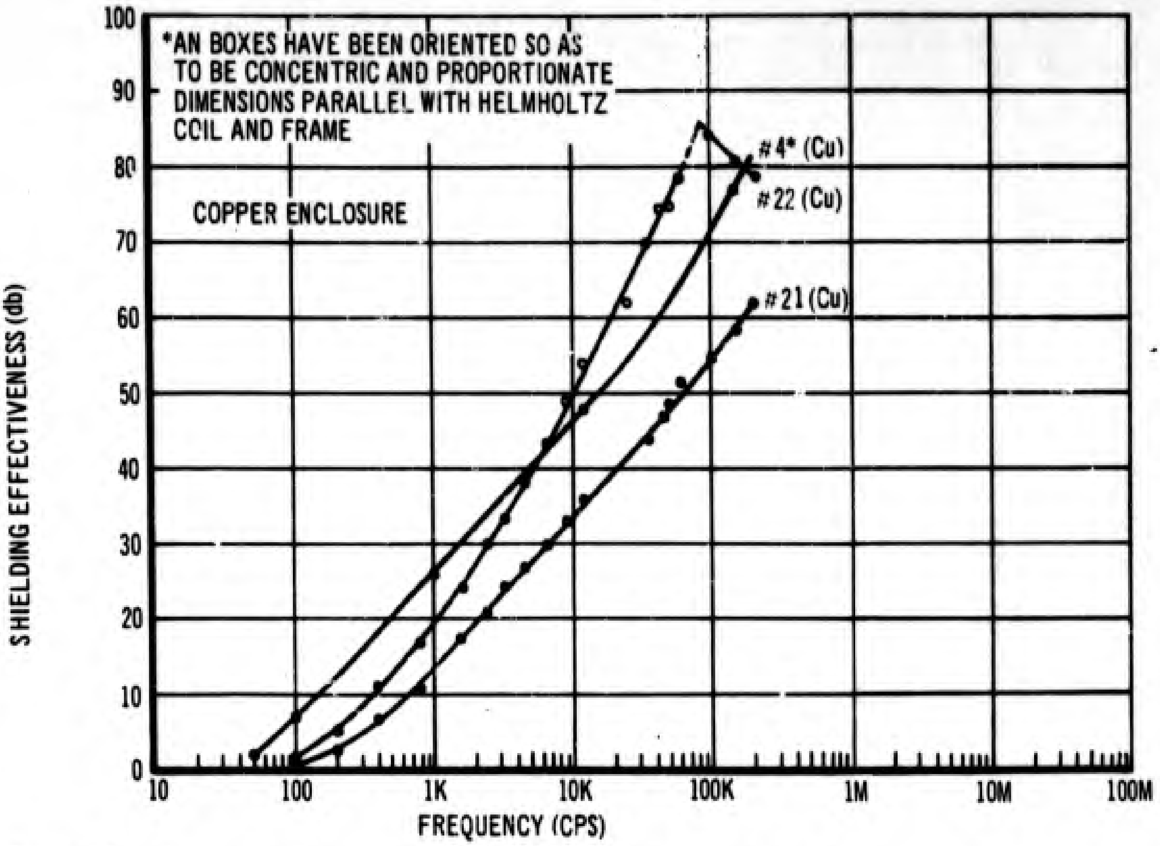

Fig. A–29 Measured Shielding Effectiveness (Single Screen vs Cell Type)

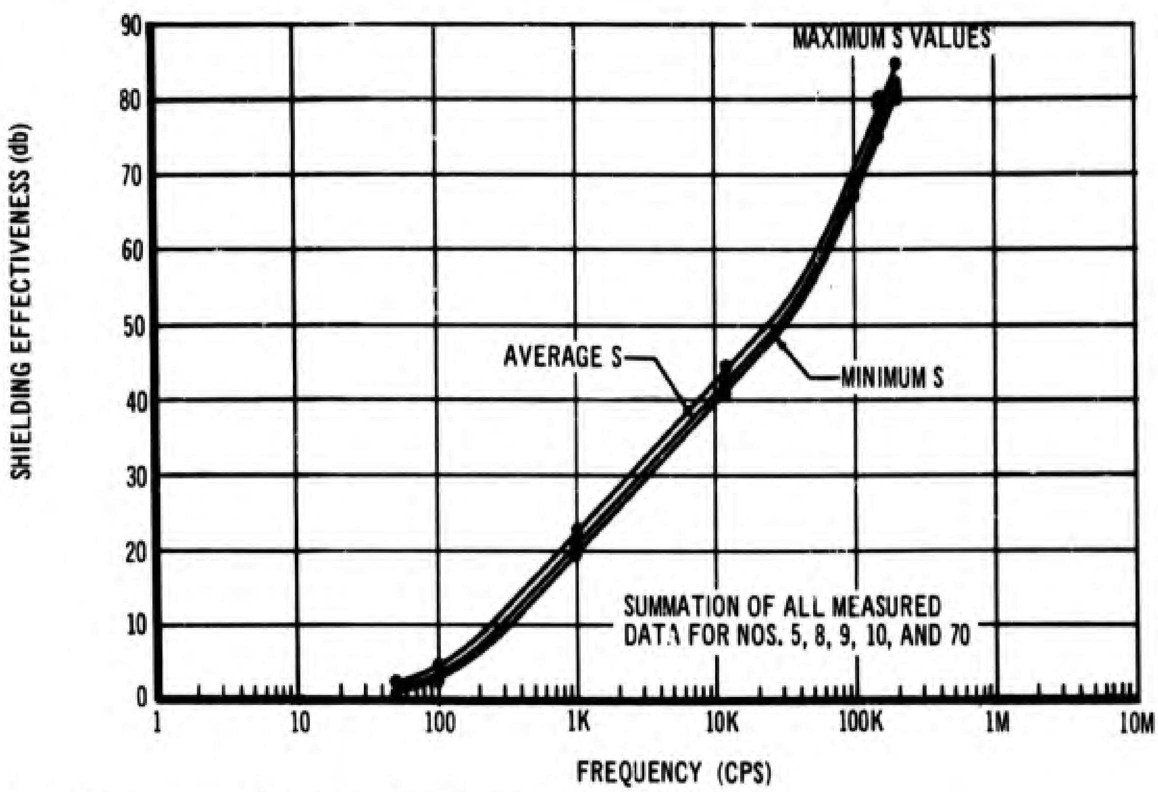

Fig. A–30 Measured Shielding Effectiveness (Shape Factor)

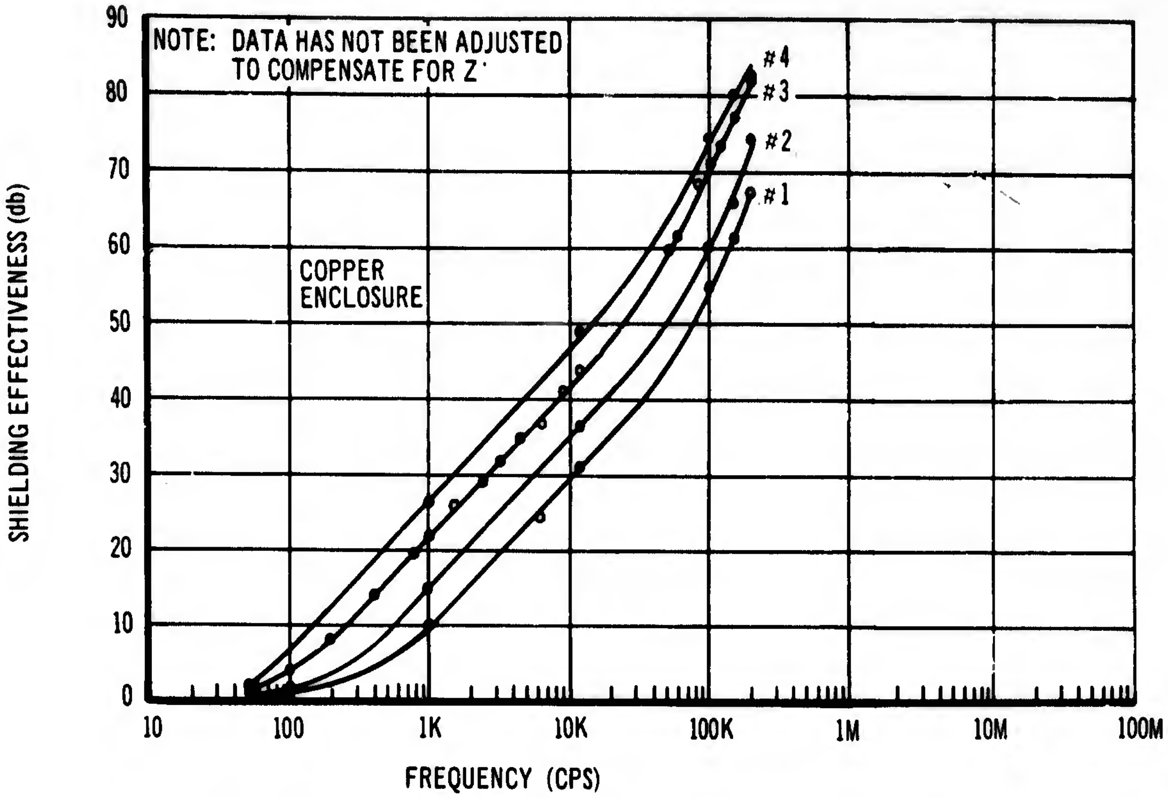

Fig. A-31 Measured Shielding Effectiveness (Size Factor)

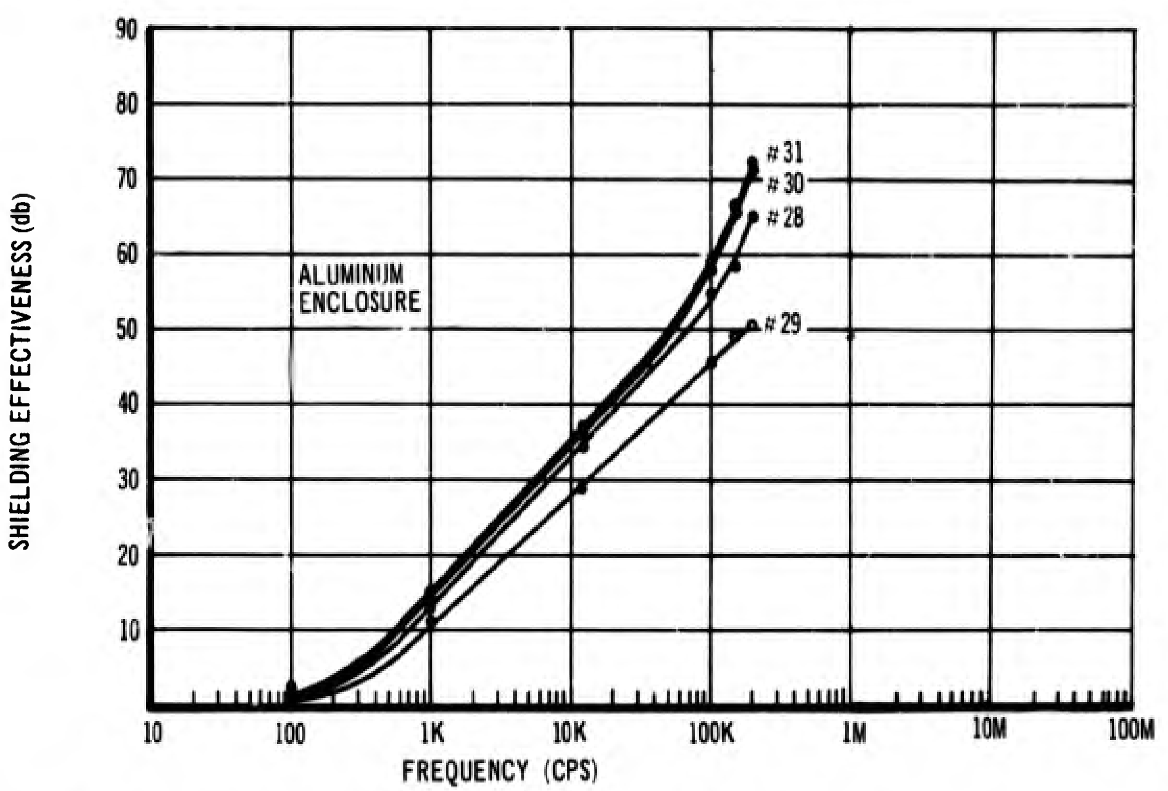

Fig. A-32 Measured Shielding Effectiveness (Fixed Seam Factor)

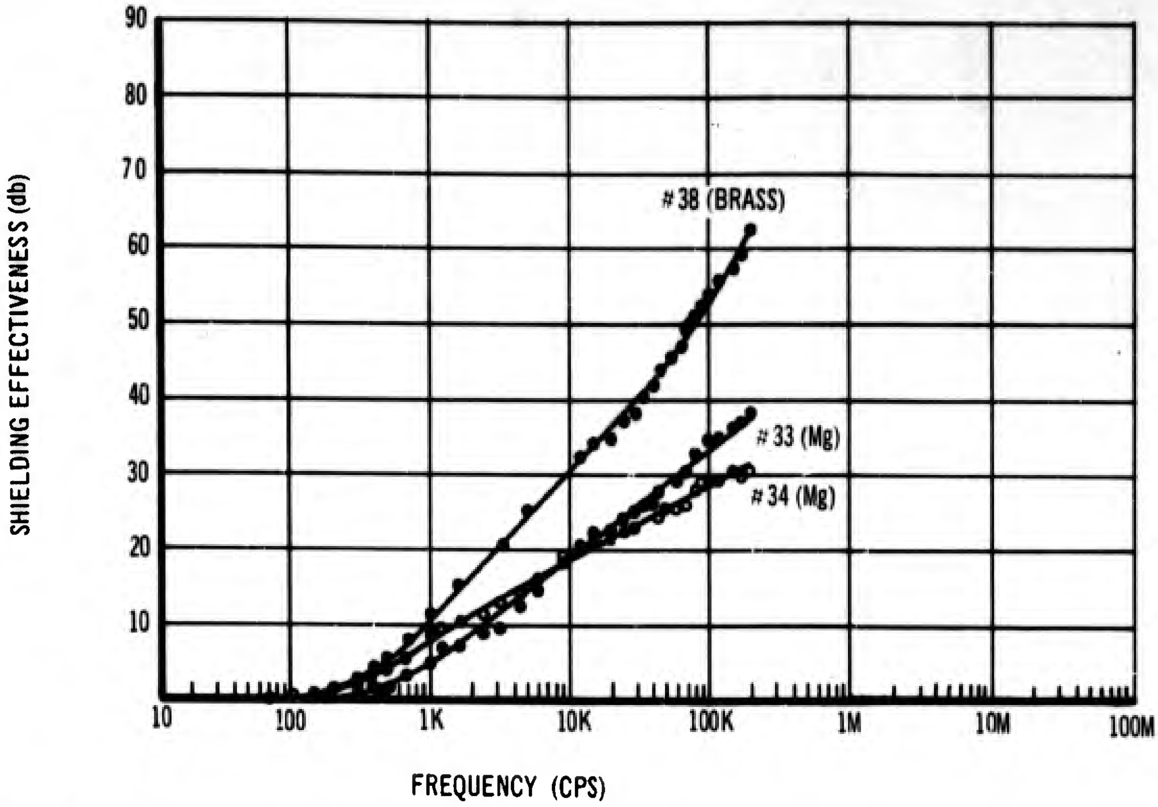

Fig. A-33 Measured Shielding Effectiveness (Fixed Seam Factor)

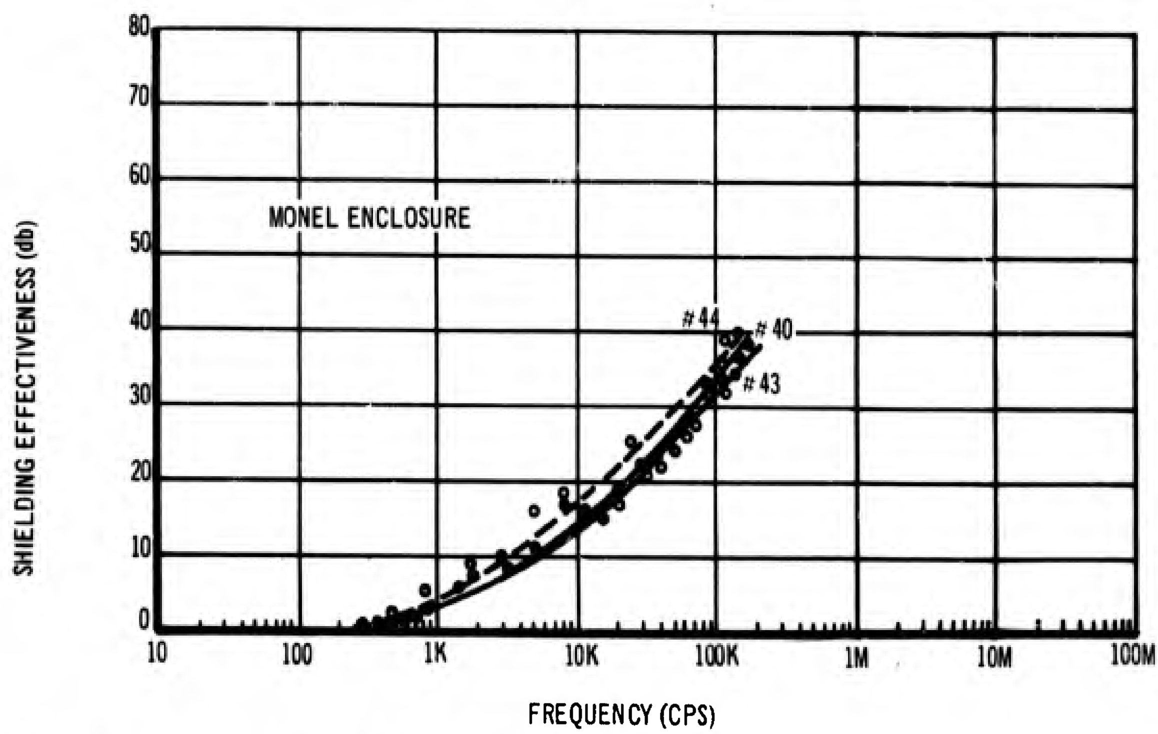

Fig. A-34 Measured Shielding Effectiveness (Fixed Seam Factor)

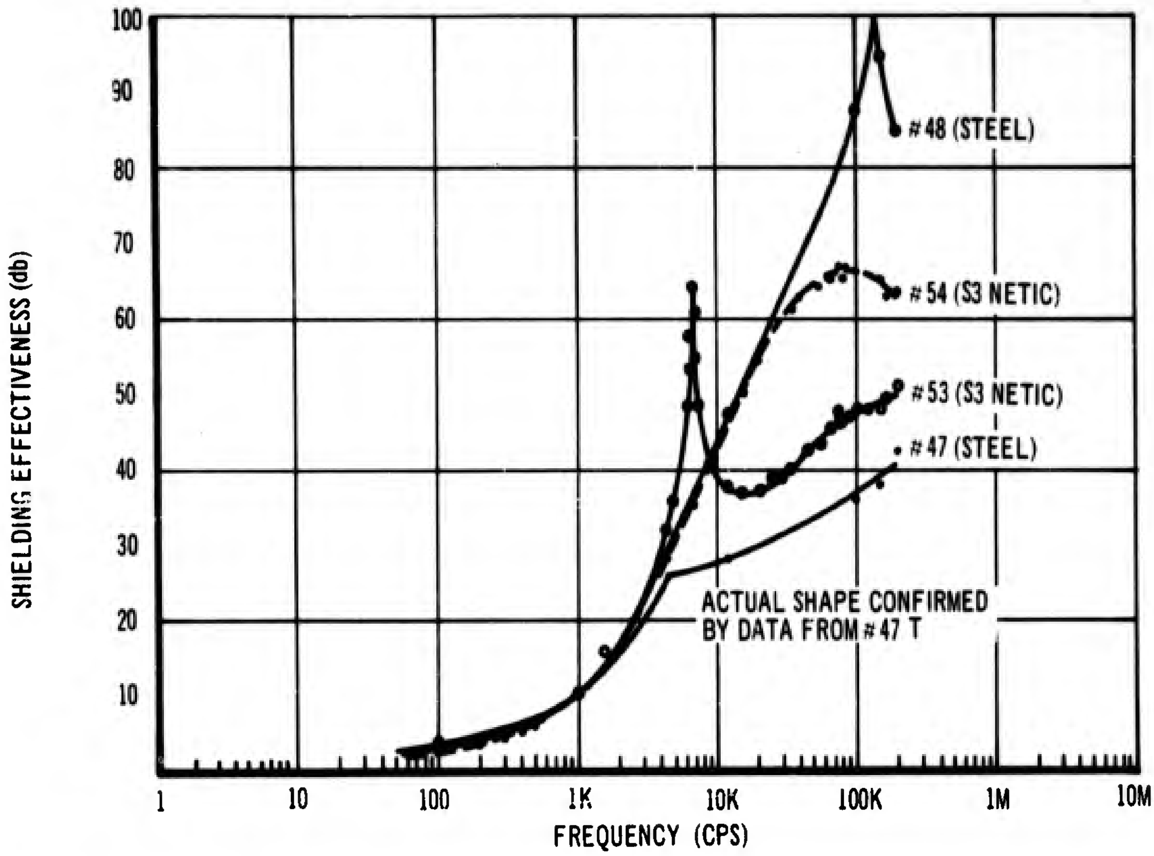

Fig. A-35 Measured Shielding Effectiveness (Fixed Seam Factor)

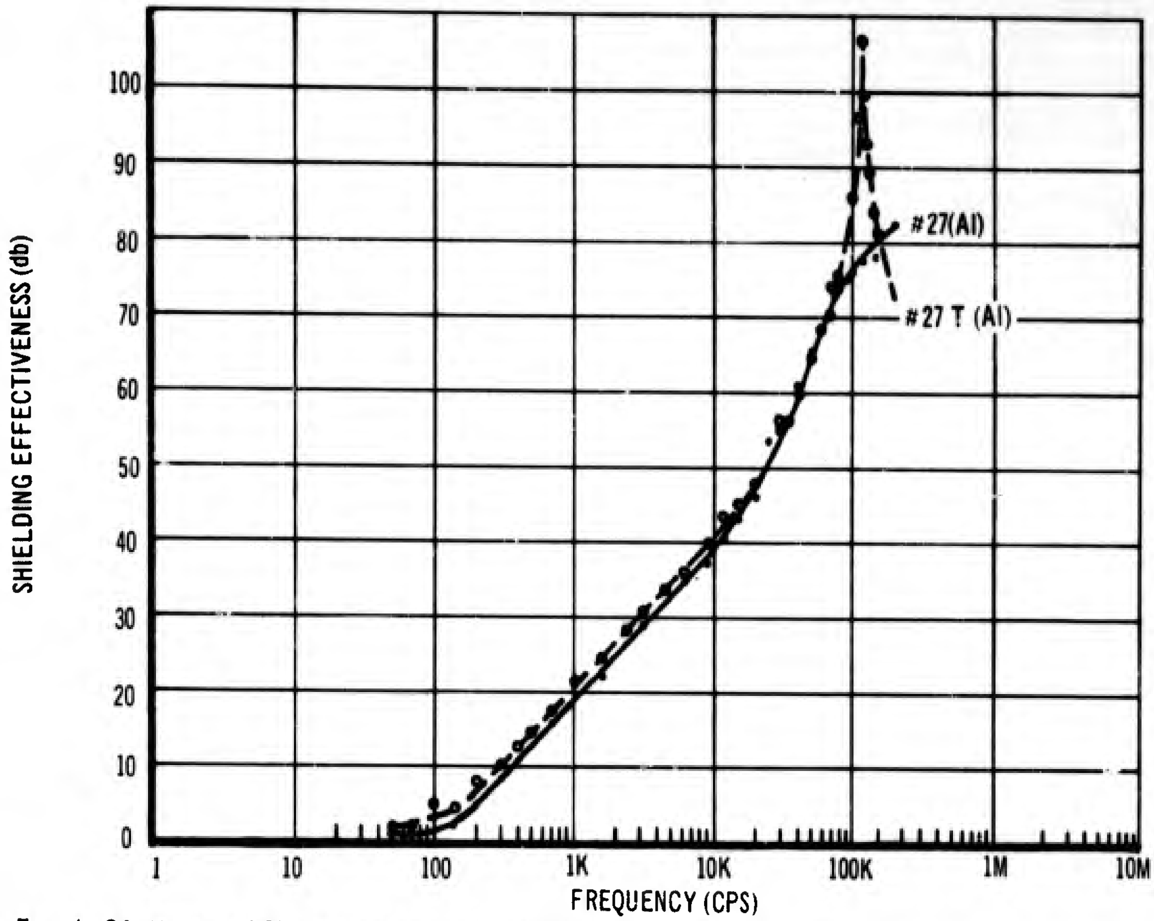

Fig. A-36 Measured Shielding Effectiveness (One vs Two Seam Lengths)

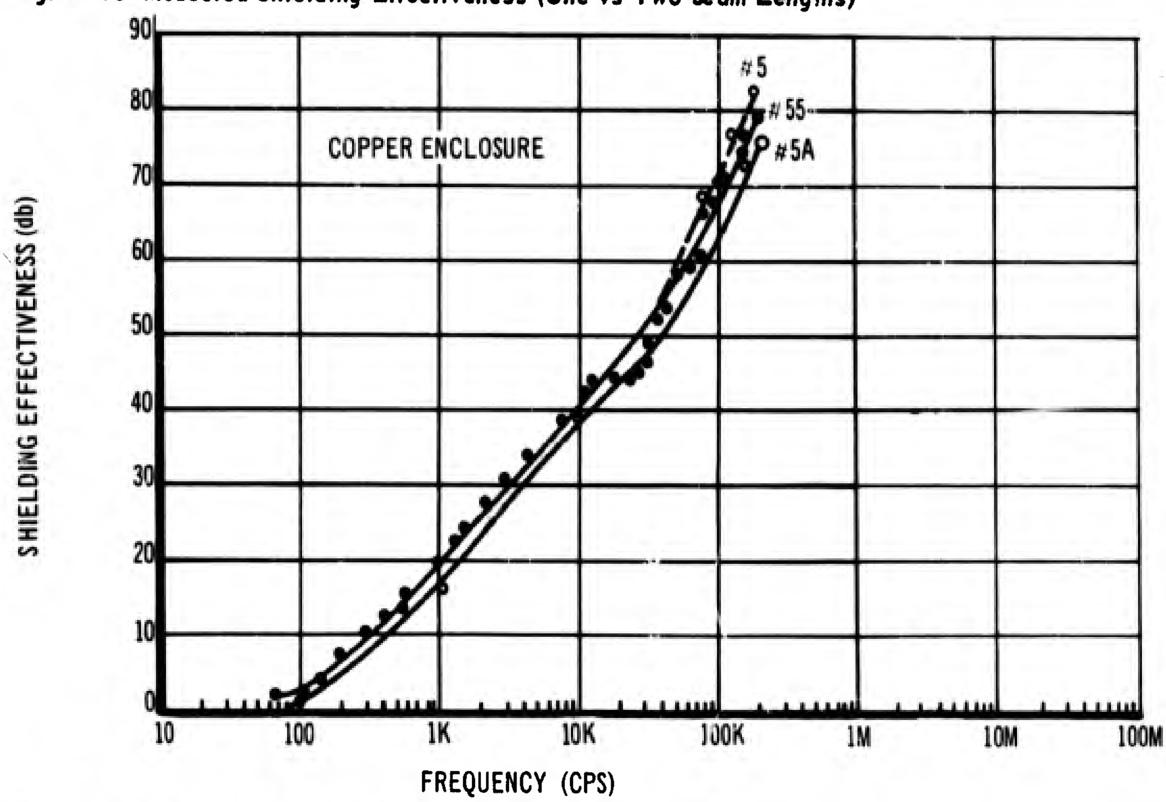

Fig. A-37 Measured Shielding Effectiveness (Access Seam Factor)

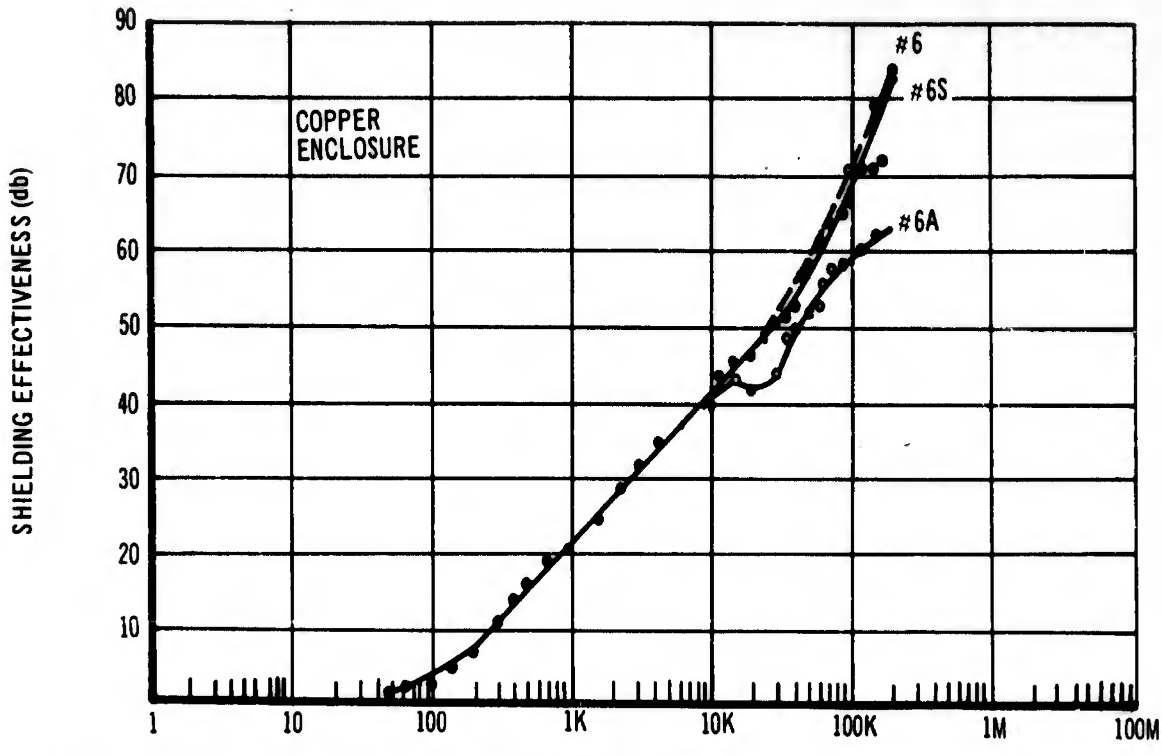

Fig. A-38 Measured Shielding Effectiveness (Access Seam Factor)

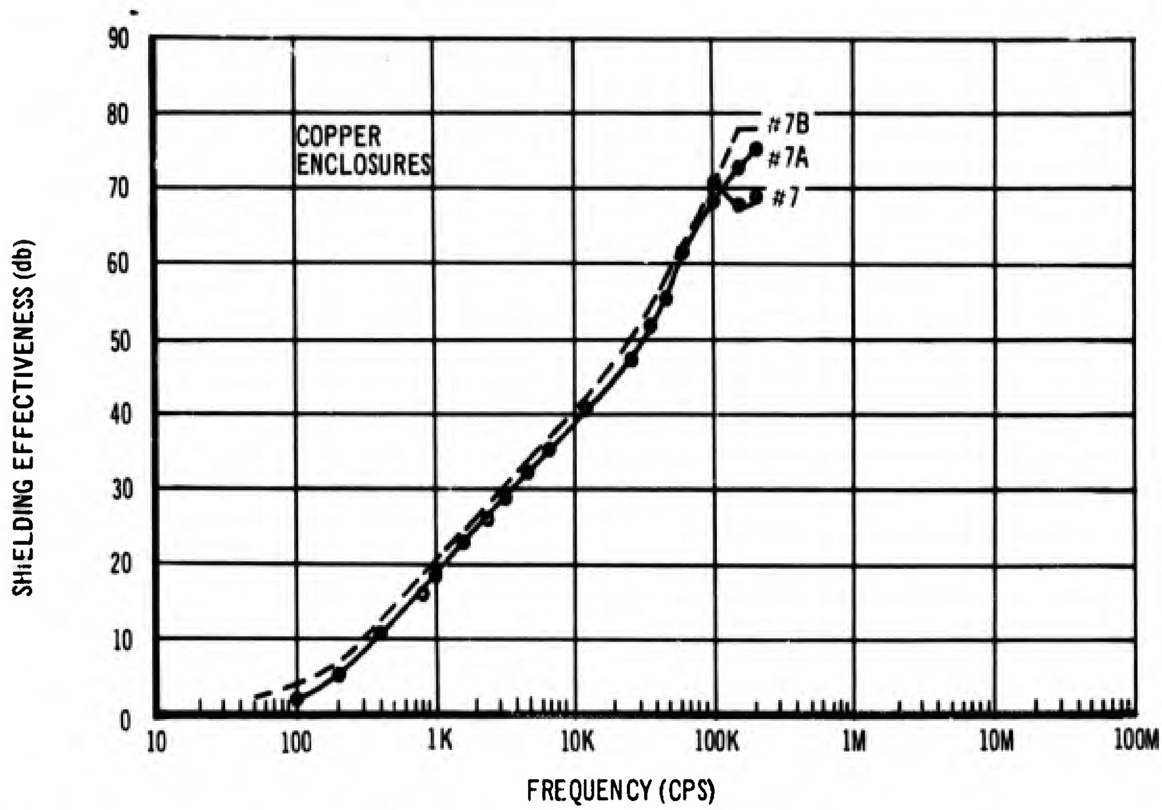

Fig. A-39 Measured Shielding Effectiveness (Access Seam Factor)

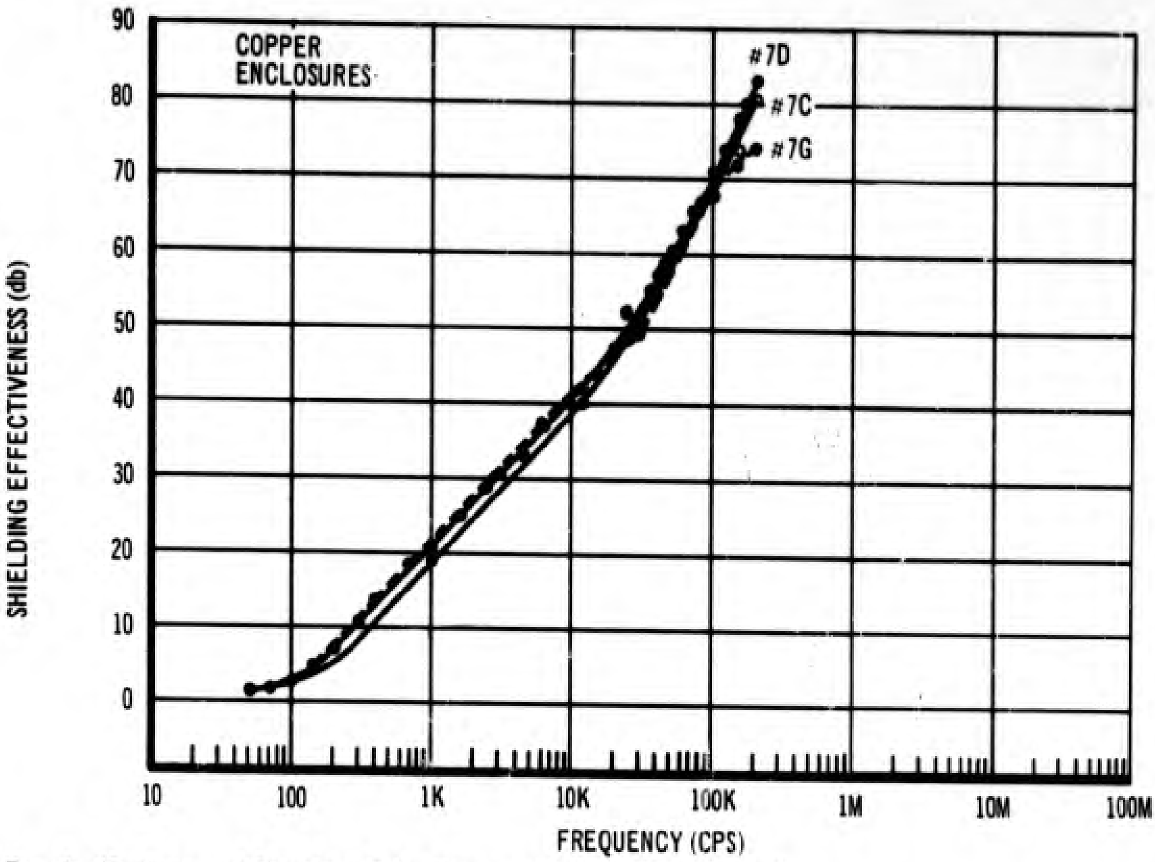

Fig. A–40 Measured Shielding Effectiveness (Access Seam Factor)

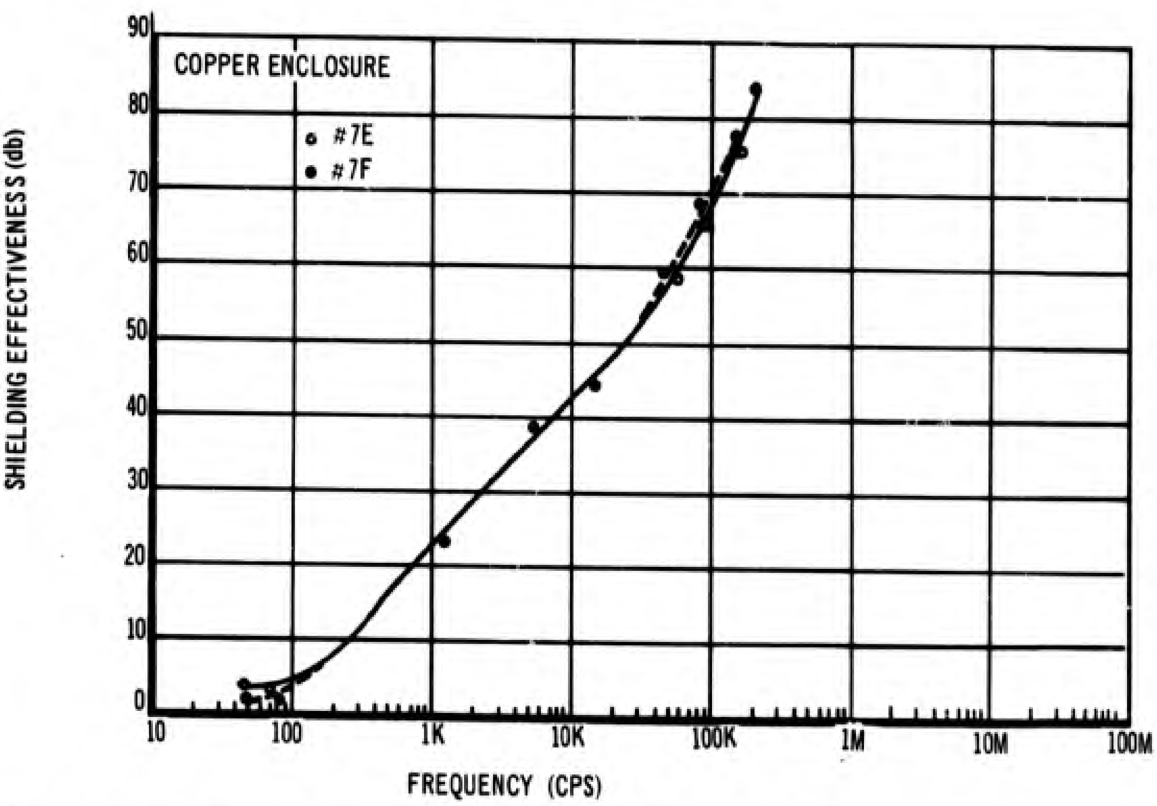

Fig. A–41 Measured Shielding Effectiveness (Access Seam Factor)

APPENDIX B MEASURED DATA 200 Kc to 1Gc.

Appendix B is a tabulation of measured shielding effectiveness data taken at four frequencies: 473 Mc, 920 Mc, 945 Mc, and 982 Mc. Measurements were made near the TE_{101} mode of the test enclosures, considered as resonant cavities. Minor variations about the TE_{101} frequency were caused by klystron difficulties.

Appendix B

Measured Shielding Effectiveness

200 Kc to 1 Gc

Box No.	473 Mc.	920 Mc.	TE_{101} 945 Mc.	TE_{101} 982 Mc.
3		≥86 db		
4	72 db			
5		83 db		
5A			40 db	
6		72 db		
6A			37 db	
7		69 db		
7A			82 db	
7B				69
7C				74
8		53 db		
9		82 db		
15		≥86 db		
16A		48 db		
16B		74 db		
17		44 db		
25				82
26		83 db		
27			69 db	
28		75 db		
29		55 db		
30		71 db		
31		88 db		
33		53 db		
34		56 db		
37		85 db		
38		69 db		
46		≥87 db		
47		56 db		
48		≥88 db		
50		≥86 db		
50-2		≥88 db		
52		≥87 db		
53		72 db		

Measured Shielding Effectiveness

200 Kc to 1 Gc

Box No.	473 Mc.	920 Mc.	TE_{101} 945 Mc.	TE_{101} 982 Mc.
54		85 db		
54A		74 db		
55		$\geqslant$ 87 db		
56		$\geqslant$ 87 db		
57		$<$ 42 db		
67		84 db		
69		78 db		

APPENDIX C MEASURED DATA 1Gc. TO 10 Gc.

Appendix C presents a tabulation of measured shielding effectiveness data at approximately the TE_{103} frequency and at 9.4 Gc. Measurements made at the latter frequency provided proof of the necessity for careful seam and access joint construction.

Appendix C

Measured Shielding Effectiveness

1.0 to 10 Gc.

Box No.	1.89 Gc.	1.914 Gc.	1.919 Gc.	9.4 Gc.
1				23 db
2	77 db			44 db
3		67 db		54 db
3S*				89 db
4				55 db
5		68 db		43 db
5A			45 db	32 db
5S				81 db
6		62 db		45 db
6A		62 db		36 db
6S				78 db
7		62 db		8 db
7A			70 db	34 db
7B			71 db	8 db
7C			71 db	35 db
7D				38 db
8		37 db		28 db
9		60 db		26 db
10		63 db		29 db
14				58 db
15		65 db		50 db
15S				87 db
16A		41 db		40 db
16B		62 db		26 db
17		38 db		2 db gain
18	40 db			3 db gain
21				25 db
22				23 db
25			69 db	33 db
26		64 db		46 db
27			50 db	26 db
28		56 db		35 db
29		59 db		12 db
30		58 db		9 db
31		41 db		27 db
33		57 db		3 db
34		62 db		3 db

Measured Shielding Effectiveness

1.0 to 10 Gc.

Box No.	1.89 Gc.	1.914 Gc.	1.919 Gc.	9.4 Gc.
36				41 db
37		67 db		17 db
38		44 db		0 db
40	≥86 db			48 db
42	84 db			36 db
43	81 db			14 db
44	≥86 db			35 db
45	24 db			21 db
46		62 db		37 db
47		52 db		19 db
47T				18 db
47 TS				18 db
48		63 db		43 db
48T				41 db
48TS				84 db
50		54 db		44 db
50S				84 db
50-2				36 db
51	78 db			57 db
52		64 db		22 db
52S				84 db
53		62 db		13 db
54		63 db		24 db
54A		64 db		14 db
55		64 db		22 db
56		62 db		24 db
57		14 db		2 db
58				2 db gain
63				24 db
67		60 db		41 db
68	39 db			8 db
69		40 db		37 db
70		57 db		38 db
71				15 db
72				23 db
74				47 db
75				35 db

* The letter "S" following a box number (No. 5S) indicates that the access cover was soldered on. "T" designates boxes which had been submitted to temperature shock.

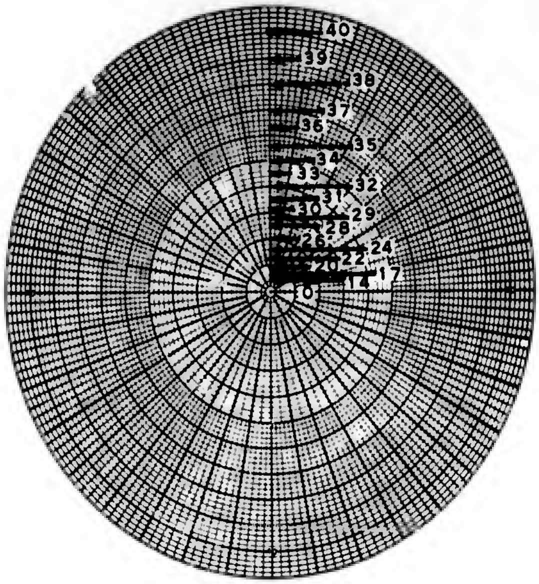

FREQUENCY 9.4 Kmc

Fig. C1 X–Band Field Pattern. Data Interpolation Chart

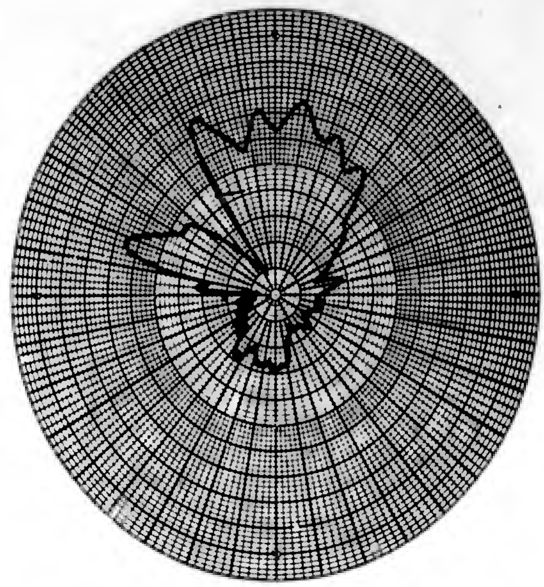

ANTENNA STUB
FREQUENCY 9.4 Kmc
ATTENUATOR 54 db
BACKGROUND 31 db
FIELD 114 db

Fig. C2 Test Box Number 1

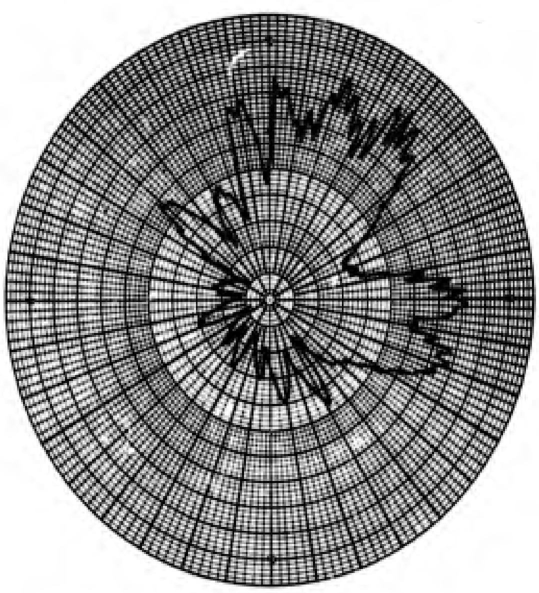

ANTENNA STUB
FREQUENCY 9.4 Kmc
ATTENUATOR 40 db
FIELD 123 db
CALCULATED S_{min} = 44 db

Fig. C3 Test Box Number 2

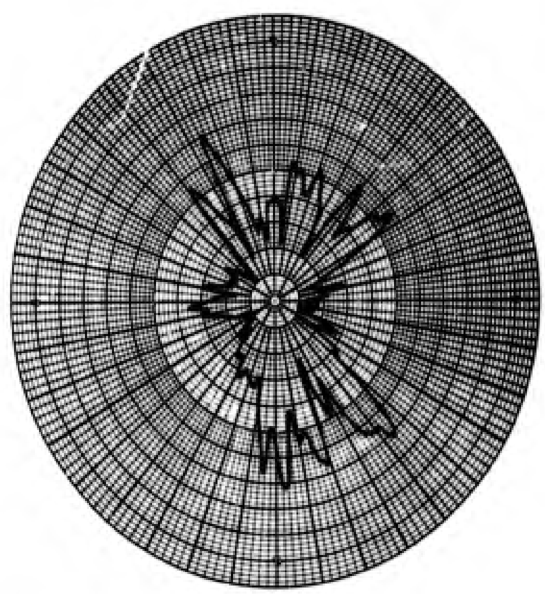

ANTENNA STUB
FREQUENCY 9.4 Kmc
ATTENUATOR 30 db
FIELD 121 db
CALCULATED S_{min} = 54 db

Fig. C4 Test Box Number 3

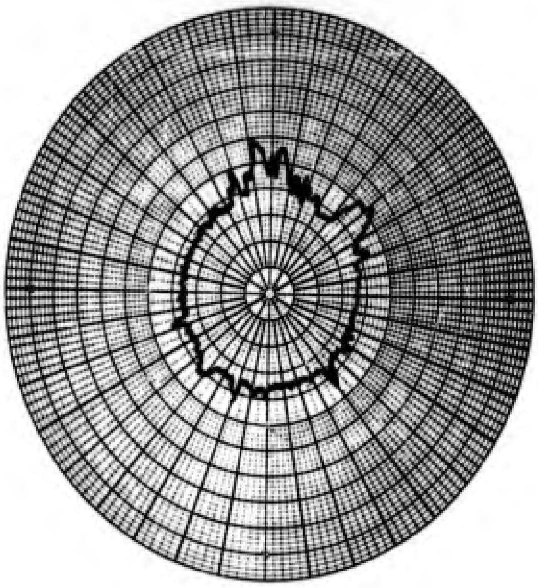

ANTENNA STUB
FREQUENCY 9.4 Kmc
ATTENUATOR 4 db

BACKGROUND 31 db (RADAR OFF)
FIELD 127 db
CALCULATED S_{min}= 89 db

Fig. C5 Test Box Number 3S, Lid Soldered

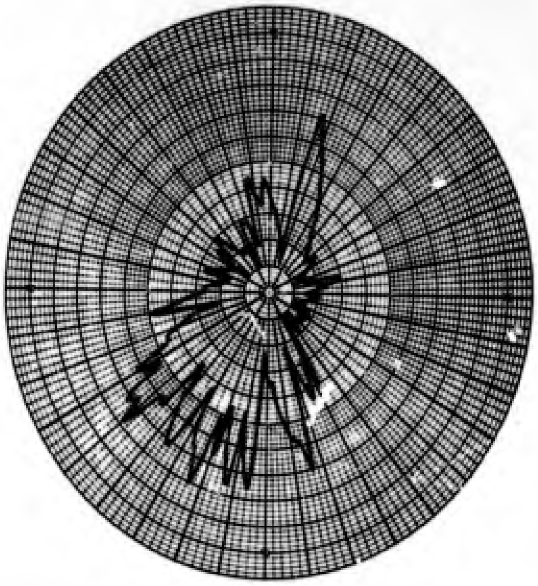

ANTENNA STUB
FREQUENCY 9.4 Kmc

ANTENNA STUB
FREQUENCY 9.4 Kmc
ATTENUATOR 30 db
FIELD 123 db

Fig. C6 Test Box Number 4

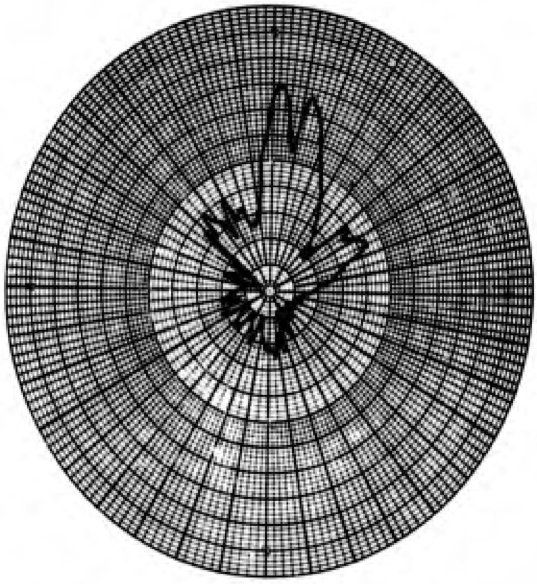

ANTENNA STUB
FREQUENCY 9.4 Kmc
ATTENUATOR 40 db

FIELD 121 db
CALCULATED S_{min} = 43 db

Fig. C7 Test Box Number 5

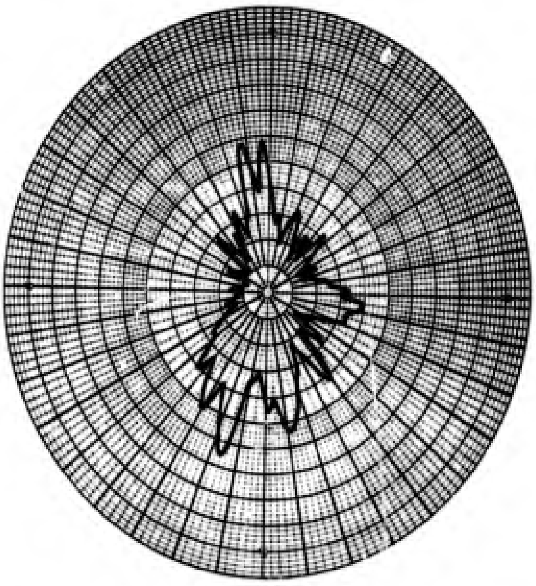

ANTENNA STUB
FREQUENCY 9.4 Kmc

ATTENUATOR 50 db
FIELD – 118

Fig. C8 Test Box Number 5A

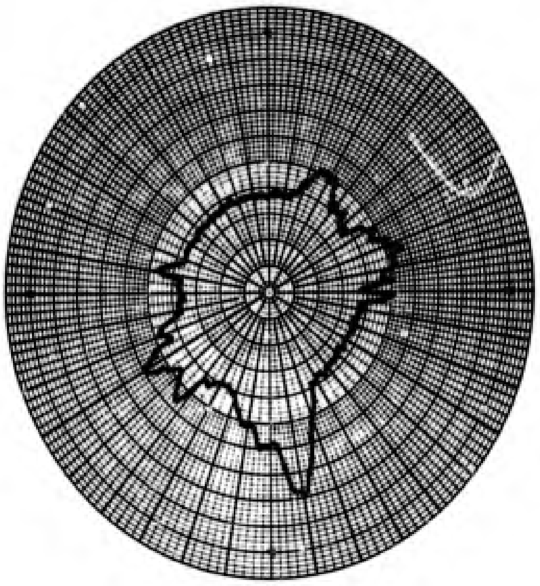

ANTENNA STUB
FREQUENCY 9.4 Kmc
ATTENUATOR 8 db
FIELD = 127 db
CALCULATED S_{min} = 81 db

Fig. C9 Test Box Number 5S, Lid Soldered

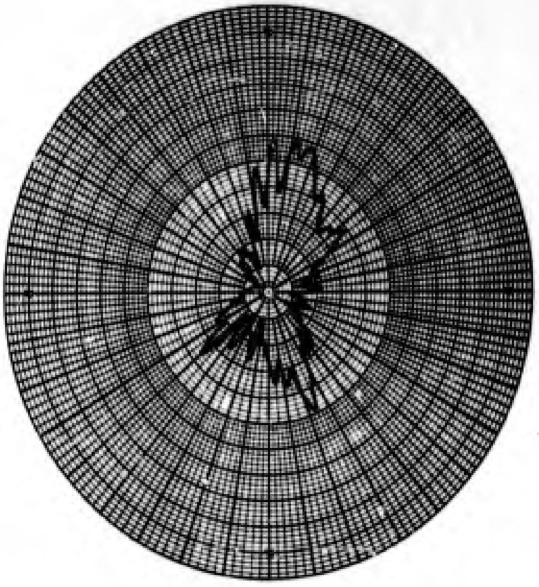

ANTENNA STUB
FREQUENCY 9.4 Kmc
ATTENUATOR 40 db
FIELD 121 db
CALCULATED S_{min} = 45 db

Fig. C10 Test Box Number 6

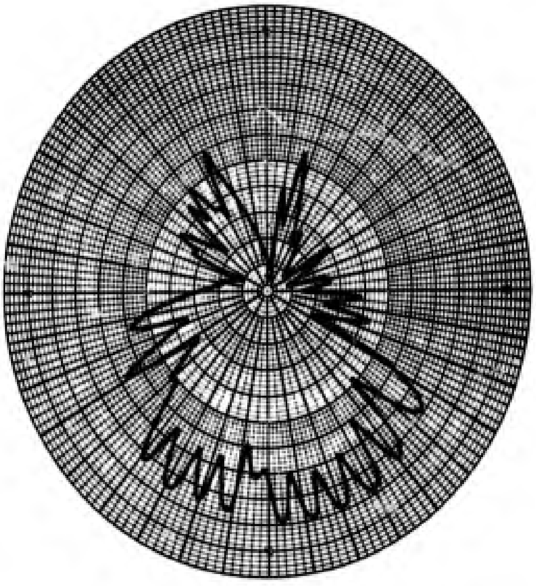

ANTENNA STUB
FREQUENCY 9.4 Kmc
ATTENUATOR 43 db
FIELD – 118

Fig. C11 Test Box Number 6A

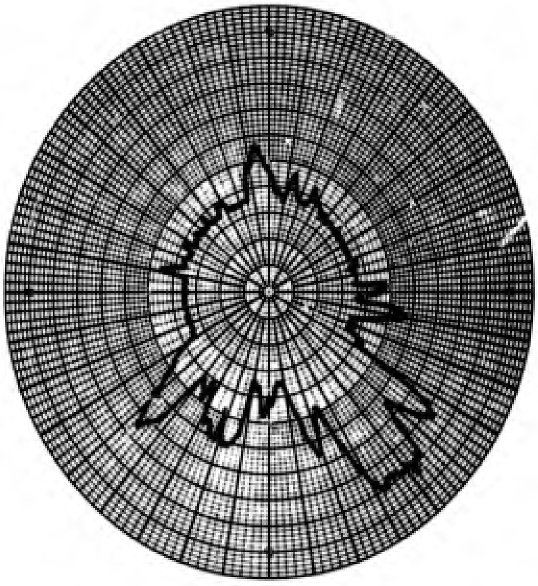

ANTENNA STUB
FREQUENCY 9.4 Kmc
ATTENUATOR 10 db
FIELD = 127
CALCULATED S_{min} = 78 db

Fig. C12 Test Box Number 6S, Lid Soldered

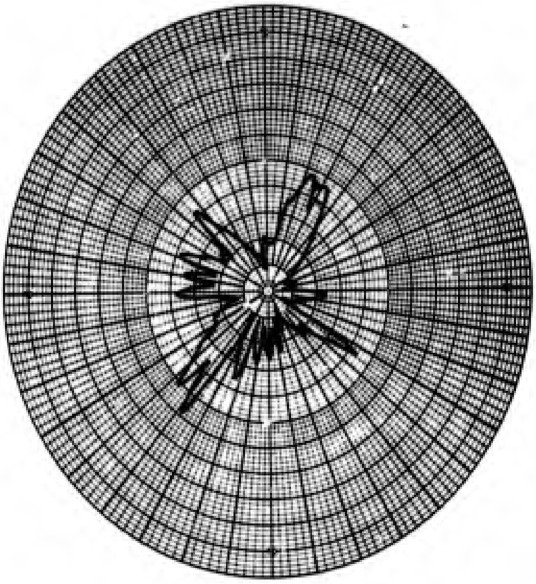

ANTENNA STUB
FREQUENCY 9.4 Kmc
ATTENUATOR 80 db
FIELD 123 db
CALCULATED S_{min} = 8 db

Fig. C13 Test Box Number 7

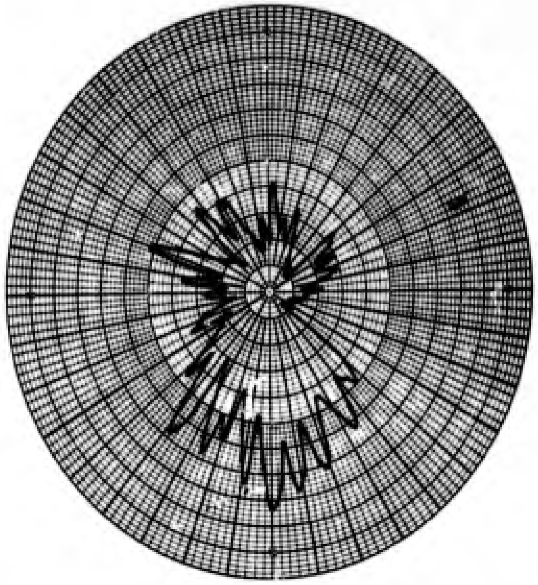

ANTENNA STUB
FREQUENCY 9.4 Kmc
ATTENUATOR 46 db
FIELD – 118 db

Fig. C14 Test Box Number 7A

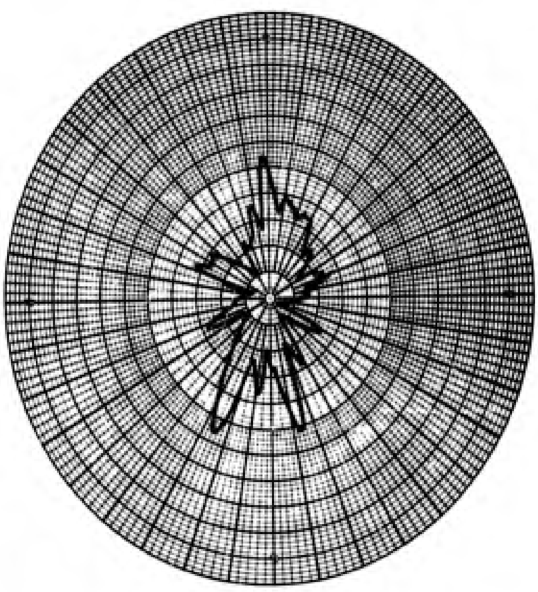

ANTENNA STUB
FREQUENCY 9.4 Kmc
ATTENUATOR 80 db
BACKGROUND 31 db
FIELD 123 db

Fig. C15 Test Box Number 7B

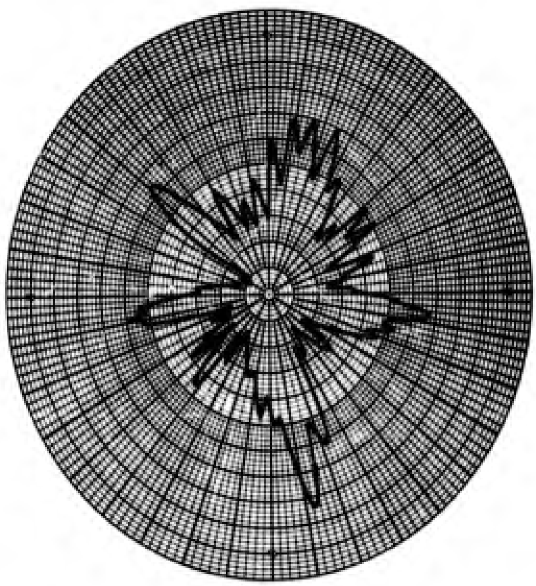

ANTENNA STUB
FREQUENCY 9.4 Kmc
ATTENUATOR 50 db
BACKGROUND 31
FIELD 123 db

Fig. C16 Test Box Number 7C

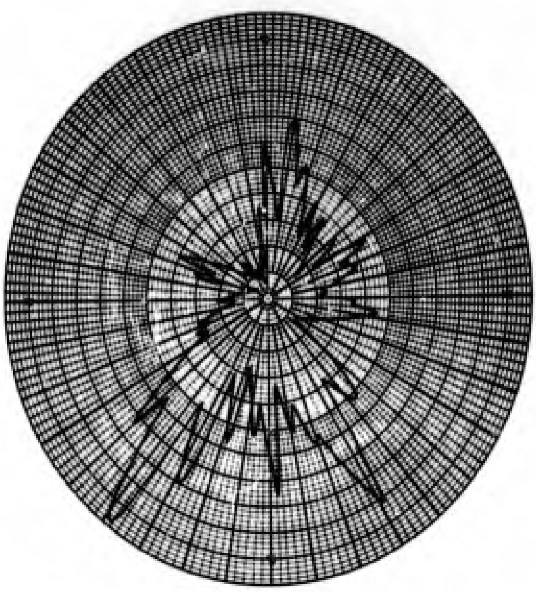

ANTENNA STUB
FREQUENCY 9.4 Kmc
ATTENUATOR 50 db
BACKGROUND 31 db

Fig. C17 Test Box Number 7D

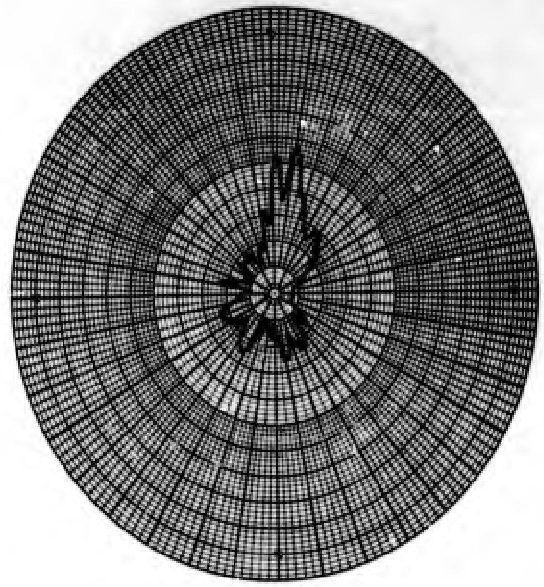

ANTENNA STUB
FREQUENCY 9.4 Kmc
ATTENUATOR 60 db
FIELD 123 db
CALCULATED S_{min} = 28 db

Fig. C18 Test Box Number 8

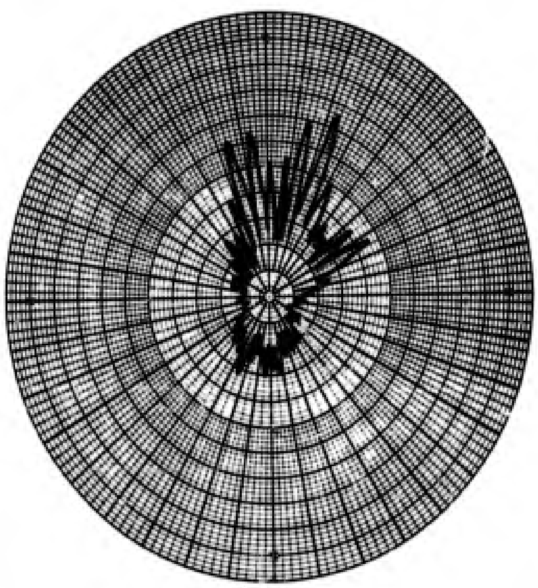

ANTENNA STUB
FREQUENCY 9.4 Kmc
ATTENUATOR 60 db
FIELD 123 db
CALCULATED S_{min} = 26 db

Fig. C19 Test Box Number 9

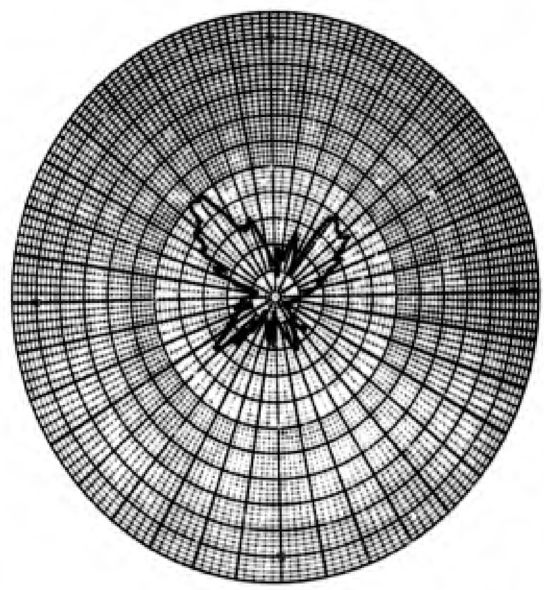

ANTENNA STUB
FREQUENCY 9.4 db
ATTENUATOR 60 db
FIELD 123 db
CALCULATED S_{min} = 29 db

Fig. C20 Test Box Number 10

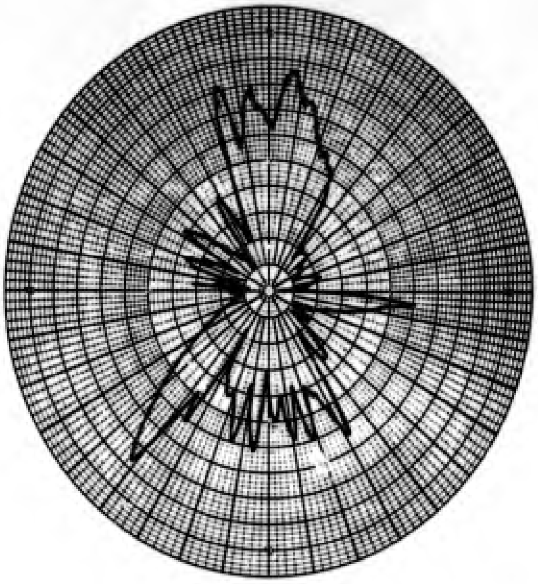

ANTENNA STUB FREQUENCY 9.4 Kmc ATTENUATOR 26 db FIELD 123 db CALCULATED S_{min} = 58 db

Fig. C21 Test Box Number 14

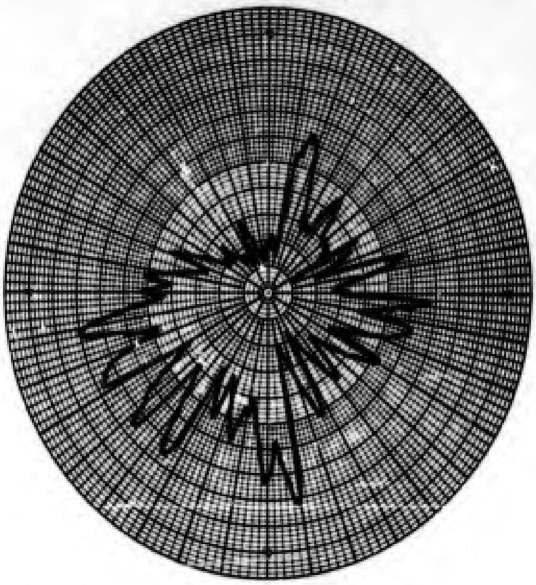

ANTENNA STUB FREQUENCY 9.4 Kmc ATTENUATOR 30 db BACKGROUND 31 db FIELD 118 db CALCULATED

Fig. C22 Test Box Number 15

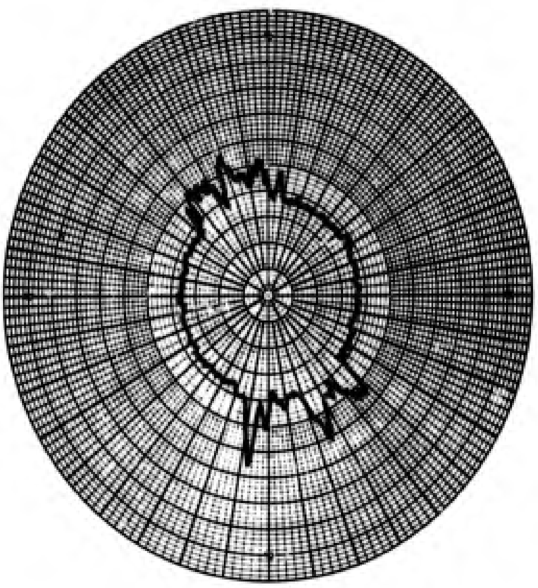

ANTENNA STUB FREQUENCY 9.4 Kmc ATTENUATOR 4 db BACKGROUND 31 db FIELD 127 db CALCULATED S_{min} = 87 db

Fig. C23 Test Box Number 15S, Lid Soldered

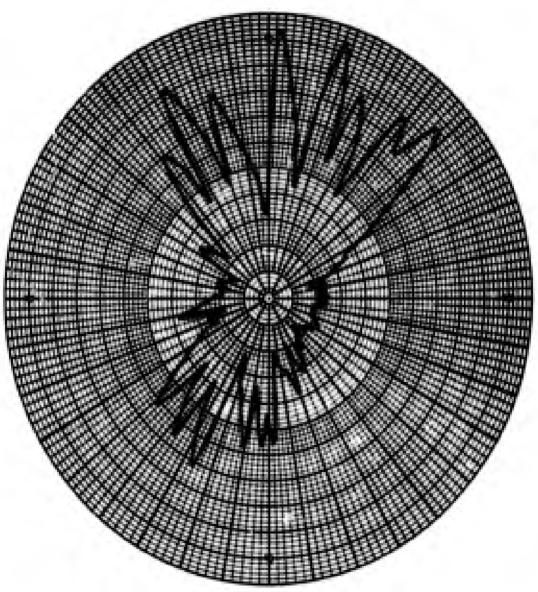

ANTENNA STUB FREQUENCY 9.4 Kmc ATTENUATOR 43 db FIELD 123 db

Fig. C24 Test Box Number 16A

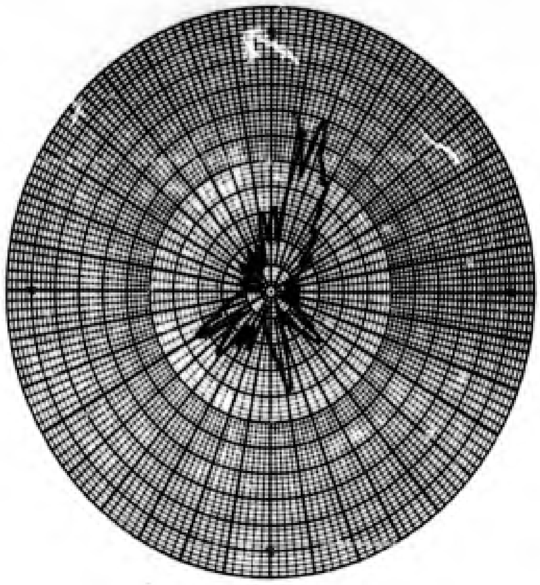

ANTENNA STUB
FREQUENCY 9.4 Kmc
ATTENUATOR 60 db

FIELD 123 db
CALCULATED
$S_{min} = 26$ db

Fig. C25 Test Box Number 16B

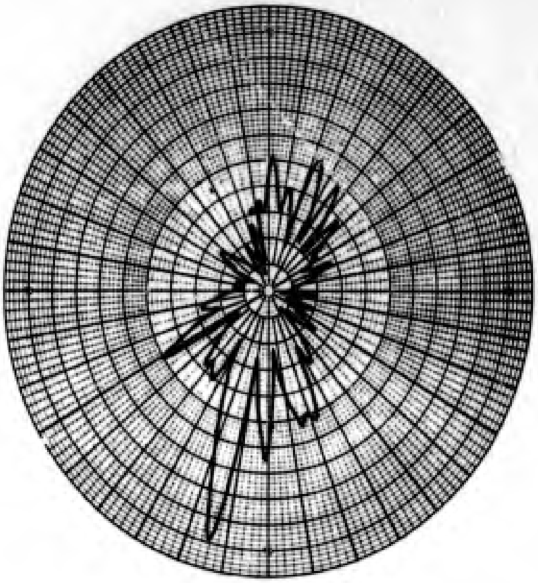

ANTENNA STUB
FREQUENCY 9.4 Kmc
ATTENUATOR 85 db

FIELD 123 db
CALCULATED
$S_{min} = 2$ db GAIN

Fig. C26 Test Box Number 17

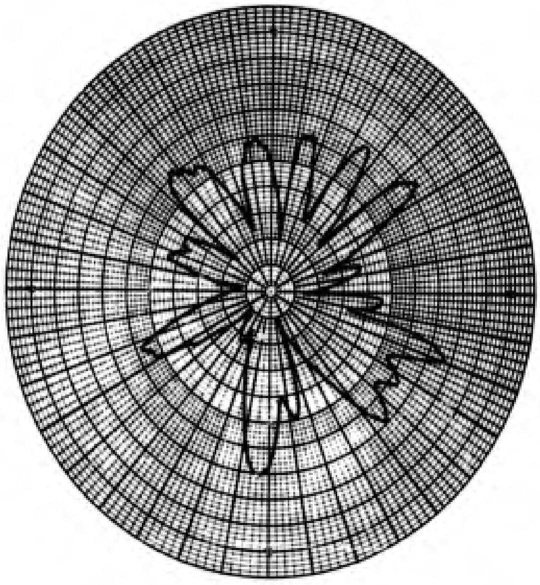

ANTENNA STUB
FREQUENCY 9.4 Kmc
ATTENUATOR 90 DB

FIELD 123 db
CALCULATED
$S_{min} = 3$ db GAIN

Fig. C27 Test Box Number 18

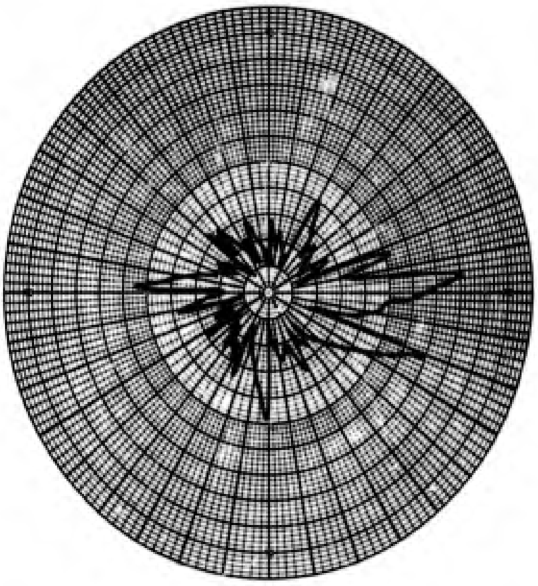

ANTENNA STUB
FREQUENCY 9.4 Kmc
ATTENUATOR 60 db

FIELD 123 DB
CALCULATED
$S_{min} = 25$ db

Fig. C28 Test Box Number 21

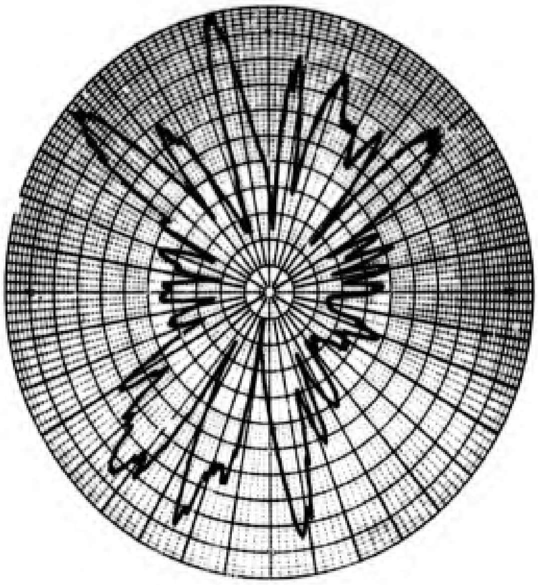

ANTENNA STUB
FREQUENCY 9.4 Kmc
ATTENUATOR 70 db
FIELD 123 db
CALCULATED S_{min} = 12 db

Fig. C28a Test Box Number 21

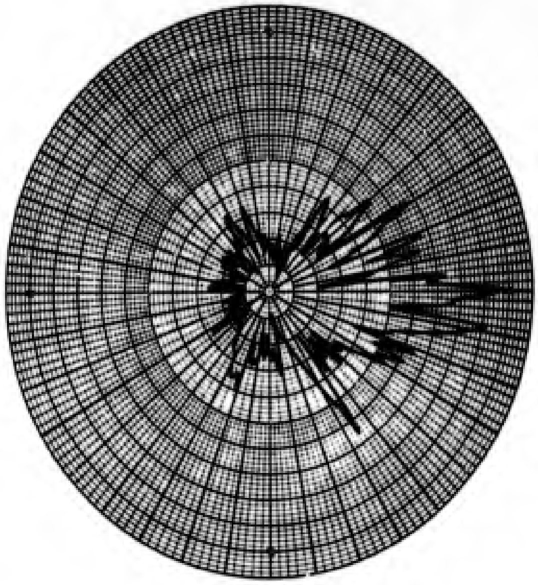

ANTENNA STUB
FREQUENCY 9.4 Kmc
ATTENUATOR 60 db
FIELD 123 db

Fig. C29 Test Box Number 22

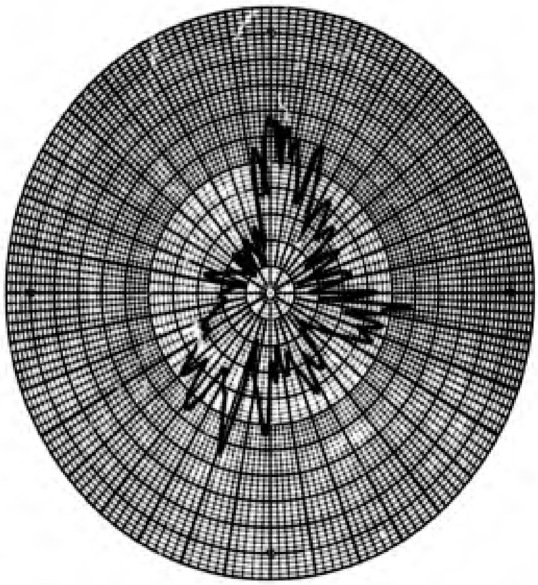

ANTENNA STUB
FREQUENCY 9.4 Kmc
ATTENUATOR 40 db
FIELD 123 db
CALCULATED S_{min} = 46 db

Fig. C30 Test Box Number 25S

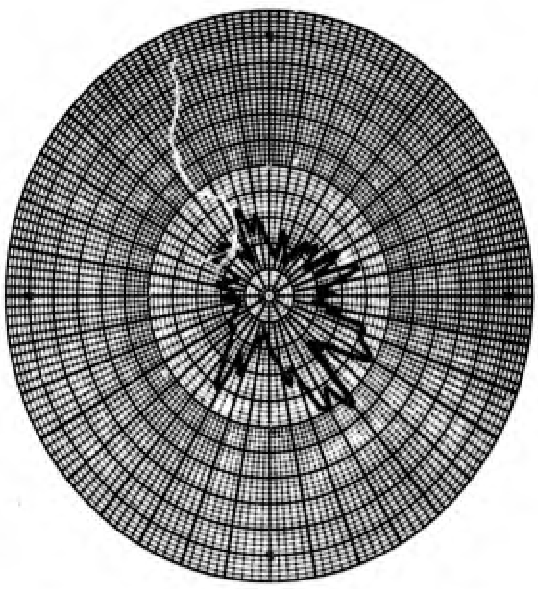

ANTENNA STUB
FREQUENCY 9.4 Kmc
ATTENUATOR 50 db
FIELD 118 db

Fig. C31 Test Box Number 26

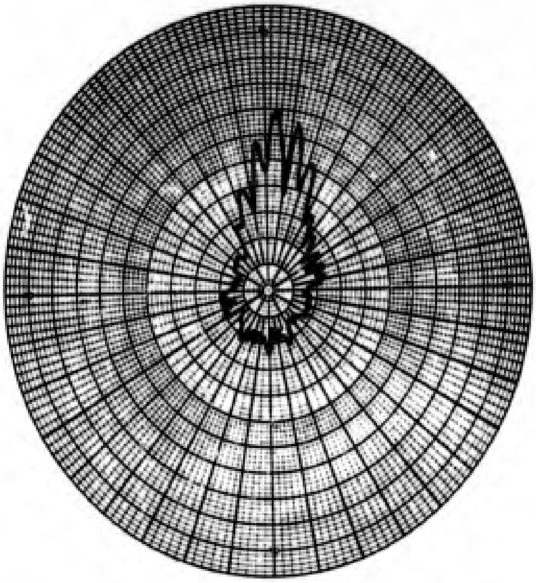

ANTENNA STUB
FREQUENCY 9.4 Kmc
ATTENUATOR 60 db

FIELD 123 db
CALCULATED $S_{min} = 26$ db

Fig. C32 Test Box Number 27

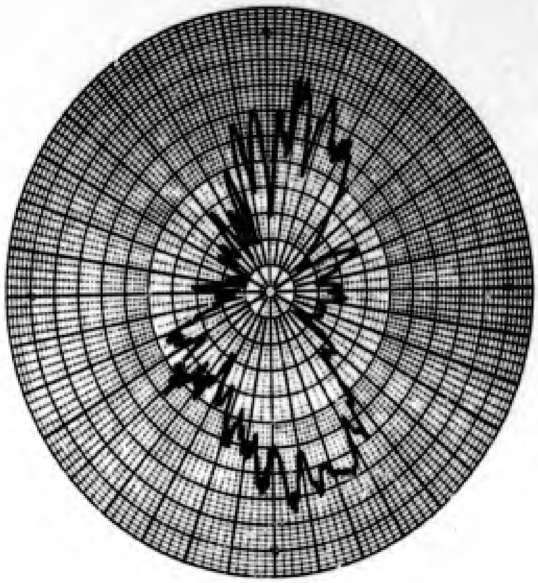

ANTENNA STUB
FREQUENCY 9.4 Kmc
ATTENUATOR 49 db

FIELD 123 db
CALCULATED $S_{min} = 35$ db

Fig. C33 Test Box Number 28

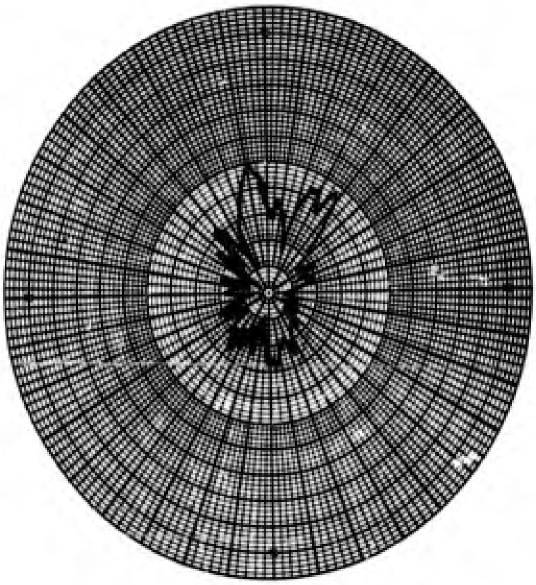

ANTENNA STUB
FREQUENCY 9.4 Kmc
ATTENUATOR 80 db

FIELD 123 db
CALCULATED $S_{min} = 9$ db

Fig. C34 Test Box Number 30

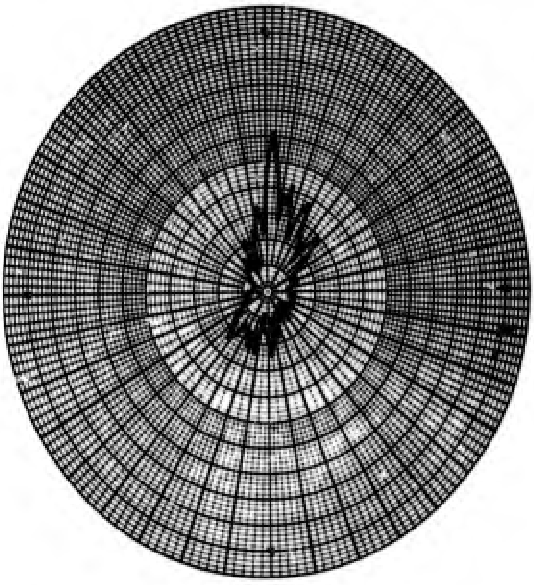

ANTENNA STUB
FREQUENCY 9.4 Kmc
ATTENUATOR 60 db

FIELD 123 db
CALCULATED $S_{min} = 27$ db

Fig. C35 Test Box Number 31

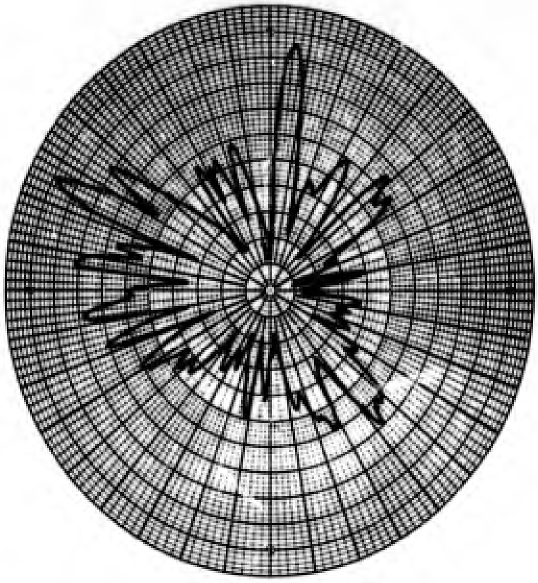

ANTENNA STUB
FREQUENCY 9.4 Kmc
ATTENUATOR 84 db
FIELD 123 db
CALCULATED $S_{min} = 3$ db

Fig. C36 Test Box Number 33

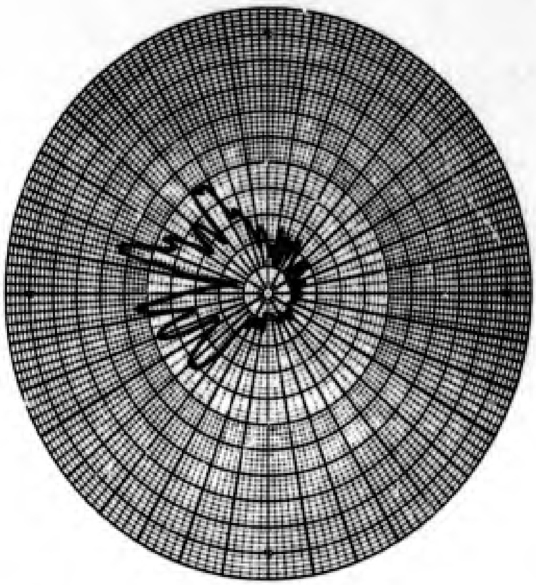

ANTENNA STUB
FREQUENCY 9.4 Kmc
ATTENUATOR 84 db
FIELD 123 db
CALCULATED $S_{min} = 3$ db

Fig. C37 Test Box Number 34

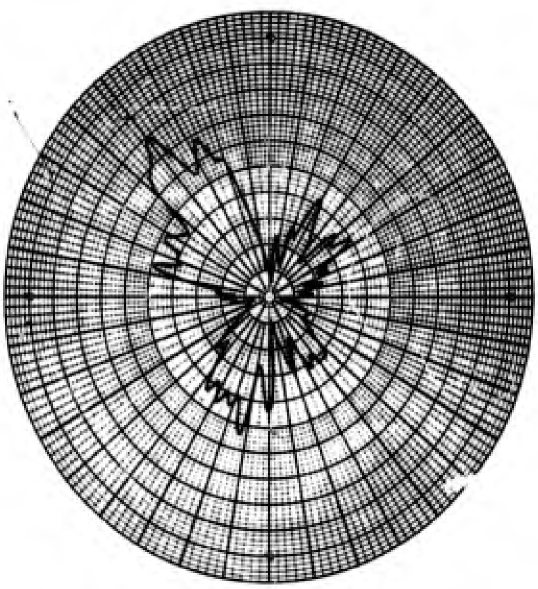

ANTENNA STUB
RAISED HORN
FREQUENCY 9.4 Kmc
ATTENUATOR 50 db
BACKGROUND 31 db
FIELD 129 db
CALCULATED $S_{min} = 41$ db

Fig. C38 Test Box Number 36

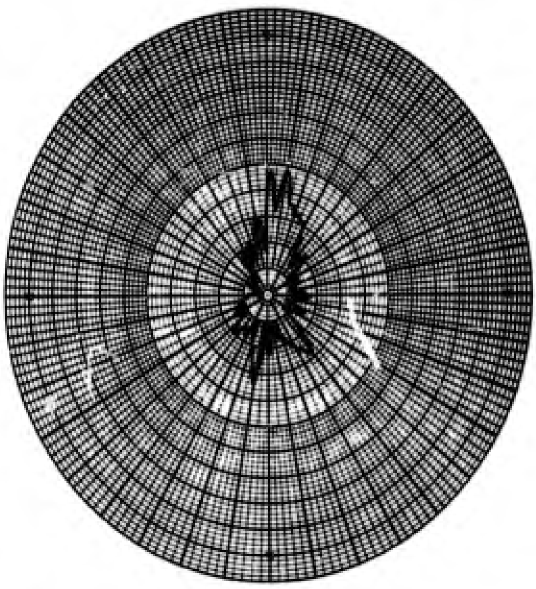

ANTENNA STUB
FREQUENCY 9.4 Kmc
ATTENUATOR 70 db
FIELD 121 db
CALCULATED $S_{min} = 17$ db

Fig. C39 Test Box Number 37

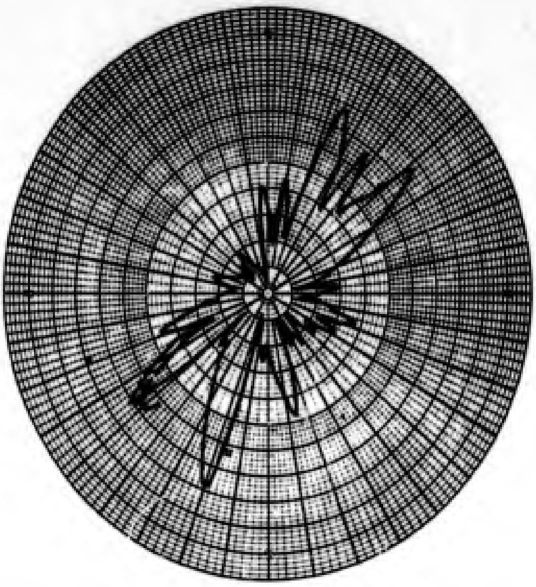

ANTENNA STUB
FREQUENCY 9.4 Kmc
ATTENUATOR 85 db
FIELD 123 db
CALCULATED $S_{min} = 0$ db

Fig. C40 Test Box Number 38

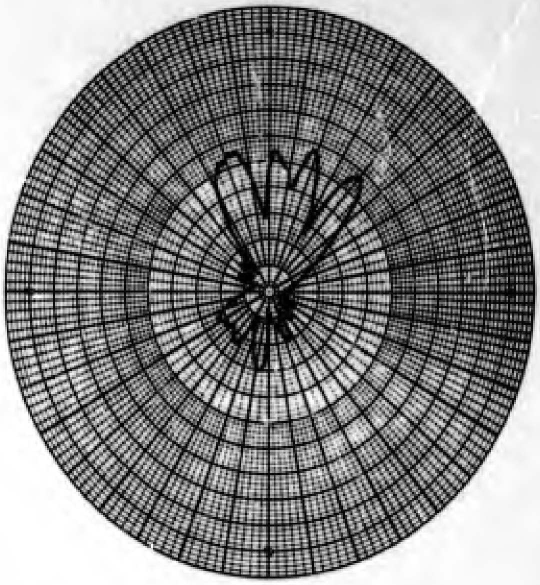

ANTENNA STUB
FREQUENCY 9.4 Kmc
ATTENUATOR 40 db
FIELD 123 db
CALCULATED $S_{min} = 48$ db

Fig. C41 Test Box Number 40

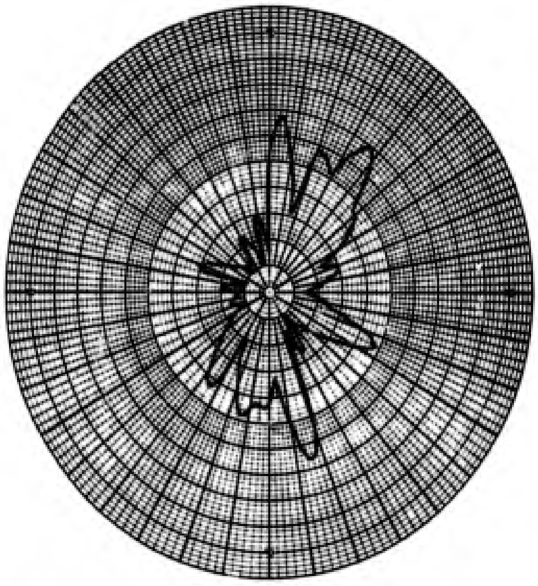

ANTENNA STUB
FREQUENCY 9.4 Kmc
ATTENUATOR 50 DB
FIELD 123 db
CALCULATED $S_{min} = 36$ db

Fig. C42 Test Box Number 42

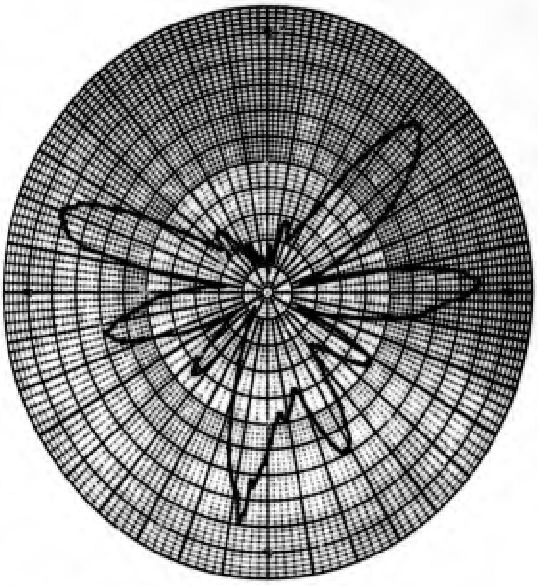

ANTENNA STUB
FREQUENCY 9.4 Kmc
ATTENUATOR 70 db
FIELD 123 db
CALCULATED $S_{min} = 14$ db

Fig. C43 Test Box Number 43

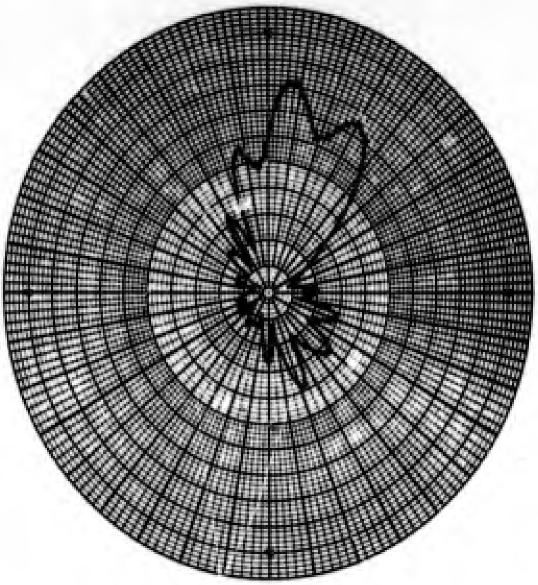

ANTENNA STUB
FREQUENCY 9.4 Kmc
ATTENUATOR 50 db
FIELD 123 db
CALCULATED S_{min} = 35 db

Fig. C44 Test Box Number 44

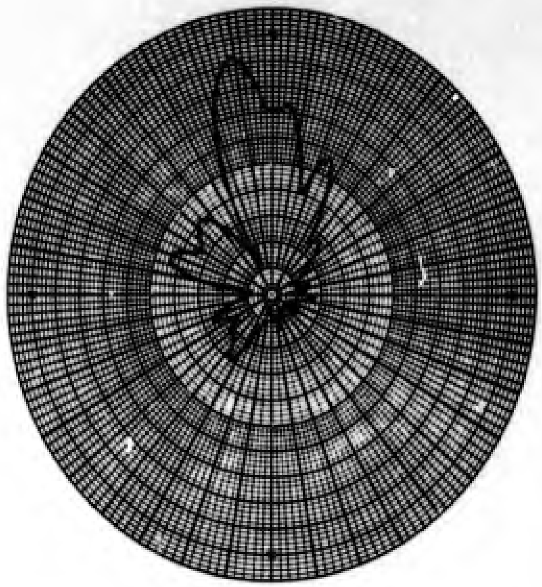

ANTENNA STUB
FREQUENCY 9.4 Kmc
ATTENUATOR 63 db
FIELD 123 db
CALCULATED S_{min} = 21 db

Fig. C45 Test Box Number 45

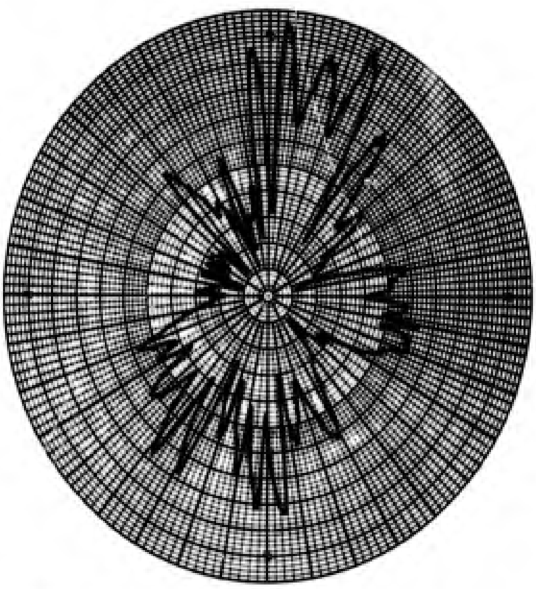

ANTENNA STUB
FREQUENCY 9.4 Kmc
ATTENUATOR 45 db
FIELD 123 db
CALCULATED S_{min} = 37 db

Fig. C46 Test Box Number 46

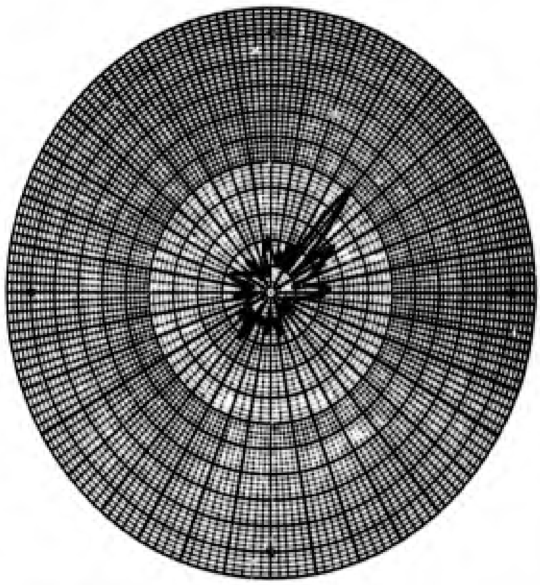

ANTENNA STUB
FREQUENCY 9.4 Kmc
ATTENUATOR 70 db
FIELD 123 db
CALCULATED S_{min} = 19 db

Fig. C47 Test Box Number 47

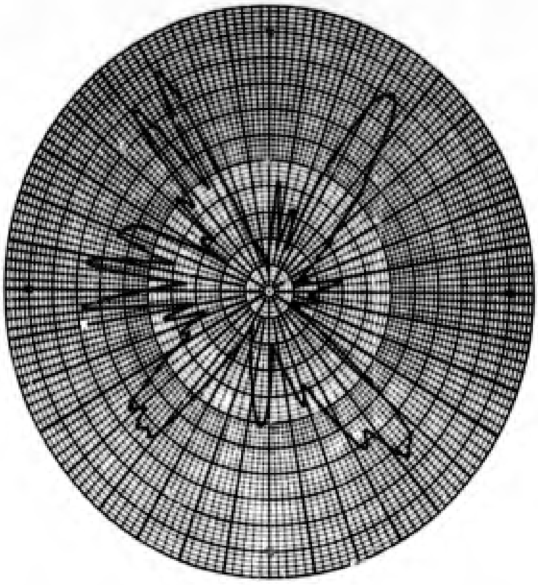

ANTENNA STUB
FREQUENCY 9.4 Kmc
ATTENUATOR 70 db
BACKGROUND 31 db
FIELD 129 db
CALCULATED S_{min} = 18 db

Fig. C48 Test Box Number 47 TS, Soldered Lid

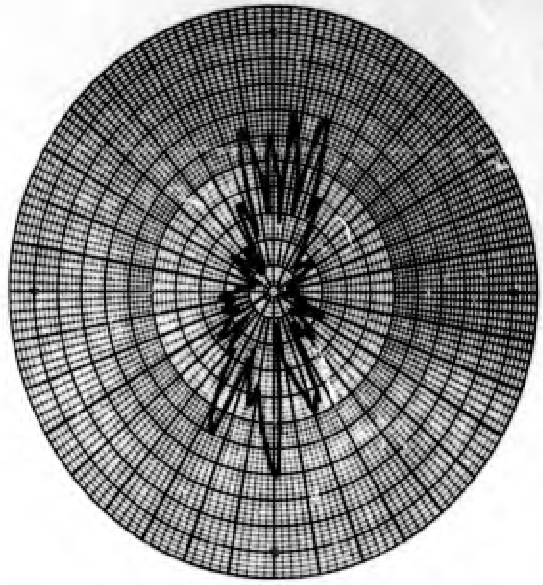

ANTENNA STUB
FREQUENCY 9.4 Kmc
ATTENUATOR 43 db
FIELD 123 db
CALCULATED S_{min} = 43 db

Fig. C49 Test Box Number 48

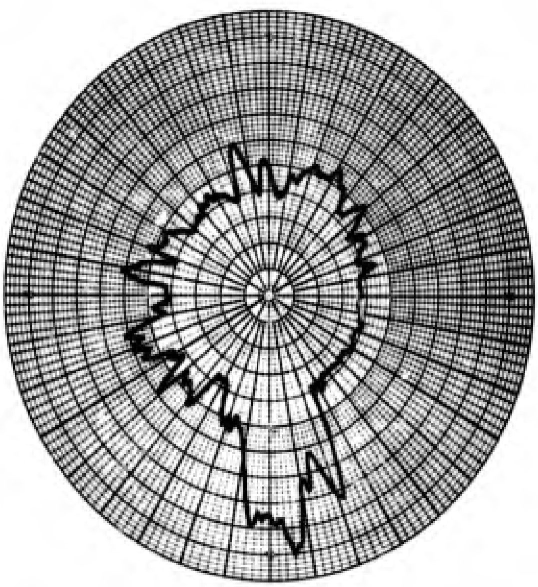

ANTENNA STUB
FREQUENCY 9.4 Kmc
ATTENUATOR 3 db
FIELD 127 db
CALCULATED S_{min} = 84 db

Fig. C50 Test Box Number 48 TS, Lid Soldered

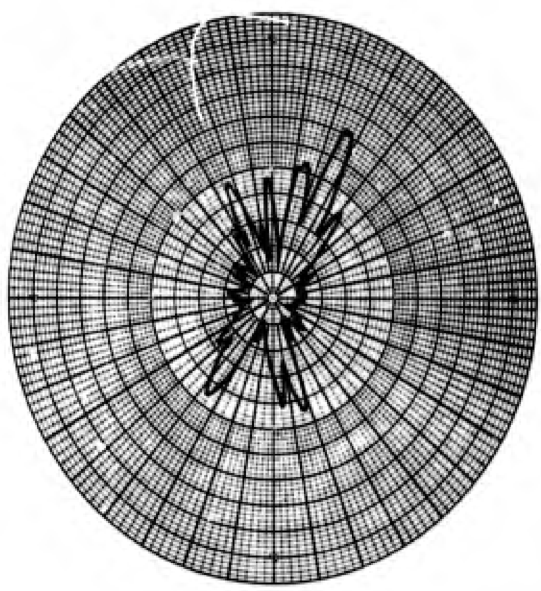

ANTENNA STUB
FREQUENCY 9.4 Kmc
ATTENUATOR 42 db
FIELD 123 db
CALCULATED S_{min} = 44 db

Fig. C51 Test Box Number 50

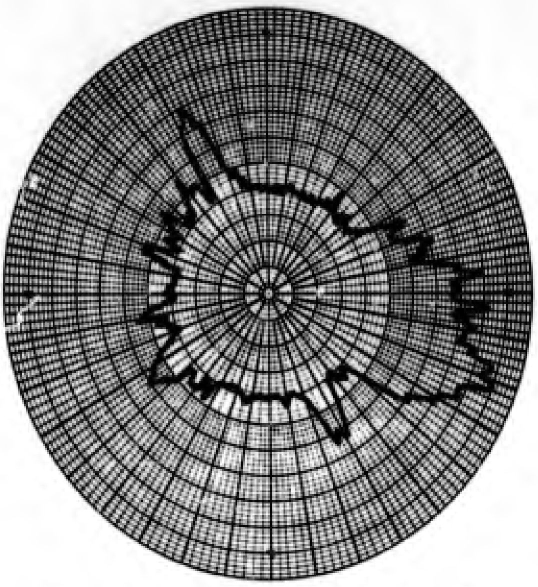

ANTENNA STUB
RAISED HORN
FREQUENCY 9.4 Kmc
ATTENUATOR 5 db
BACKGROUND 31 db
FIELD 129 db
CALCULATED S_{min}=84db

Fig. C52 Test Box Number 50-S, Soldered Lid

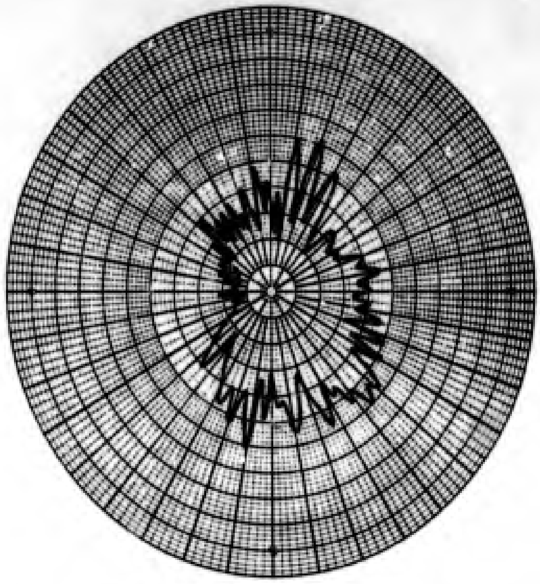

ANTENNA STUB
FREQUENCY 9.4 Kmc
ATTENUATOR 50 db
FIELD 123 db
CALCULATED S_{min} = 37 db

Fig. C53 Test Box Number 50-2

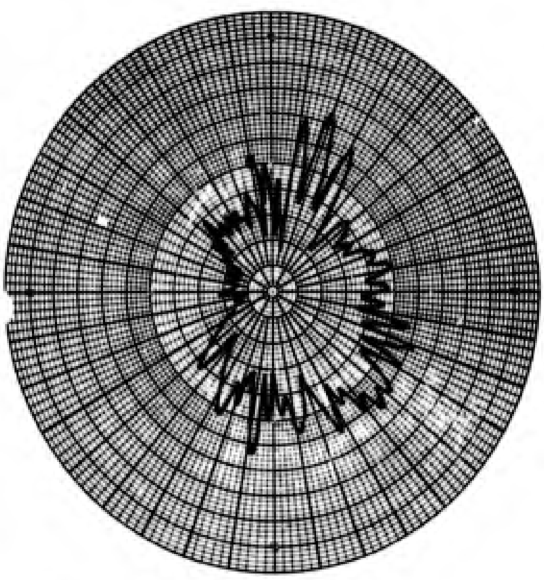

ANTENNA STUB
FREQUENCY 9.4 Kmc
ATTENUATOR 50 db
FIELD 123 db
CALCULATED S_{min}=36 db

Fig. C54 Test Box Number 50-2

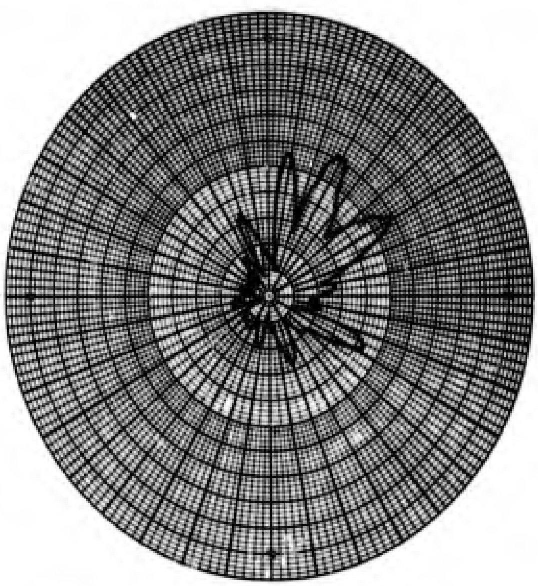

ANTENNA STUB
FREQUENCY 9.4 Kmc
ATTENUATOR 30 db
FIELD 123 db
CALCULATED S_{min}=57 db

Fig. C55 Test Box Number 51

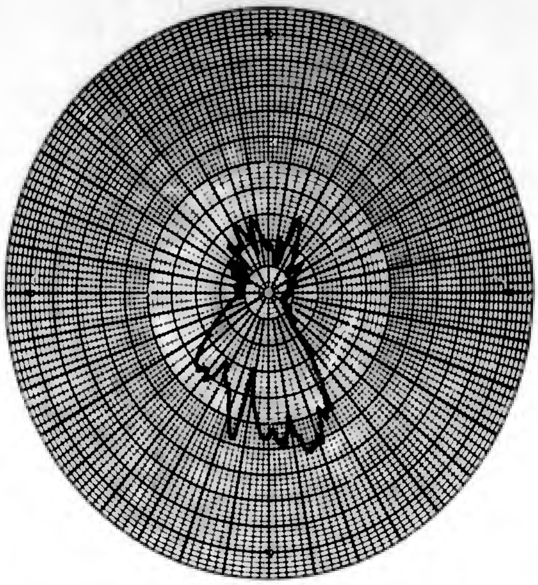

ANTENNA STUB
FREQUENCY 9.4 Kmc
ATTENUATOR 3 db

FIELD 127 db
CALCULATED S_{min}=84 db

Fig. C56 Test Box Number 52

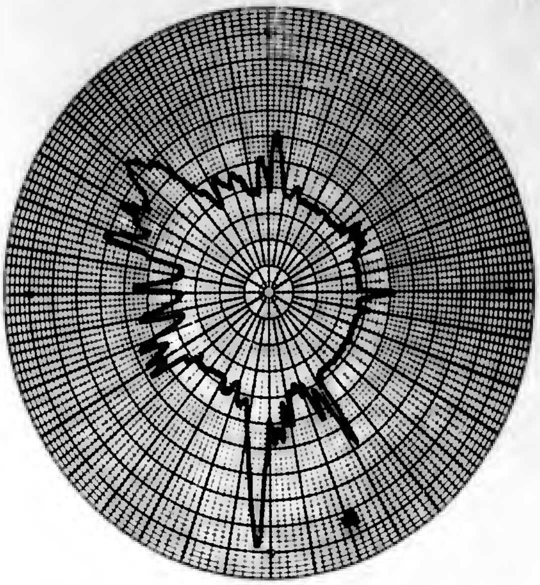

ANTENNA STUB
FREQUENCY 9.4 Kmc
ATTENUATOR 65 db

FIELD 123 db
CALCULATED S_{min}=22 db

Fig. C57 Test Box Number 52S, Soldered Lid

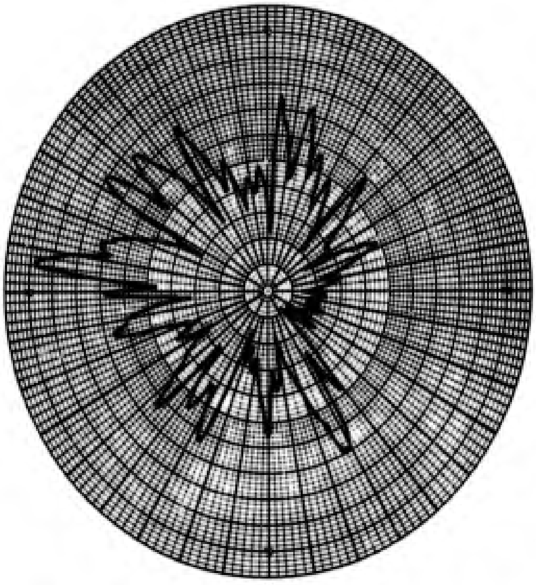

ANTENNA STUB
FREQUENCY 9.4 Kmc
ATTENUATOR 70 db

FIELD 123 db
CALCULATED S_{min}=13 db

Fig. C58 Test Box Number 53

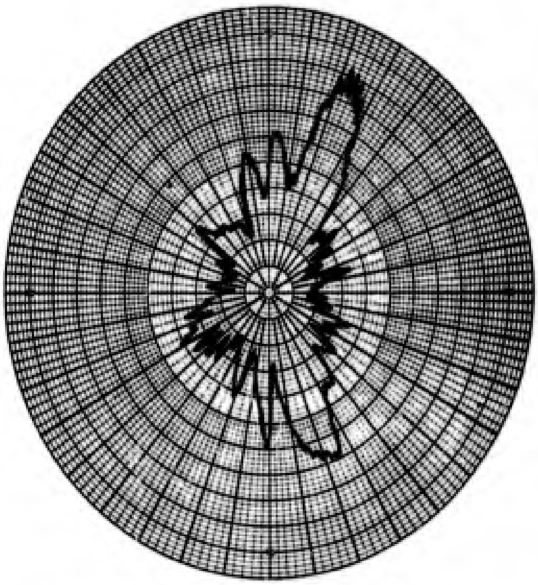

ANTENNA STUB
FREQUENCY 9.4 Kmc
ATTENUATOR 60 db

FIELD 123 db
CALCULATED S_{min}=24 db

Fig. C59 Test Box Number 54

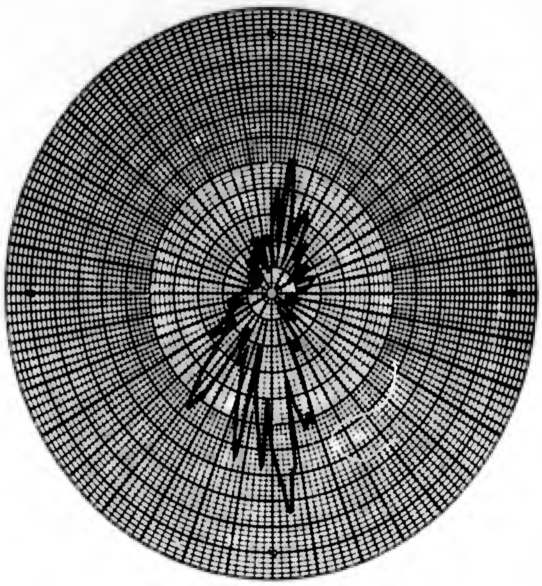

ANTENNA STUB FIELD 123 db
FREQUENCY 9.4 db CALCULATED S_{min}=14 db
ATTENUATOR 70 db

Fig. C60 Test Box Number 54A

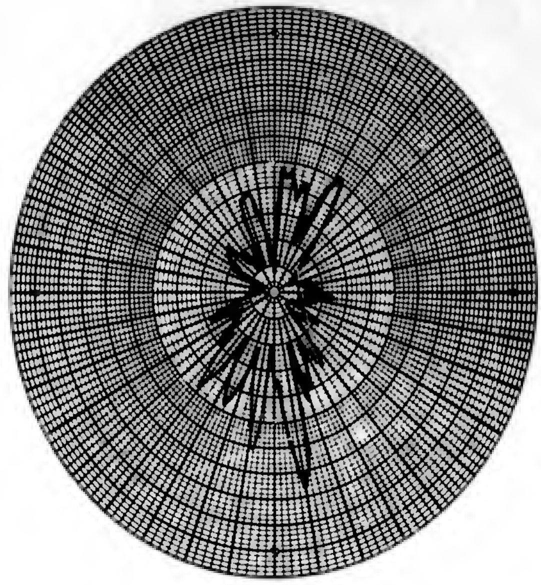

ANTENNA STUB FIELD 123 db
FREQUENCY 9.4 Kmc CALCULATED S_{min}=22 db
ATTENUATOR 63 db

Fig. C61 Test Box Number 55

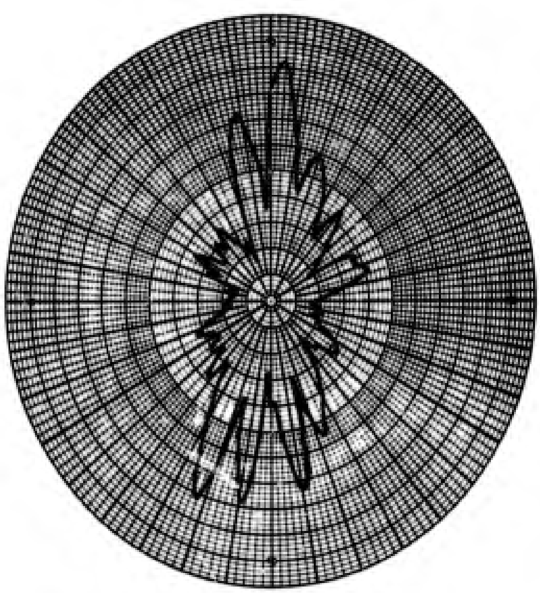

ANTENNA STUB FIELD 123 db
FREQUENCY 9.4 Kmc CALCULATED S_{min}=24 db
ATTENUATOR 60 db

Fig. C62 Test Box Number 56

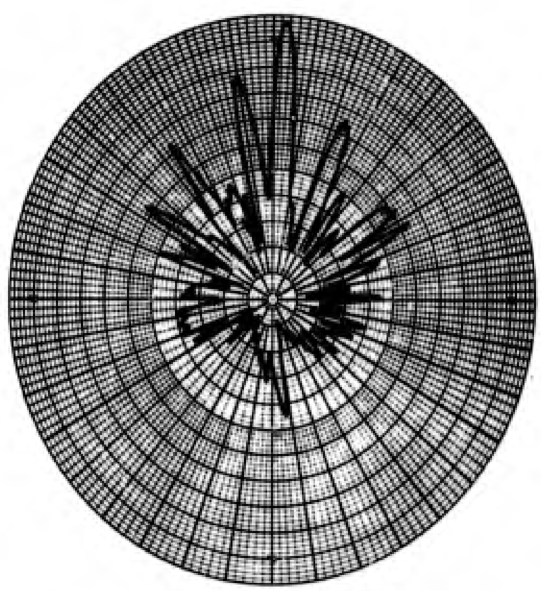

ANTENNA STUB FIELD 123 db
FREQUENCY 9.4 Kmc CALCULATED S_{min}=2 db
ATTENUATOR 80 db

Fig. C63 Test Box Number 57

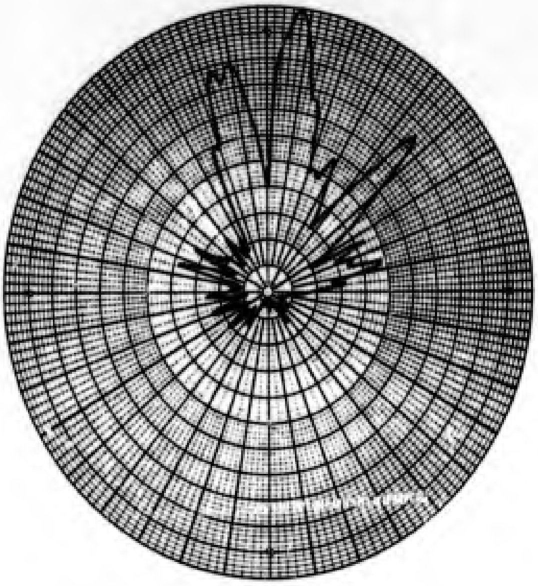

ANTENNA STUB
FREQUENCY 9.4 Kmc
ATTENUATOR 90 db
FIELD 129 db
CALCULATED S_{min}=−2 db

Fig. C64 Test Box Number 58, Raised Horn

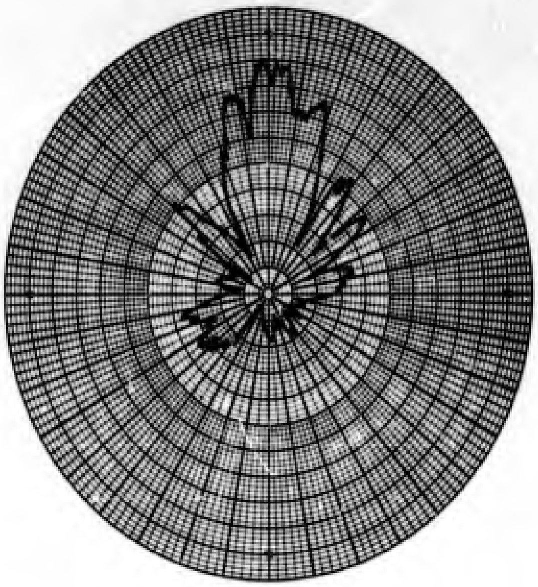

ANTENNA STUB
FREQUENCY 9.4 Kmc
ATTENUATOR 60 db
FIELD 123 db
CALCULATED S_{min}=24 db

Fig. C65 Test Box Number 63

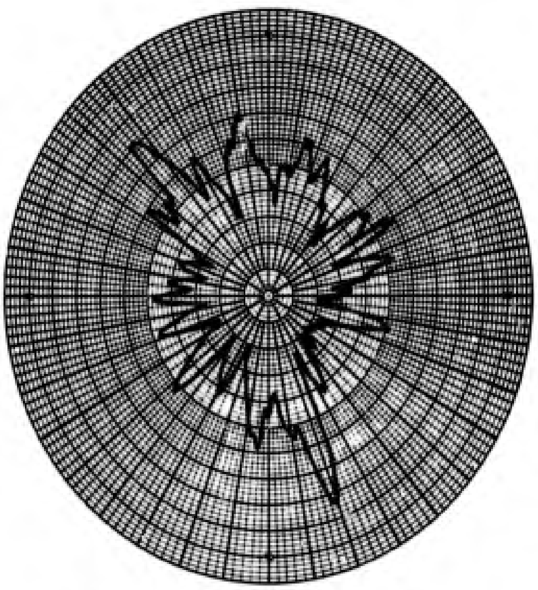

ANTENNA STUB
FREQUENCY 9.4 Kmc
ATTENUATOR 43 db
FIELD 123 db
CALCULATED S_{min}=41 db

Fig. C66 Test Box Number 67

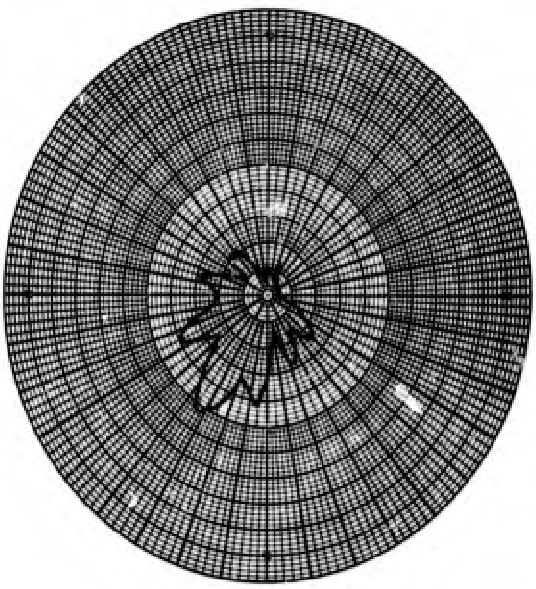

ANTENNA STUB
FREQUENCY 9.4 Kmc
ATTENUATOR 80 db
FIELD 123 db
CALCULATED S_{min}=8 db

Fig. C67 Test Box Number 68

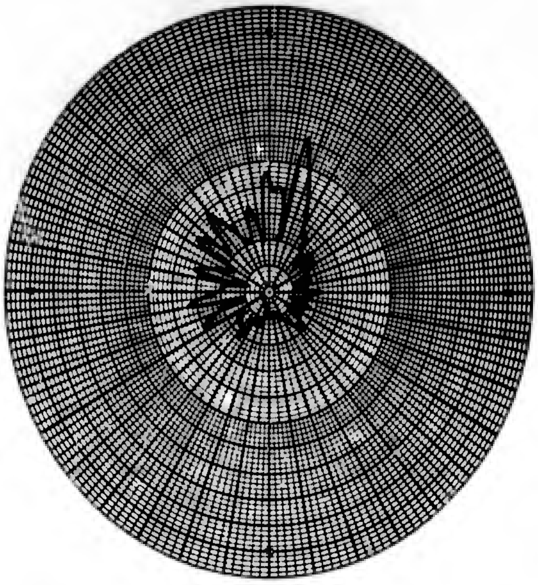

ANTENNA STUB
FREQUENCY 9.4 Kmc
ATTENUATOR 50 db
FIELD 123 db
CALCULATED S_{min}=37 db

Fig. C68 Test Box Number 69

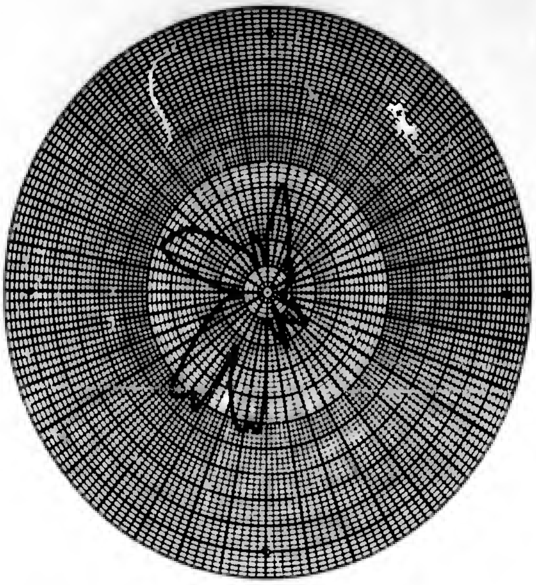

ANTENNA STUB
FREQUENCY 9.4 Kmc
ATTENUATOR 60 db
FIELD 123 db
CALCULATED S_{min}=28 db

Fig. C69 Test Box Number 70

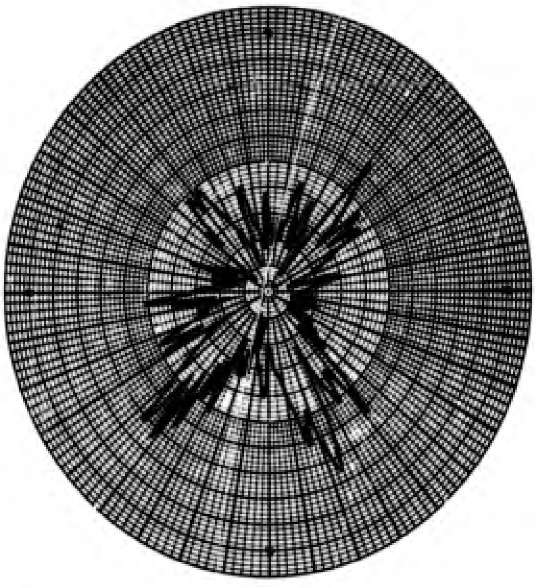

ANTENNA STUB
FREQUENCY 9.4 Kmc
ATTENUATOR 70 db
FIELD 123 db

Fig. C70 Test Box Number 71

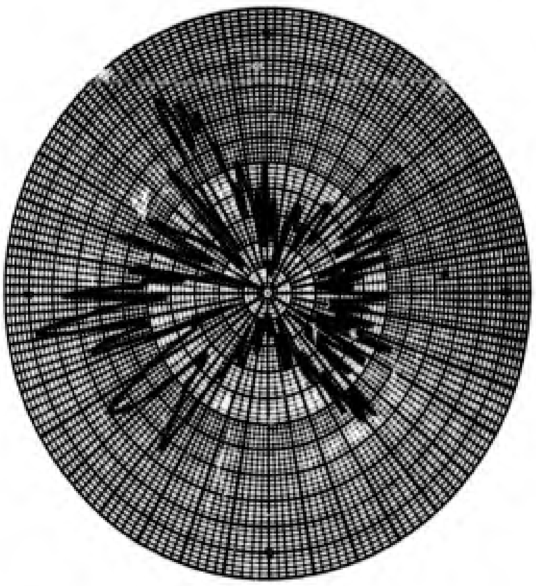

ANTENNA STUB
FREQUENCY 9.4 Kmc
ATTENUATOR 60 db
FIELD 123 db
CALCULATED

Fig. C71 Test Box Number 72

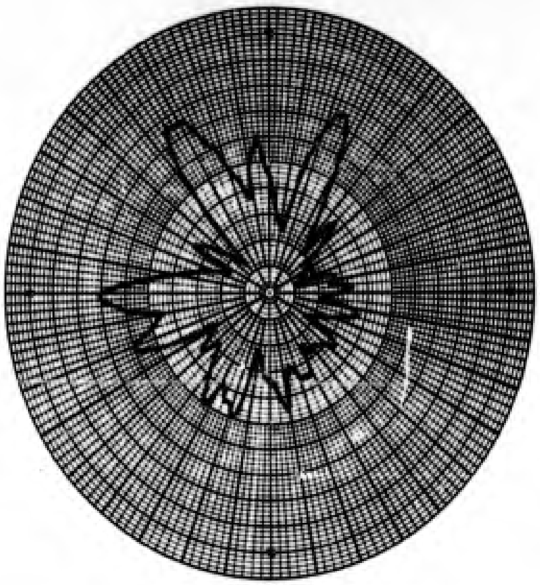

ANTENNA STUB
FREQUENCY 9.4 Kmc
ATTENUATOR 33 db
BACKGROUND 31 db
FIELD 118 db

Fig. C72 Test Box Number 74

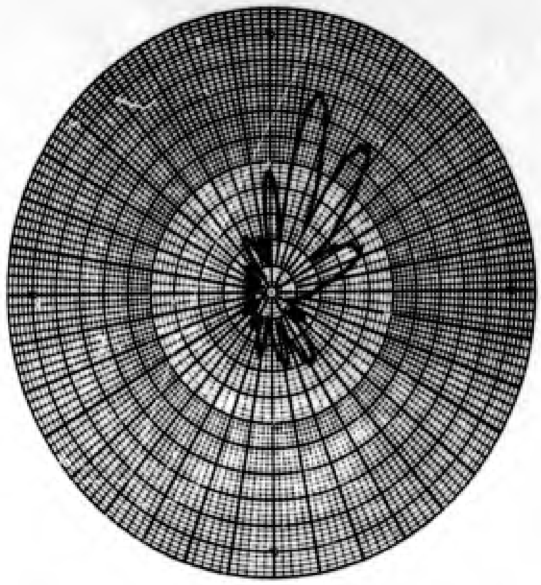

ANTENNA STUB
FREQUENCY 9.4 Kmc
ATTENUATOR 50 db
FIELD 123 db
CALCULATED S_{min}=35 db

Fig. C73 Test Box Number 75

DOCUMENT CONTROL DATA—R&D

(Security classification of title, body of abstract and indexing annotation must be entered when the overall report is classified)

1. ORIGINATING ACTIVITY (Corporate author) The Boeing Company Airplane Company Renton, Washington	2a. REPORT SECURITY CLASSIFICATION FOR OFFICIAL USE ONLY 2b. GROUP N/A

3. REPORT TITLE

"Feasibility Study of Shielding Techniques".

4. DESCRIPTIVE NOTES (Type of report and inclusive dates)
Final Report - 4 June 1963 - 30 November 1964

5. AUTHOR(S) (Last name, first name, initial)
PLANTZ, Vellar C.
BRUSH, David R.
SCHULZ, Richard B.

6. REPORT DATE	7a. TOTAL NO. OF PAGES	7b. NO. OF REFS.
9 April 1965	180	12

8a. CONTRACT OR GRANT NO. DA36-039 AMC-02308(E) b. PROJECT NO. 1E6-20501-D-449 c. Task Nr. -01 d. Subtask Nr. -18	9a. ORIGINATOR'S REPORT NUMBER(S) D6-8597-5 9b. OTHER REPORT NO.(S) (Any other numbers that may be assigned this report) N/A

10. AVAILABILITY/LIMITATION NOTICES
For Official Use Only. DDC release to CFSTI not authorized. U.S. Government agencies may obtain copies of this report directly from DDC. Release or announcement to the public is not authorized.

11. SUPPLEMENTARY NOTES N/A	12. SPONSORING MILITARY ACTIVITY U.S. Army Electronics Command Fort Monmouth, New Jersey (AMSEL-RD-GFR)

13. ABSTRACT

(U) This final report of an 18-month research and study program presents two significant results of fundamental utility in understanding and designing electromagnetic shielding for a given application.

(U) a. Shielding Design. A technique has been developed for the design of optimum shielding enclosures. This technique is substantiated by theoretical development and by laboratory data obtained in the course of the research. The basic theoretical approach is to consider the transmission of electromagnetic energy through the shielding material in a manner analagous to conventional transmission-line theory. Transmission through each leakage path in a shield such as a seam, air inlet, closure or other discontinuity was considered to be in parallel with that through the shield material itself. Design data resulting from this approach and substantiating experimental data are given. Utilization of this overall approach and design techniques resulting therefrom yield good agreement between theory and predicted performance of practical shielding enclosures.

(U) b. Low-Frequency Resonance. During the study, resonance effects in a number of shielding enclosures were observed in the frequency range of 5 kc to 150 kc. These are explained on the basis of large differences in phase shift between parallel transmission paths through the material and through seams under certain conditions of transmission. These effects are believed to be described for the first time herein.

14. KEY WORDS	LINK A		LINK B		LINK C	
	ROLE	WT.	ROLE	WT.	ROLE	WT.
Shielding (U) Electromagnetic Shielding (U) Electromagnetic Shielding Theory (U) Electromagnetic Shielding Design (U) Electromagnetic Shielding Materials (U) Electromagnetic Shielding Joints (U) Electromagnetic Shielding Effectiveness (U) VLF Shielding (U) LF Shielding (U) Microwave Shielding (U)						

INSTRUCTIONS

1. ORIGINATING ACTIVITY: Enter the name and address of the contractor, subcontractor, grantee, Department of Defense activity or other organization *(corporate author)* issuing the report.

2*a*. REPORT SECURITY CLASSIFICATION: Enter the overall security classification of the report. Indicate whether "Restricted Data" is included. Marking is to be in accordance with appropriate security regulations.

2*b*. GROUP: Automatic downgrading is specified in DoD Directive 5200.10 and Armed Forces Industrial Manual. Enter the group number. Also, when applicable, show that optional markings have been used for Group 3 and Group 4 as authorized.

3. REPORT TITLE: Enter the complete report title in all capital letters. Titles in all cases should be unclassified. If a meaningful title cannot be selected without classification, show title classification in all capitals in parenthesis immediately following the title.

4. DESCRIPTIVE NOTES: If appropriate, enter the type of report, e.g., interim, progress, summary, annual, or final. Give the inclusive dates when a specific reporting period is covered.

5. AUTHOR(S): Enter the name(s) of author(s) as shown on or in the report. Enter last name, first name, middle initial. If military, show rank and branch of service. The name of the principal author is an absolute minimum requirement.

6. REPORT DATE: Enter the date of the report as day, month, year; or month, year. If more than one date appears on the report, use date of publication.

7*a*. TOTAL NUMBER OF PAGES: The total page count should follow normal pagination procedures, i.e., enter the number of pages containing information.

7*b*. NUMBER OF REFERENCES: Enter the total number of references cited in the report.

8*a*. CONTRACT OR GRANT NUMBER: If appropriate, enter the applicable number of the contract or grant under which the report was written.

8*b*, 8*c*, & 8*d*. PROJECT NUMBER: Enter the appropriate military department identification, such as project number, subproject number, system numbers, task number, etc.

9*a*. ORIGINATOR'S REPORT NUMBER(S): Enter the official report number by which the document will be identified and controlled by the originating activity. This number must be unique to this report.

9*b*. OTHER REPORT NUMBER(S): If the report has been assigned any other report numbers *(either by the originator or by the sponsor)*, also enter this number(s).

10. AVAILABILITY/LIMITATION NOTICES: Enter any limitations on further dissemination of the report, other than those imposed by security classification, using standard statements such as:

(1) "Qualified requesters may obtain copies of this report from DDC."

(2) "Foreign announcement and dissemination of this report by DDC is not authorized."

(3) "U. S. Government agencies may obtain copies of this report directly from DDC. Other qualified DDC users shall request through ______________."

(4) "U. S. military agencies may obtain copies of this report directly from DDC. Other qualified users shall request through ______________."

(5) "All distribution of this report is controlled. Qualified DDC users shall request through ______________."

If the report has been furnished to the Office of Technical Services, Department of Commerce, for sale to the public, indicate this fact and enter the price, if known.

11. SUPPLEMENTARY NOTES: Use for additional explanatory notes.

12. SPONSORING MILITARY ACTIVITY: Enter the name of the departmental project office or laboratory sponsoring *(paying for)* the research and development. Include address.

13. ABSTRACT: Enter an abstract giving a brief and factual summary of the document indicative of the report, even though it may also appear elsewhere in the body of the technical report. If additional space is required, a continuation sheet shall be attached.

It is highly desirable that the abstract of classified reports be unclassified. Each paragraph of the abstract shall end with an indication of the military security classification of the information in the paragraph, represented as *(TS), (S), (C), or (U)*.

There is no limitation on the length of the abstract. However, the suggested length is from 150 to 225 words.

14. KEY WORDS: Key words are technically meaningful terms or short phrases that characterize a report and may be used as index entries for cataloging the report. Key words must be selected so that no security classification is required. Identifiers, such as equipment model designation, trade name, military project code name, geographic location, may be used as key words but will be followed by an indication of technical context. The assignment of links, rules, and weights is optional.

SUPPLEMENTARY

INFORMATION

AD 466 293

THE BOEING COMPANY

AIRPLANE GROUP

September 29, 1965

6-1100-28-466

To: Commander
Defense Documentation Center
Cameron Station
Alexandria, Virginia 22314

Attention:

Subject: Final Report Boeing Document D6-8597-5
Contract DA36-039-AMC02308(E)
"Feasibility Study of Shielding Techniques"

1. The subject report was forwarded via U. S. Mail to the addressee, under date of July 8, 1965, in accordance with our contract with the U. S. Army Electronics Command.

2. Subsequent to the issuance of this document several typographical and technical changes have been noted as detailed on the attached sheet titled "List of Errata".

3. Kindly notate your copy or copies of the subject document to incorporate the clarifying information contained in this errata.

THE BOEING COMPANY

L. W. Taylor,
Assistant Manager
Contract Administration
Product Development

Enclosure:

cc: Wm. Stirratt
USAEC-AMSEL-RD-GFR

C. G. Widdis
USAEC-AMSEL-CM-JR-6

FEASIBILITY STUDY OF SHIELDING TECHNIQUES

FINAL REPORT - DOCUMENT D6-8597-5

LIST OF ERRATA

Page 15, Following the equation in rule (6), change line of text to read "and the corresponding wave impedance, resulting from two separate waves, is"

Page 33, Equations (100), (101), and (102). In the expression $4\frac{\eta_w}{Z_w}$, delete the factor "4" and substitute "2"

Page 34, first line. Delete "4" in expression $4\frac{\eta_w}{Z_w}$, and substitute "2"

Equation (103), first line. Delete "4" in expression $4\frac{\eta_w}{Z_w}$ and "4" following the = sign, and substitute "2" in each case

Equation (103), first and third lines. Delete "2.77" and substitute "1.39" in three places

Page 77, Equation (153). Delete "2.25" and substitute "25.5"

Page 100, Equation (165), fourth line. Delete "(n + 1)A" and substitute "(n - 1)A"

Page 102, Figure 46. Delete that portion of the straight diagonal line extending below the point at which it meets the broken line

Page 104, Line 8, beginning "So that". Add "from Equations (97) and (98)"

Line 9, Delete expression " ΔS_{m2}" and substitute "B_{m2}"